CW MEASUREMENTS OF RIGHT CIRCULAR CONES

Eugene F. Knott, et al

Michigan University

Prepared for:

Air Force Cambridge Research Laboratories

April 1973

Unclassified
Security Classification

AD 769976

DOCUMENT CONTROL DATA - R & D

(Security classification of title, body of abstract and indexing annotation must be entered when the overall report is classified)

1. ORIGINATING ACTIVITY *(Corporate author)*
The University of Michigan Radiation Laboratory
2216 Space Research Bldg., North Campus
Ann Arbor, Michigan 48105

2a. REPORT SECURITY CLASSIFICATION
Unclassified

2b. GROUP

3. REPORT TITLE

CW MEASUREMENTS OF RIGHT CIRCULAR CONES

4. DESCRIPTIVE NOTES *(Type of report and inclusive dates)*
Scientific. Interim.

5. AUTHOR(S) *(First name, middle initial, last name)*
Eugene F. Knott
Thomas B. A. Senior

6. REPORT DATE	7a. TOTAL NO. OF PAGES	7b. NO. OF REFS
April 1973	179	0

8a. CONTRACT OR GRANT NO.
F19628-73-C-0126
b. PROJECT, Task, Work Unit Nos.
5635-02-01
c. DoD Element 61102F
d. DoD Subelement 681305

9a. ORIGINATOR'S REPORT NUMBER(S)
011758-1-T
Scientific Report No. 1

9b. OTHER REPORT NO(S) *(Any other numbers that may be assigned this report)*
AFCRL-TR-0269

10. DISTRIBUTION STATEMENT
This document has been approved for public release and sale; its distribution is unlimited.

11. SUPPLEMENTARY NOTES
TECH, OTHER

12. SPONSORING MILITARY ACTIVITY
Air Force Cambridge Research Laboratories (LZ)
L. G. Hanscom Field
Bedford, Massachusetts 01730

13. ABSTRACT

The measured backscattering characteristics of two metallic right circular cones, with and without absorbing pads on their bases, are shown in 328 patterns. The absorber pads were used to reduce second order diffraction across the base of the cones. Measurements were carried out at closely spaced frequencies from 8.0 to 12.0 GHz, for both horizontal and vertical polarizations, using a CW cancellation method.

DD FORM 1473

Unclassified

14. KEY WORDS	LINK A		LINK B		LINK C	
	ROLE	WT	ROLE	WT	ROLE	WT
Backscattering						
Cones						
Measurements						

CW MEASUREMENTS OF RIGHT CIRCULAR CONES

by
Eugene F. Knott
Thomas B.A. Senior

The University of Michigan
Radiation Laboratory
2455 Hayward
Ann Arbor, Michigan 48105

Contract No. F19628-73-C-0126
Project No. 5635
Task No. 563502
Work Unit No. 56350201

Scientific Report No. 1

April 1973

Contract Monitor: John K. Schindler
Microwave Physics Laboratory

Prepared for

AIR FORCE CAMBRIDGE RESEARCH LABORATORIES
AIR FORCE SYSTEMS COMMAND
UNITED STATES AIR FORCE
BEDFORD, MASSACHUSETTS 01730

ABSTRACT

The measured backscattering characteristics of two metallic right circular cones, with and without absorbing pads on their bases, are shown in 328 patterns. The absorber pads were used to reduce second order diffraction across the base of the cones. Measurements were carried out at closely spaced frequencies from 8.0 to 12.0 GHZ for both horizontal and vertical polarizations, using a CW cancellation method.

CW MEASUREMENTS OF RIGHT CIRCULAR CONES

The intent of this report is to display in a convenient format the measured backscattering characteristics of a pair of metallic right circular cones. The original purpose of the measurements was to collect a comprehensive body of data to be used in analyzing the diffraction of electromagnetic waves by the base of a cone and to provide experimental tests of theoretical work that has been in progress for several years at the Radiation Laboratory. Having performed the measurements, it occurred to us that others might also find the data useful and we decided to publish the data for the benefit of all.

The cones were machined from cold-rolled aluminum billets and care was taken to maintain sharp tips and sharp edges where the slanted sides meet the base. Their half-angles were 15.00 ± 0.05 and 40.00 ± 0.05 degrees and their base diameters were 3.937 ± 0.001 and 6.010 ± 0.002 inches, respectively. The large half-angle of the latter model was chosen to provide a substantial range in aspect angle over which the entire rim of the base remains visible. A short cylindrical beaded foam pedestal was cemented to each cone to speed their installation on and removal from a beaded foam support column used in the measurements. The cones were measured both with and without circular pads of Emerson and Cuming AN-73 absorbing material cemented to their bases, whose purpose was to reduce second order diffraction across the base.

The measurements were carried out at X-band frequencies in a large anechoic chamber using the time-honored CW cancellation method. A stable signal was produced by the use of a phase-locked frequency stabilizer and residual chamber reflections were cancelled by means of a reference signal sample of controllable phase and amplitude. A single pyramidal antenna was used as transmitter and receiver, hence the measured returns are proportional to the target's backscattering cross section. The received signal was detected by a superheterodyne receiver and recorded on a conventional antenna pattern recorder.

The recorded patterns were calibrated by a substitution method, in which the target obstacle is removed and replaced by a known scatterer, leaving all equipment gain settings undisturbed. We used a precision aluminum sphere 2.945 inches in diameter for calibration and, based on its theoretical radar cross section, we have marked each pattern with a reference line whose amplitude is 10 square wavelengths. This line extends horizontally across the entire pattern.

The frequencies used in the measurements ranged from 8.0 to 12.0 GHz and were nominally spaced 0.1 GHz apart, producing a total of 41 frequencies. Occasionally the klystron signal source failed to produce the necessary power at the desired frequency, whereupon the frequency was shifted slightly in order to achieve more satisfactory operation. However, the frequency was always measured, whatever it turned out to be (with an estimated accuracy of better than 0.01 GHz), and the measured value was multiplied by the constants 1.047922 and 1.599698 in order to obtain the electrical circumference $ka = 2\pi a/\lambda$ of the 15° and 40° cones, respectively, at each frequency. Each pattern is prominently labelled with this value.

The cone targets were installed on the support column with their axes in a horizontal plane and the column was rotated about a vertical axis. The angular scale shown at the bottom of each pattern is the aspect angle subtended by the line of sight and the cone axis, with zero degrees being nose-on incidence. The traces are not always perfectly centered on the patterns, but the misalignment is seldom greater than 0.5 degree. Total aspect angle coverage was limited to slightly more than 90 degrees on either side of nose-on, sufficient to include at least the first two side lobes beyond the specular flash from the side of the cone.

Both horizontal and vertical polarizations were used and the various combinations of frequency, polarization, model and model condition (with or without absorber pad) produced a total of 328 patterns. The patterns of the 15-degree cone are reproduced on pages 10 through 91 and those of the 40-degree cone are reproduced on pages 94 through 175. The format used in displaying the patterns is simple and convenient: when the reader turns to any page he will be looking at a collection of four patterns. The pair on the left-hand page is for horizontal polarization and

the pair on the right for vertical. The upper pattern on either page is for the bare object and the lower for the object having the absorber pad cemented to its base.

The measurements were started off with horizontal polarization at the highest frequency (12.0 GHz) and the models were initially bare. After patterns of the bare objects had been recorded, the absorber pads were applied and another pair of patterns recorded. The frequency was then decremented 0.1 GHz and the absorber-treated models measured again; the pads were removed and another pair of patterns taken. This procedure was followed until the lowest frequency had been reached, whereupon the polarization was rolled over to the vertical. Then, with alternate application and removal of the pads, the frequency was advanced by 0.1 GHz increments until the highest frequency had been completed. We mention this measurement sequence so that the reader will be aware that although the patterns in a given set are physically adjacent to each other on the pages of this report, the time interval separating them may have been several days. In a few instances the frequency used for the vertical polarization was not quite the same as for horizontal and the reader will perceive occasional slight differences in the ka values displayed for a complete set of patterns; see pages 168 and 169, for example.

In order to give the reader some feeling for the consistency of the data, we have abstracted from the patterns the radar cross sections of the cones at nose-on and specular aspects, and these are displayed in Figs. 1 through 3. The values plotted in Fig. 1 are the means of the horizontal and vertical nose-on cross sections when adjusted according to the 10 square wavelength calibration line on the patterns. The circles are datum points for the bare objects and the squares for the absorber-treated models. The marked undulatory pattern traced out by the bare 15-degree cone cross sections shows that a significant contribution arises from second order diffraction across the shadowed base. The application of the absorber pad reduces this source of return, as evidenced by the more gentle undulation, but does not completely suppress it. The fact that minima and maxima exchange positions shows, in addition, that the absorber also changes the phase of the cross-base diffraction.

The corresponding variations in the 40-degree cone data are weaker than those for the 15-degree cone and, aside from what seem to be random errors, the

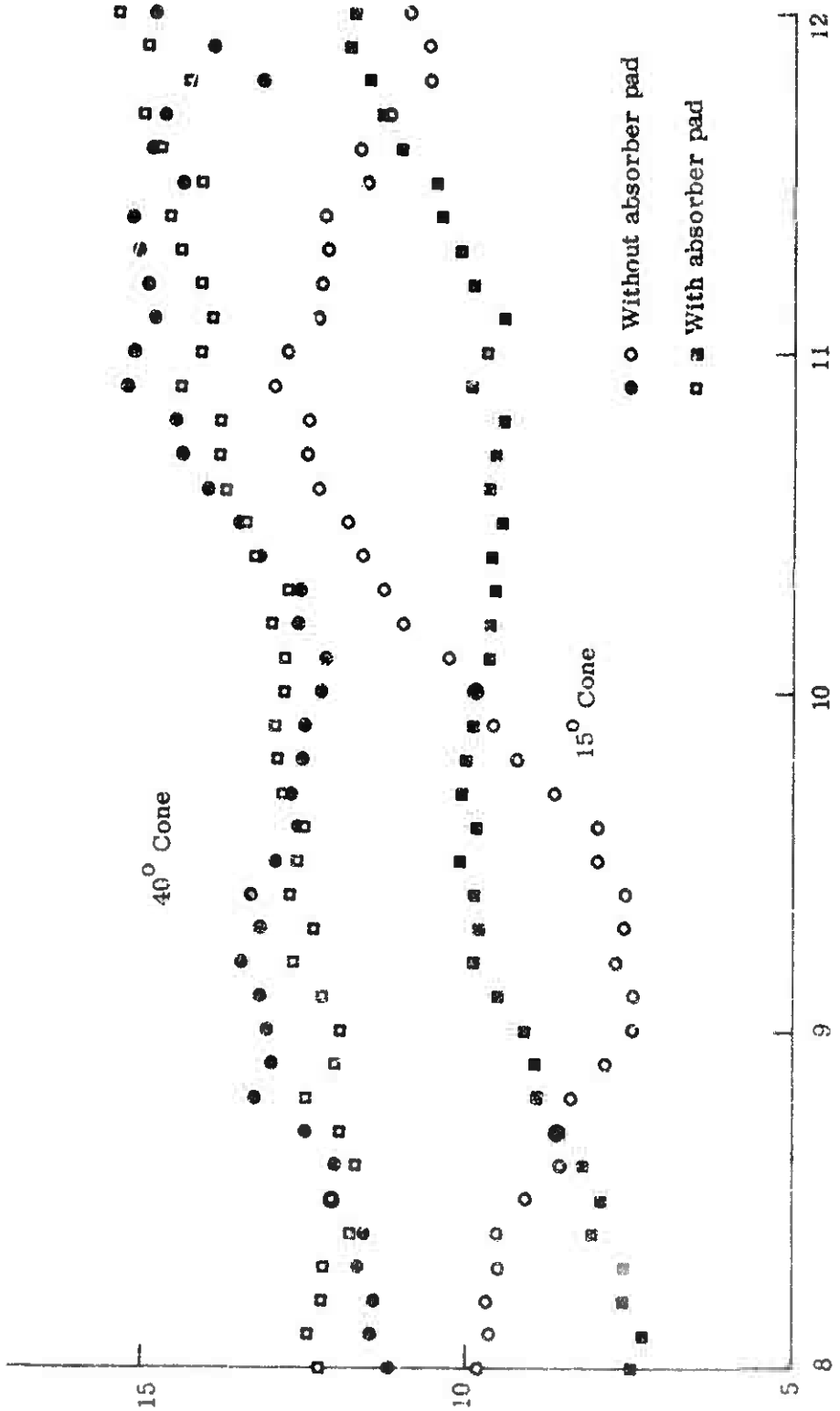

Figure 1: Summary of Nose-on Measurements.

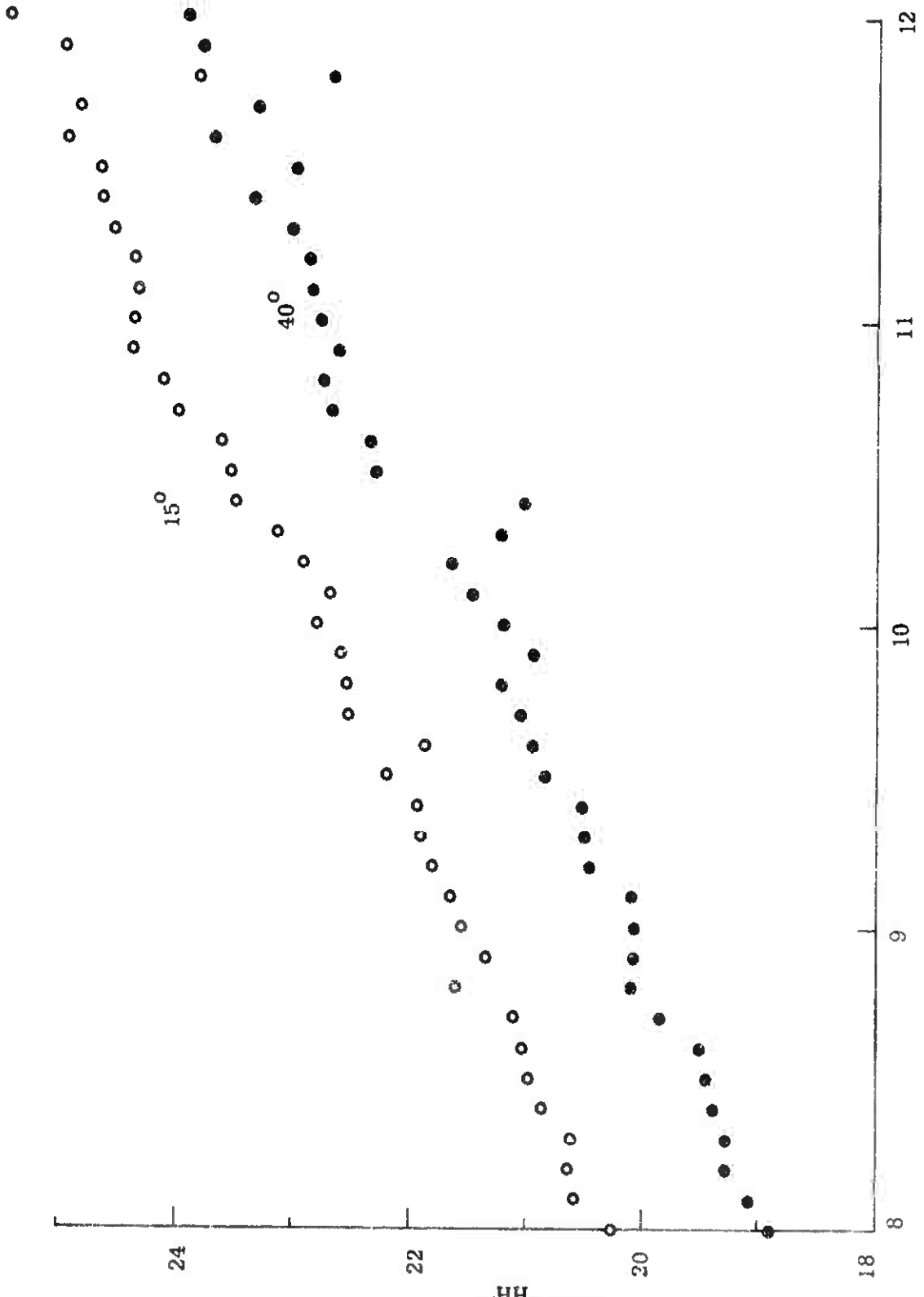

Figure 2: Specular Radar Cross Sections for Horizontal Polarization.

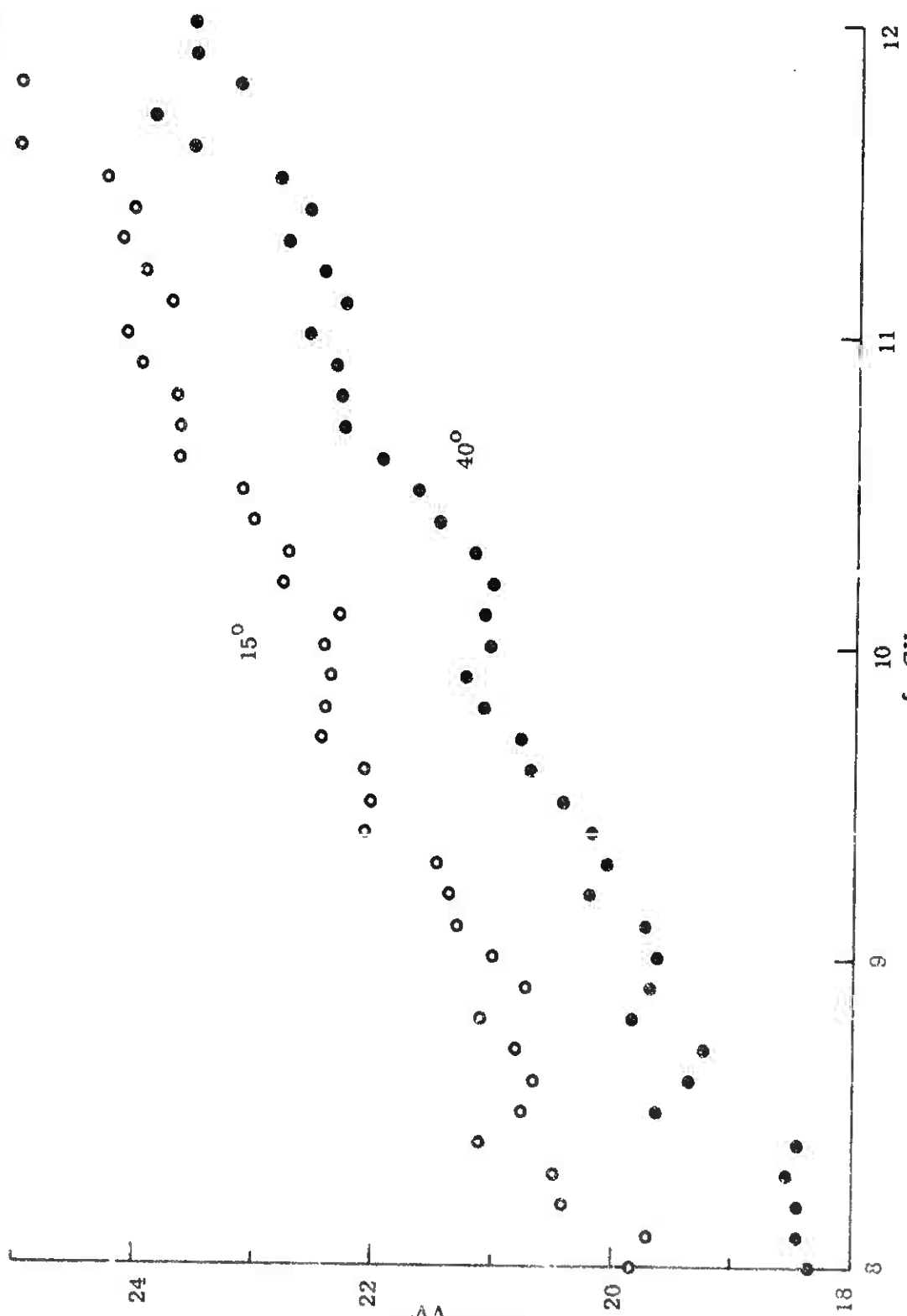

Figure 3: Specular Radar Cross Section for Vertical Polarization.

absorber pad produces a reasonably smoothly increasing cross section with increasing frequency. The results suggest that the larger cone has a smaller second order contribution than the smaller cone. Note that all four data sets take simultaneous jumps at certain frequencies (e.g., 9.2, 10.9, 11.2 GHz), while only those for one cone or the other do so at other frequencies (e.g., 8.8, 10.2, 11.8 GHz).

The specular radar cross sections of the cones are shown as functions of frequency in Fig. 2 for horizontal polarization in Fig. 3 for vertical. In both figures the upper string of datum points are those of the 15-degree cone and the lower data, of the 40-degree cone. The reader will immediately note the displacement of several datum points from the prevailing trend, notably those at 10.4 and 11.8 GHz in Fig. 2, and those at 8.4 and 10.7 GHz in Fig. 3. Undoubtedly the calibration levels of the patterns that produced these points should be adjusted, but we leave it to the reader to decide precisely how much adjustment is required. Aside from the disparities noted above, the data as a complete set seem to be accurate within 0.5 dB. Finally, a close comparison of Figs. 2 and 3 show that the specular returns for vertical polarization are on the average about 0.25 dB lower than those for horizontal polarization. We believe this to be a real difference, and not due to a consistent experimental error between the polarizations.

absorber pad produces a reasonably smoothly increasing cross section with increasing frequency. The results suggest that the larger cone has a smaller second order contribution than the smaller cone. Note that all four data sets take simultaneous jumps at certain frequencies (e.g., 9.2, 10.9, 11.2 GHz), while only those for one cone or the other do so at other frequencies (e.g., 8.8, 10.2, 11.8 GHz).

The specular radar cross sections of the cones are shown as functions of frequency in Fig. 2 for horizontal polarization in Fig. 3 for vertical. In both figures the upper string of datum points are those of the 15-degree cone and the lower data, of the 40-degree cone. The reader will immediately note the displacement of several datum points from the prevailing trend, notably those at 10.4 and 11.8 GHz in Fig. 2, and those at 8.4 and 10.7 GHz in Fig. 3. Undoubtedly the calibration levels of the patterns that produced these points should be adjusted, but we leave it to the reader to decido precisely how much adjustment is required. Aside from the disparities noted above, the data as a complete set seem to be accurate within 0.5 dB. Finally, a close comparison of Figs. 2 and 3 show that the specular returns for vertical polarization are on the average about 0.25 dB lower than those for horizontal polarization. We believe this to be a real difference, and not due to a consistent experimental error between the polarizations.

15° CONE

Preceding page blank

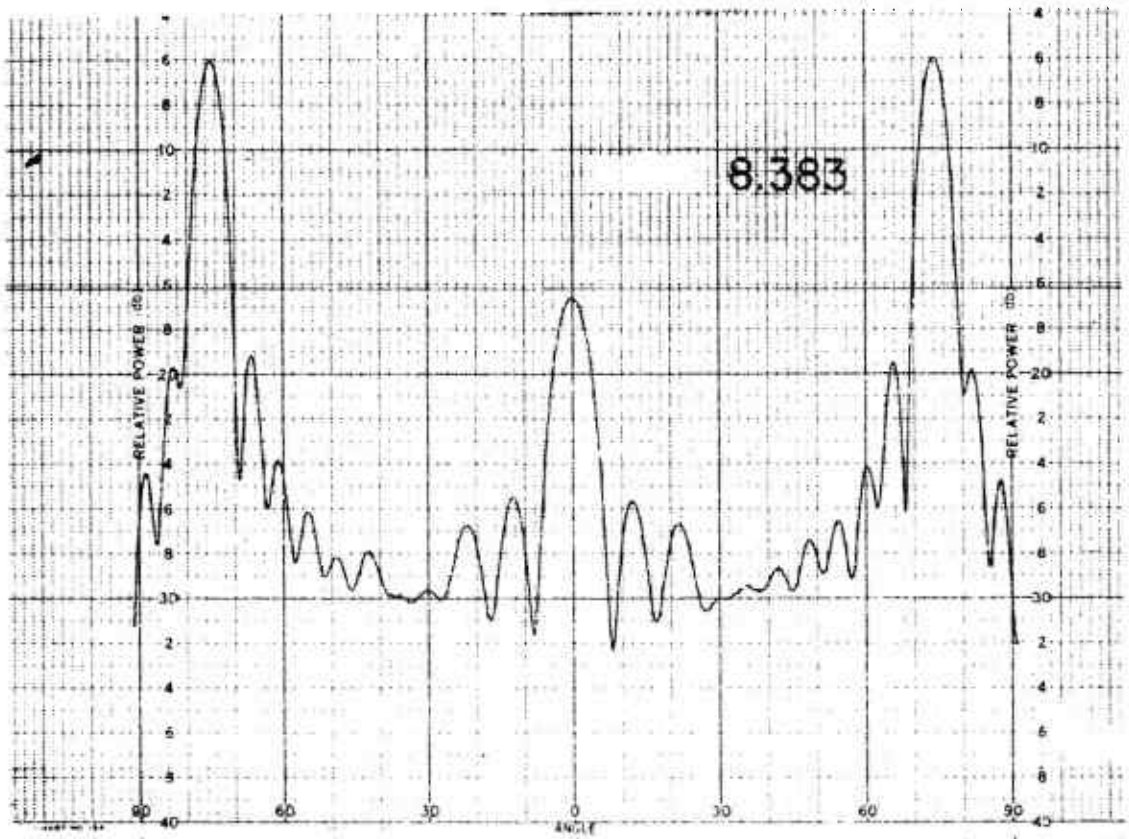
8.383
RELATIVE POWER dB
ANGLE

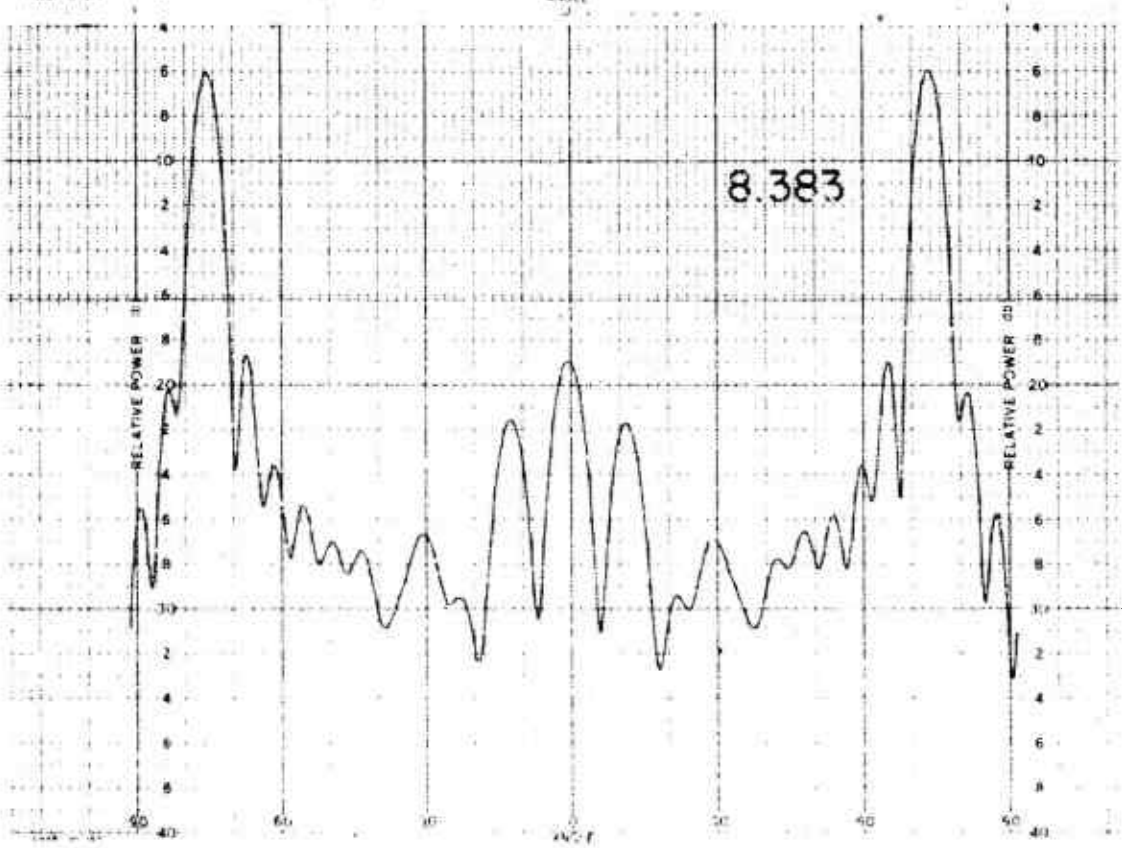
8.383
RELATIVE POWER dB

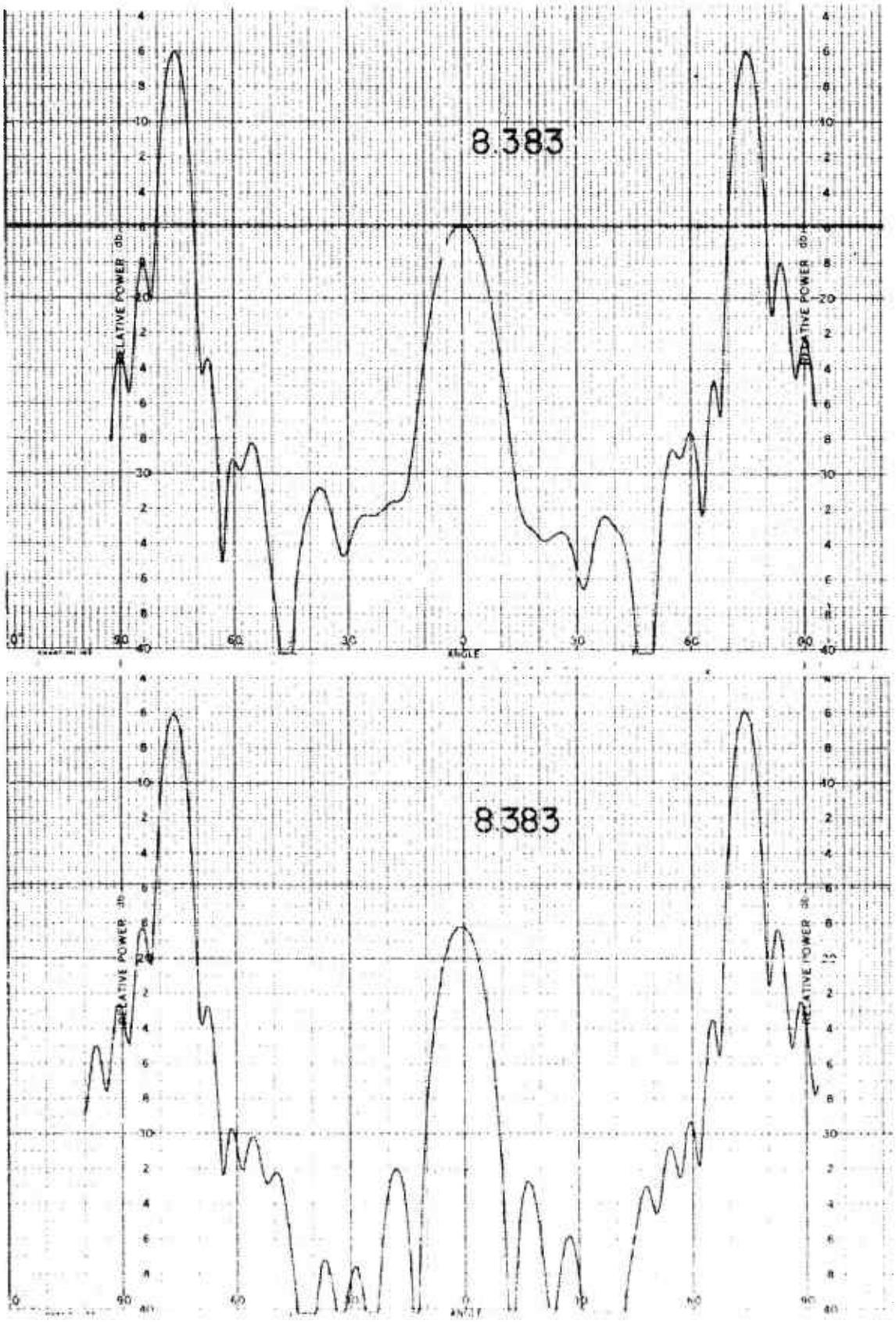
8.383
RELATIVE POWER db
ANGLE
8.383
RELATIVE POWER db
ANGLE

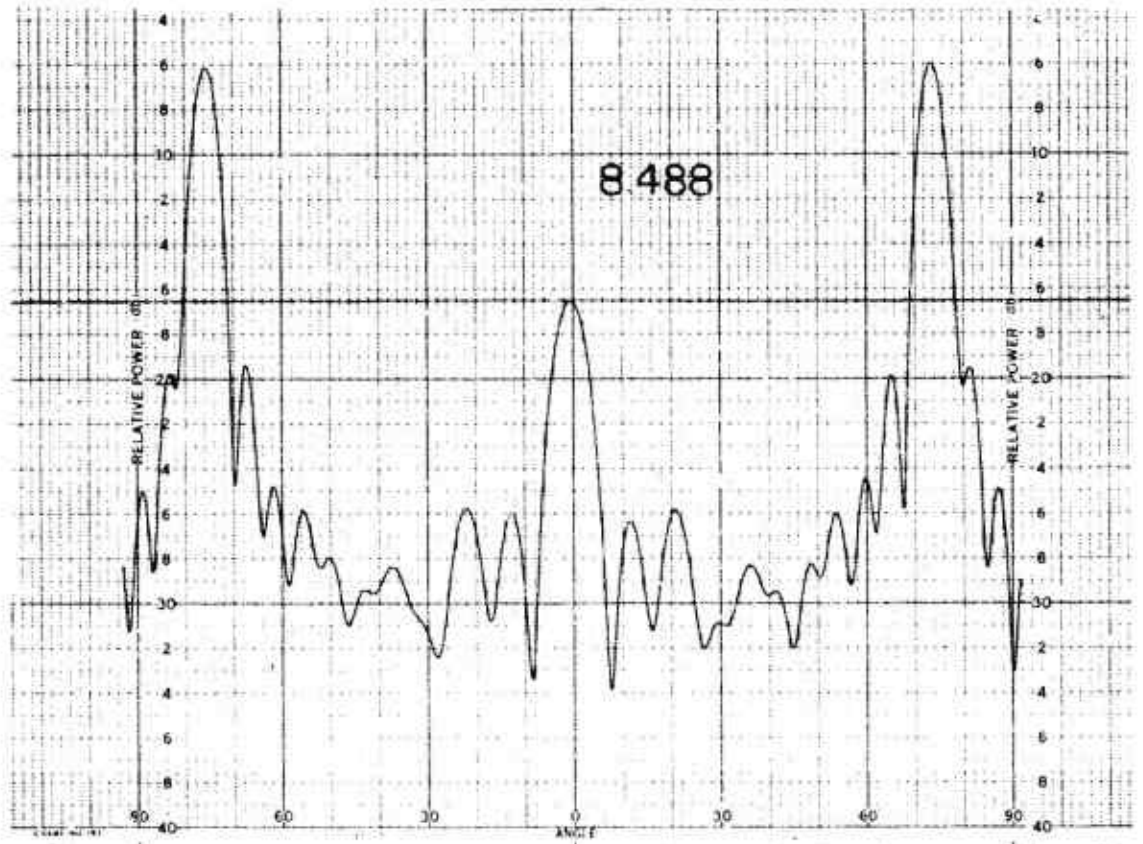
8.488
RELATIVE POWER dB
90
60
30
0
30
60
90
ANGLE

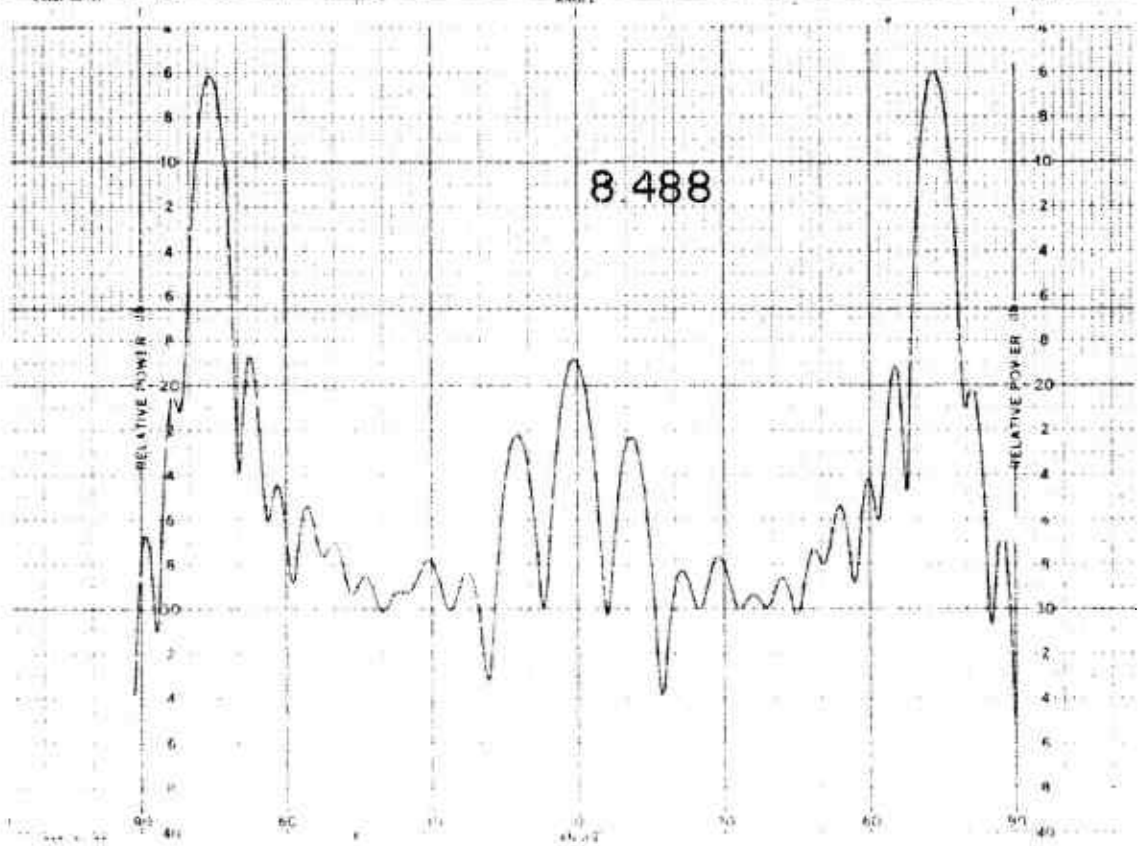
8.488
RELATIVE POWER dB
90
60
30
0
30
60
90
ANGLE

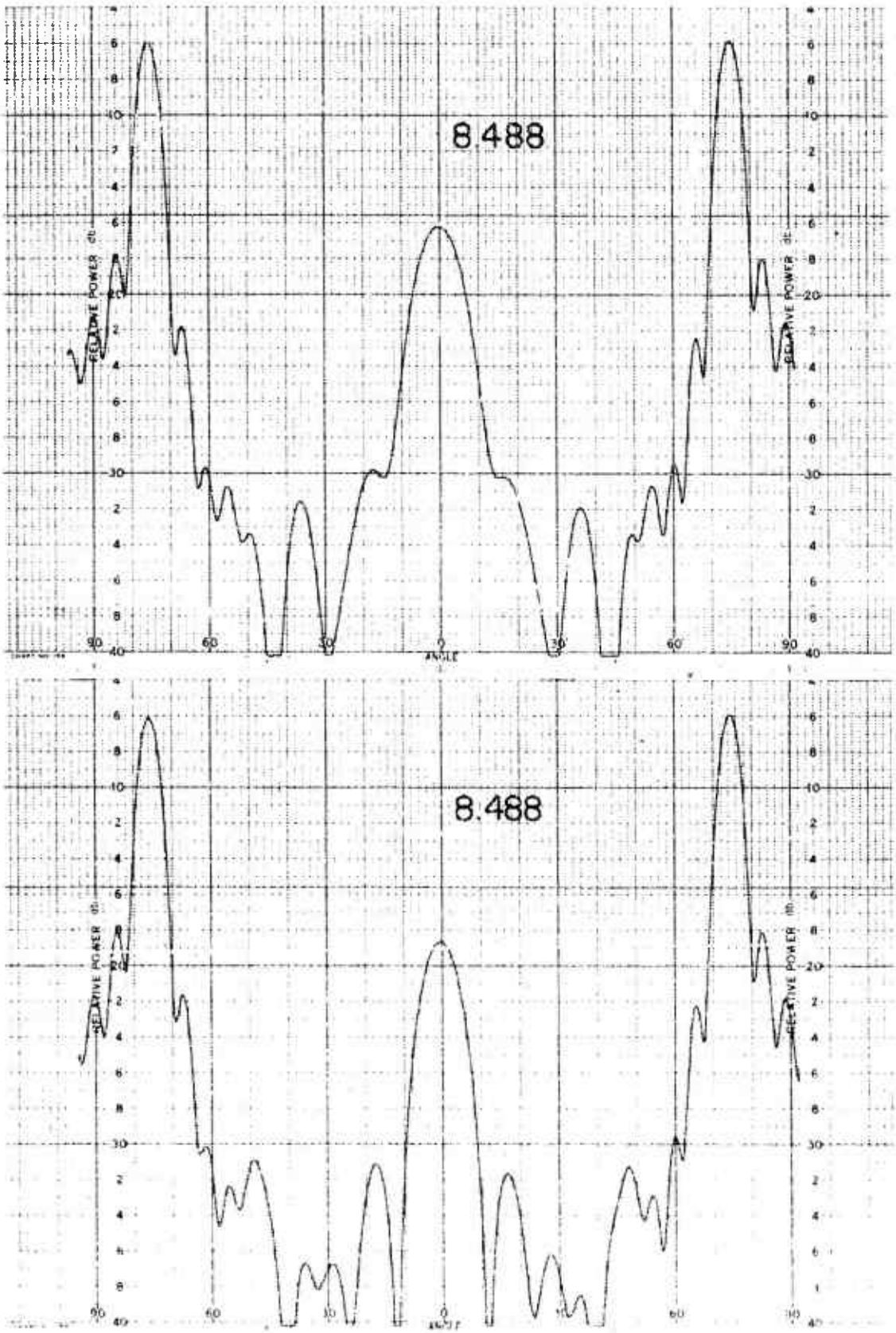
8.488
RELATIVE POWER db
ANGLE
8.488
RELATIVE POWER db
ANGLE

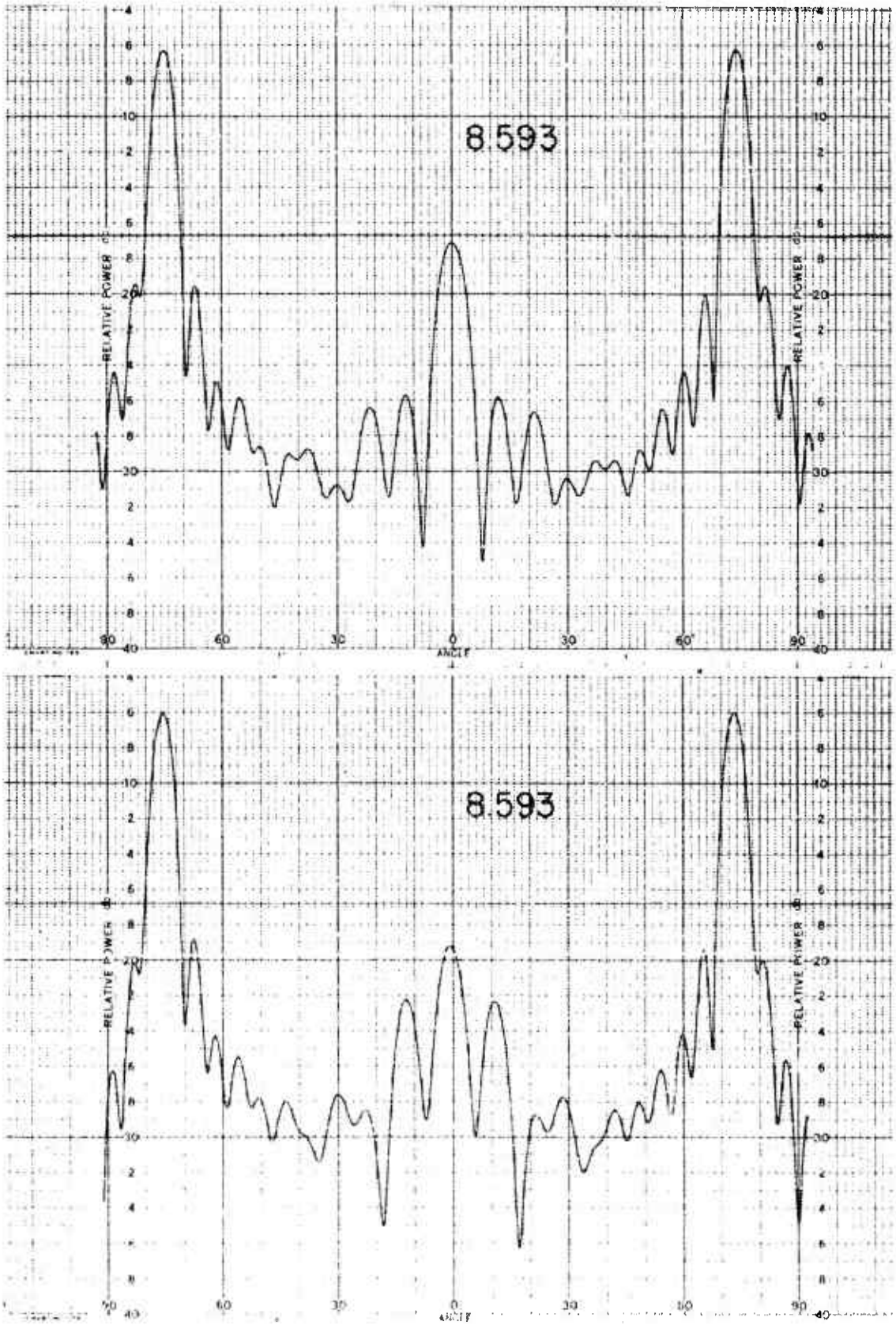
8.593
RELATIVE POWER dB
ANGLE
8.593
RELATIVE POWER dB
ANGLE

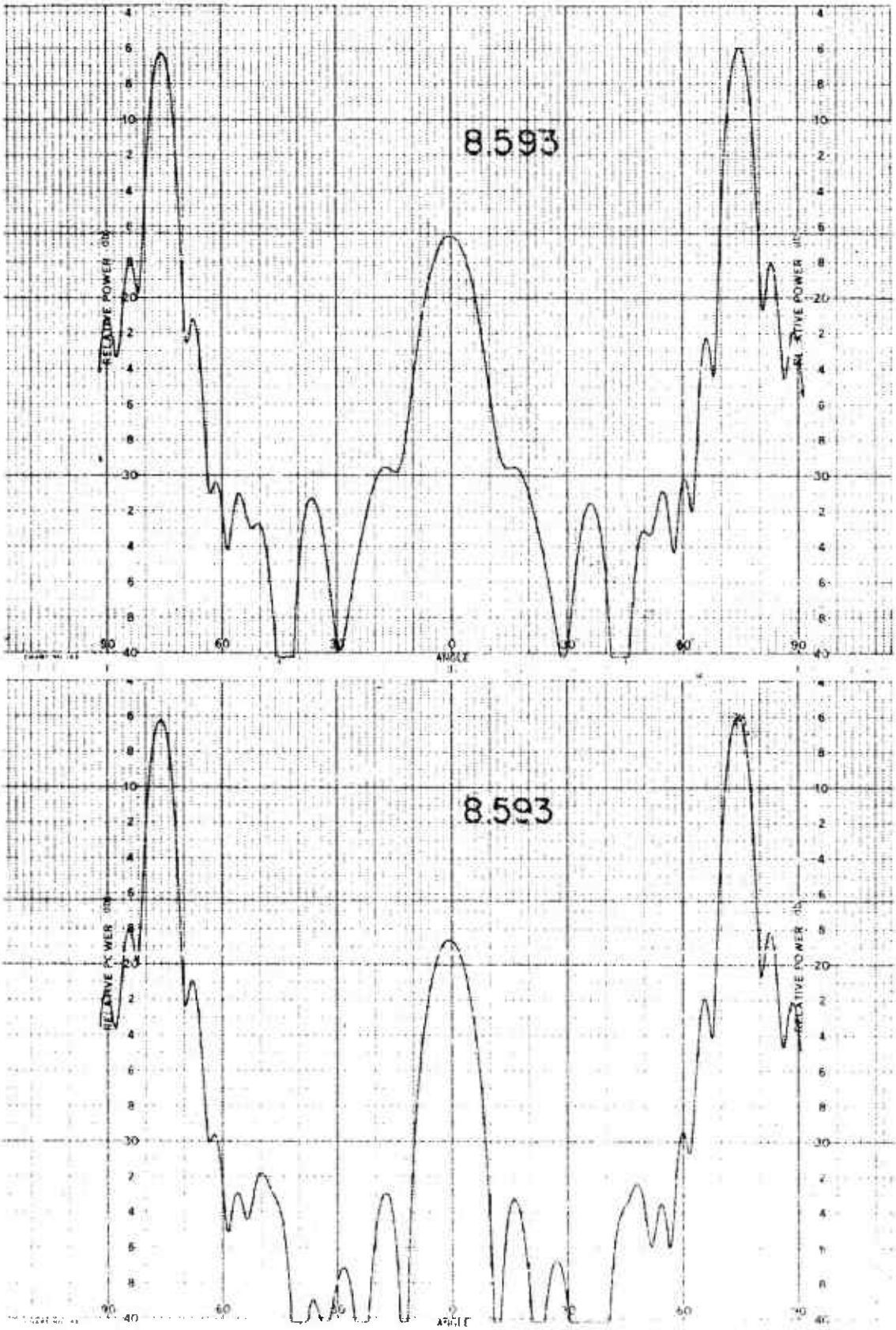
8.593
RELATIVE POWER
ANGLE
8.593
RELATIVE POWER
ANGLE

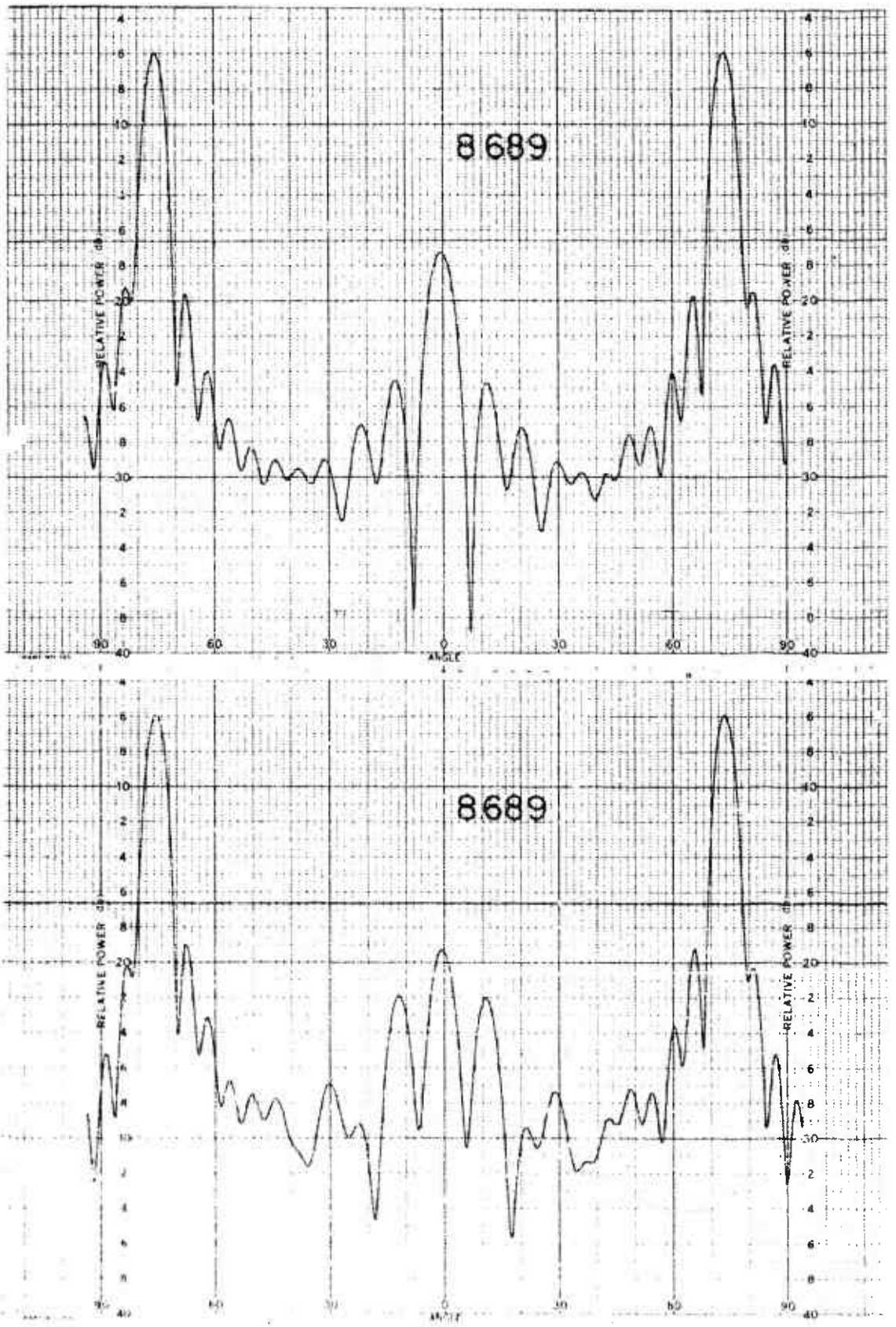
8689
RELATIVE POWER dB
ANGLE
8689
RELATIVE POWER dB
ANGLE

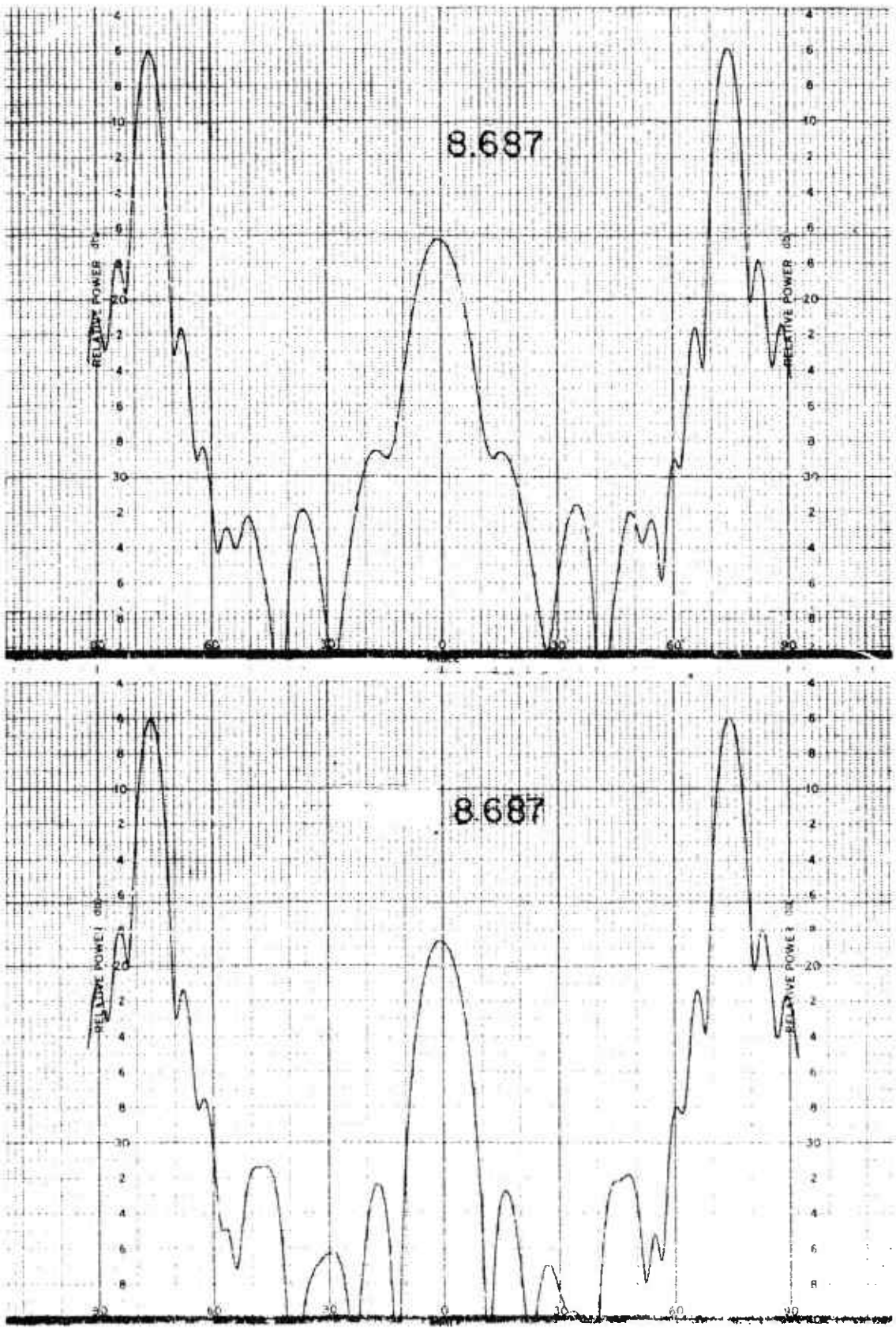
8.687
RELATIVE POWER dB
8.687
RELATIVE POWER dB

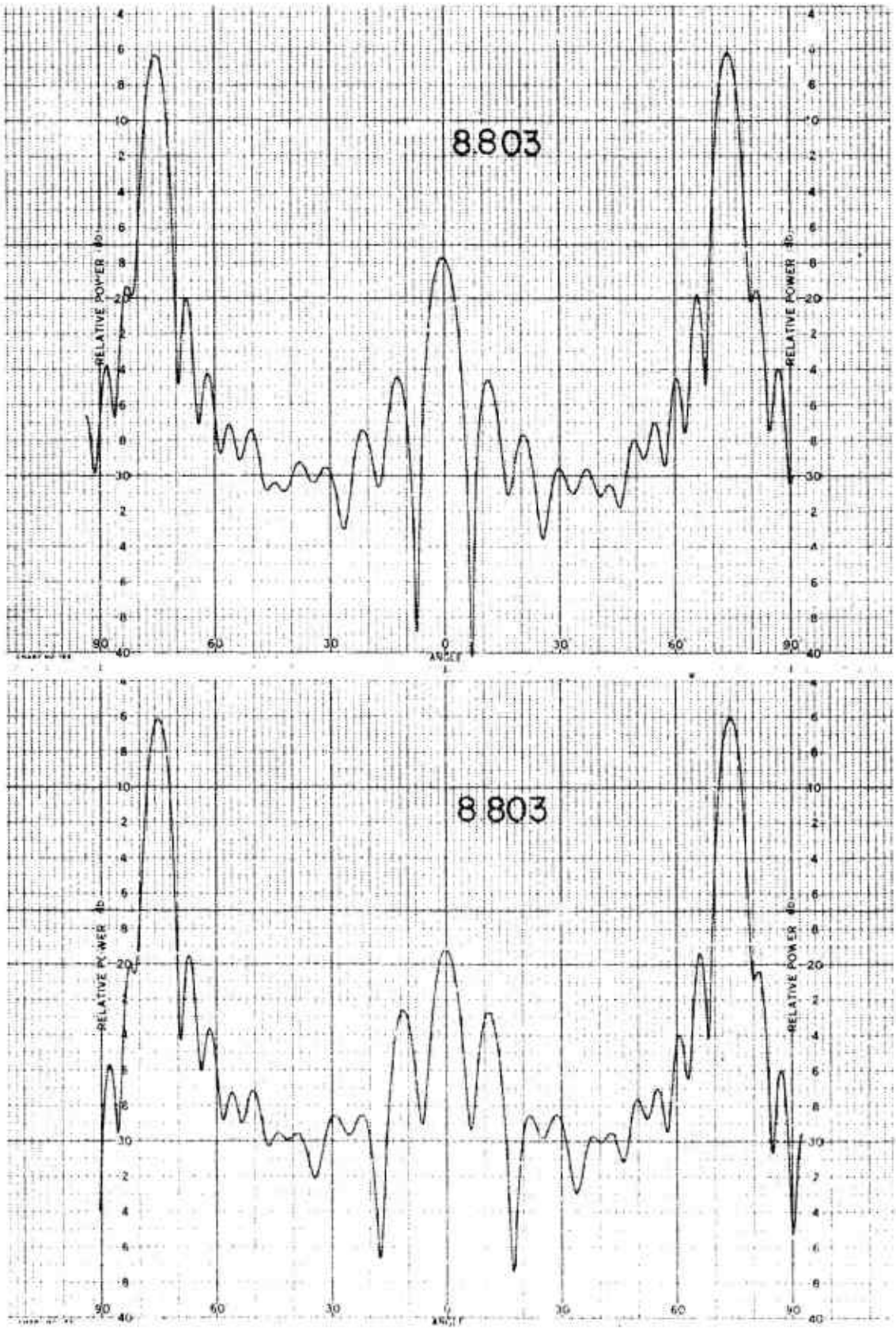
8803
RELATIVE POWER db
90
60
30
0
30
60
90
8803
RELATIVE POWER db

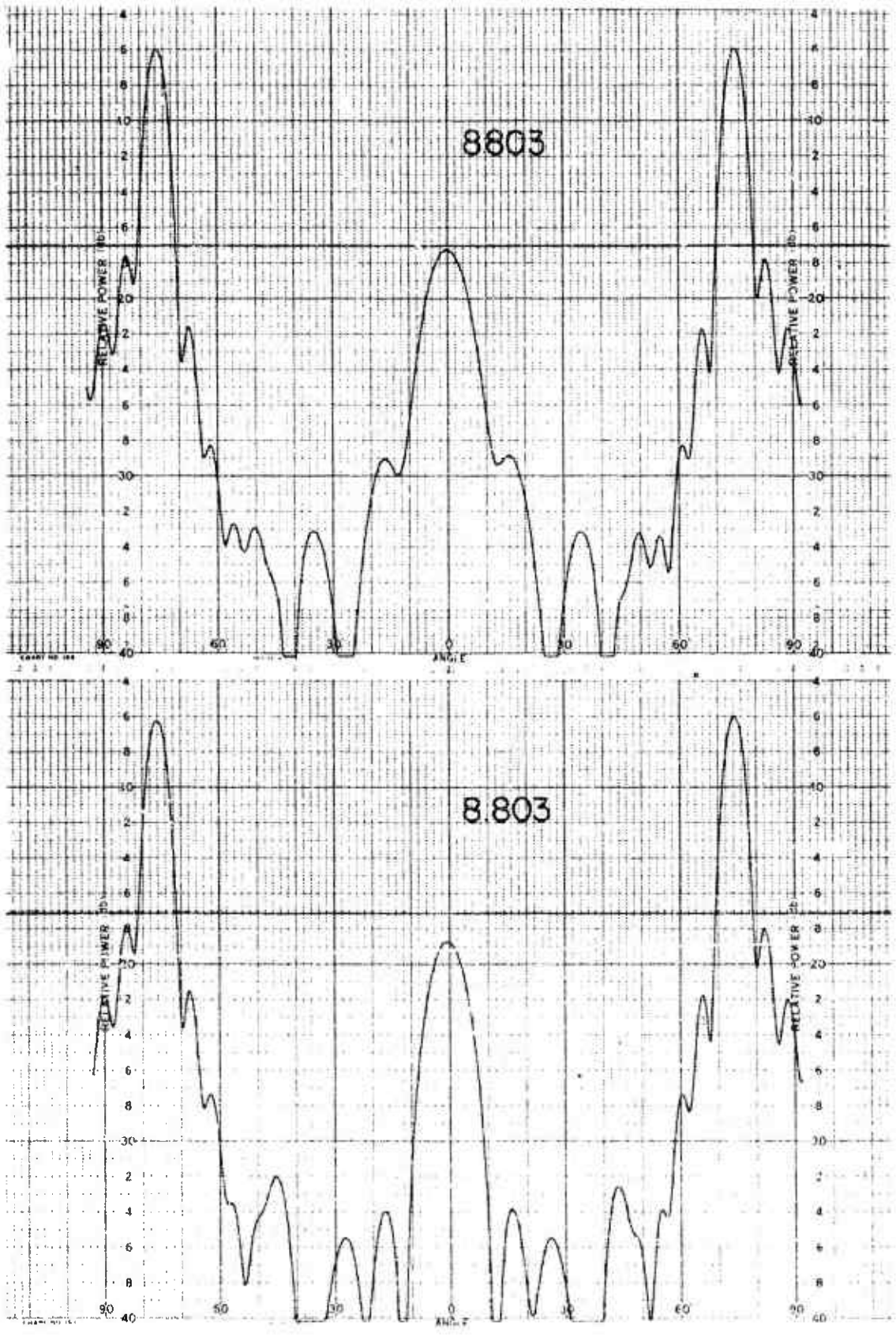
8803
8.803
RELATIVE POWER (db)
ANGLE

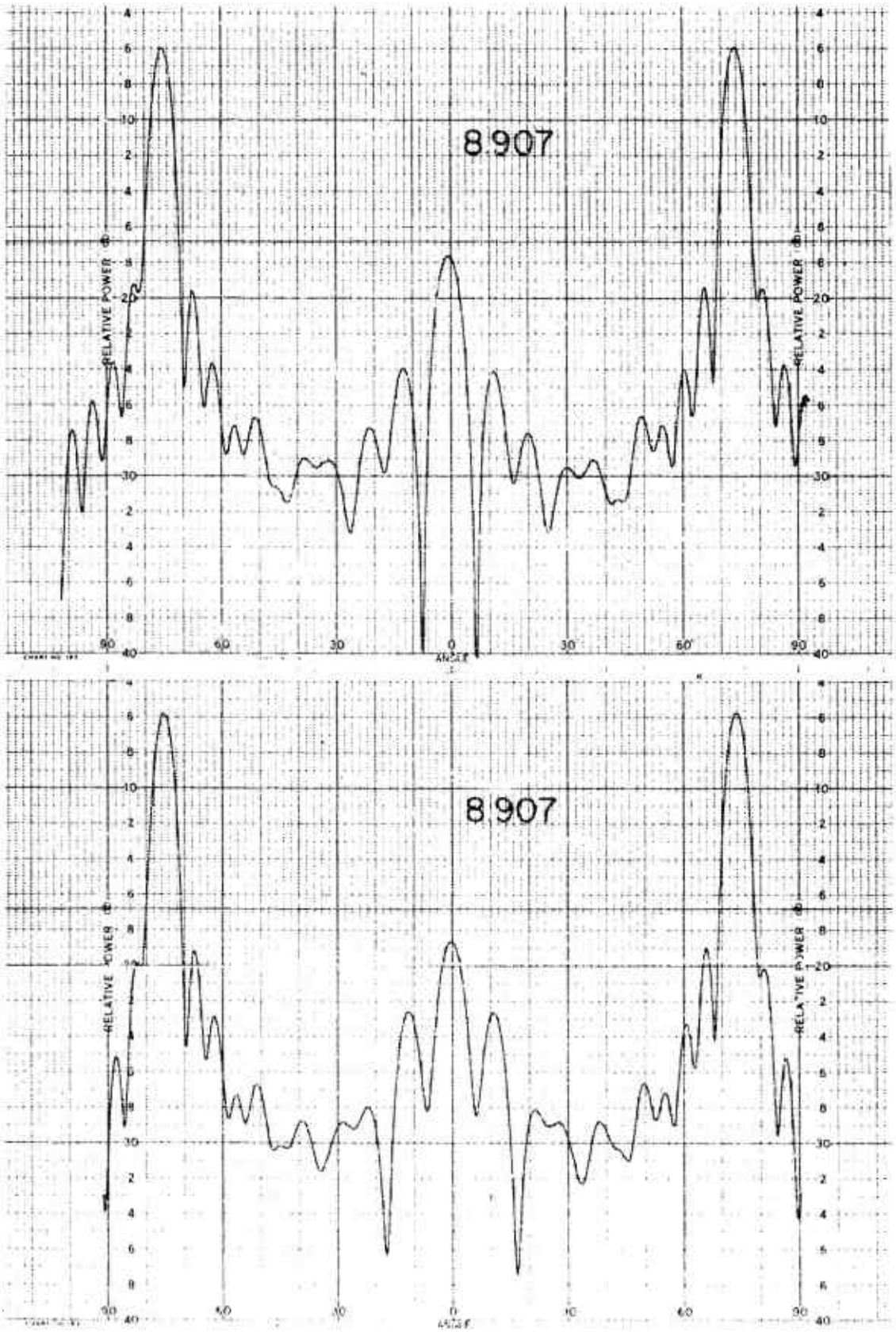
8.907
RELATIVE POWER (dB)
ANGLE
8.907
RELATIVE POWER (dB)
ANGLE

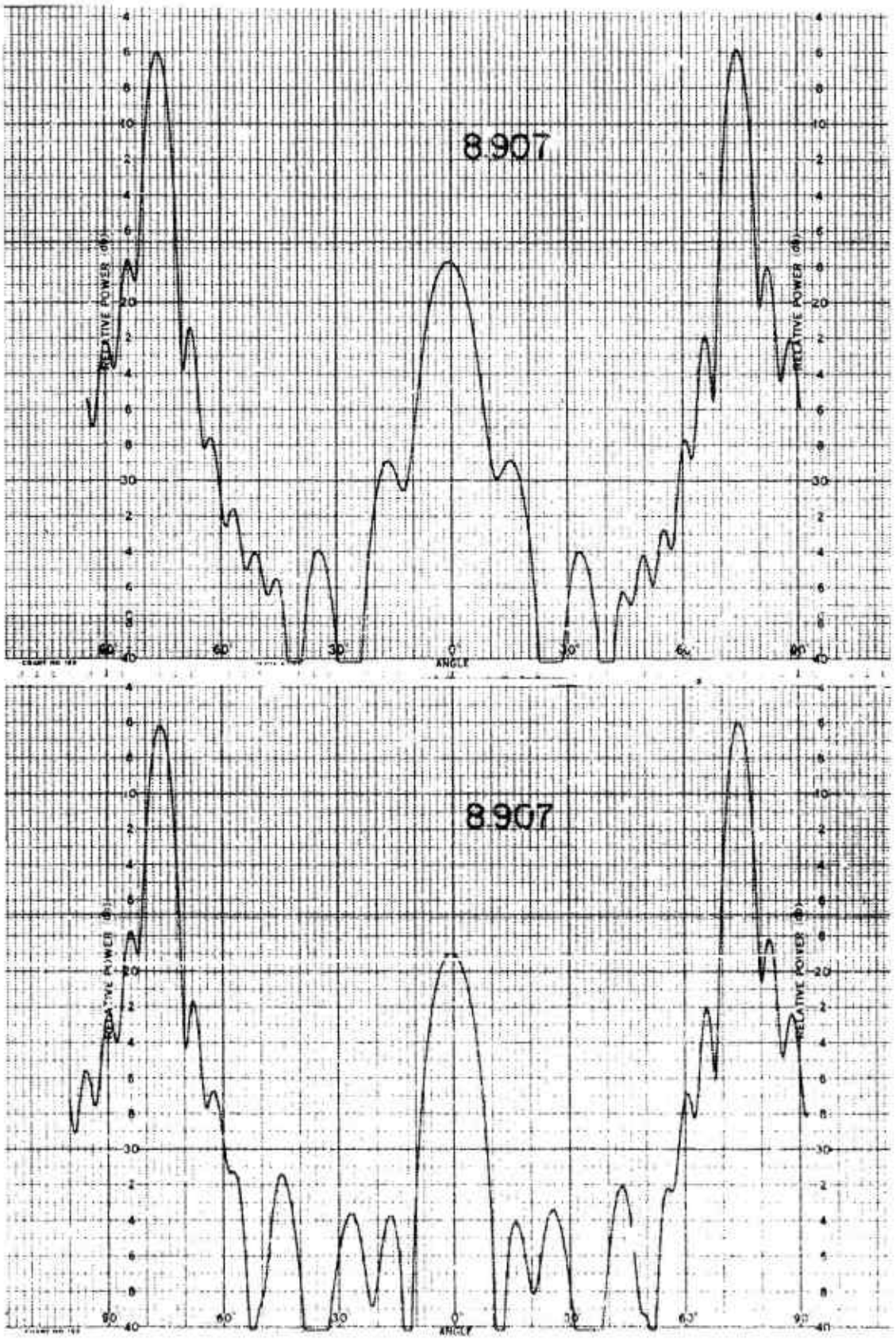
8.907
RELATIVE POWER (dB)
ANGLE
8.907
RELATIVE POWER (dB)
ANGLE

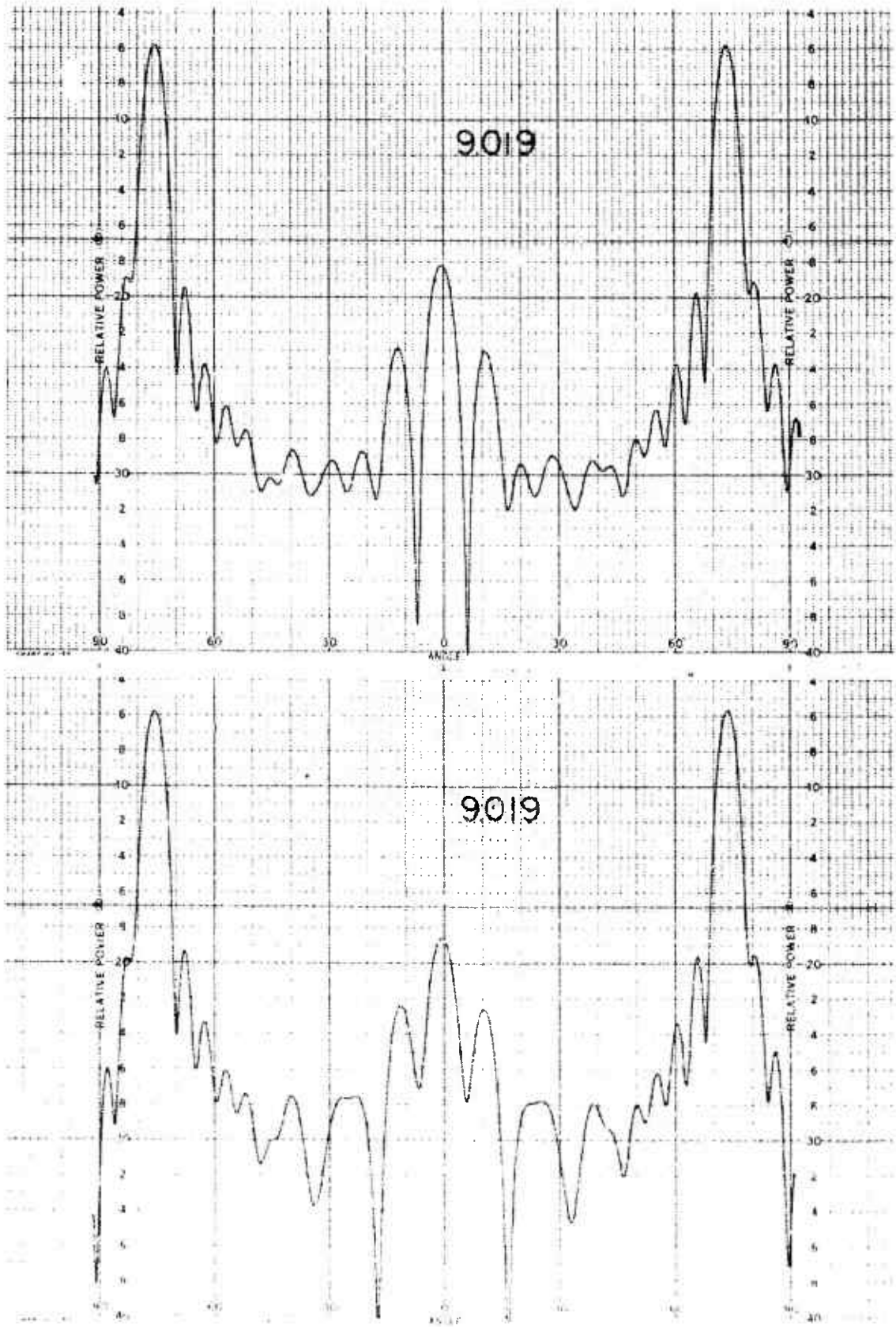
9019
RELATIVE POWER (dB)
ANGLE
9019
RELATIVE POWER (dB)

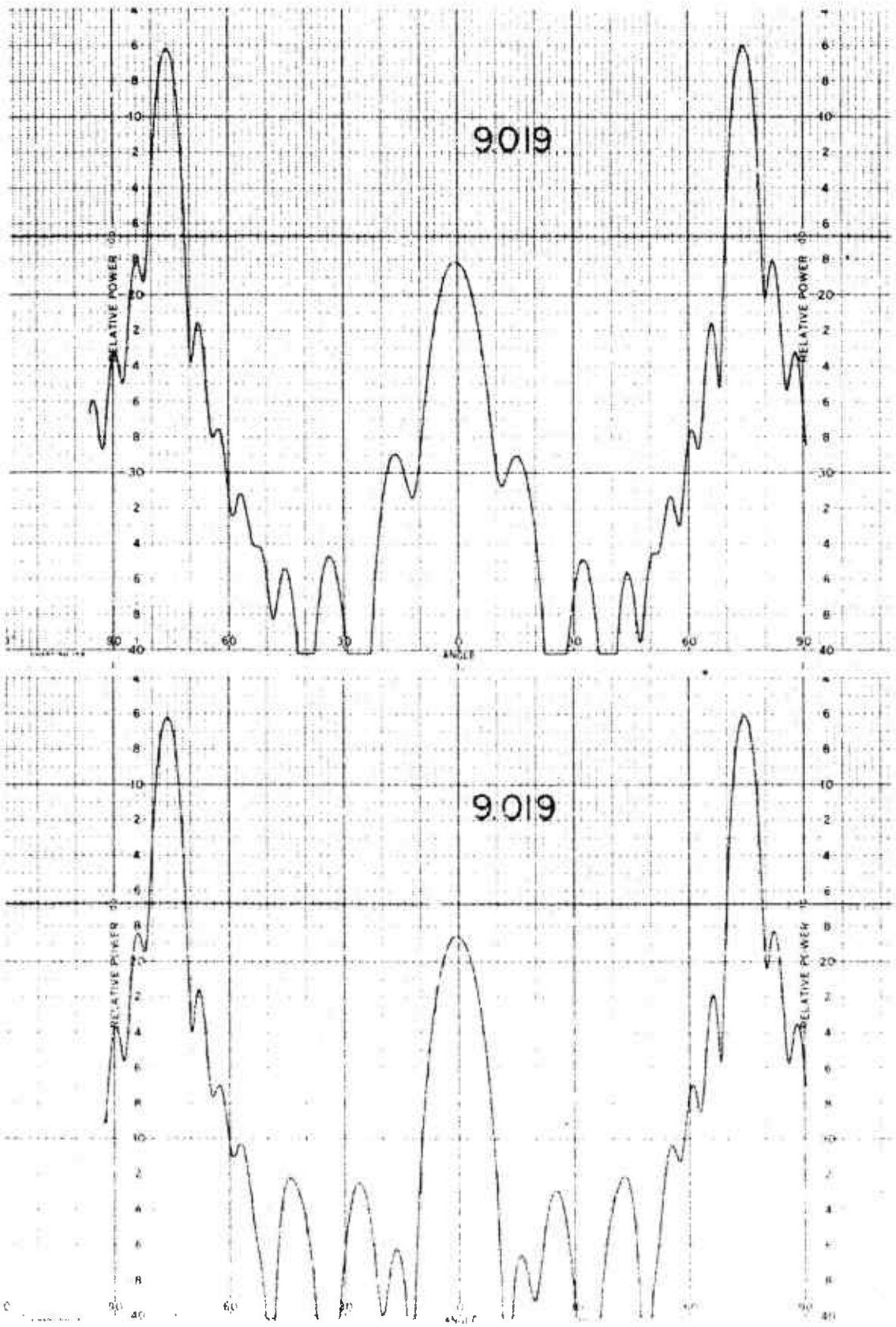
9.019
RELATIVE POWER
ANGLE
9.019
RELATIVE POWER

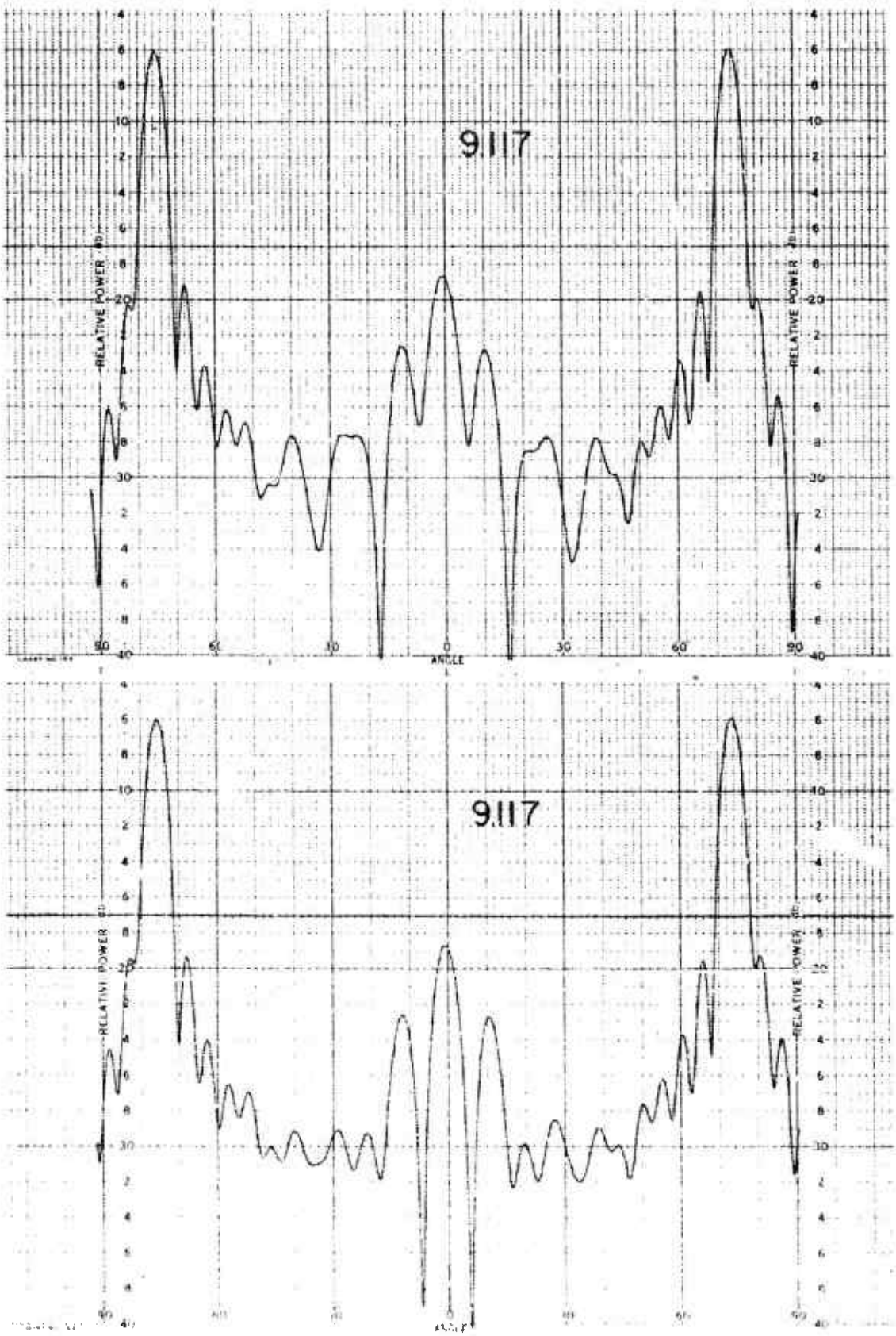
9.117
RELATIVE POWER (dB)
ANGLE
9.117
RELATIVE POWER (dB)

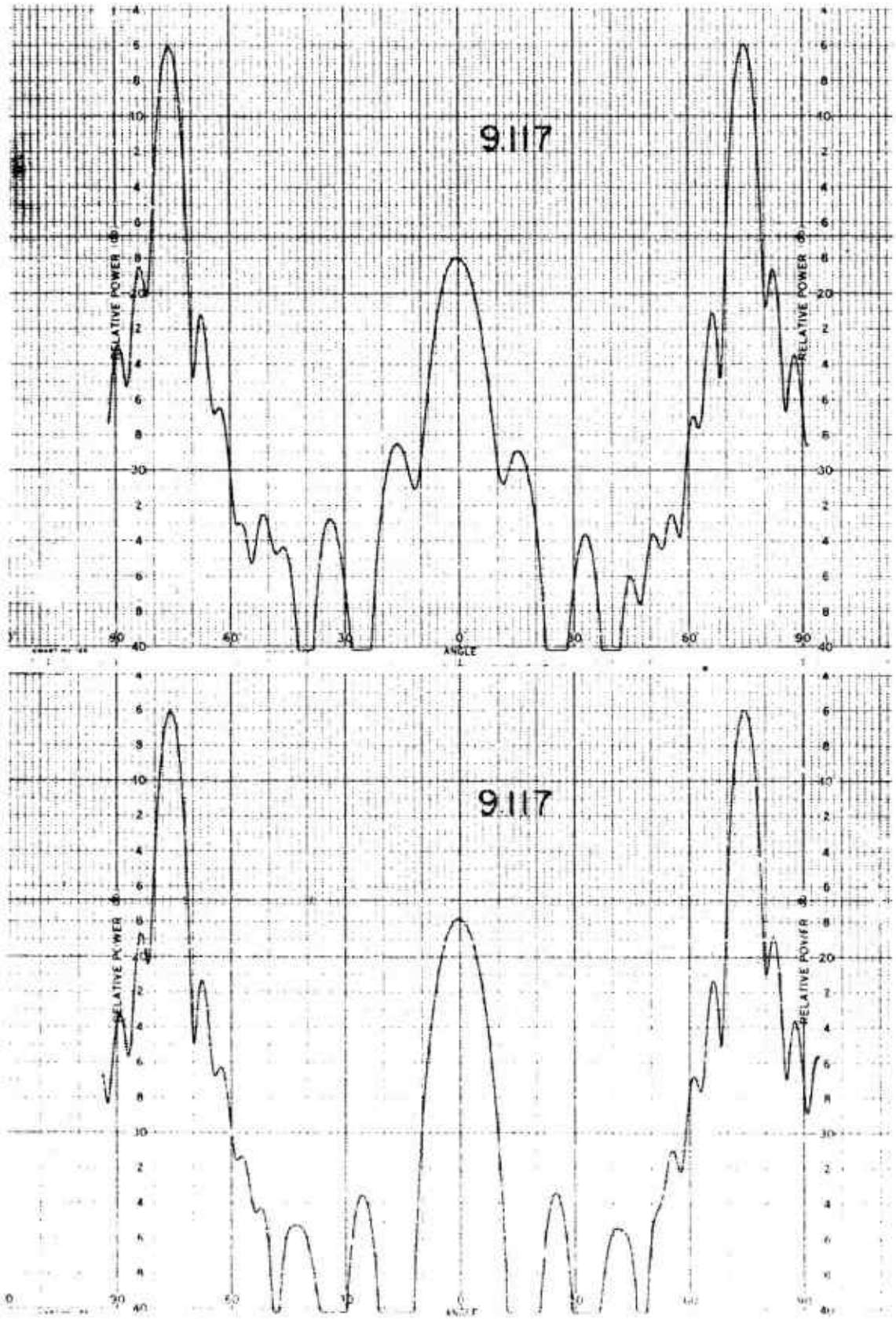
9.117
RELATIVE POWER (dB)
ANGLE
9.117
RELATIVE POWER (dB)

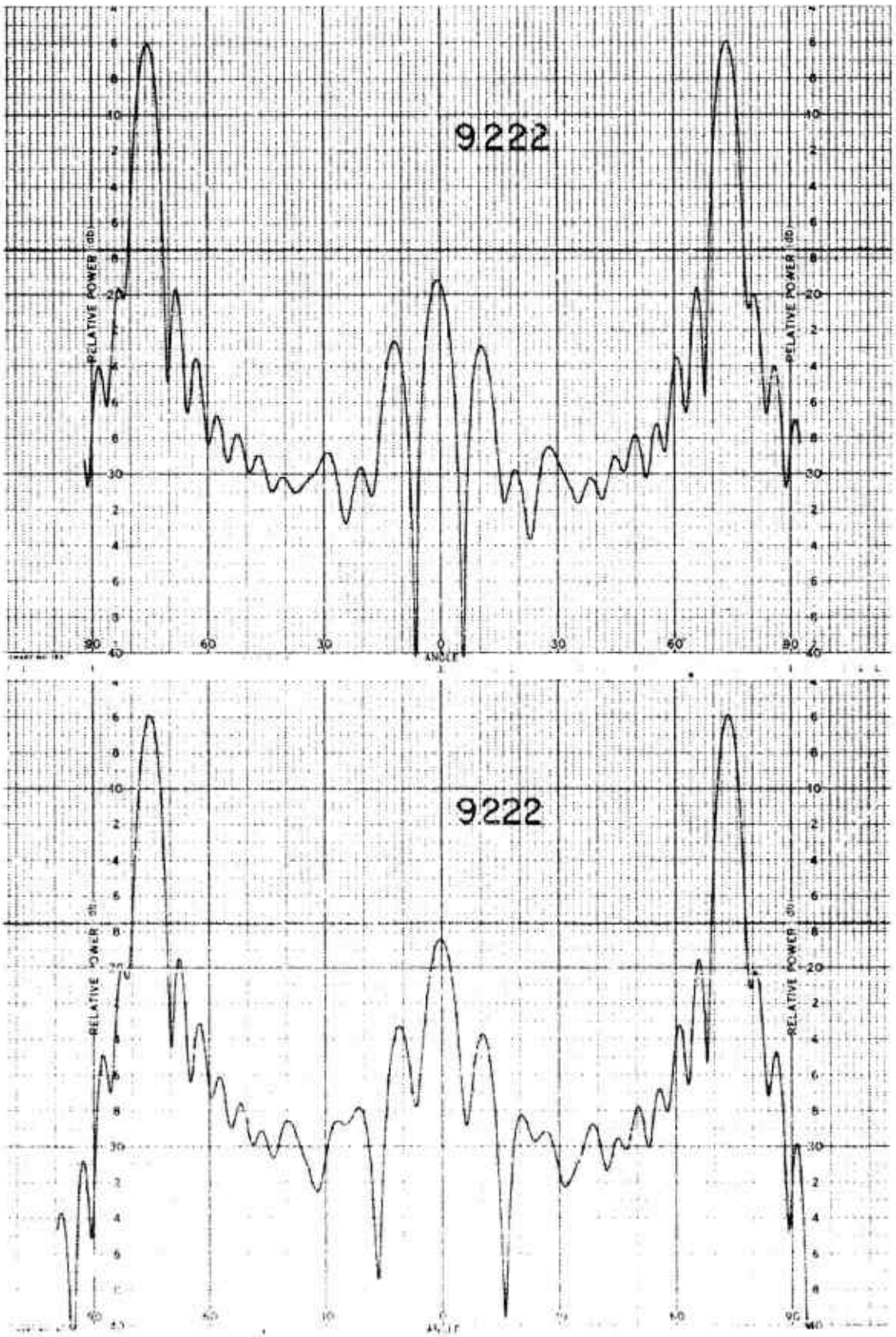
9222
RELATIVE POWER (dB)
ANGLE
9222
RELATIVE POWER (dB)

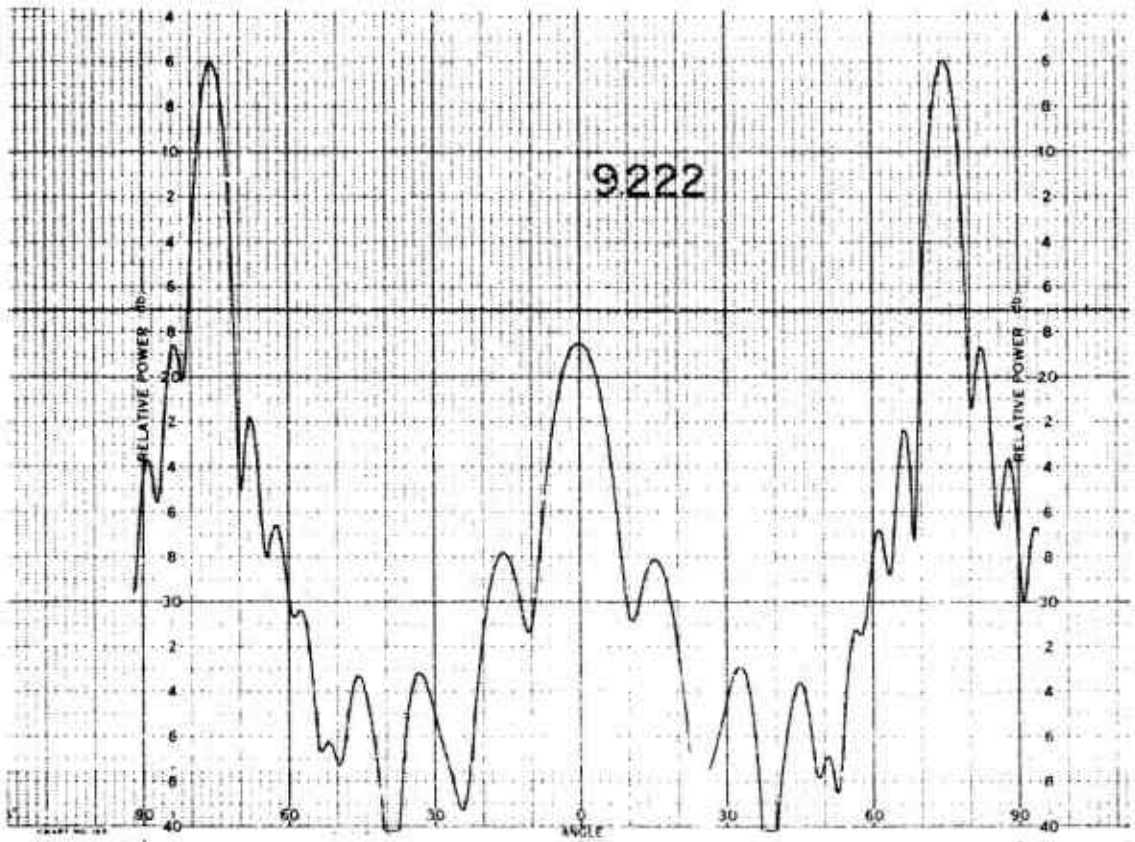
9222
RELATIVE POWER db
ANGLE

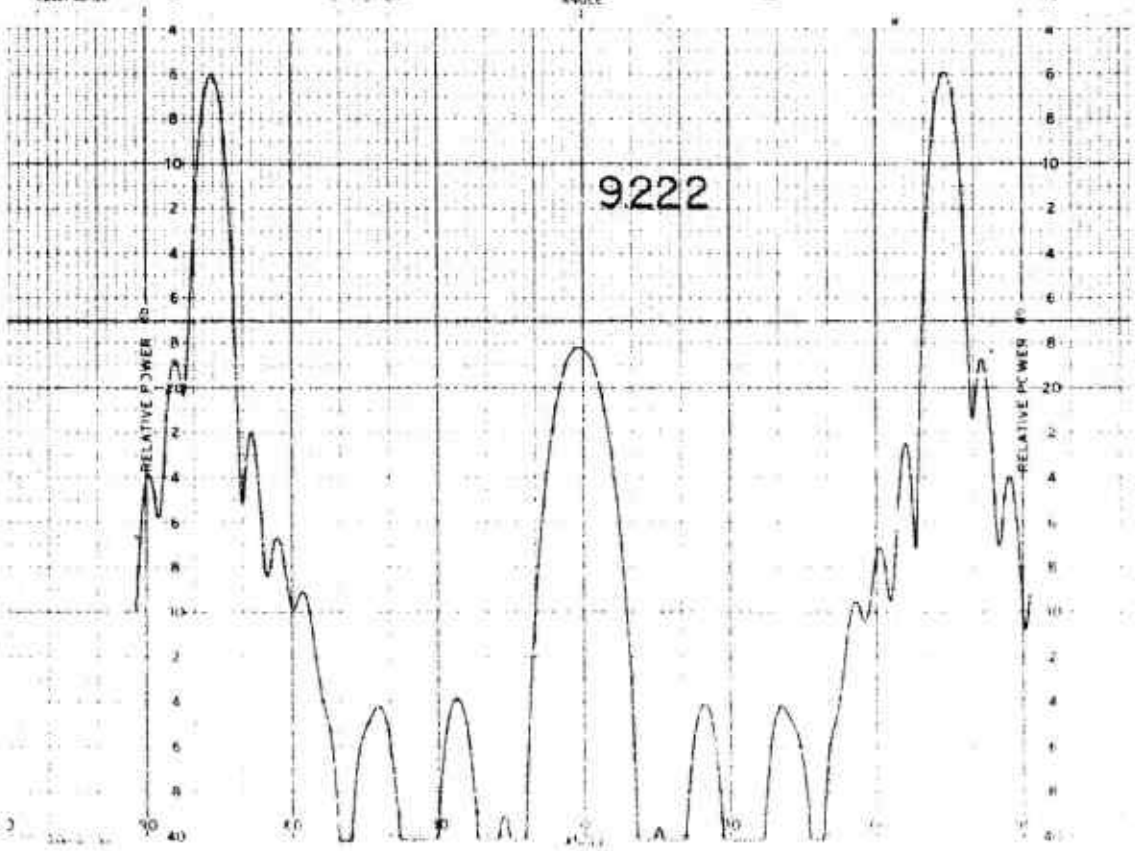
9222
RELATIVE POWER db

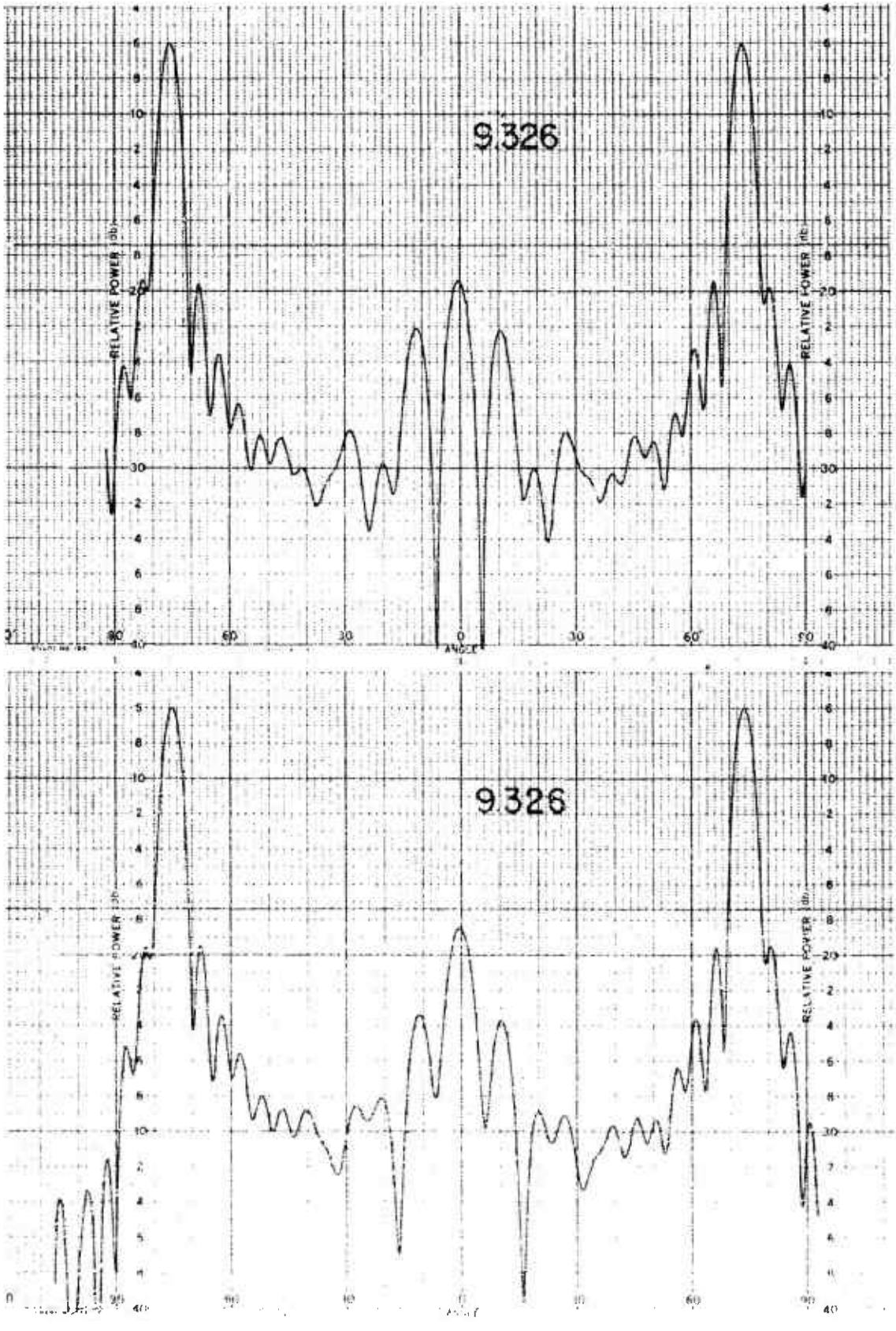
9.326
RELATIVE POWER (db)
ANGLE
9.326
RELATIVE POWER (db)

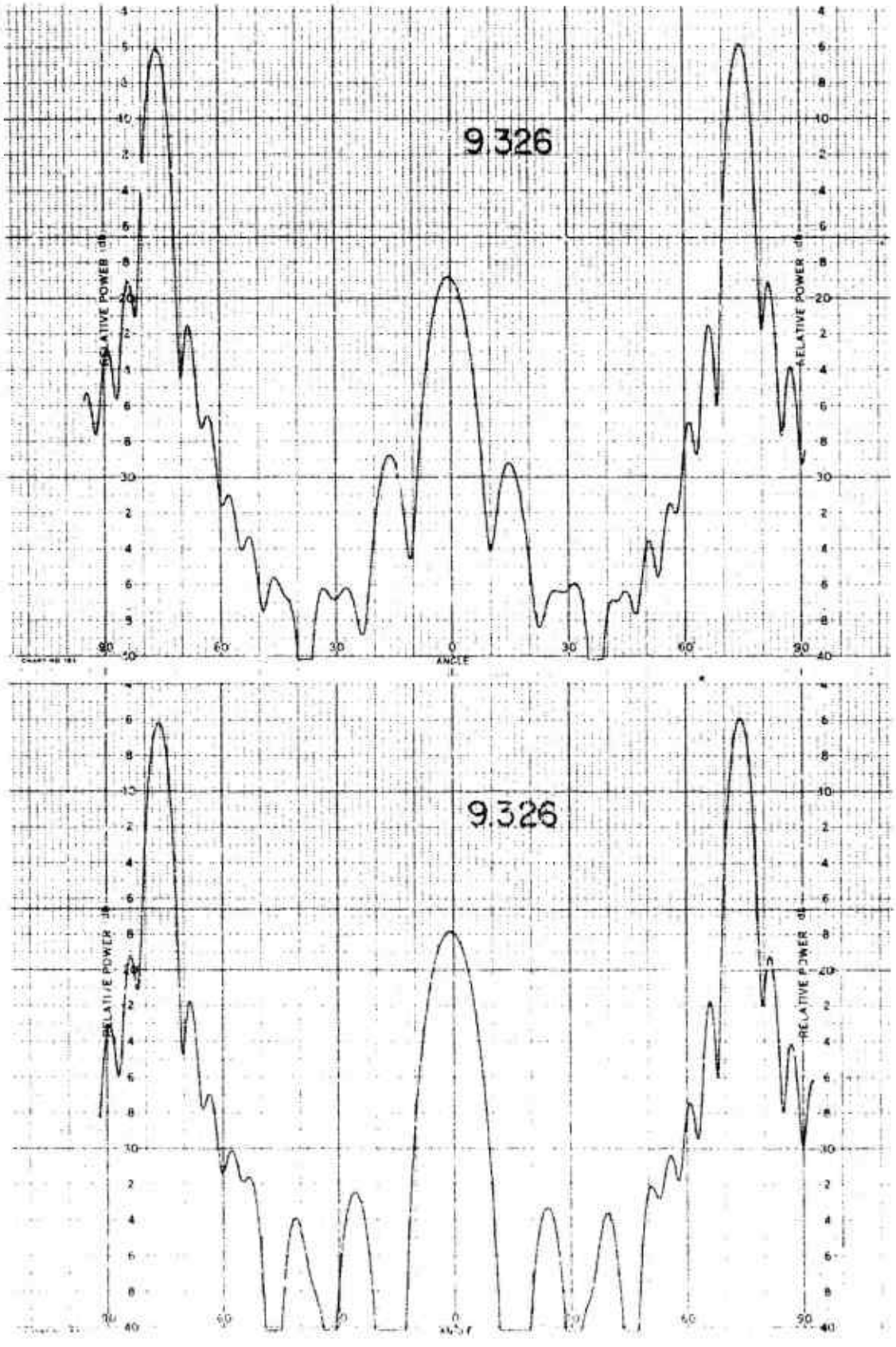
9.326
RELATIVE POWER dB
ANGLE
9.326
RELATIVE POWER dB

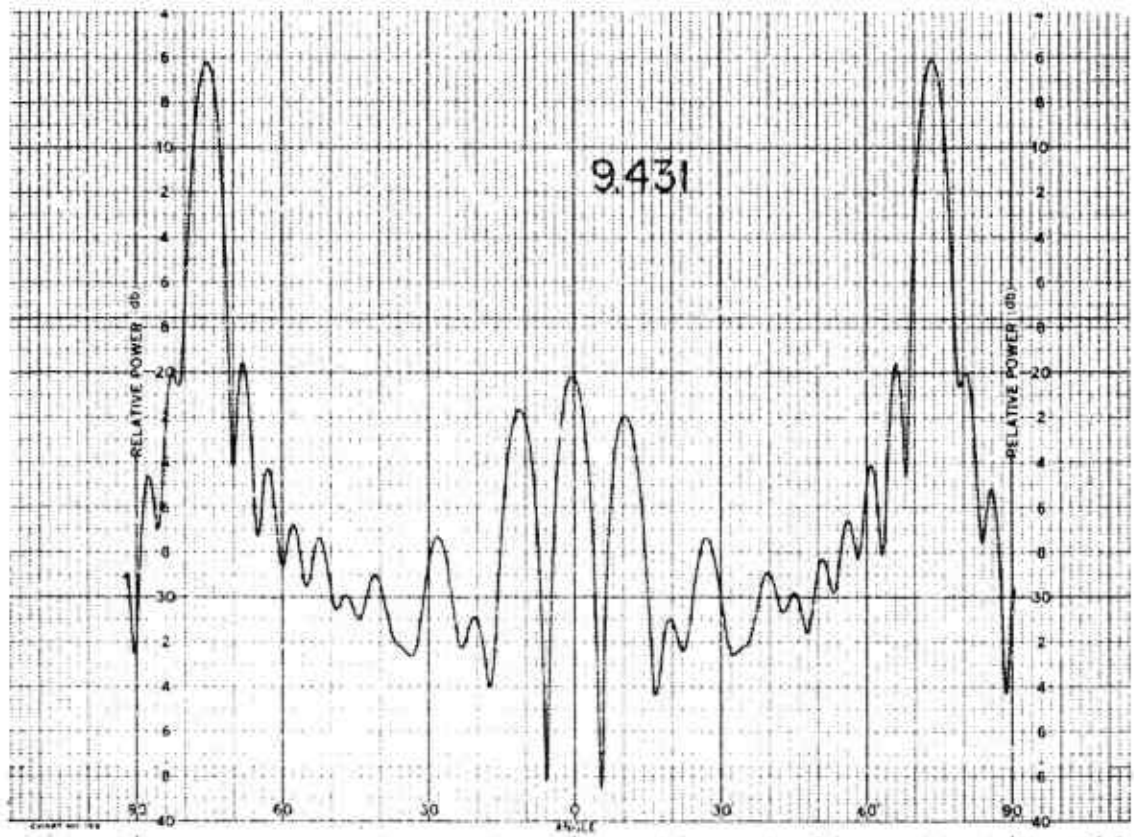
9.431
RELATIVE POWER db
RELATIVE POWER (db)
90
60
30
0
30
60
90
ANGLE

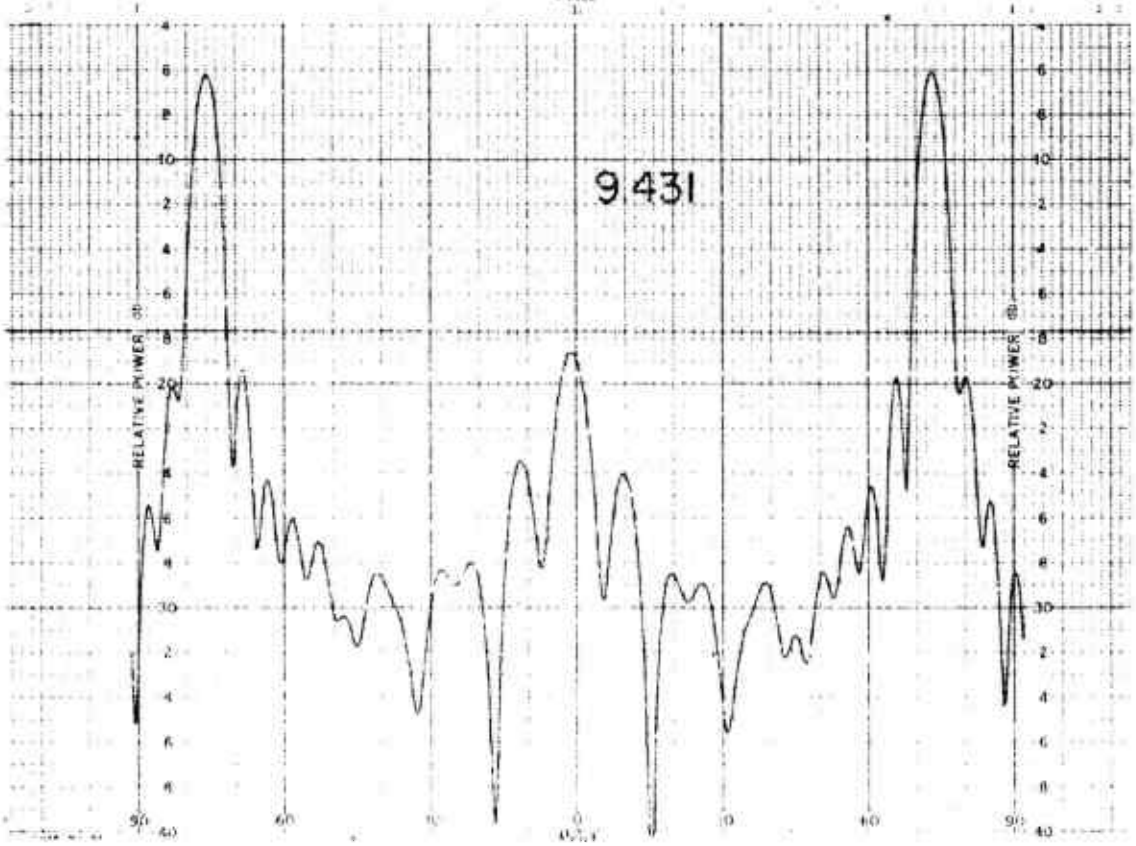
9.431
RELATIVE POWER db
RELATIVE POWER (db)
90
60
30
0
30
60
90
ANGLE

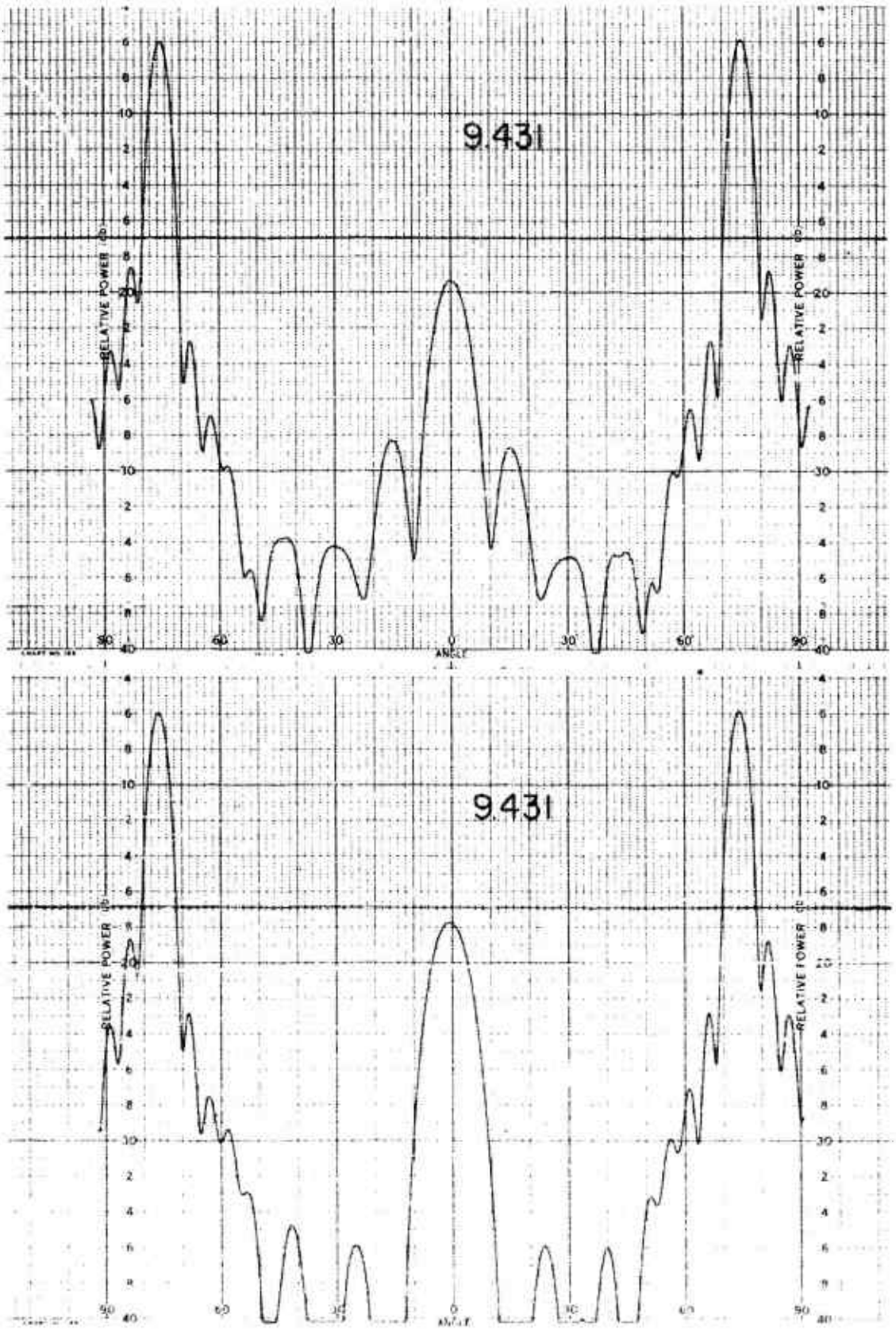
9.431
RELATIVE POWER (dB)
ANGLE
9.431
RELATIVE POWER (dB)
ANGLE

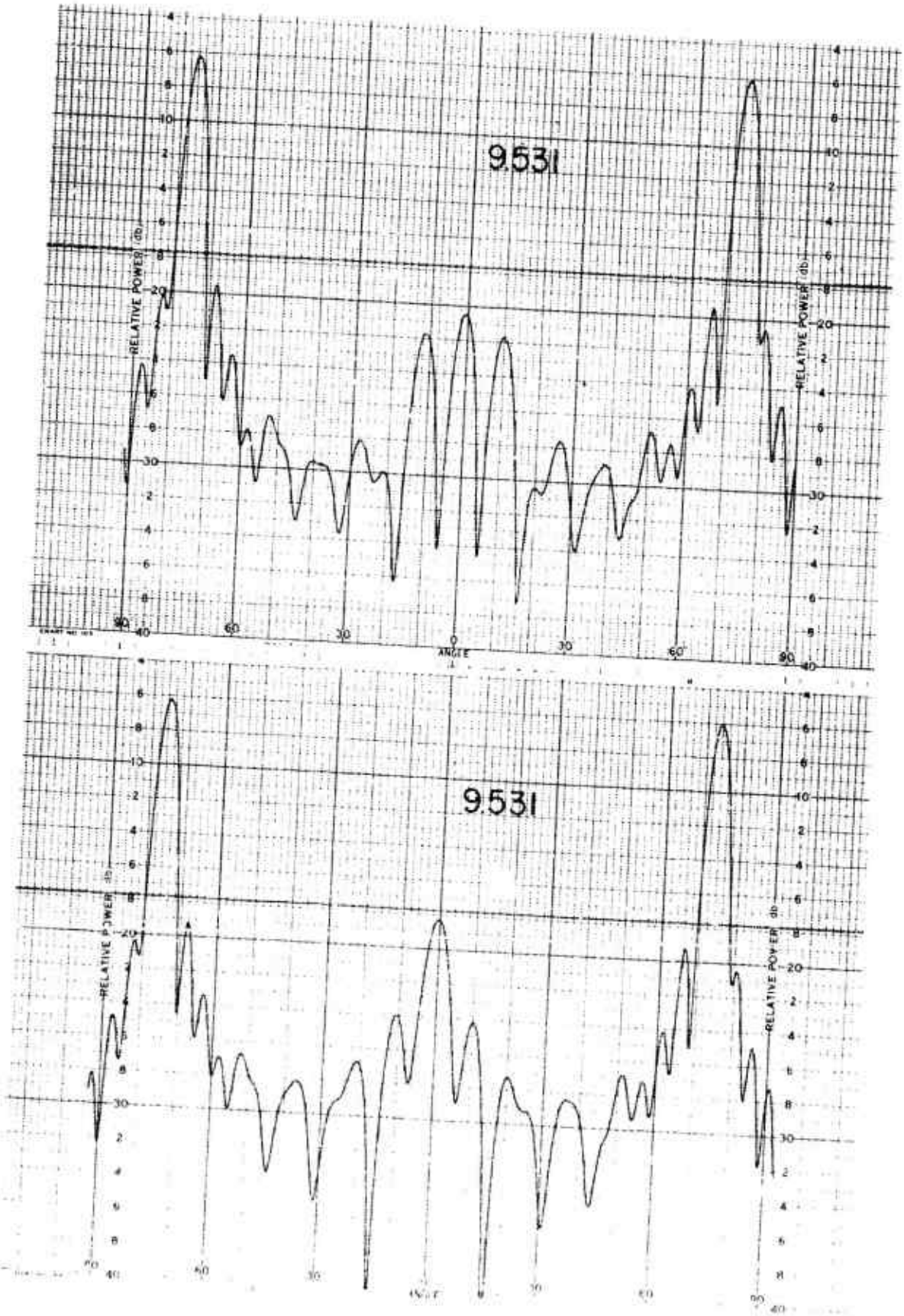
9.531
RELATIVE POWER (db)
ANGLE
9.531
RELATIVE POWER (db)

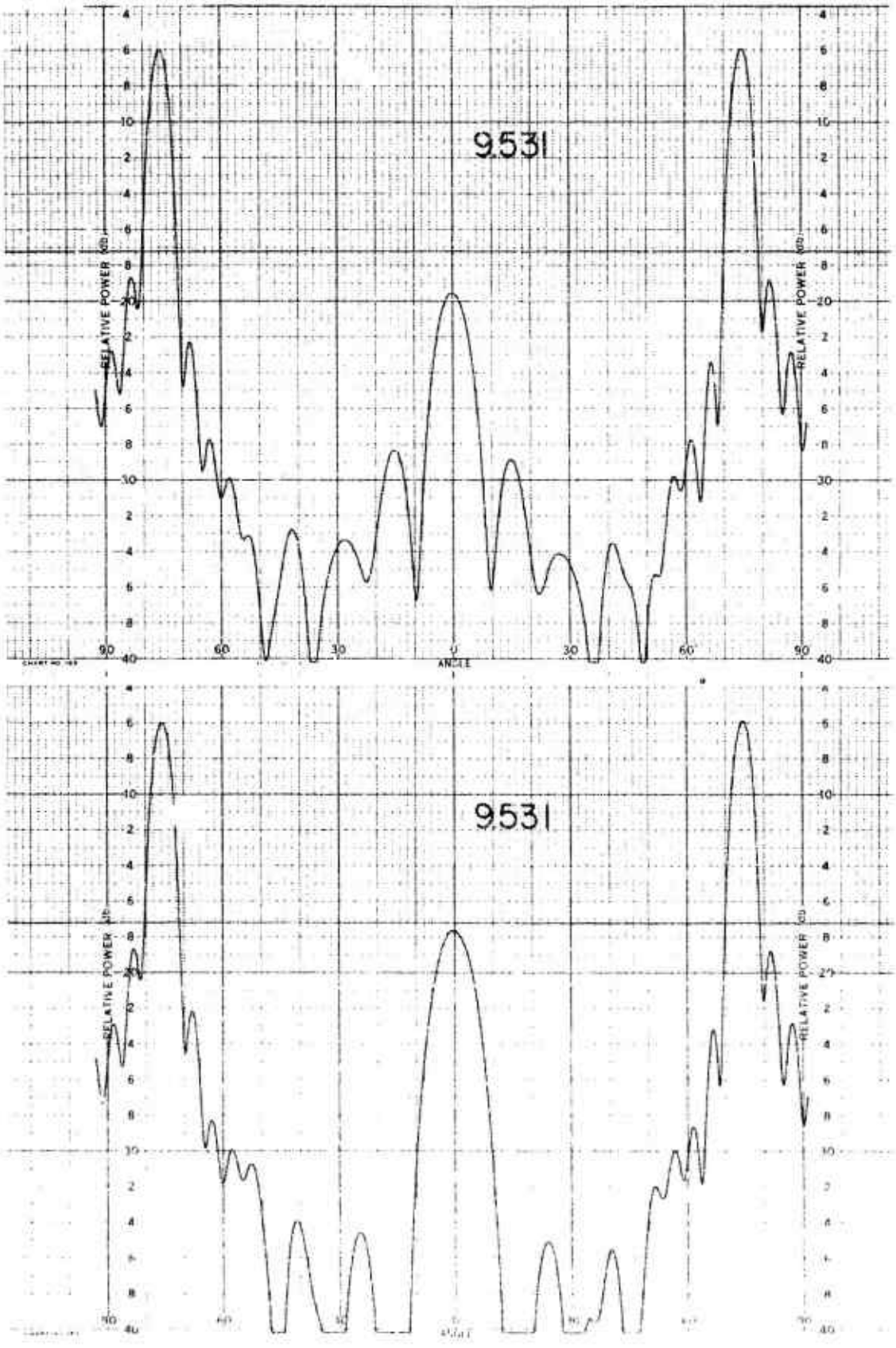
9531
RELATIVE POWER (DB)
ANGLE
9531
RELATIVE POWER (DB)

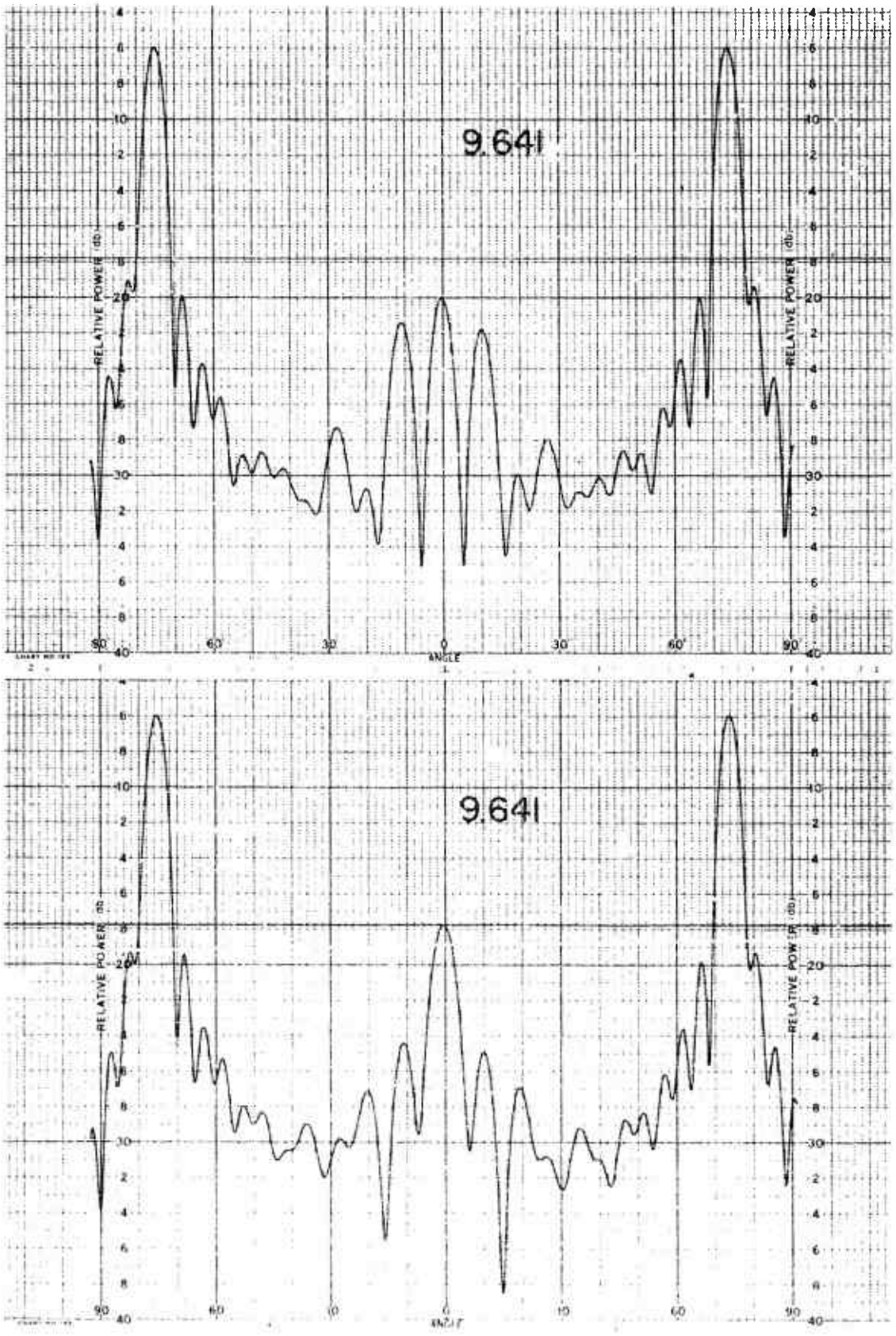
9.641
RELATIVE POWER (db)
ANGLE
9.641
RELATIVE POWER (db)
ANGLE

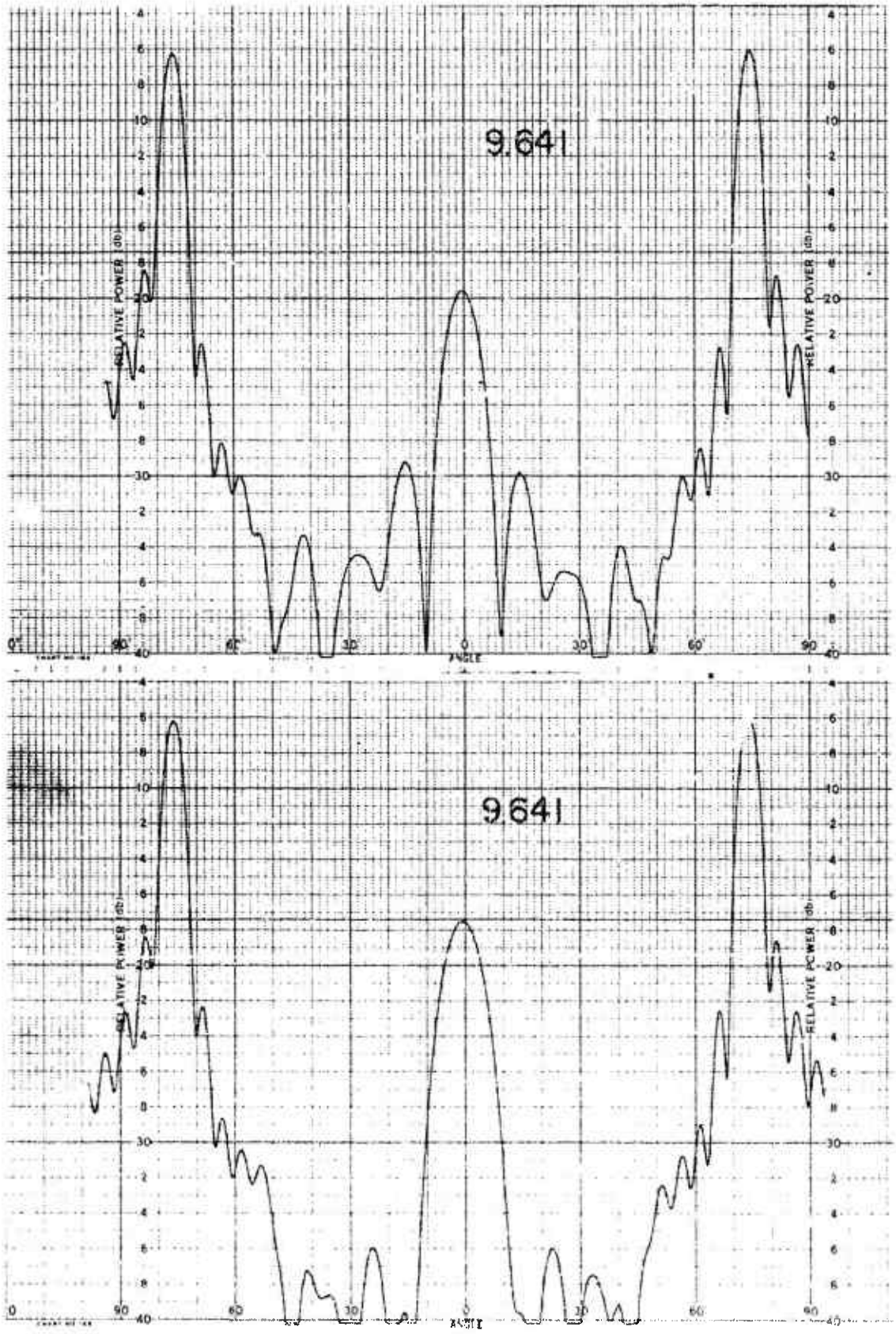
9.641
RELATIVE POWER (db)
ANGLE
9.641
RELATIVE POWER (db)
ANGLE

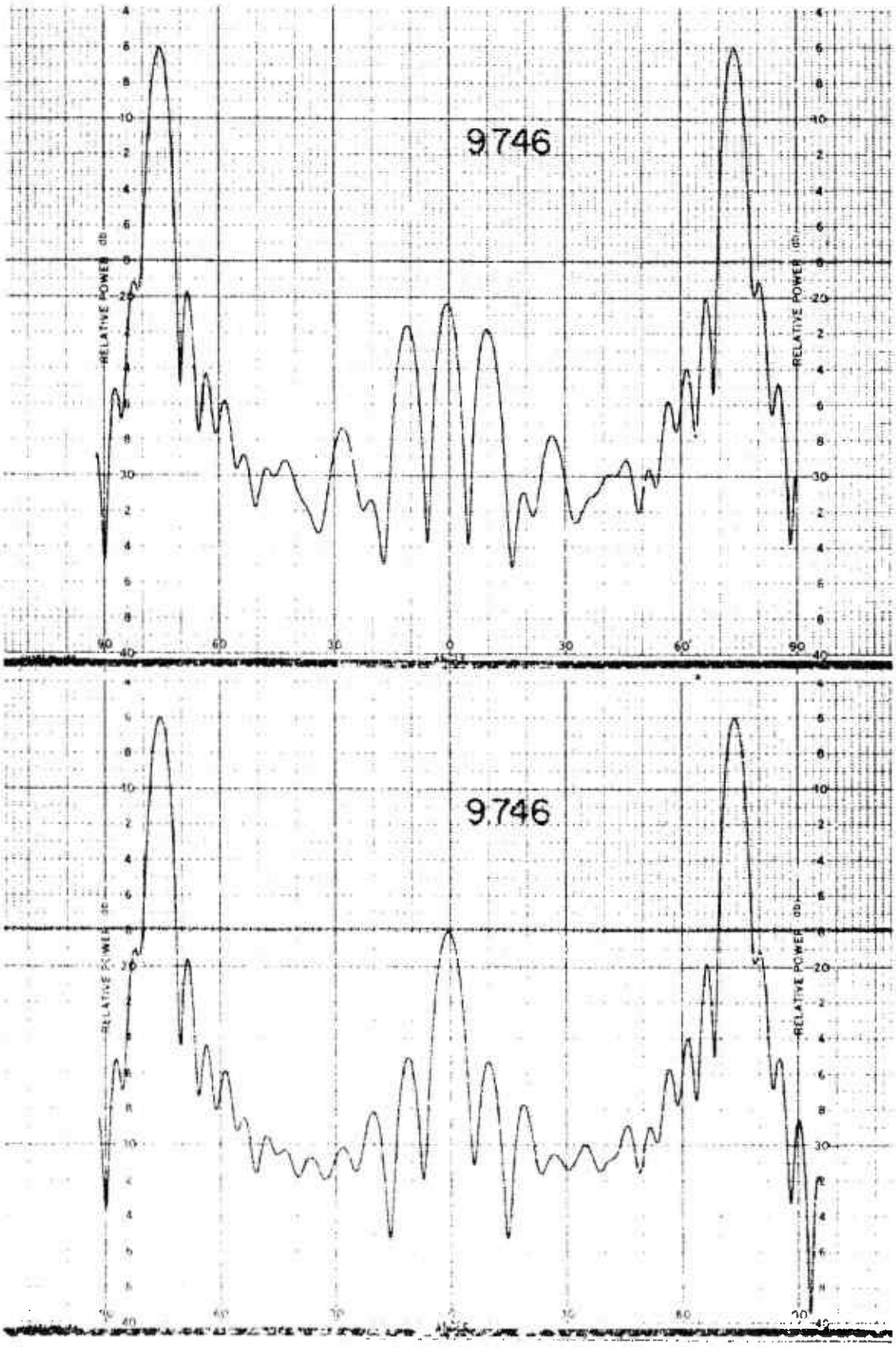
9.746
RELATIVE POWER dB
9.746
RELATIVE POWER dB

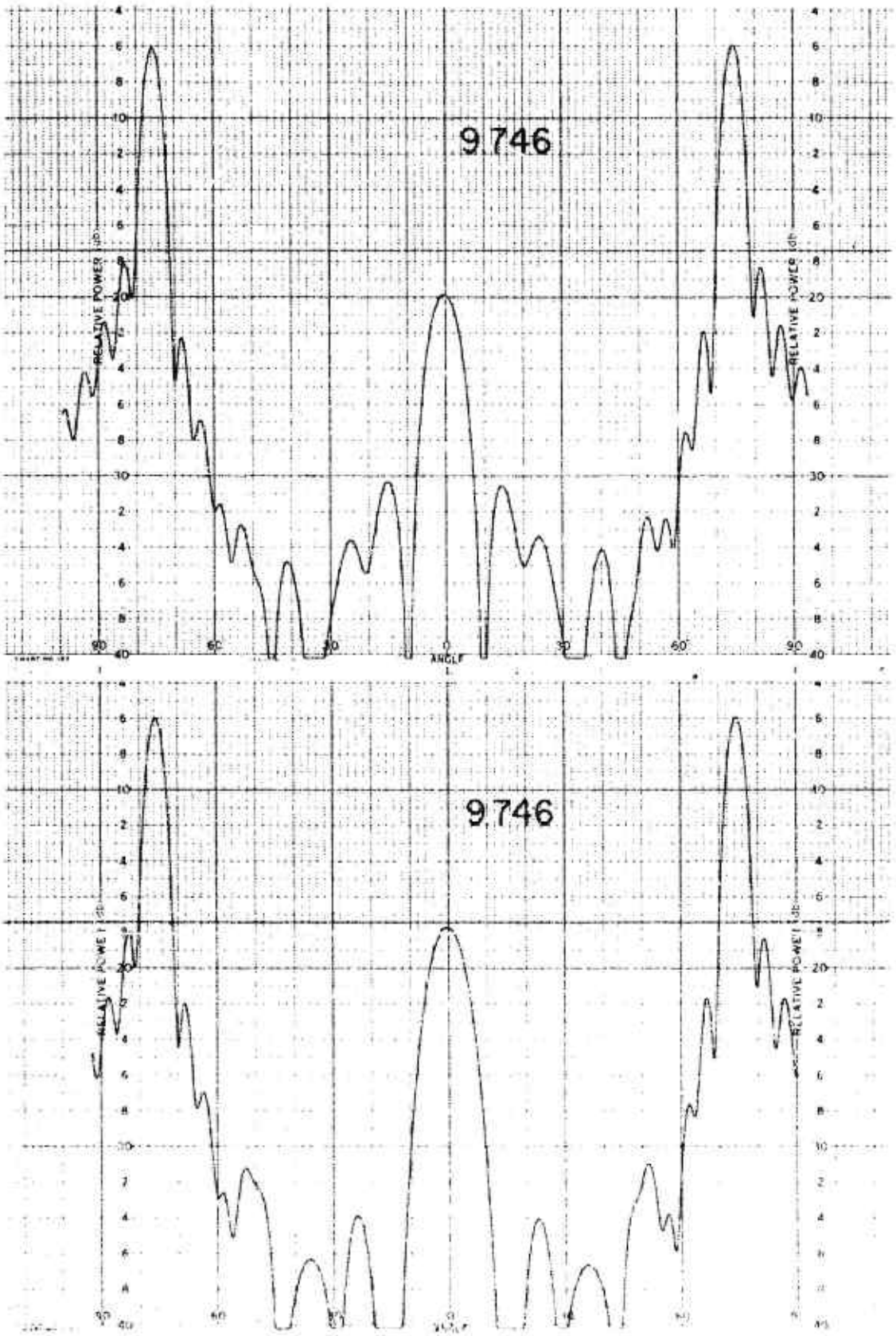
9.746
RELATIVE POWER (dB)
ANGLE
9.746
RELATIVE POWER (dB)

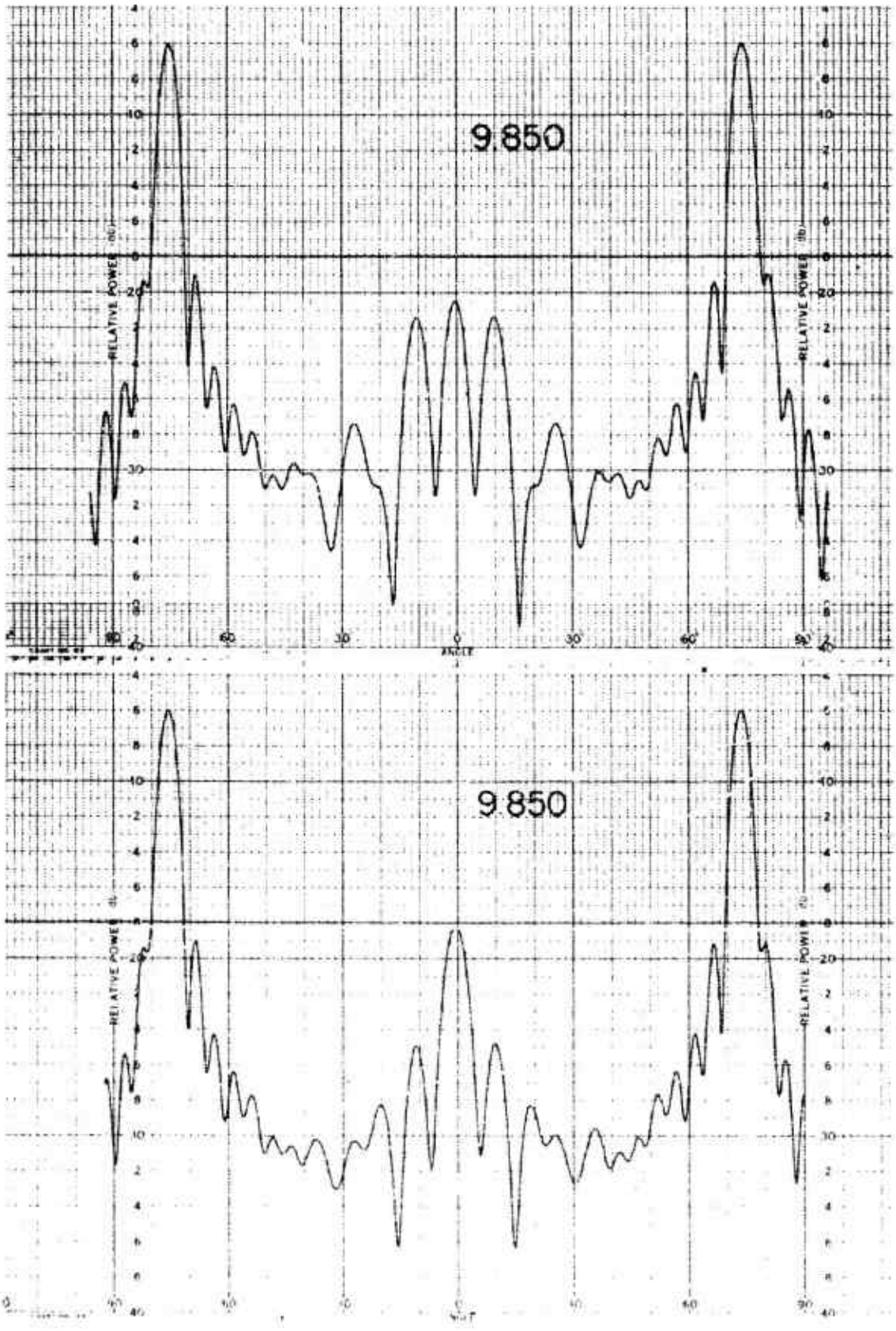
9.850
RELATIVE POWER (dB)
ANGLE
9.850
RELATIVE POWER (dB)

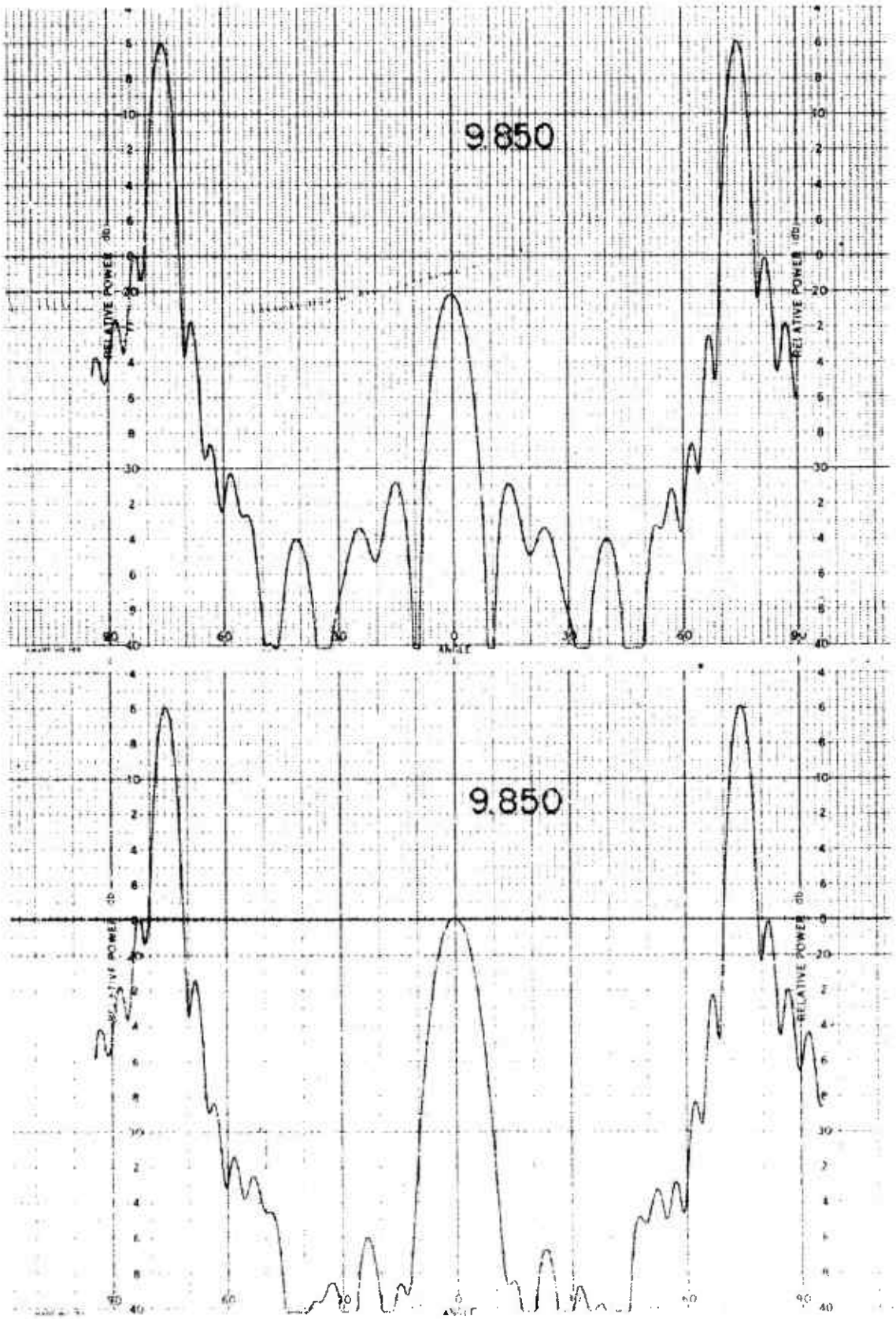
9.850
RELATIVE POWER
ANGLE
9.850
RELATIVE POWER
ANGLE

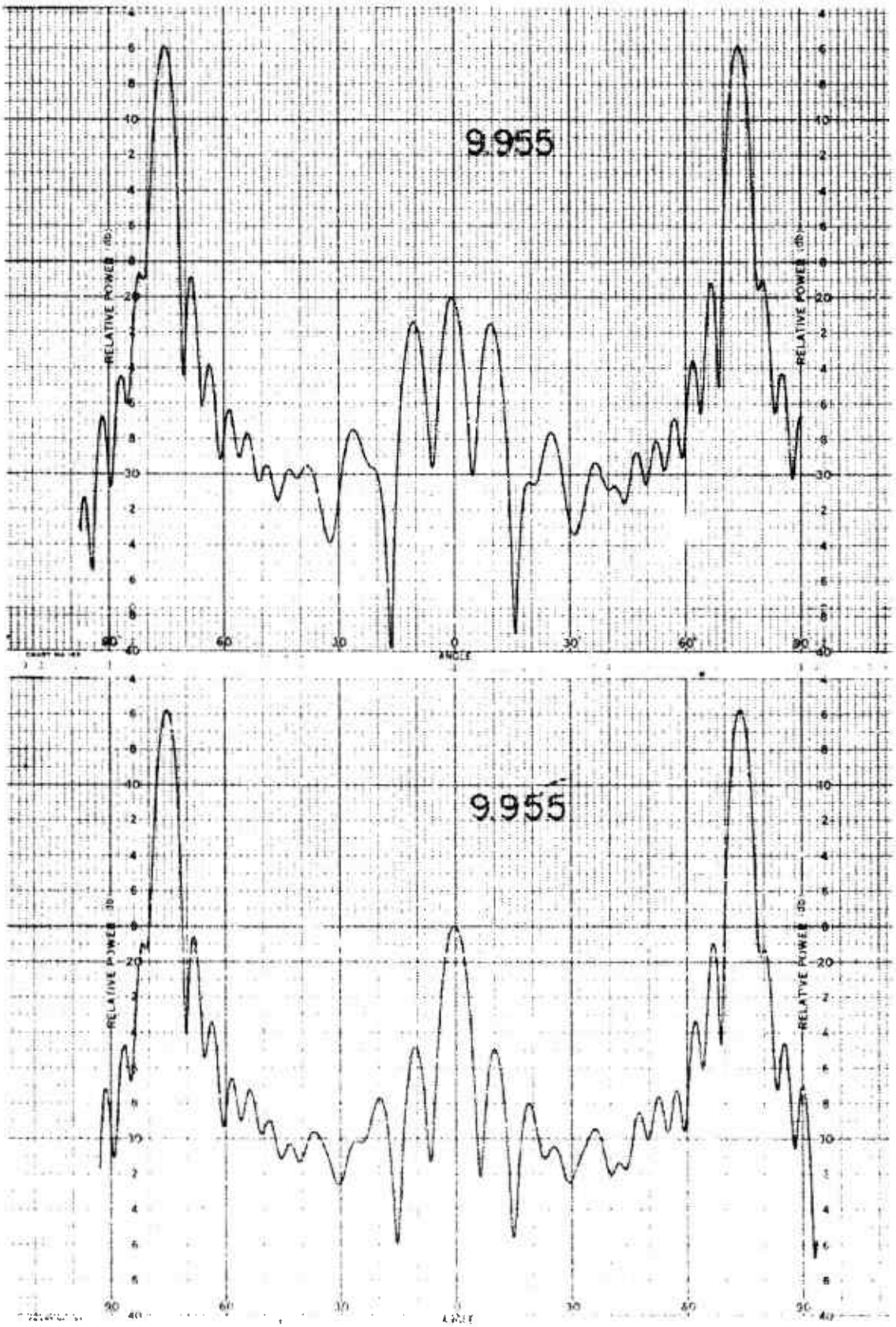
9.955
RELATIVE POWER (db)
ANGLE
9.955
RELATIVE POWER (db)

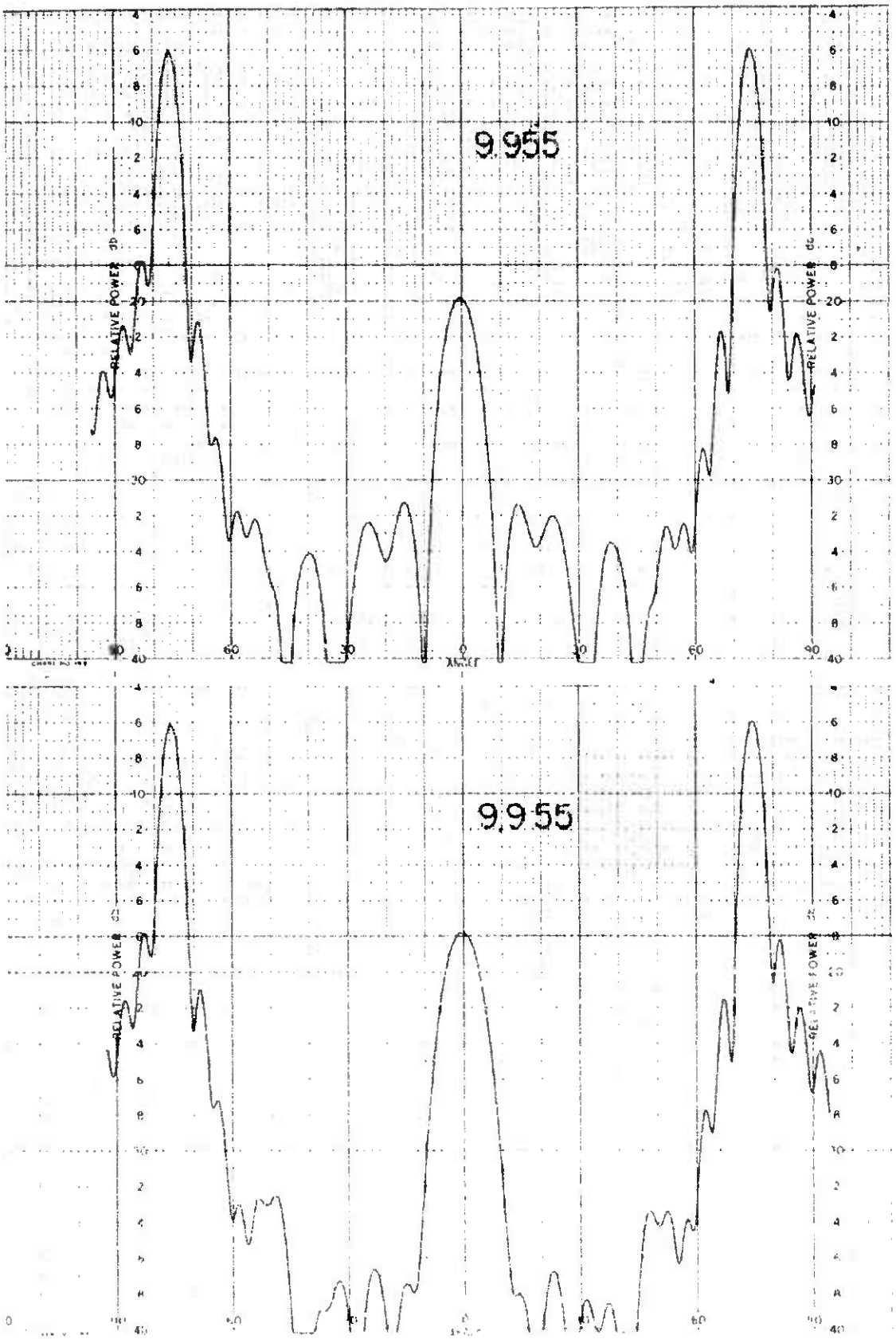
9.955
RELATIVE POWER dB
ANGLE
9.955
RELATIVE POWER dB

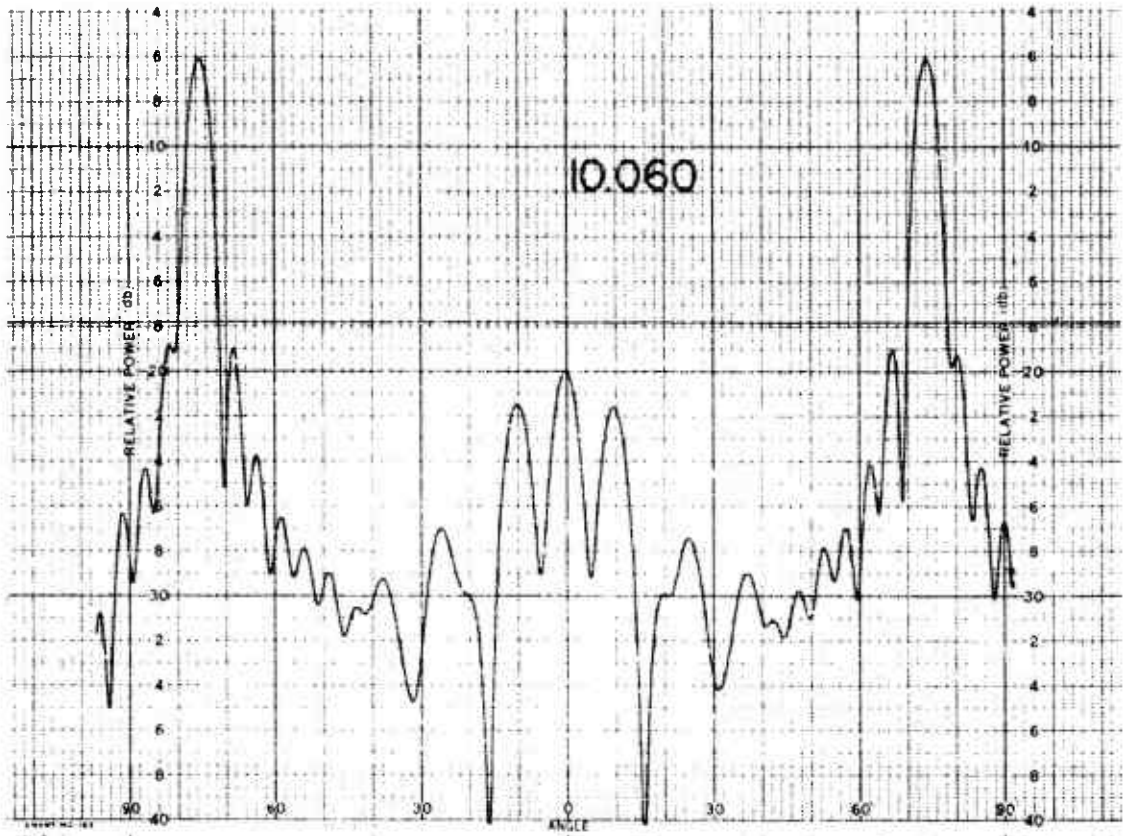
10.060
RELATIVE POWER (db)
ANGLE

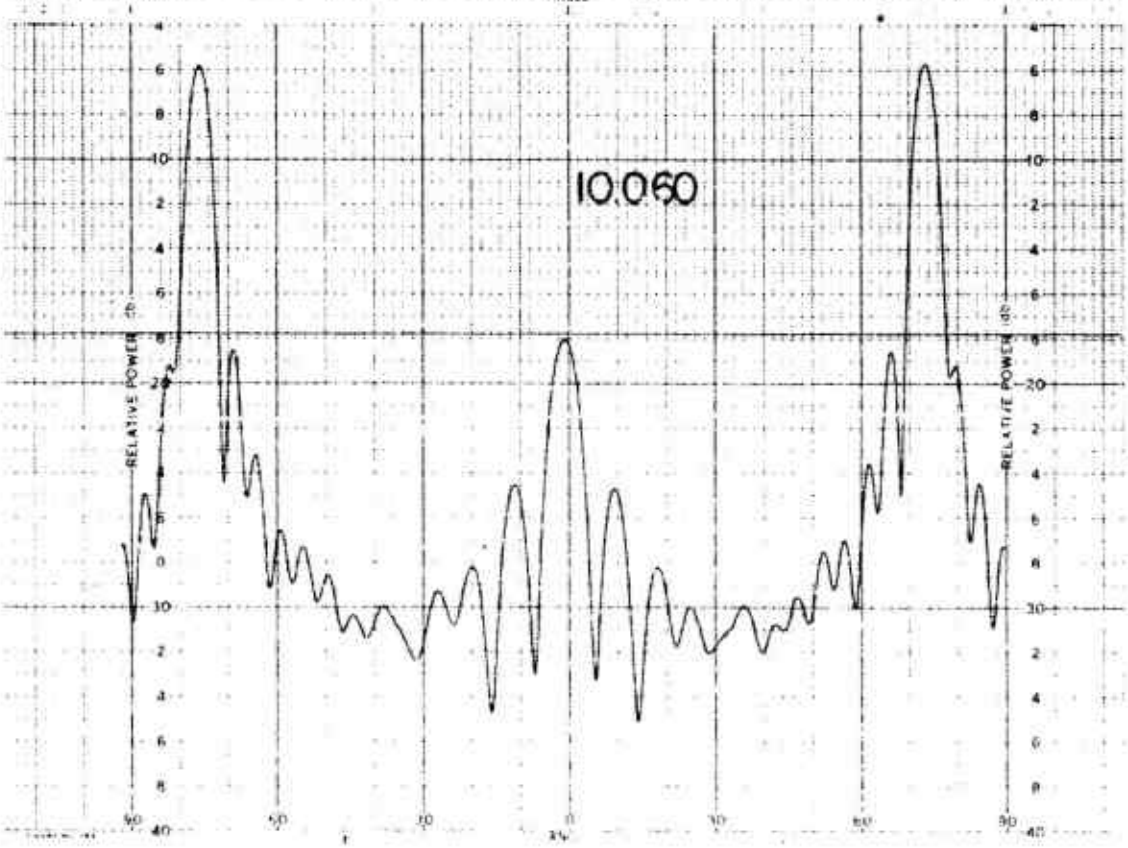
10.060
RELATIVE POWER

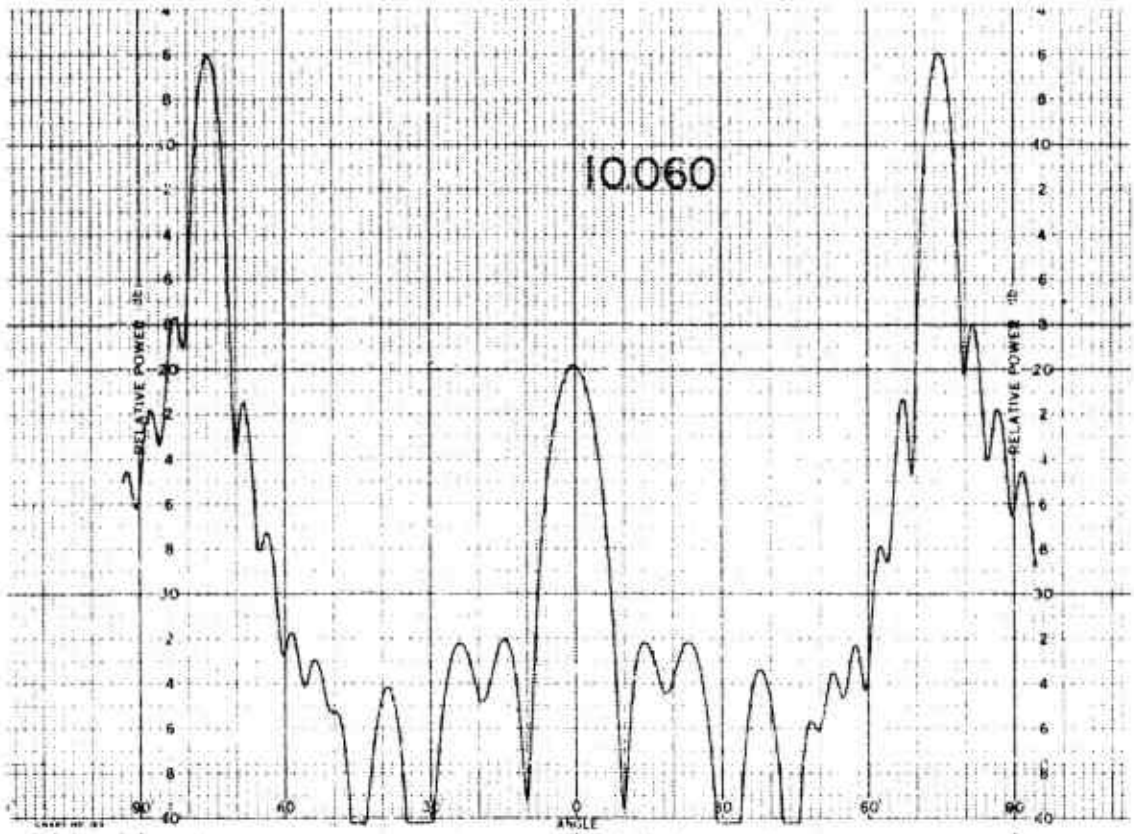
10.060
RELATIVE POWER
ANGLE

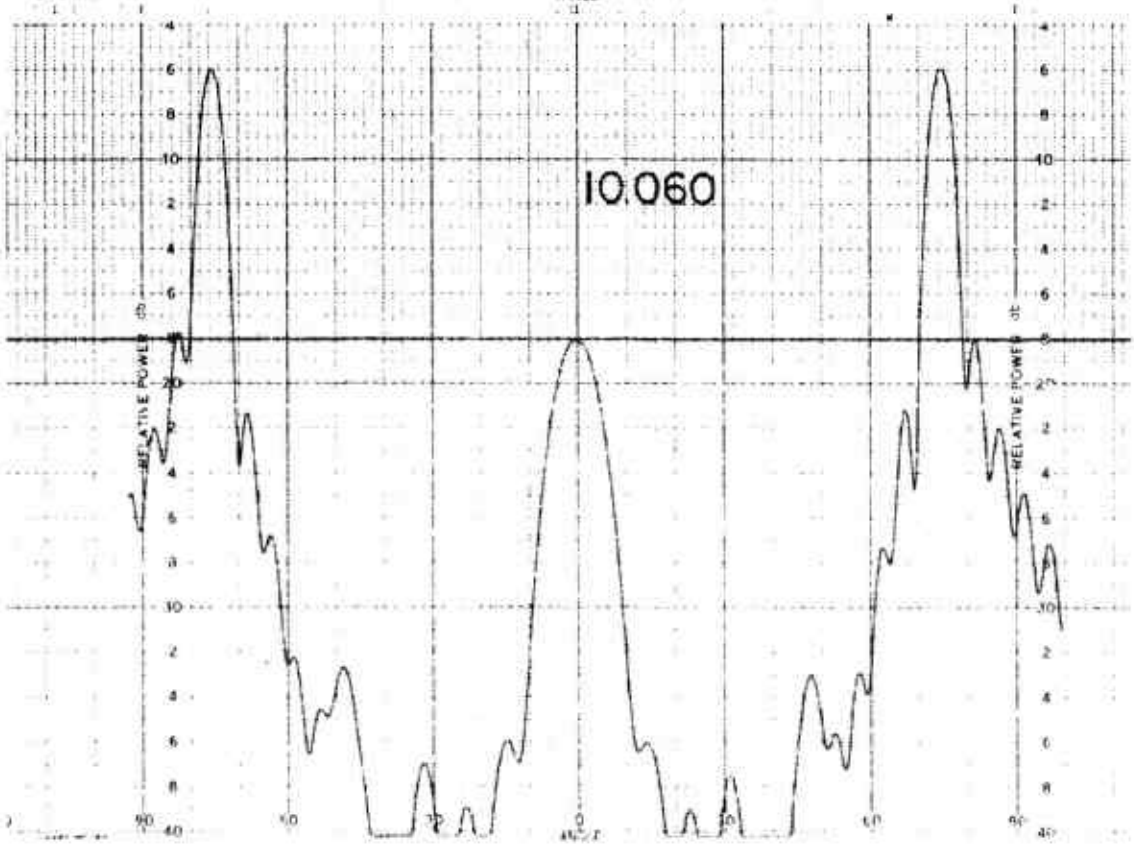
10.060
RELATIVE POWER

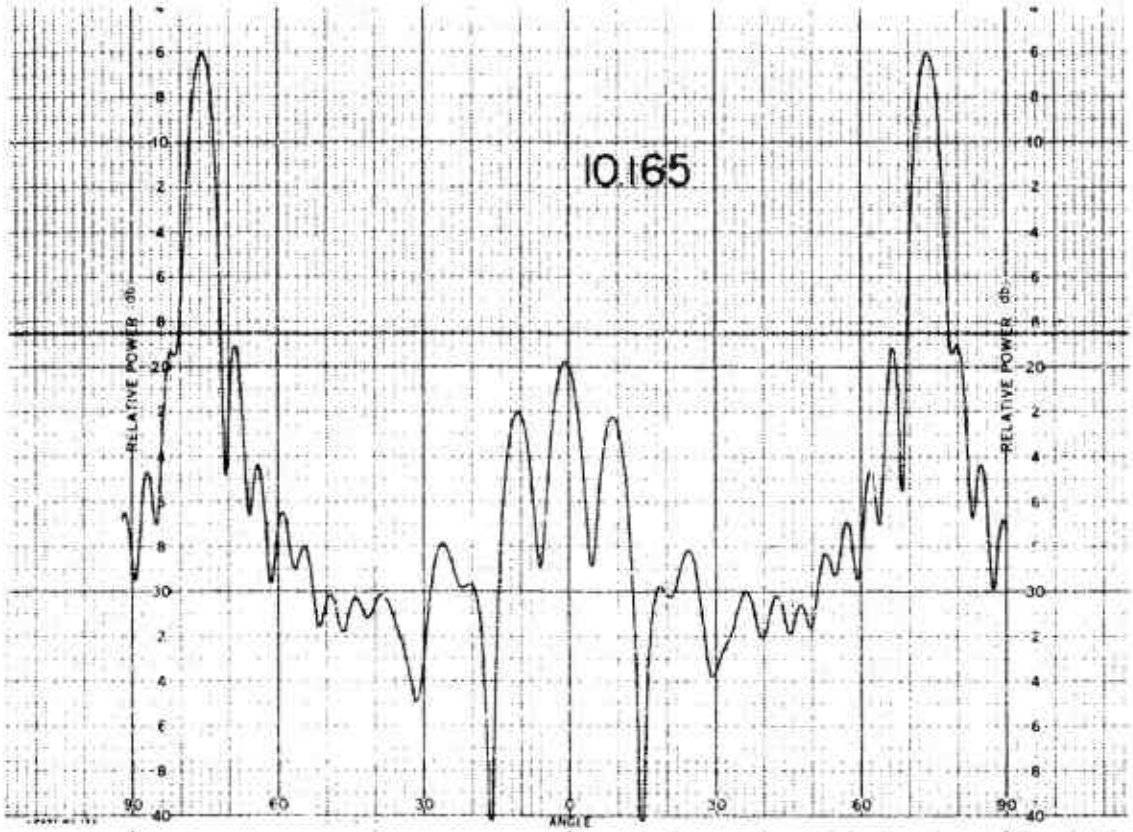
10.165
RELATIVE POWER db
ANGLE
90
60
30
0
30
60
90

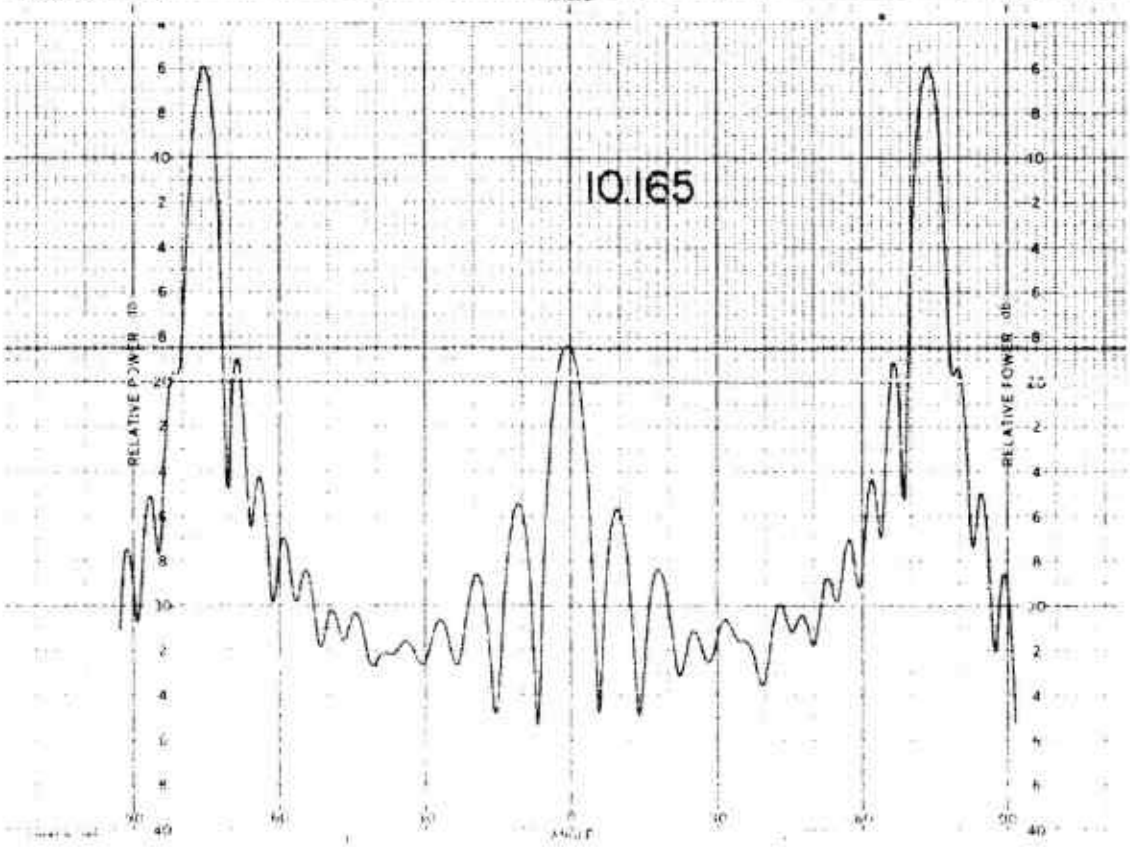
10.165
RELATIVE POWER db
ANGLE

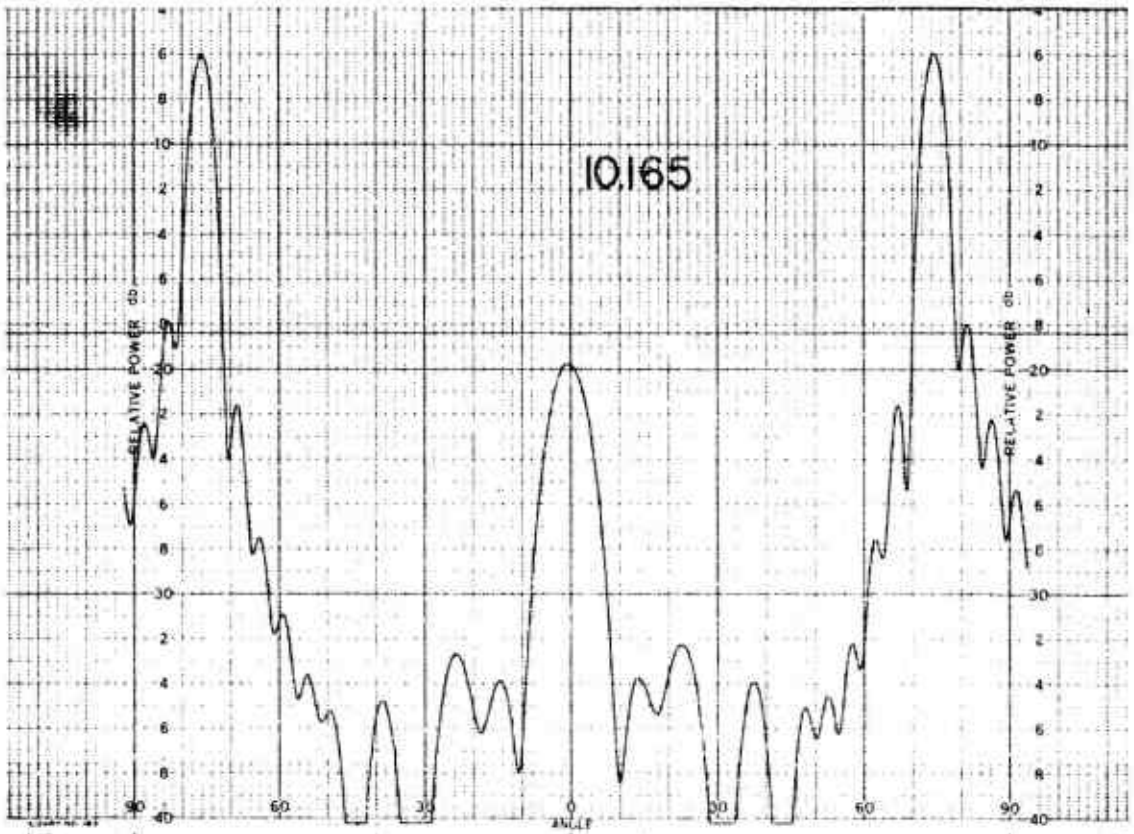
10.165
RELATIVE POWER dB
ANGLE

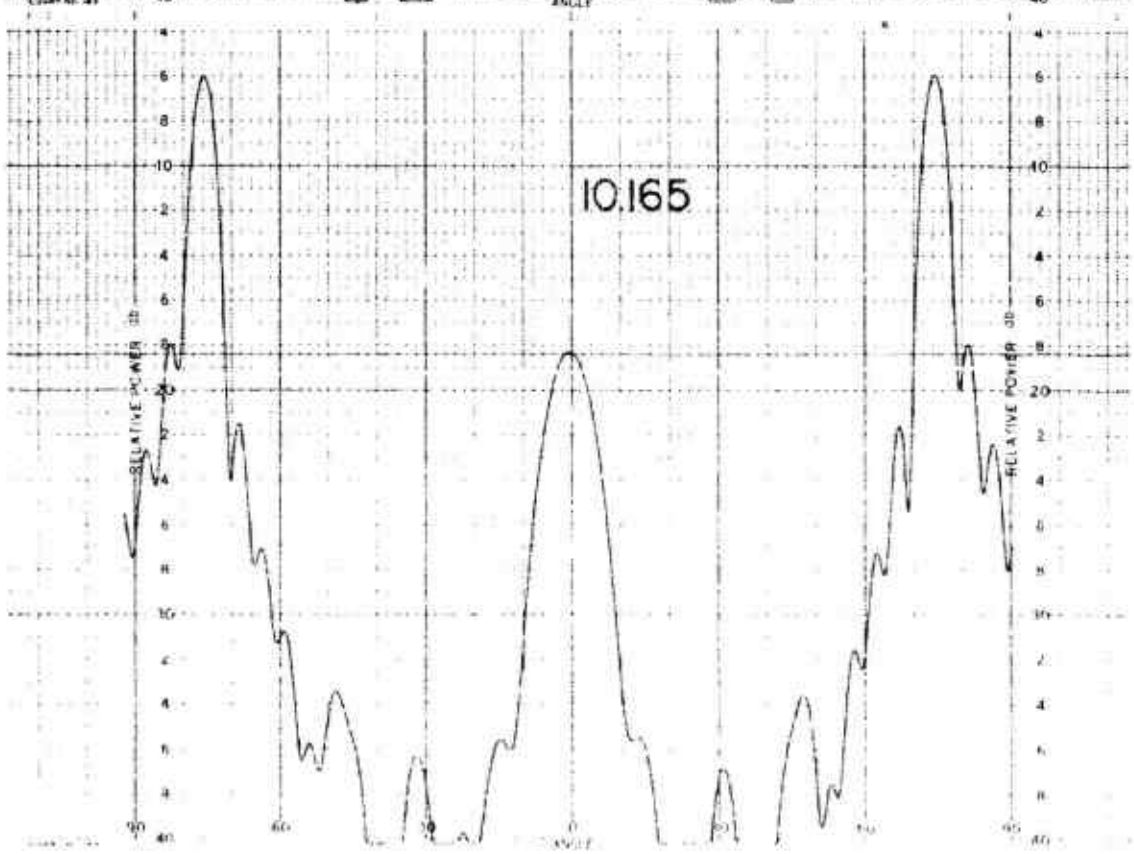
10.165
RELATIVE POWER dB
ANGLE

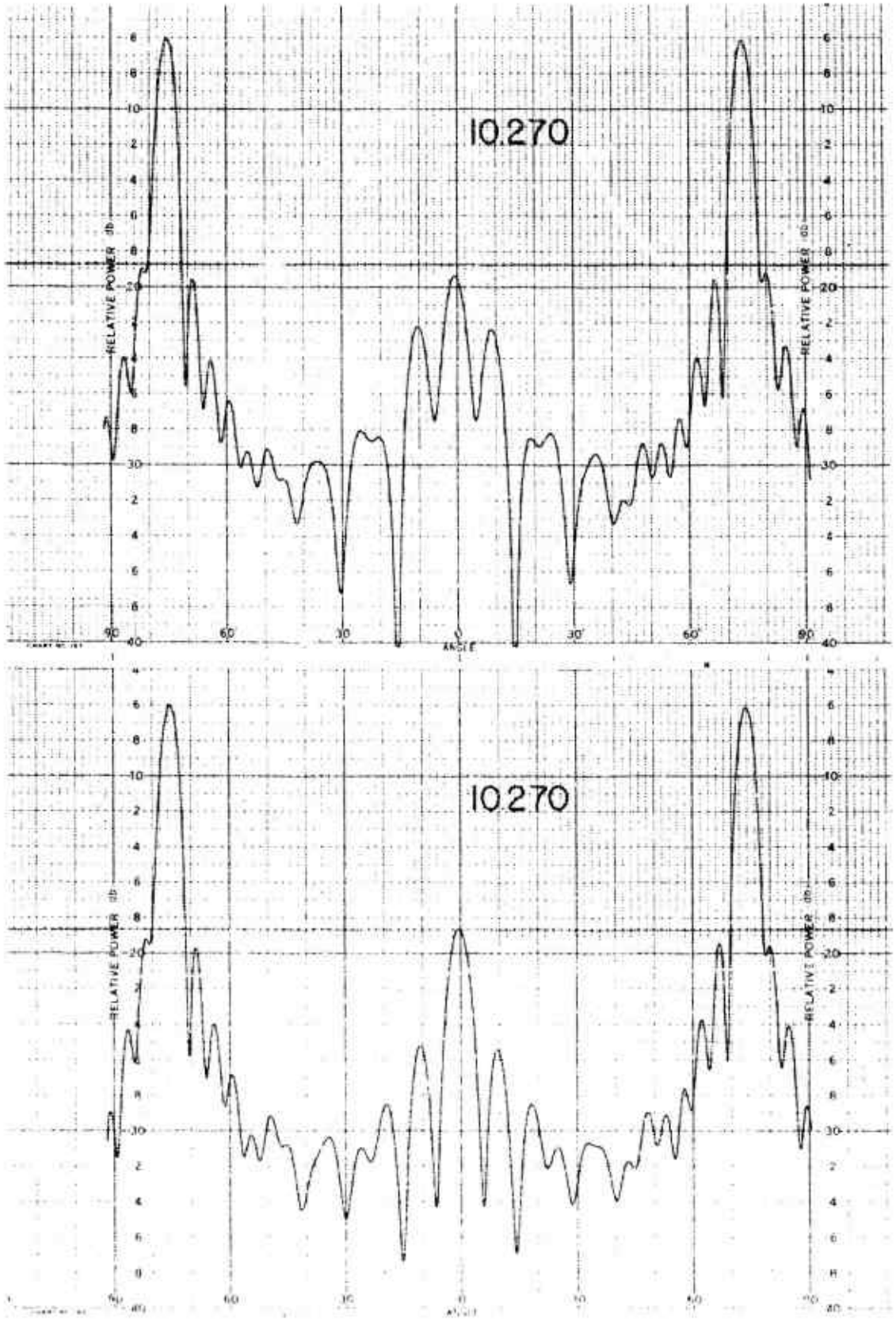
10.270
RELATIVE POWER db
ANGLE
10.270
RELATIVE POWER db

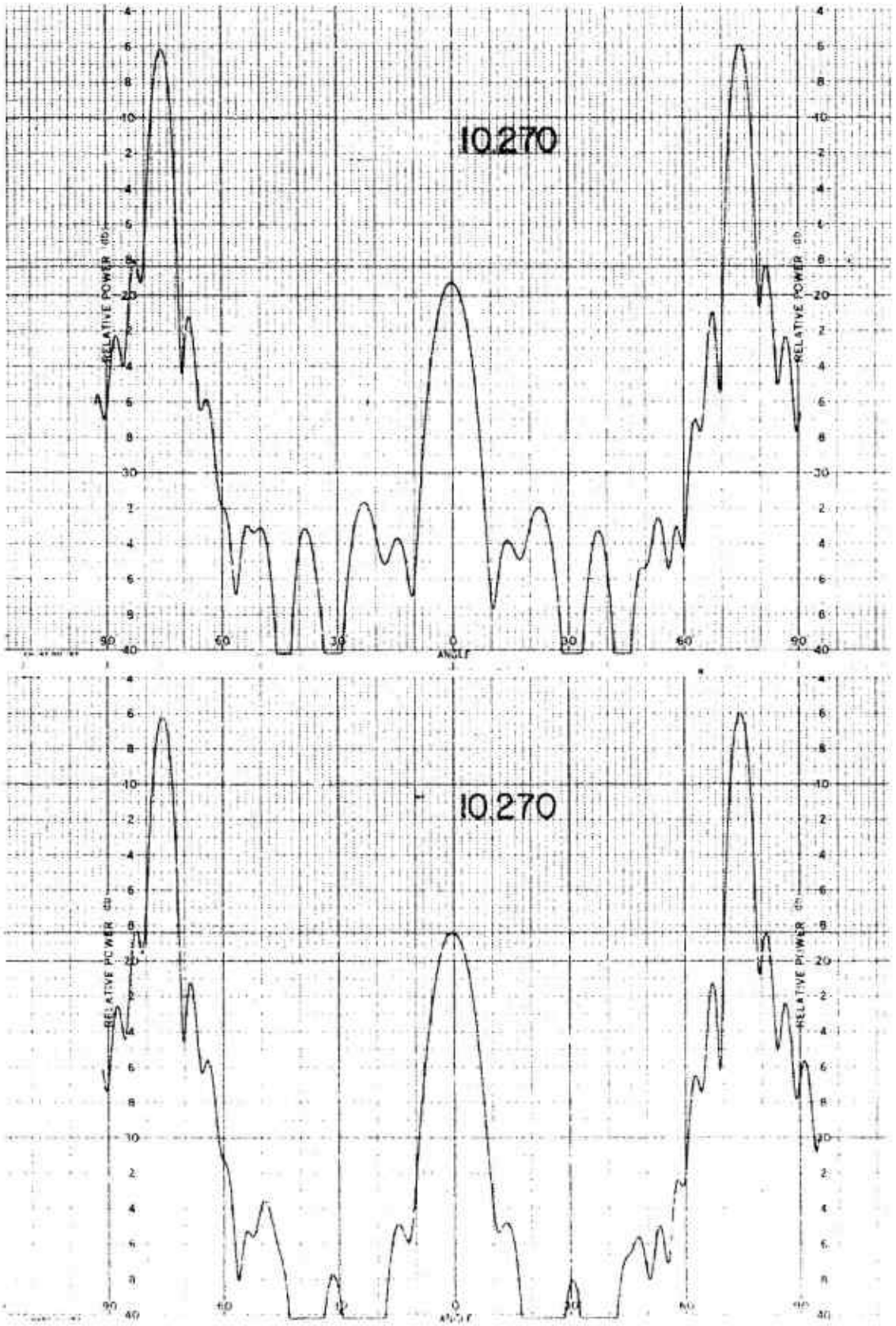
10.270
RELATIVE POWER dB
ANGLE
10.270
RELATIVE POWER dB
ANGLE

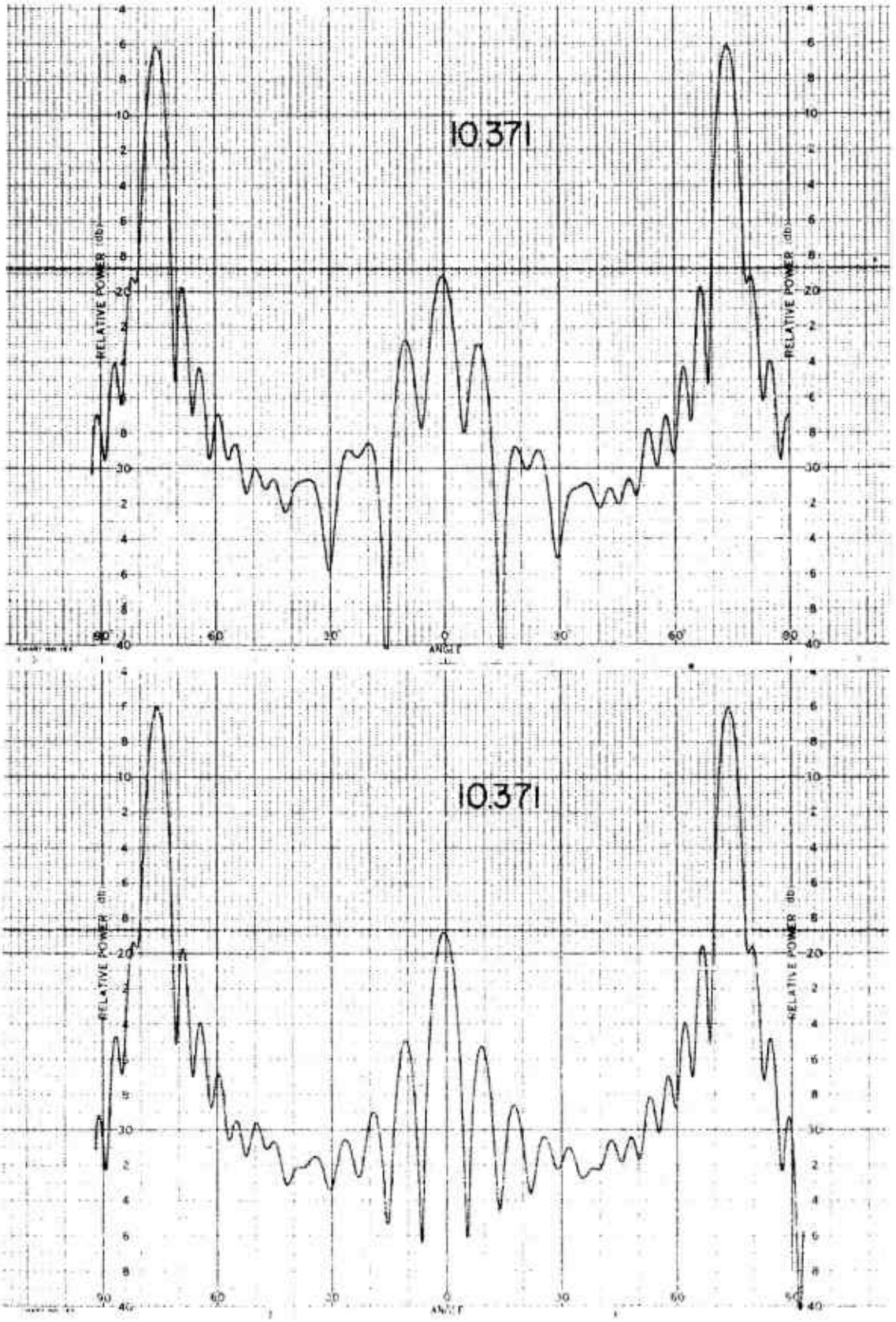
10.371
RELATIVE POWER (db)
ANGLE
10.371
RELATIVE POWER (db)
ANGLE

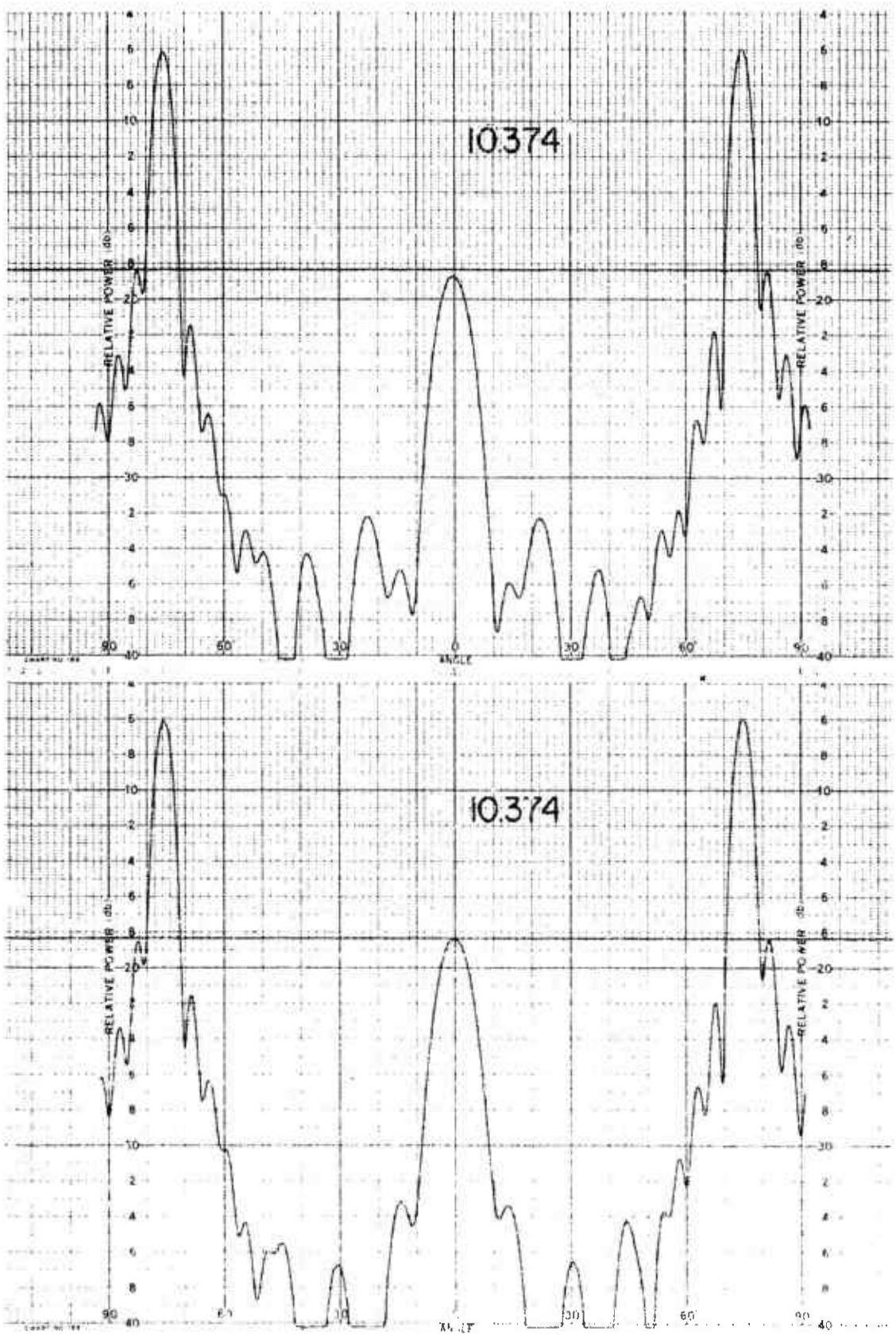
10.374
RELATIVE POWER (dB)
90
60
30
0
30
60
90
ANGLE
10.374
RELATIVE POWER (dB)

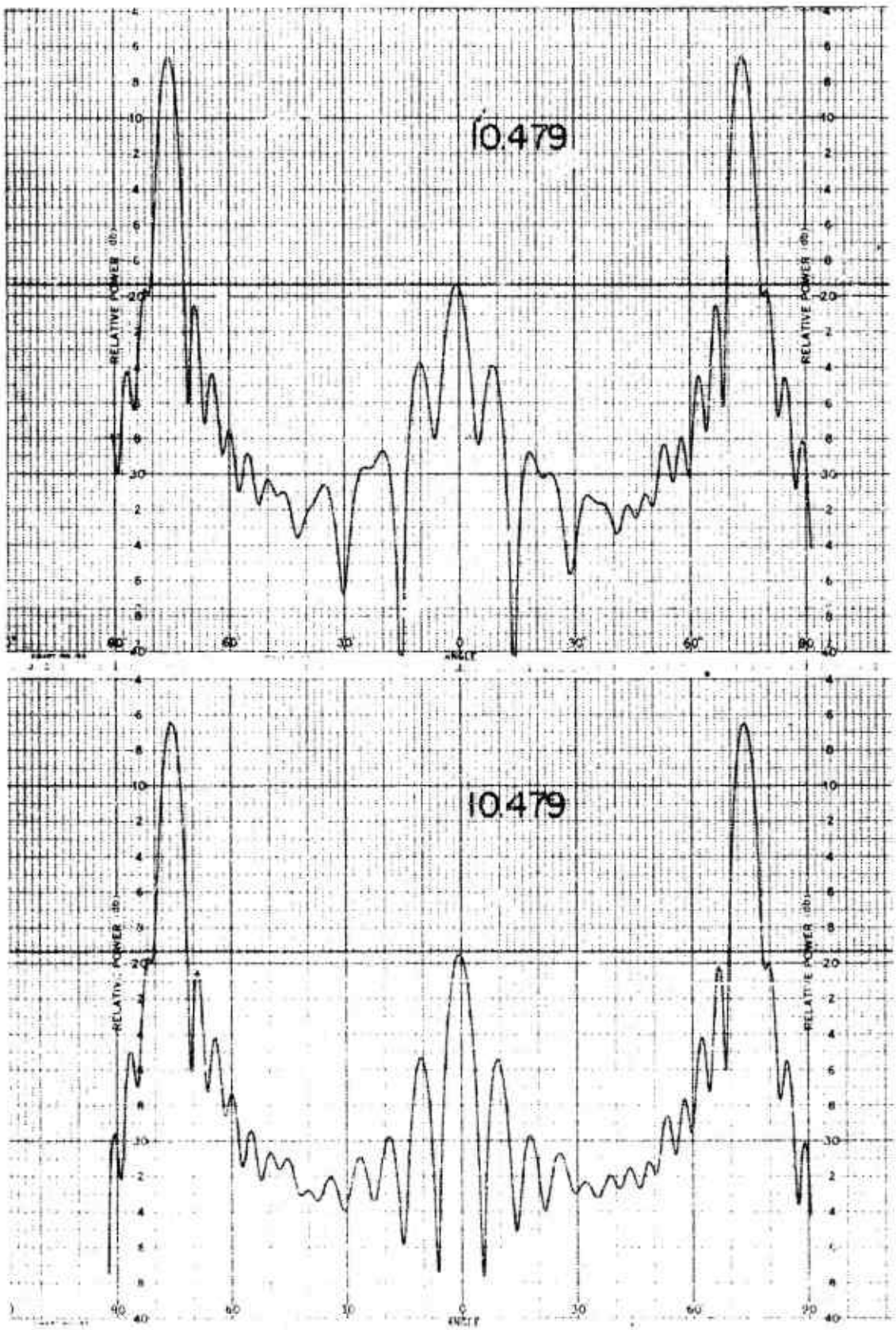
10.479
RELATIVE POWER (db)
10.479
RELATIVE POWER (db)

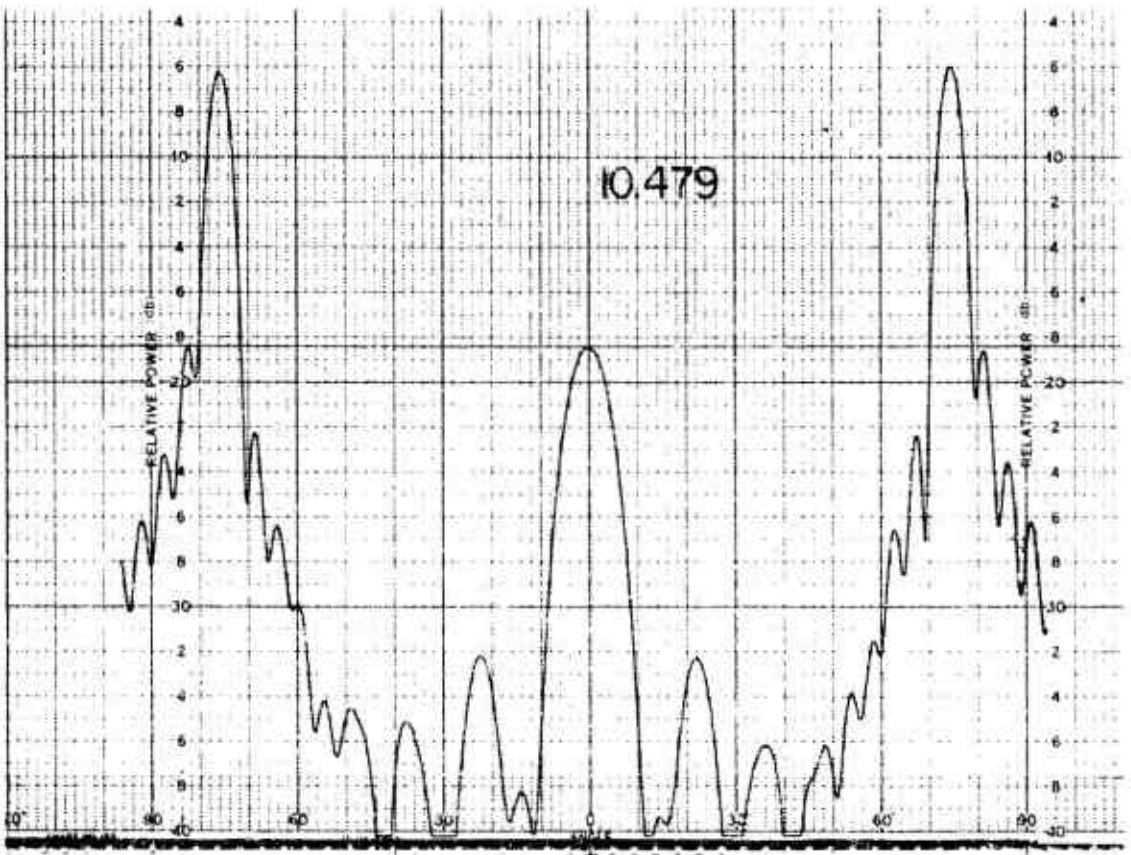
10.479
RELATIVE POWER db

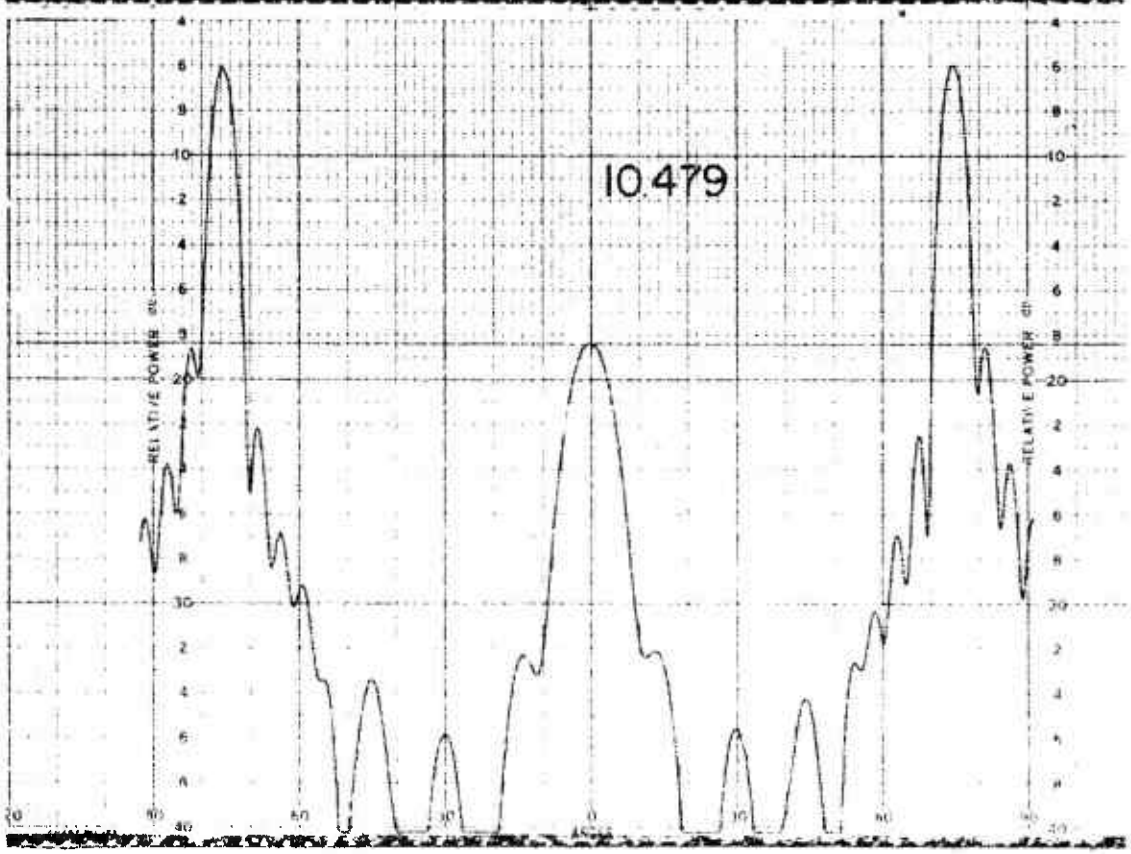
10.479
RELATIVE POWER db

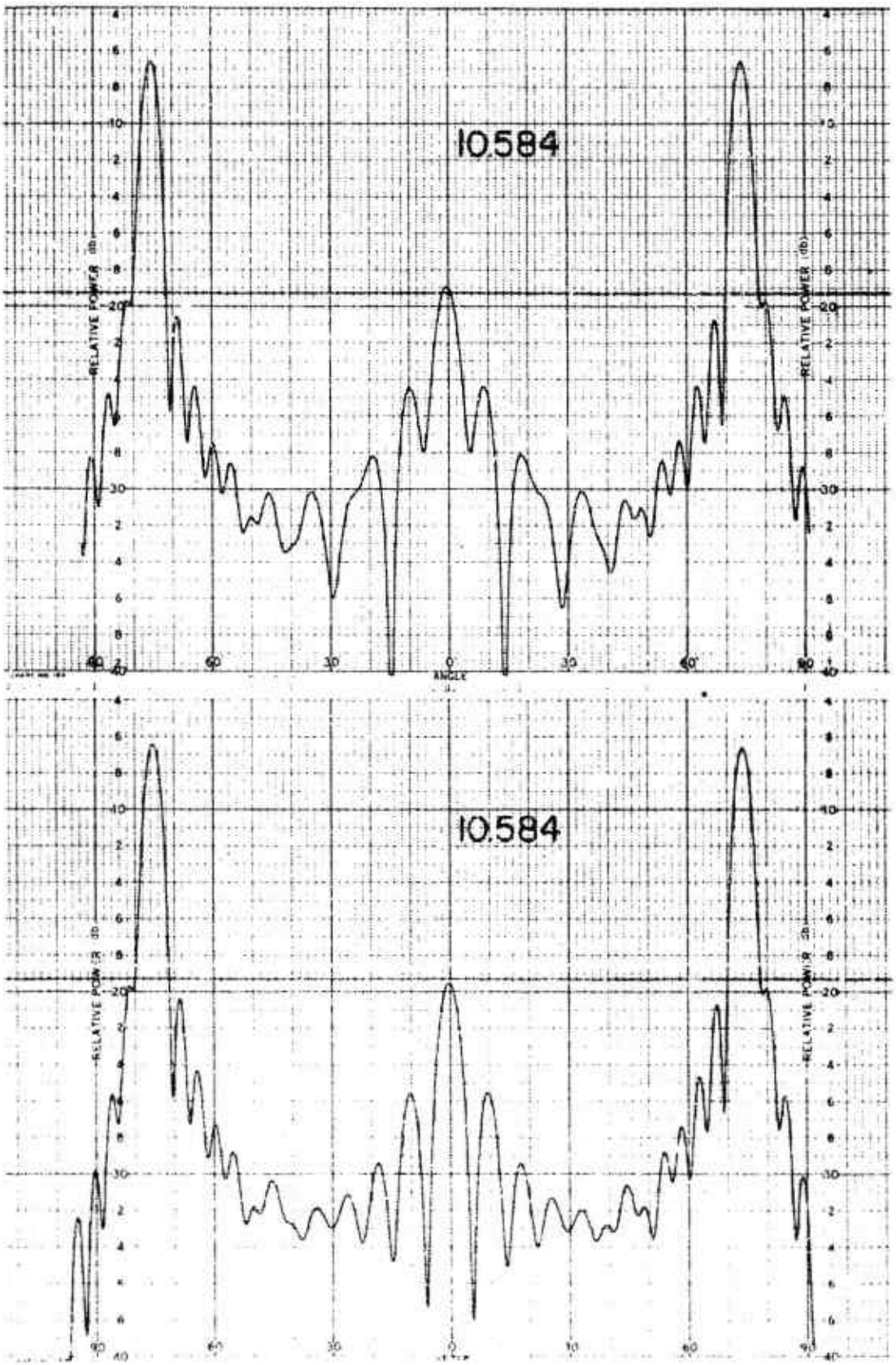
10.584
RELATIVE POWER (dB)
ANGLE
10.584
RELATIVE POWER (dB)

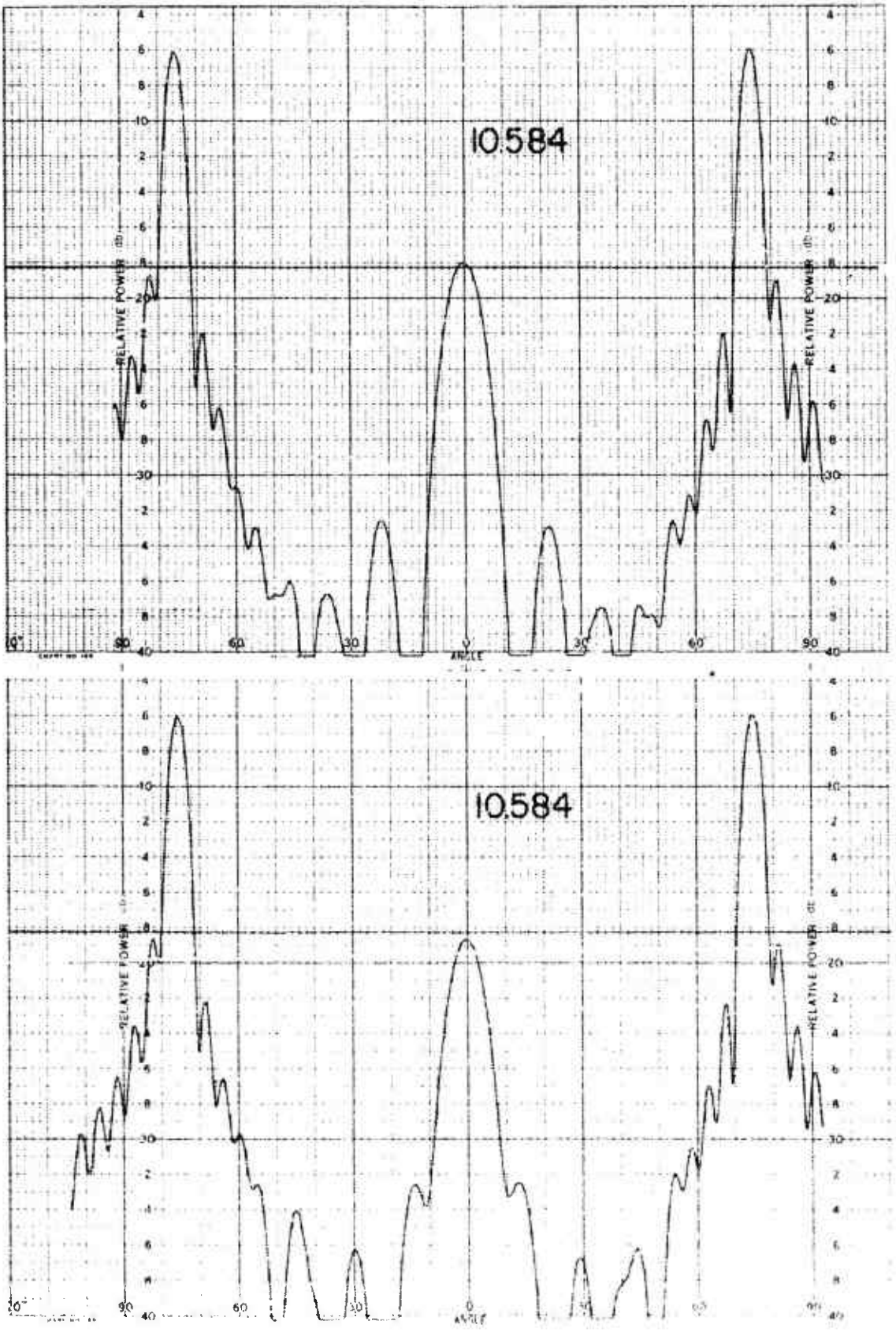
10.584
RELATIVE POWER (db)
ANGLE
10.584
RELATIVE POWER (db)
ANGLE

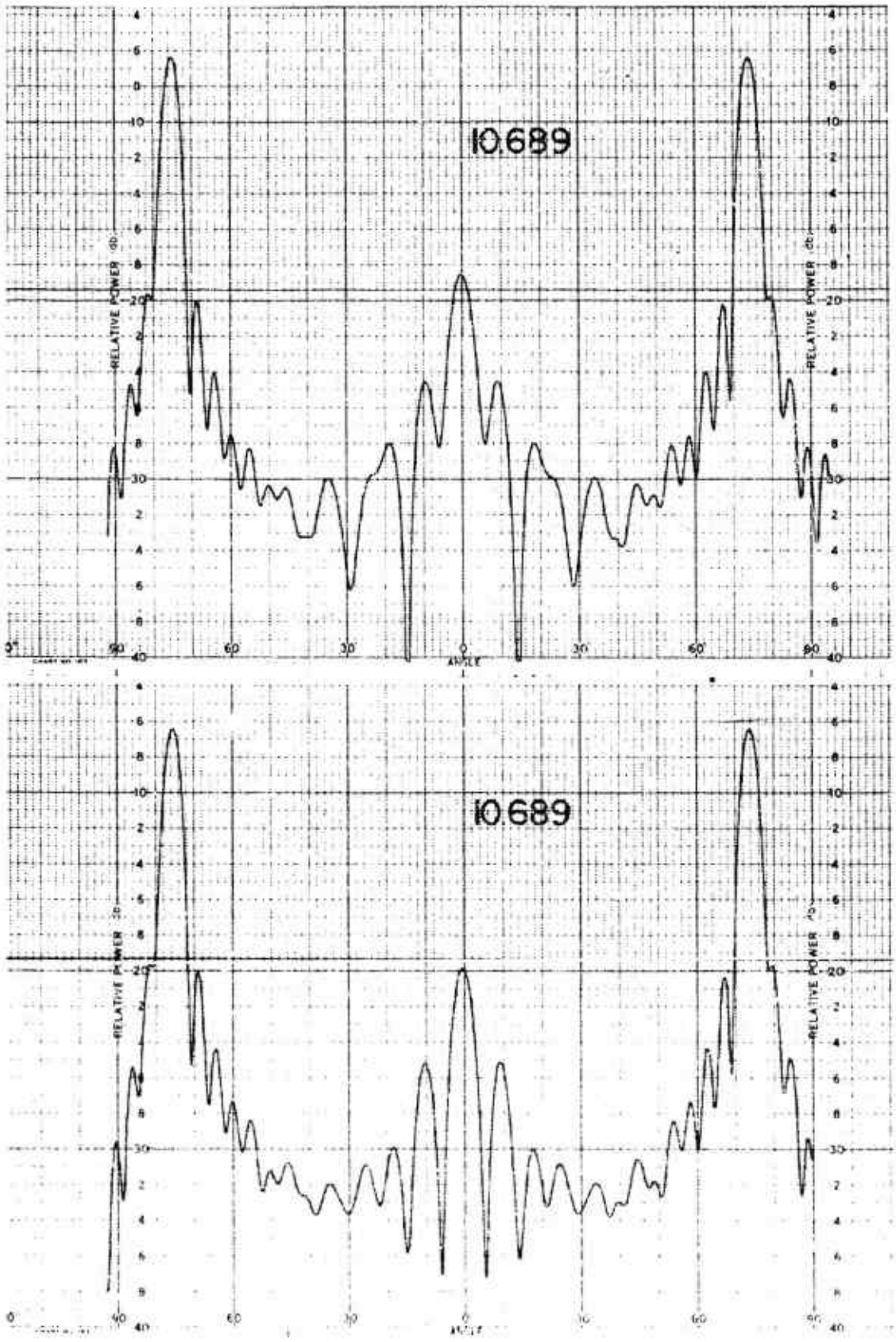
10.689
RELATIVE POWER (db)
ANGLE
10.689
RELATIVE POWER (db)
ANGLE

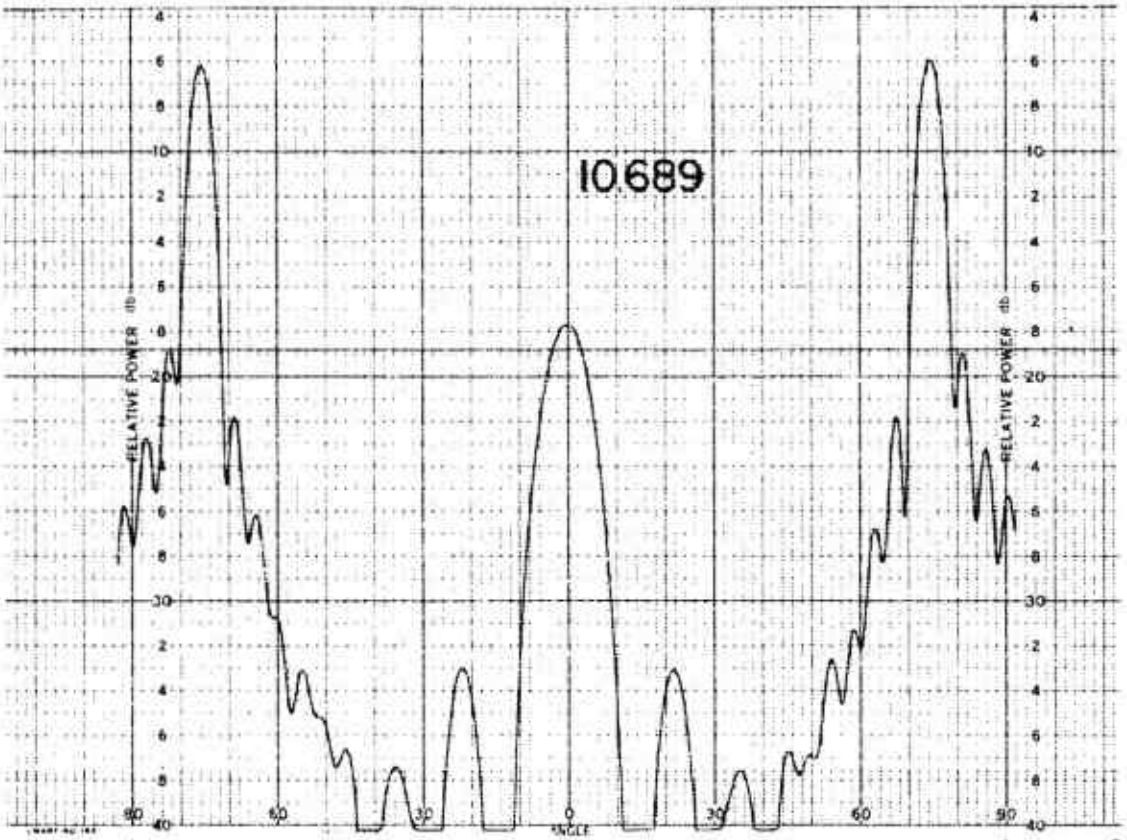
10.689
RELATIVE POWER db
ANGLE

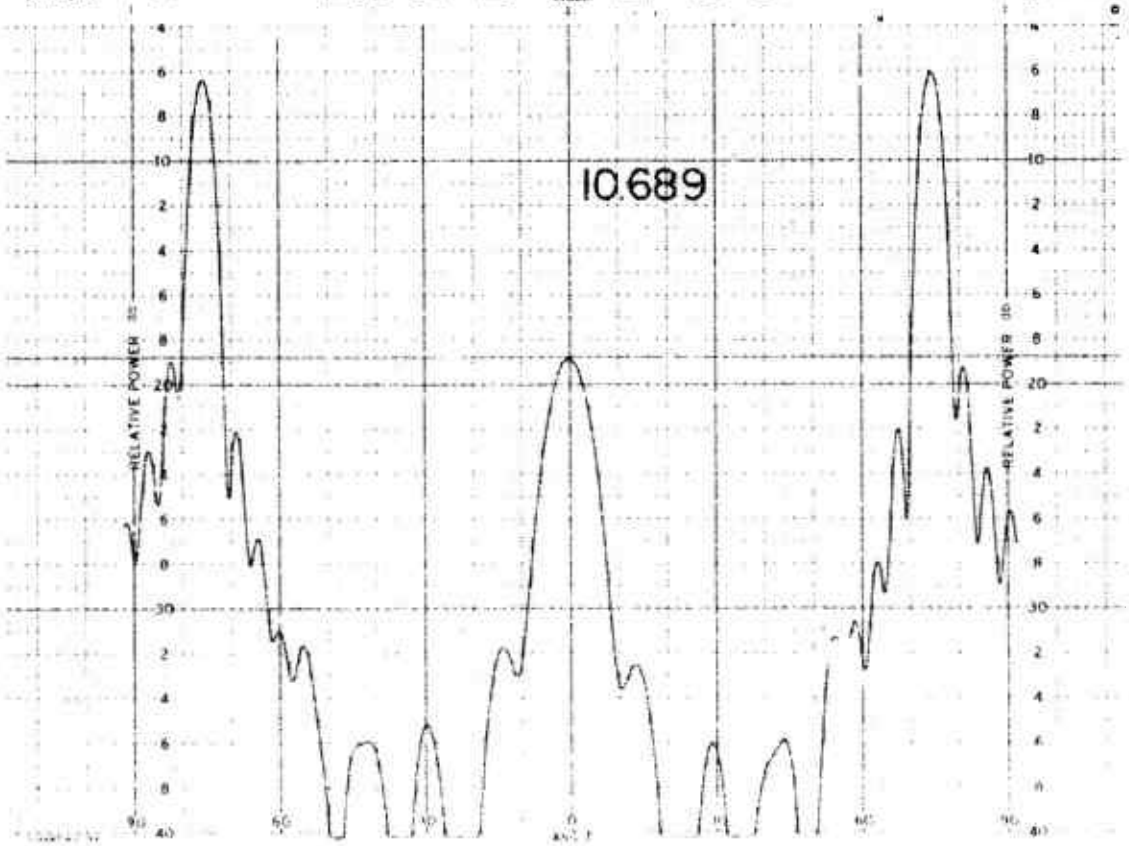
10.689
RELATIVE POWER db

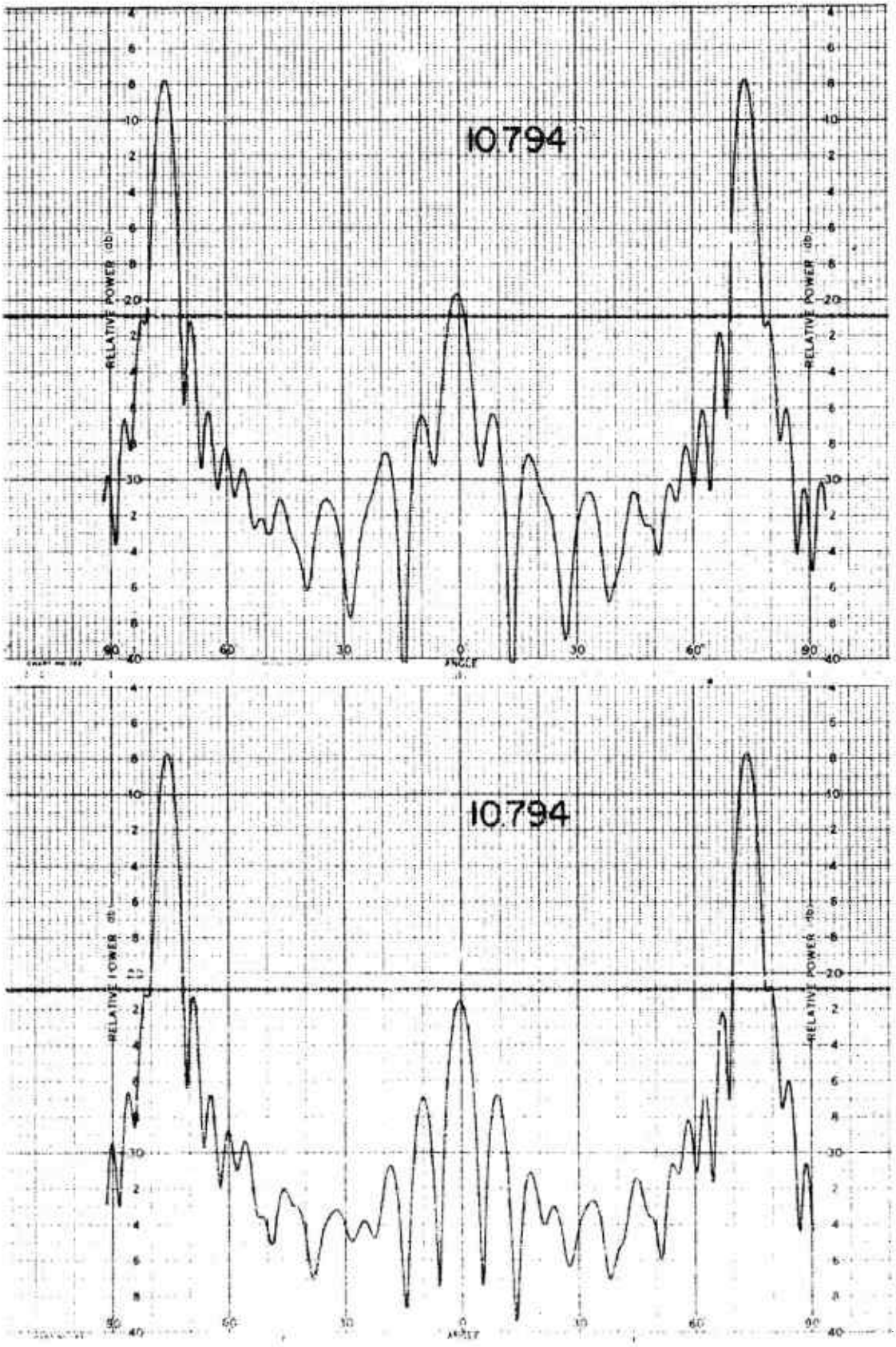
10794
RELATIVE POWER db
ANGLE
10794
RELATIVE POWER db
ANGLE

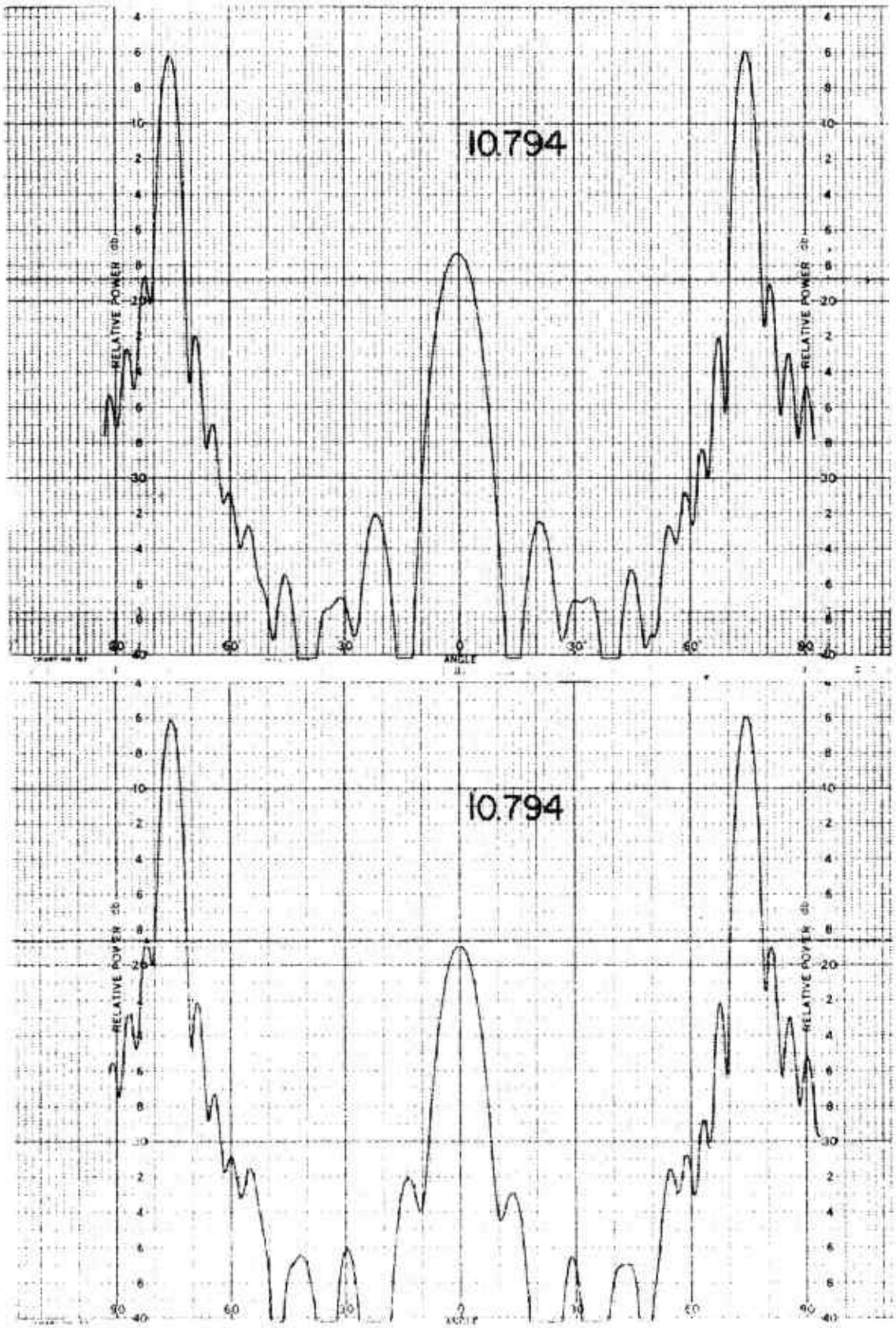
10.794
RELATIVE POWER db
ANGLE
10.794
RELATIVE POWER db

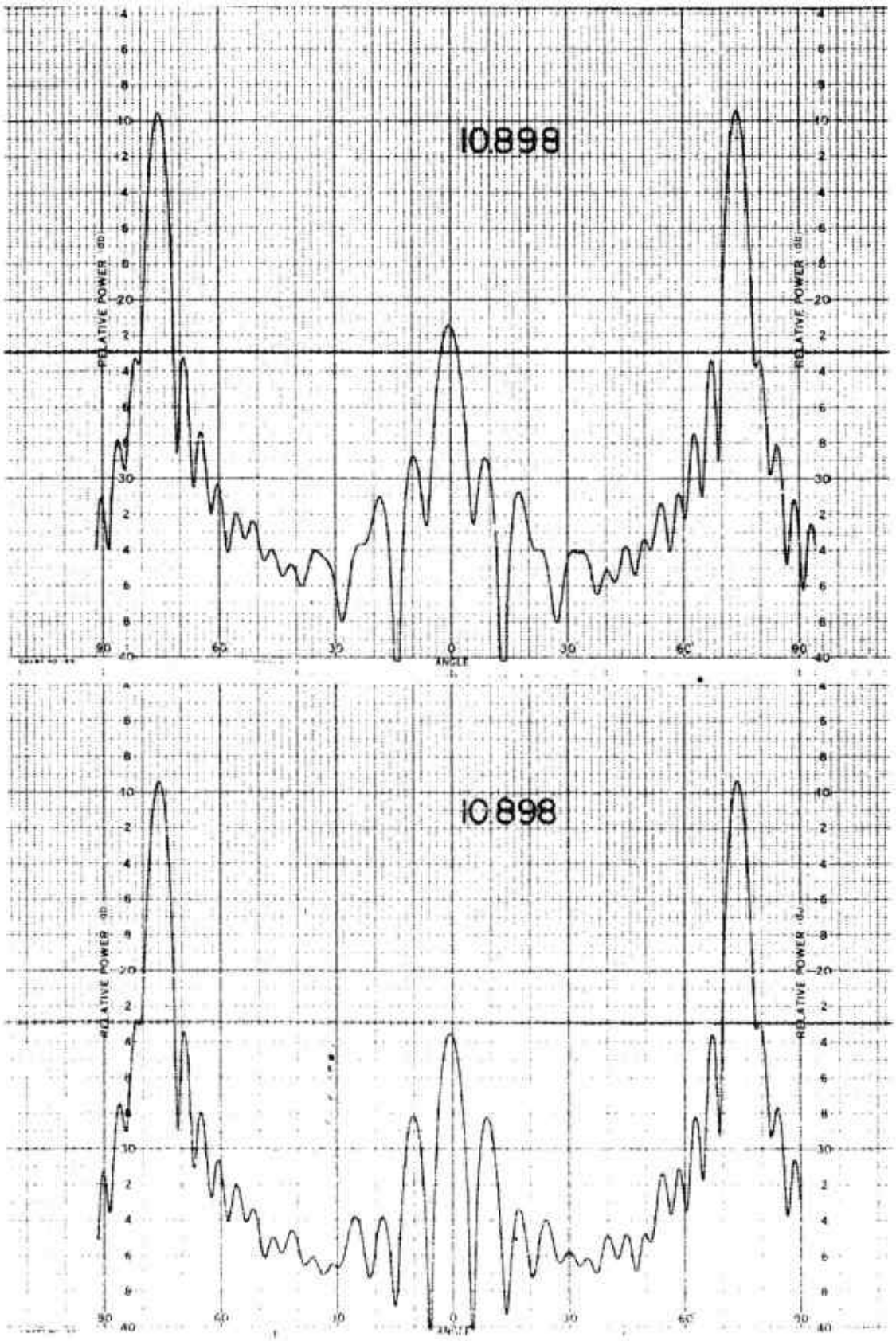
10898
RELATIVE POWER (dB)
ANGLE
10898
RELATIVE POWER (dB)
ANGLE

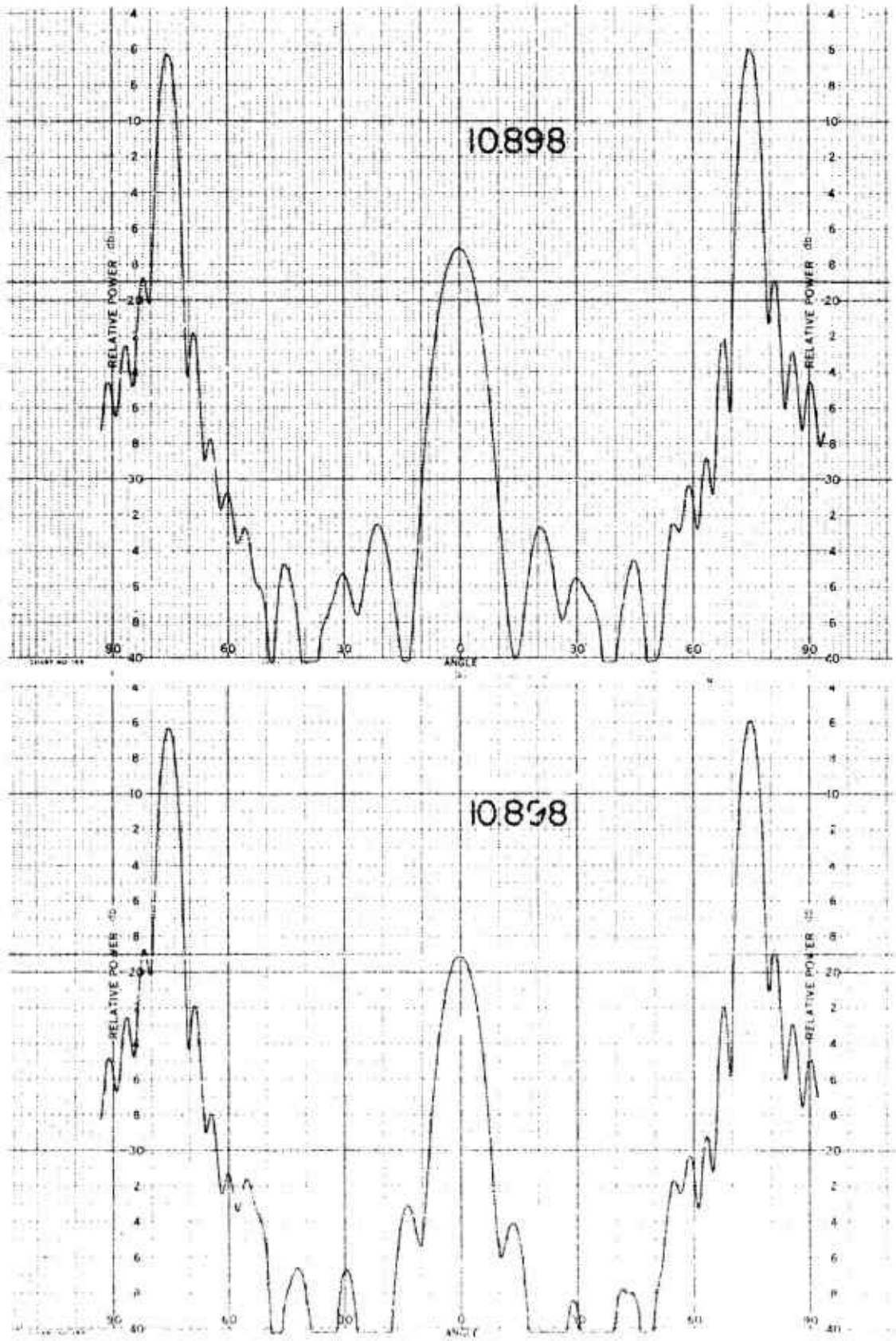
10.898
RELATIVE POWER db
ANGLE
10.898
RELATIVE POWER db
ANGLE

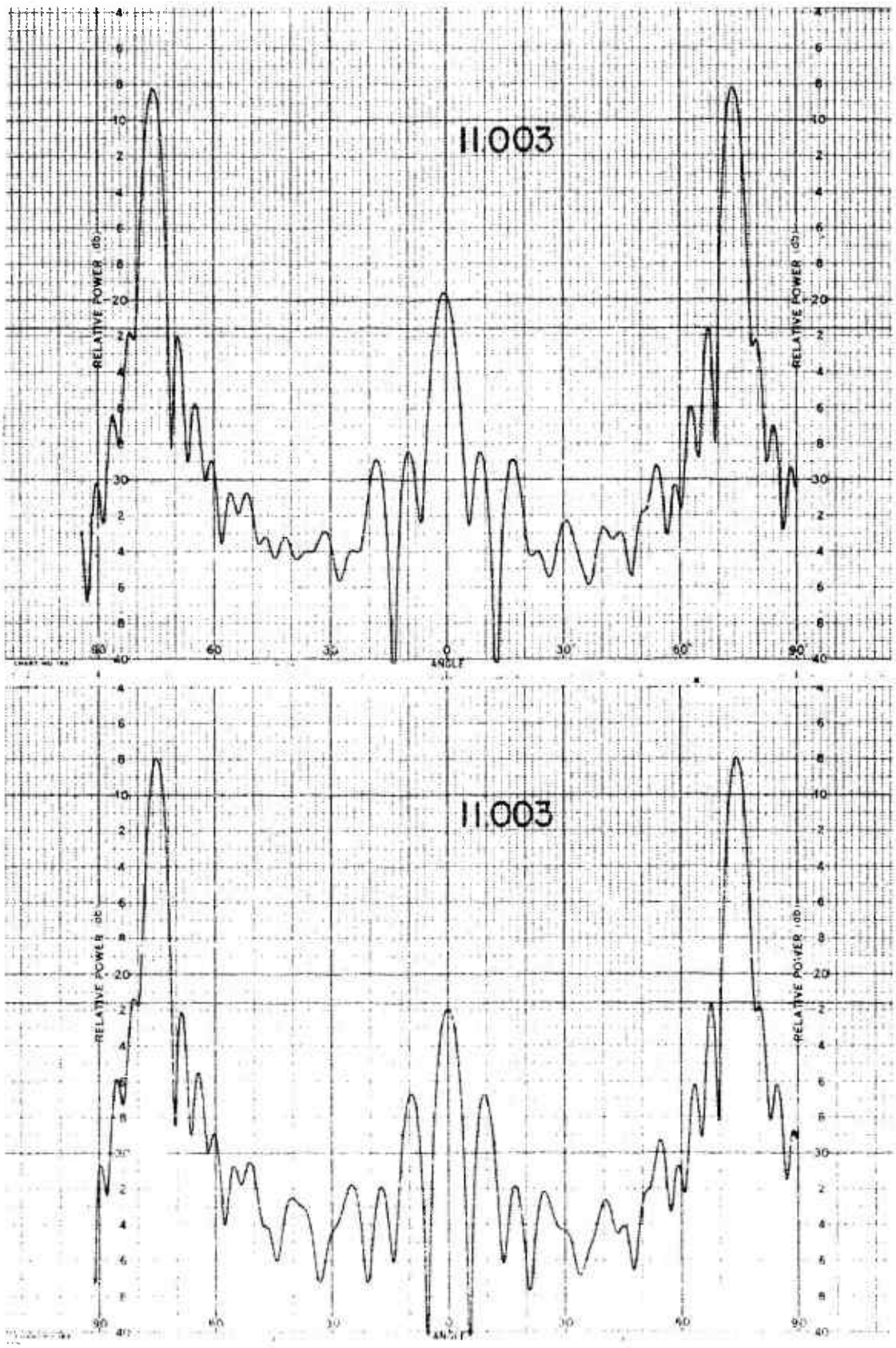
11.003
RELATIVE POWER (dB)
ANGLE
11.003
RELATIVE POWER (dB)
ANGLE

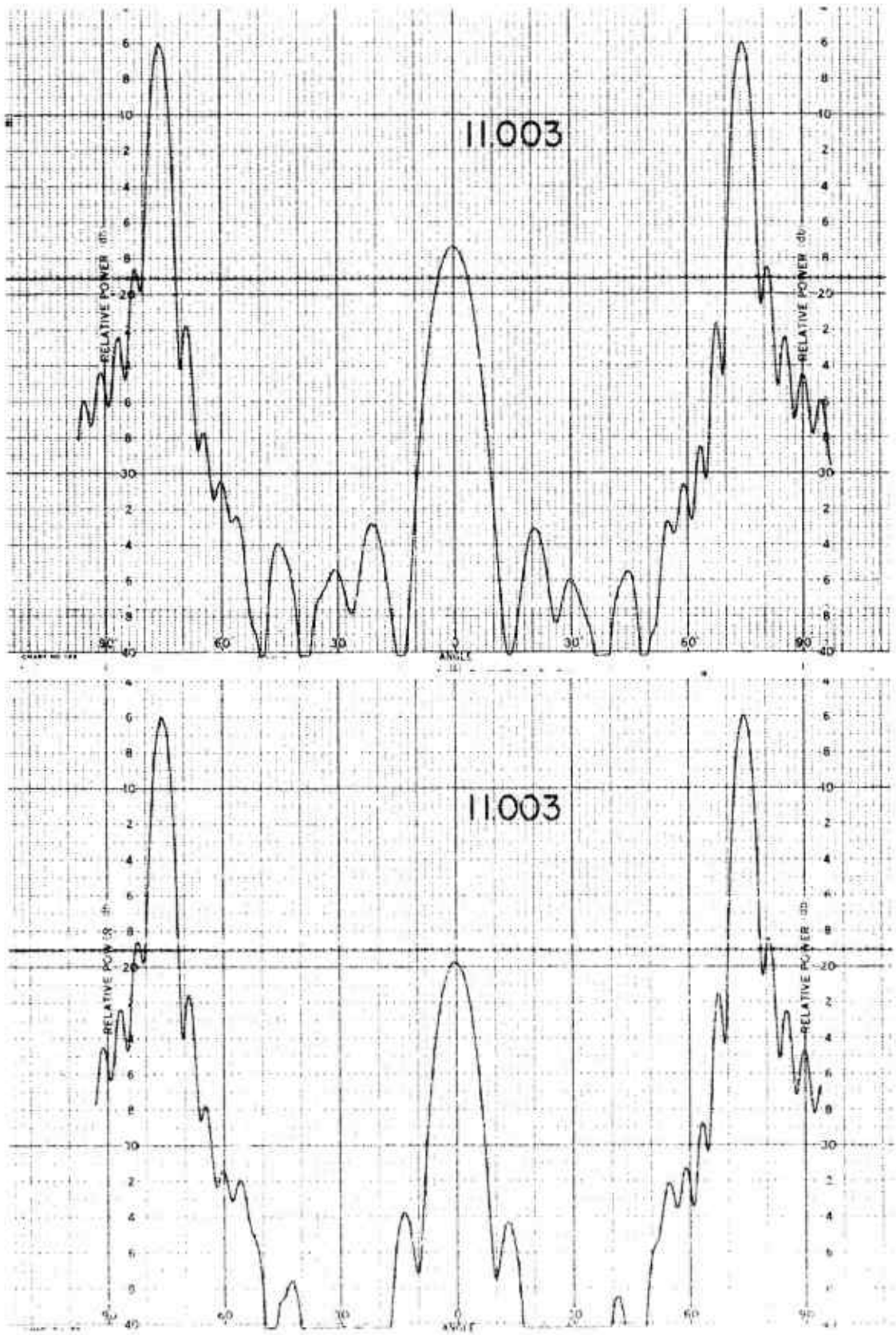
11.003
RELATIVE POWER (db)
ANGLE
11.003
RELATIVE POWER (db)
ANGLE

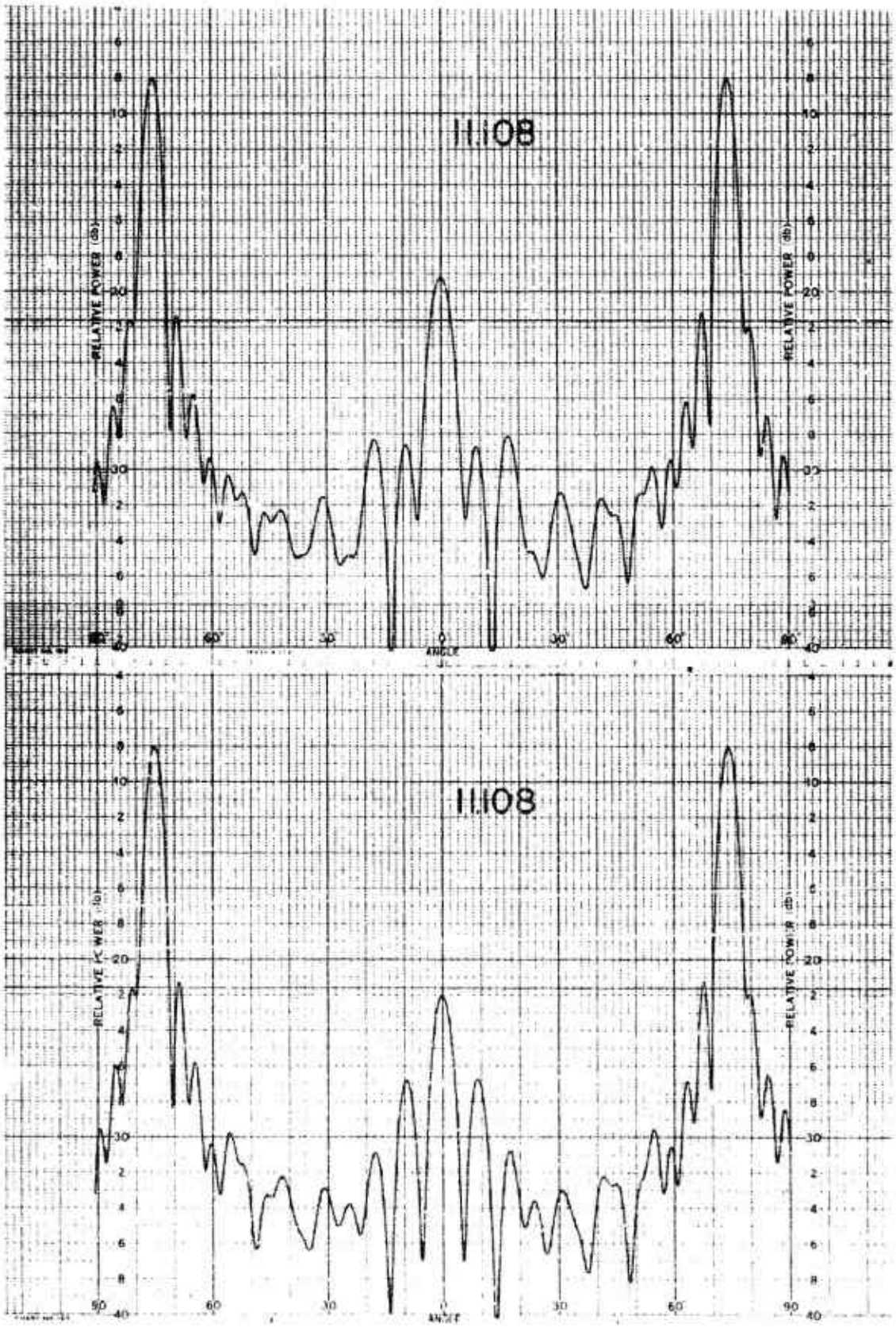
11.108
RELATIVE POWER (db)
ANGLE
11.108
RELATIVE POWER (db)
ANGLE

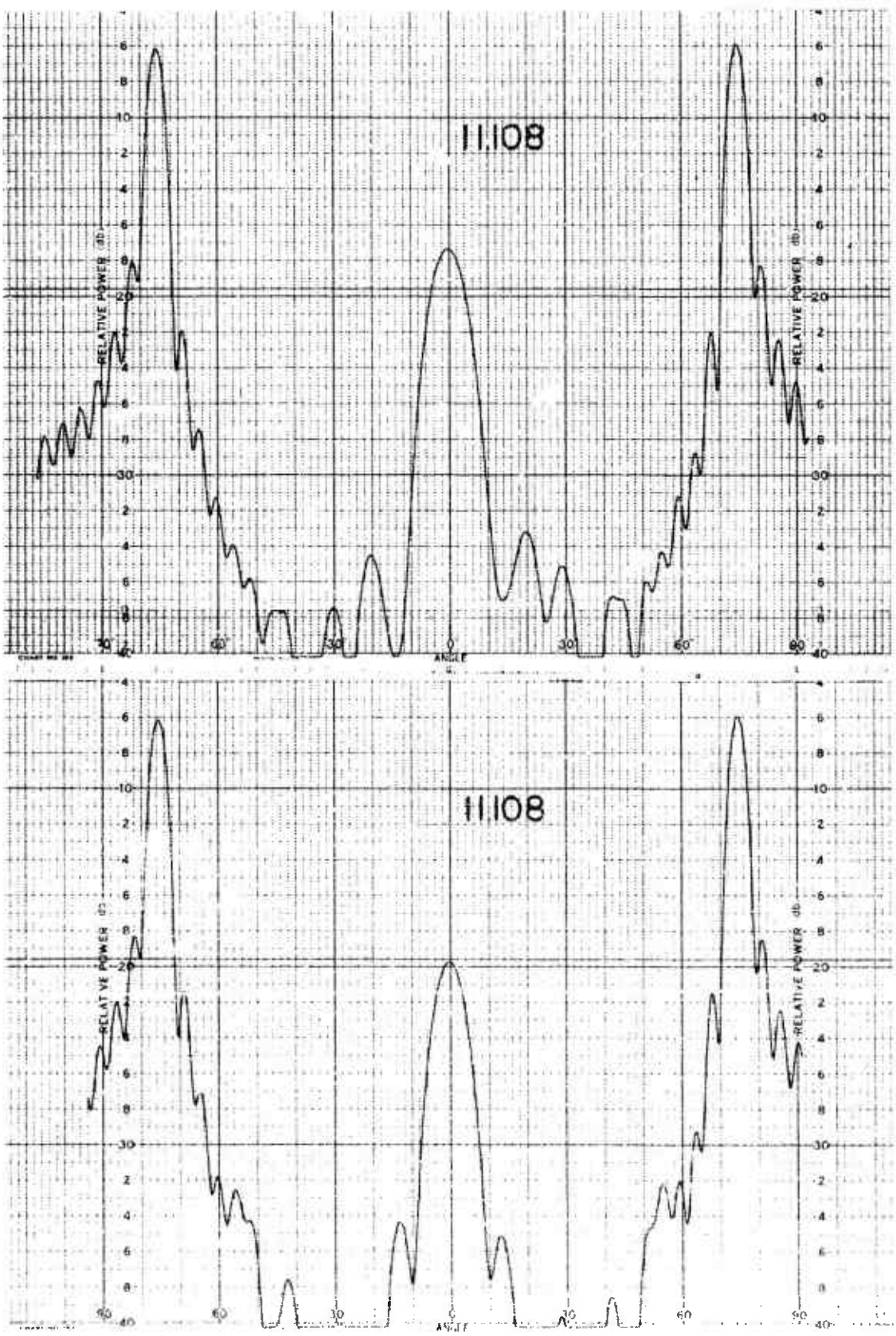
11108
RELATIVE POWER db
ANGLE
11108
RELATIVE POWER db
ANGLE

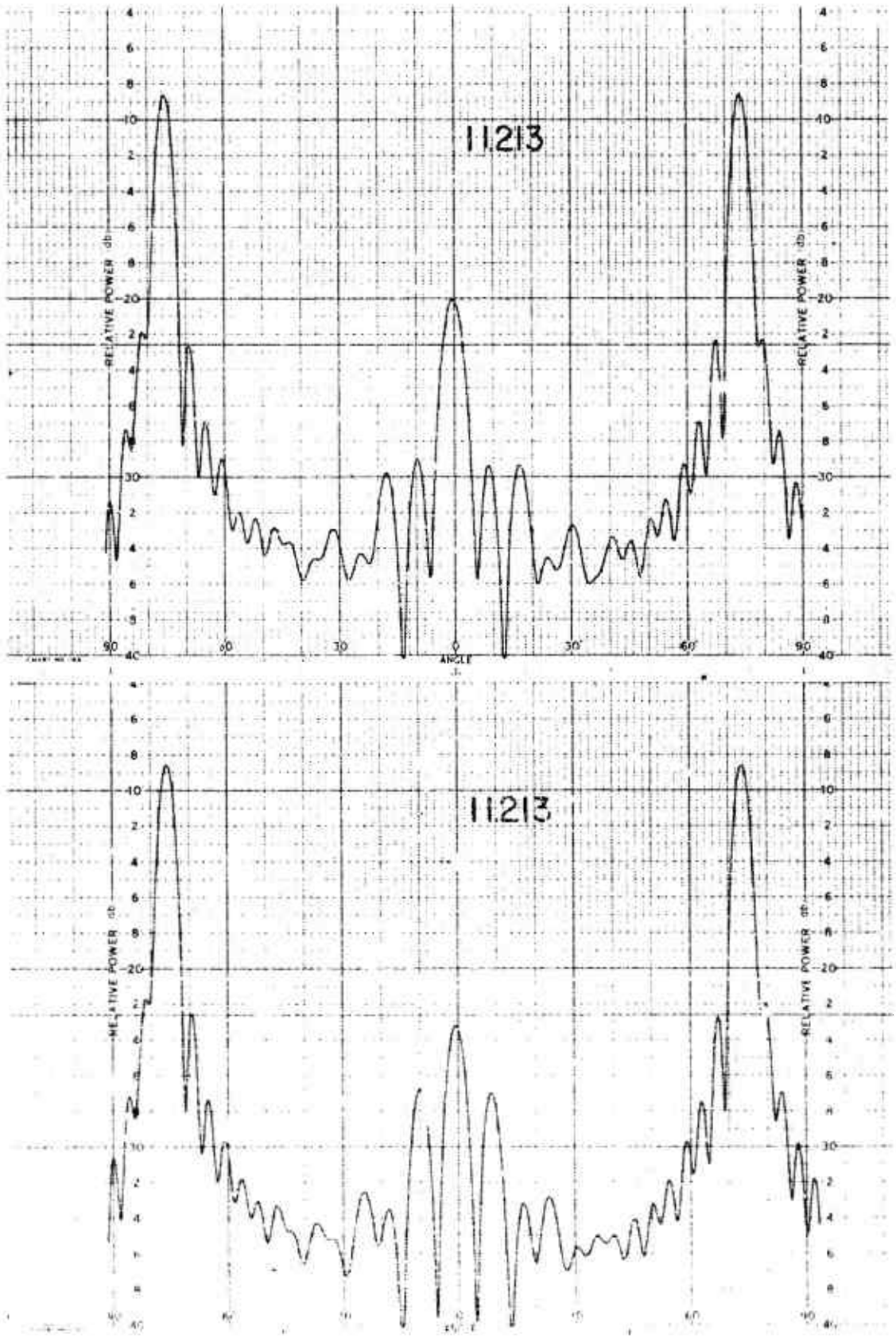
11.213
RELATIVE POWER db
ANGLE
11.213
RELATIVE POWER db

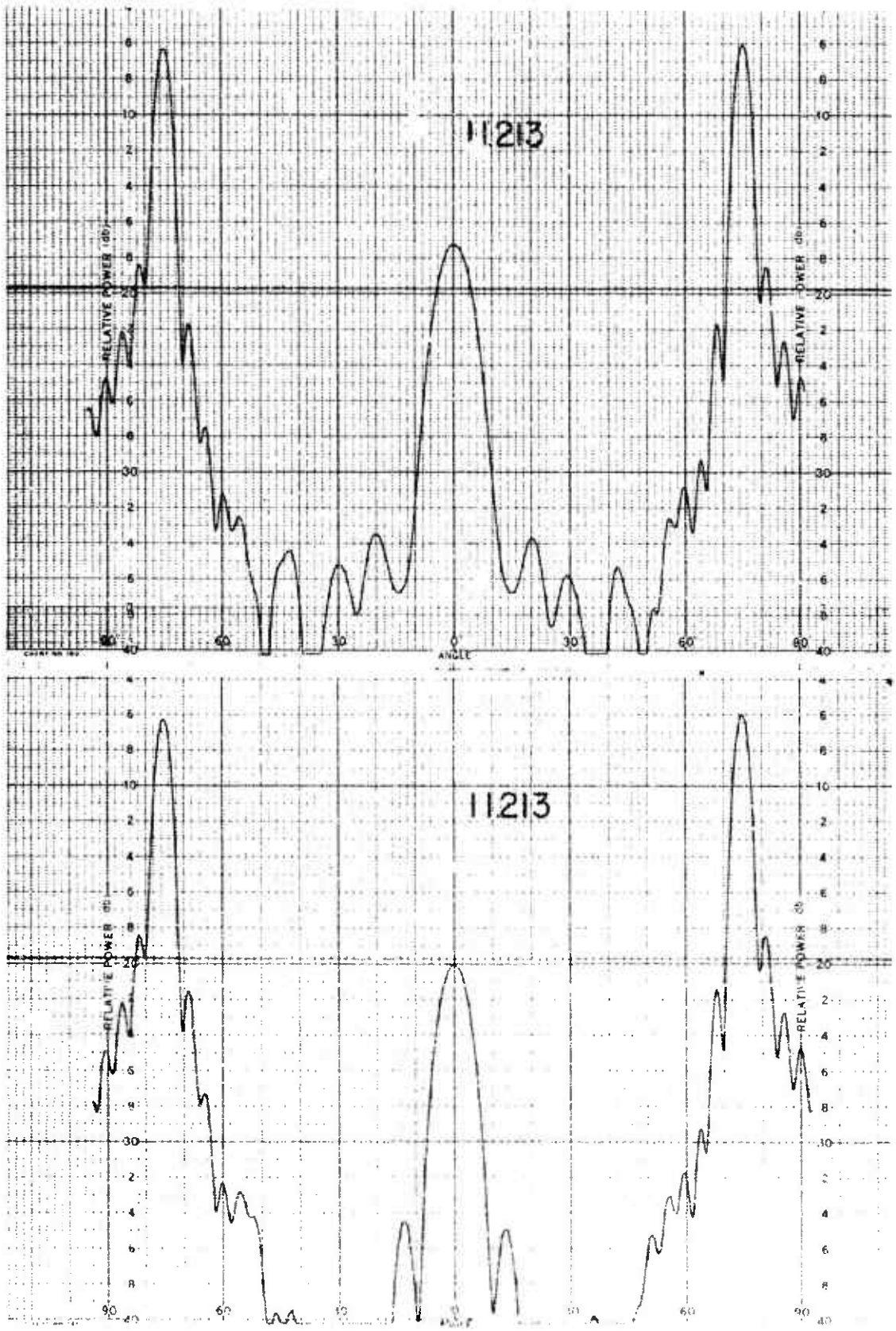
11213
RELATIVE POWER db
ANGLE
11213
RELATIVE POWER db

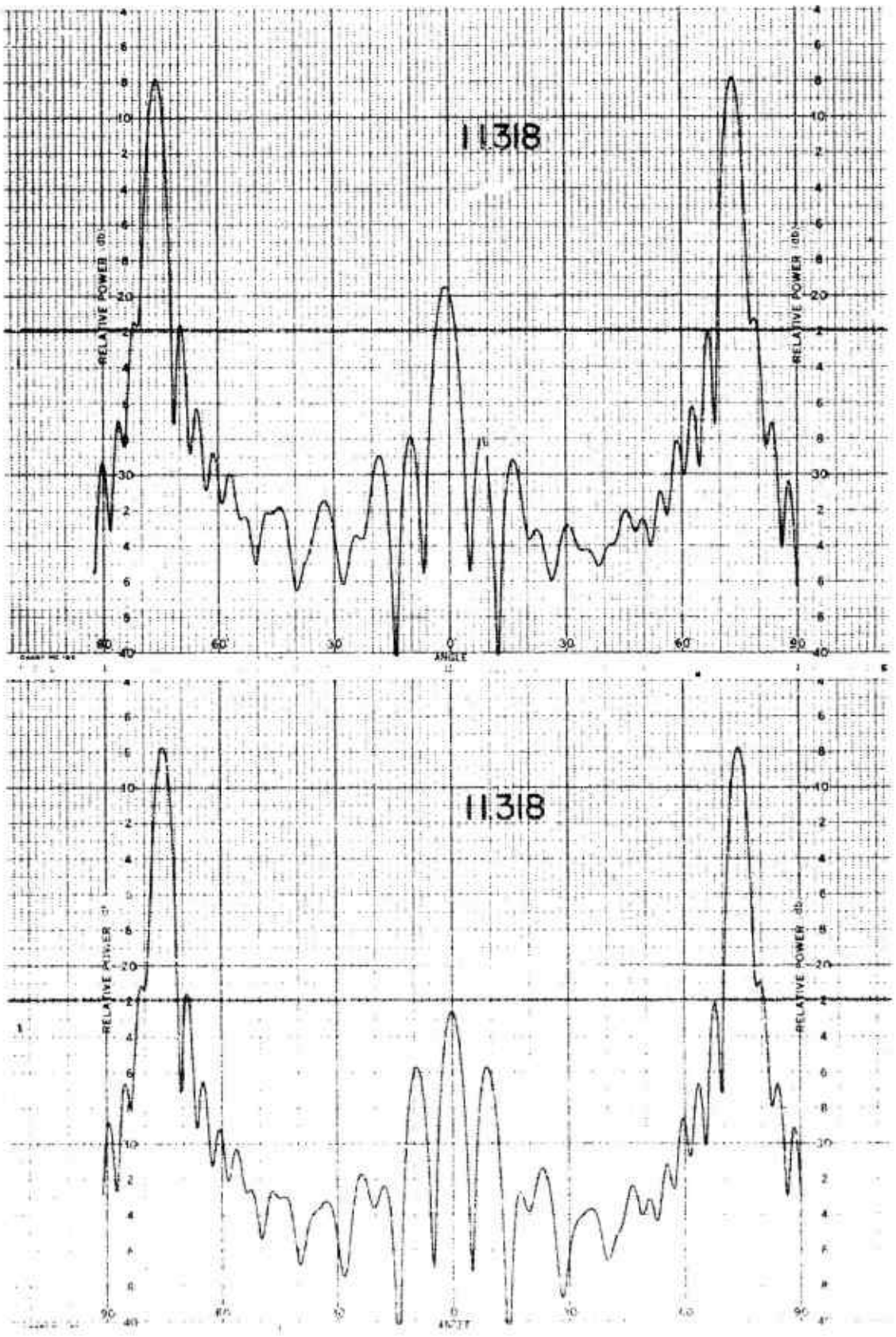
11318
RELATIVE POWER (db)
ANGLE
11318
RELATIVE POWER (db)

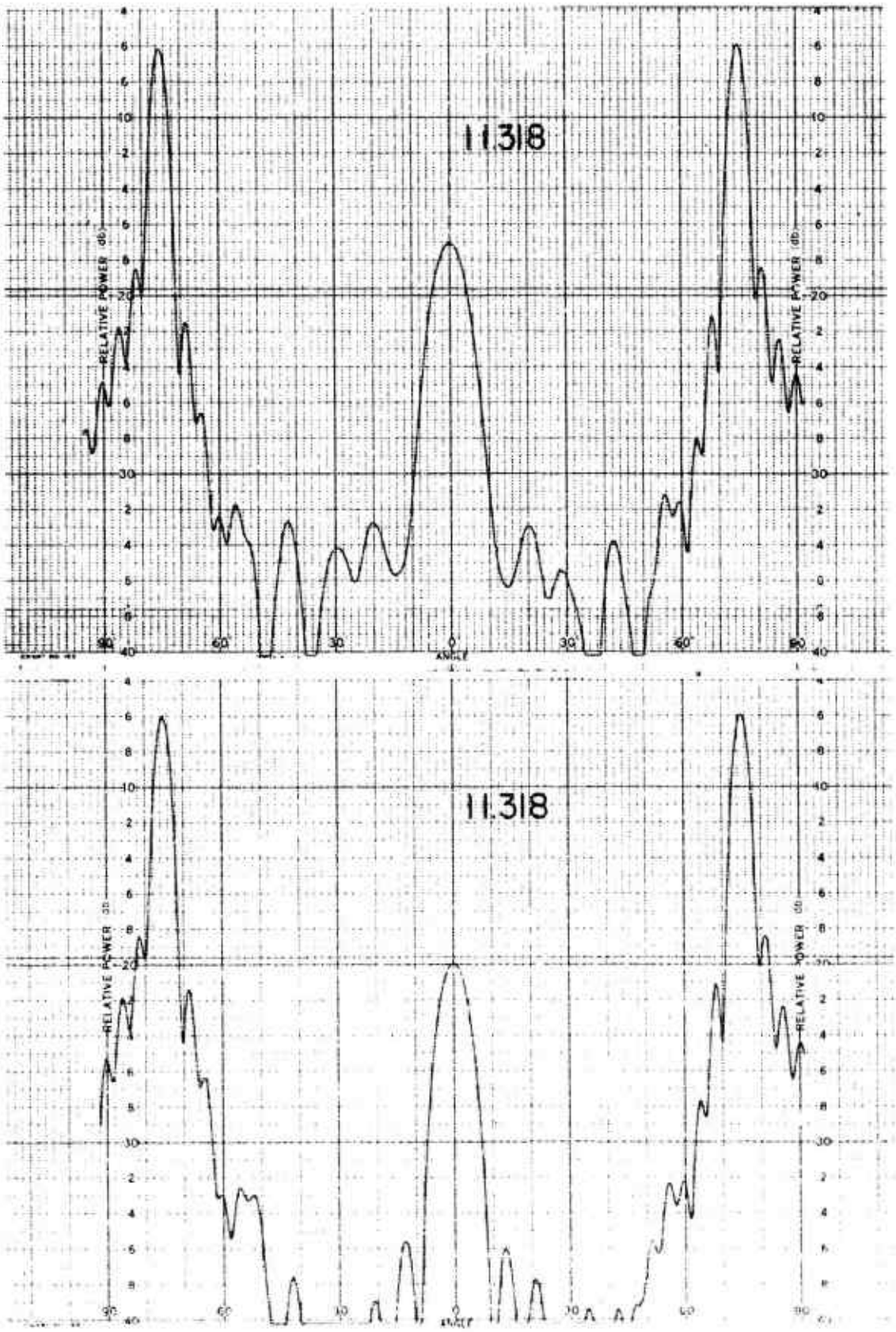
11.318
RELATIVE POWER (db)
ANGLE
11.318
RELATIVE POWER (db)
ANGLE

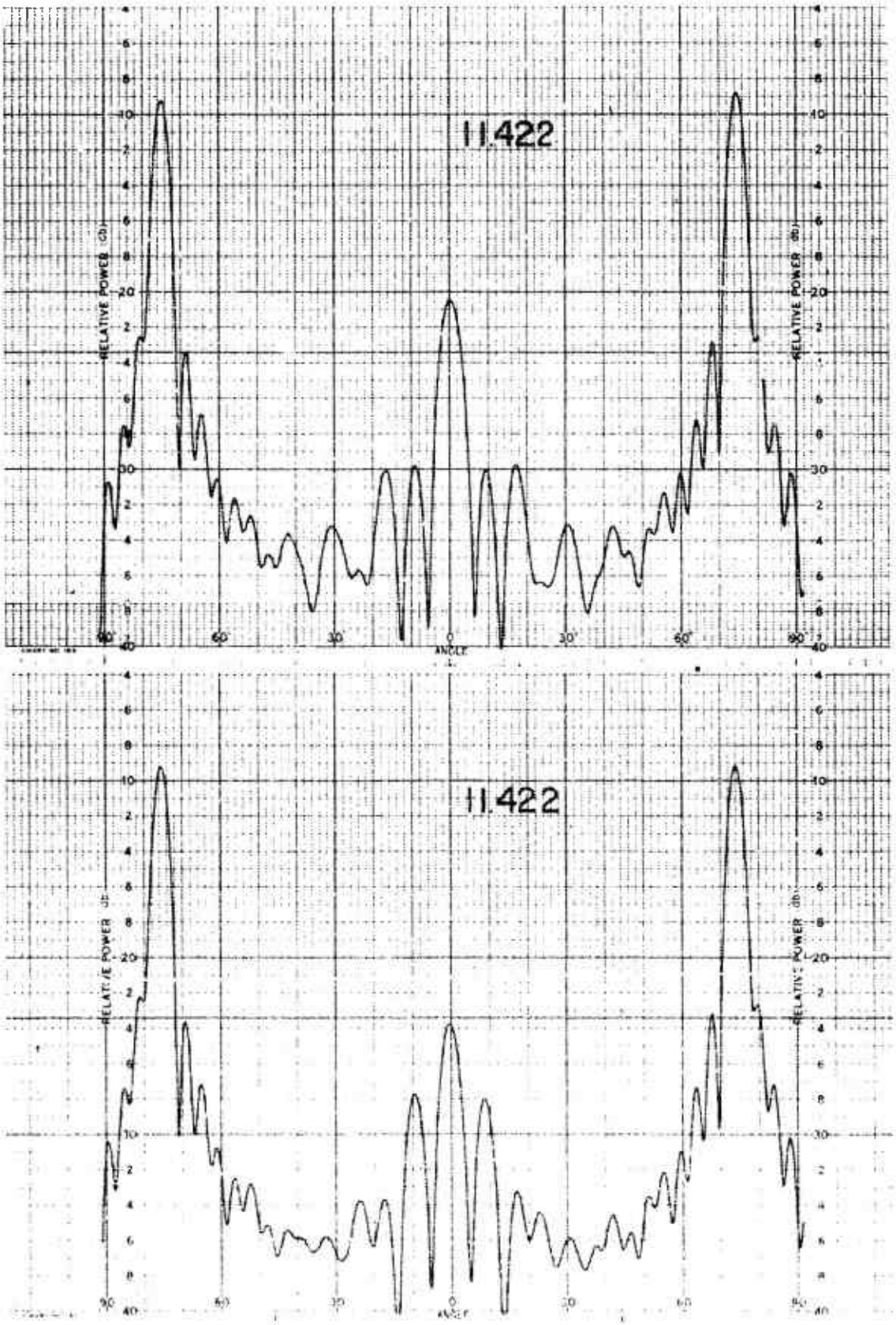
11.422
RELATIVE POWER (DB)
ANGLE
11.422
RELATIVE POWER (DB)
ANGLE

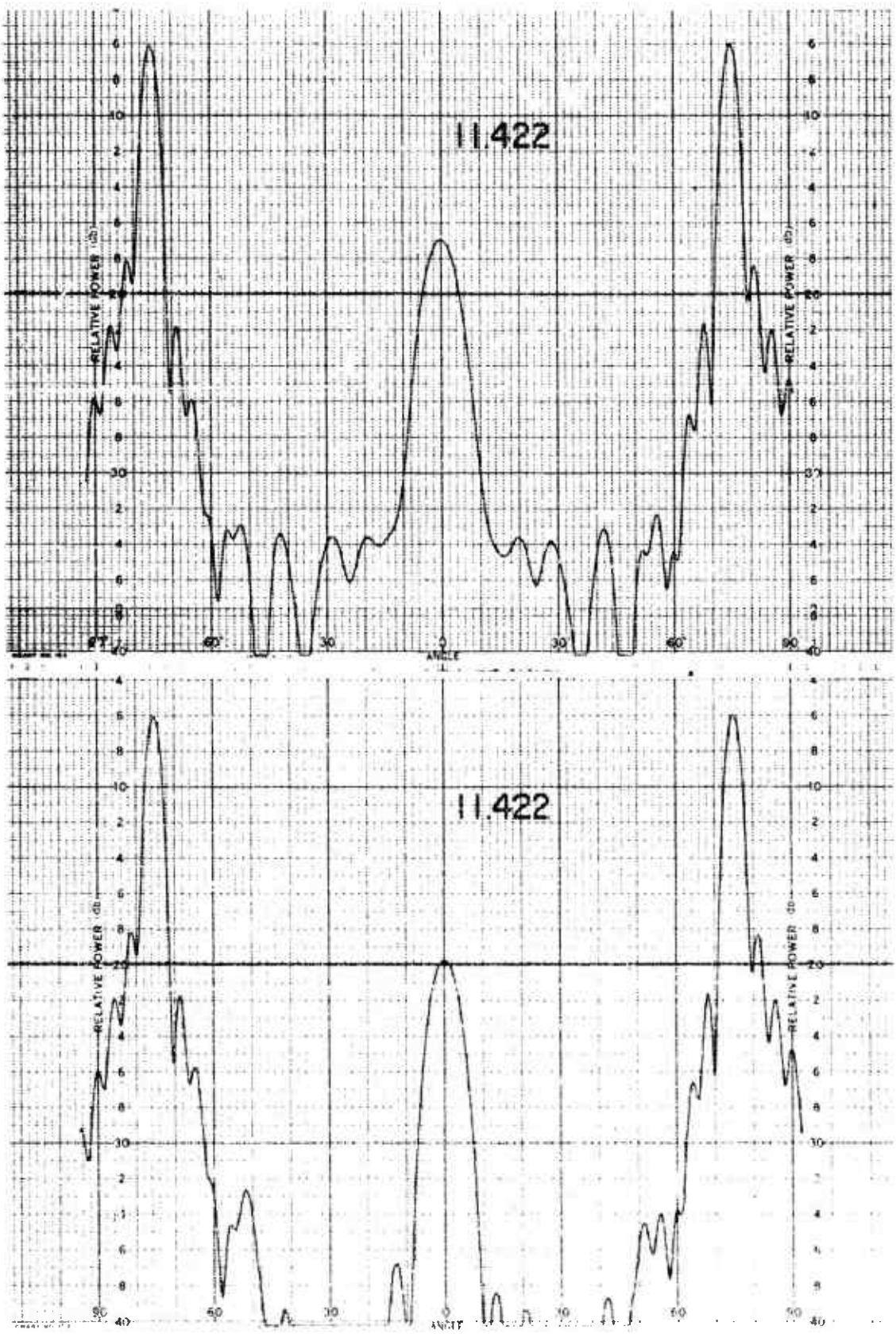
11.422
RELATIVE POWER (dB)
ANGLE
11.422
RELATIVE POWER (dB)
ANGLE

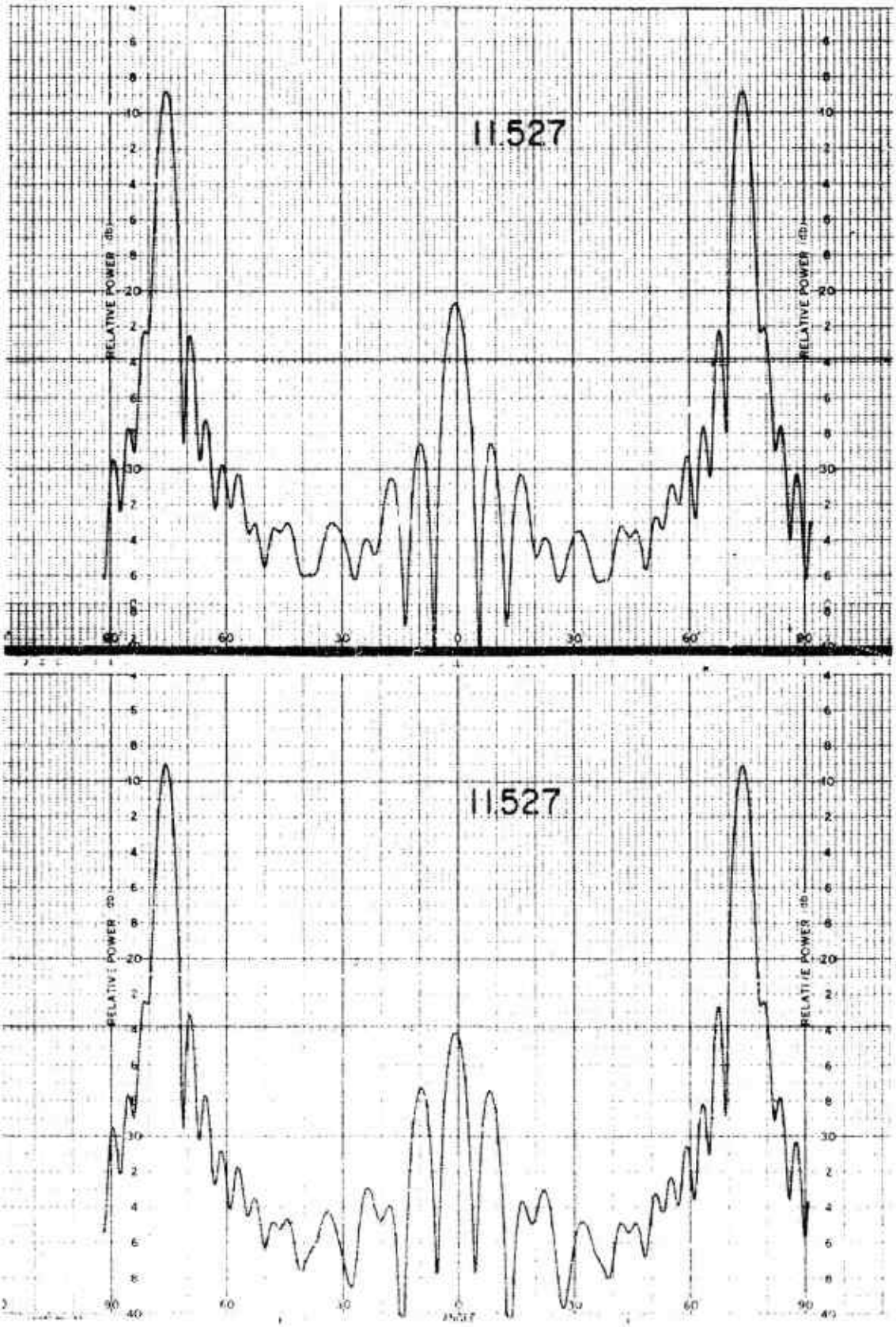
11.527
RELATIVE POWER (dB)
11.527
RELATIVE POWER (dB)

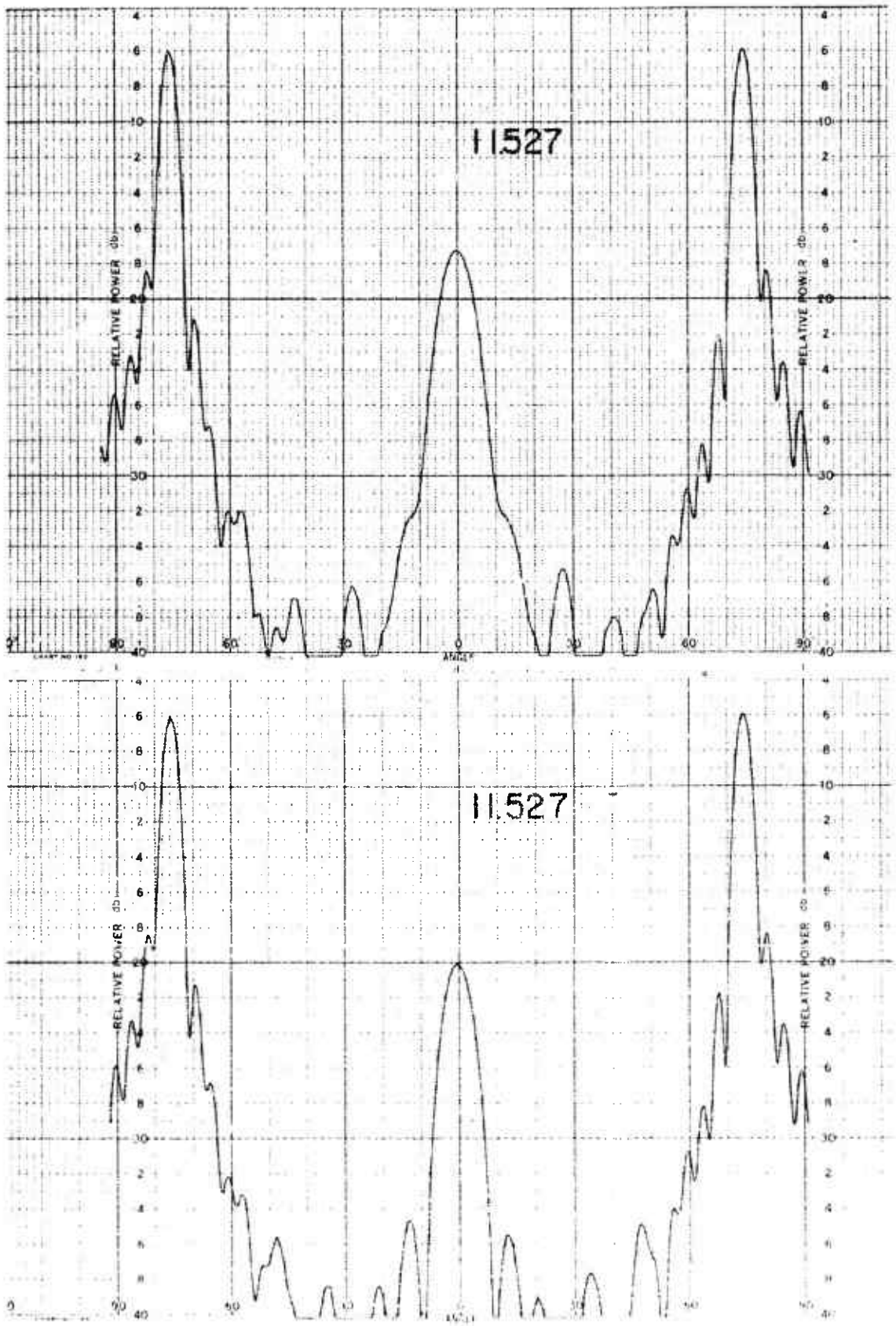
11527
RELATIVE POWER db
ANGLE
11.527
RELATIVE POWER db

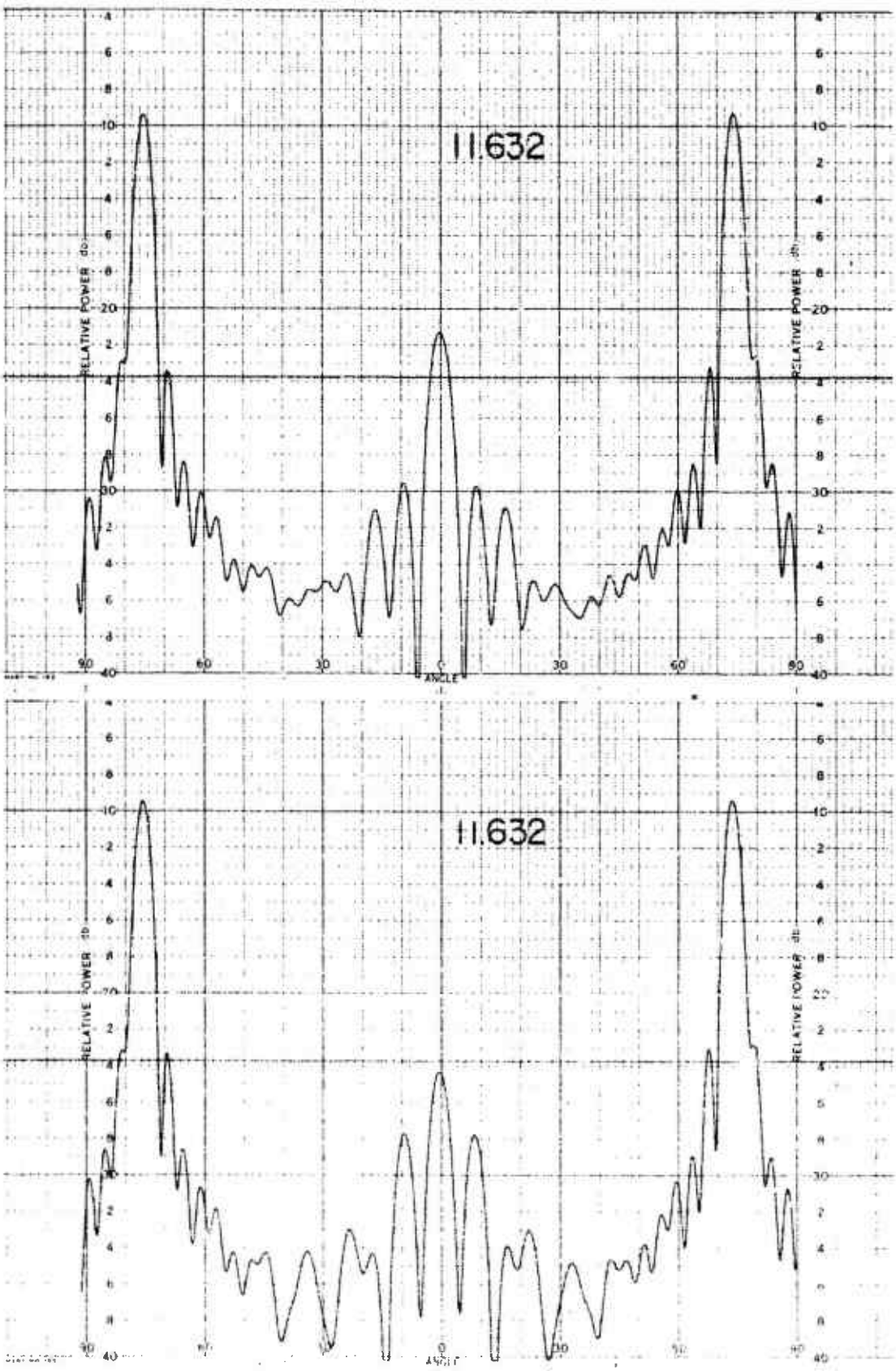
11.632
RELATIVE POWER dB
ANGLE
11.632
RELATIVE POWER dB

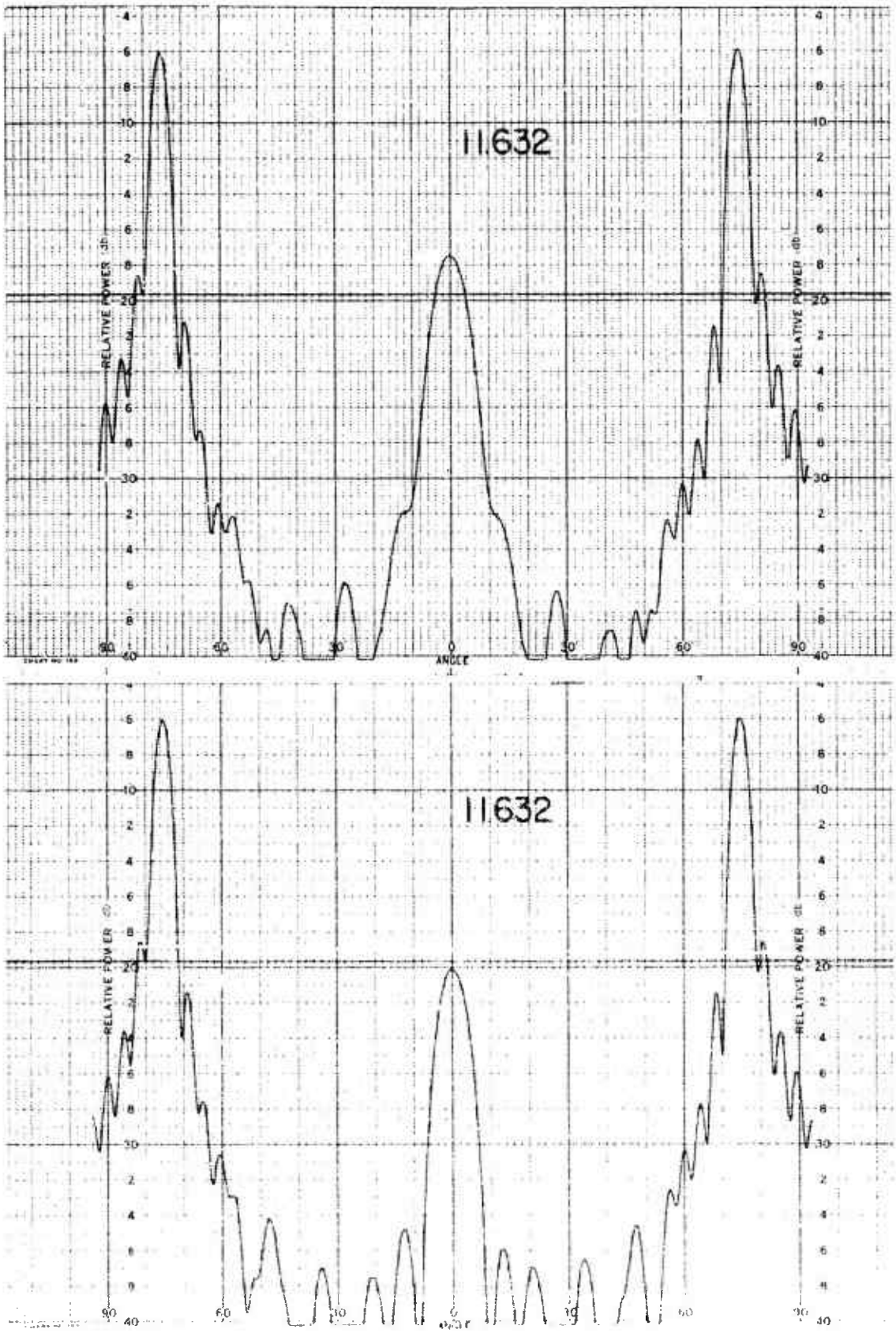
11.632
RELATIVE POWER
ANGLE
11.632
RELATIVE POWER

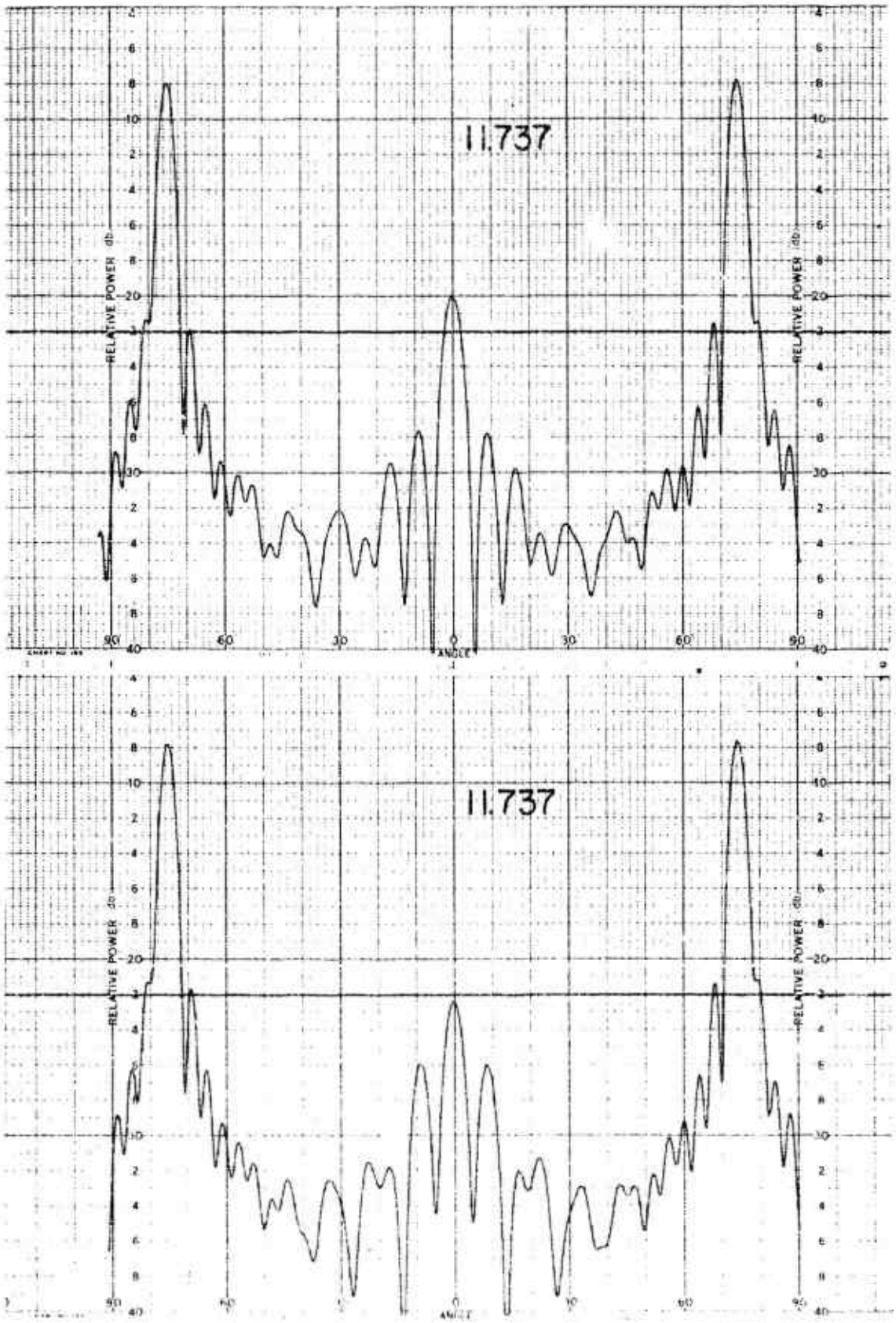
11.737
RELATIVE POWER db
ANGLE
11.737
RELATIVE POWER db
ANGLE

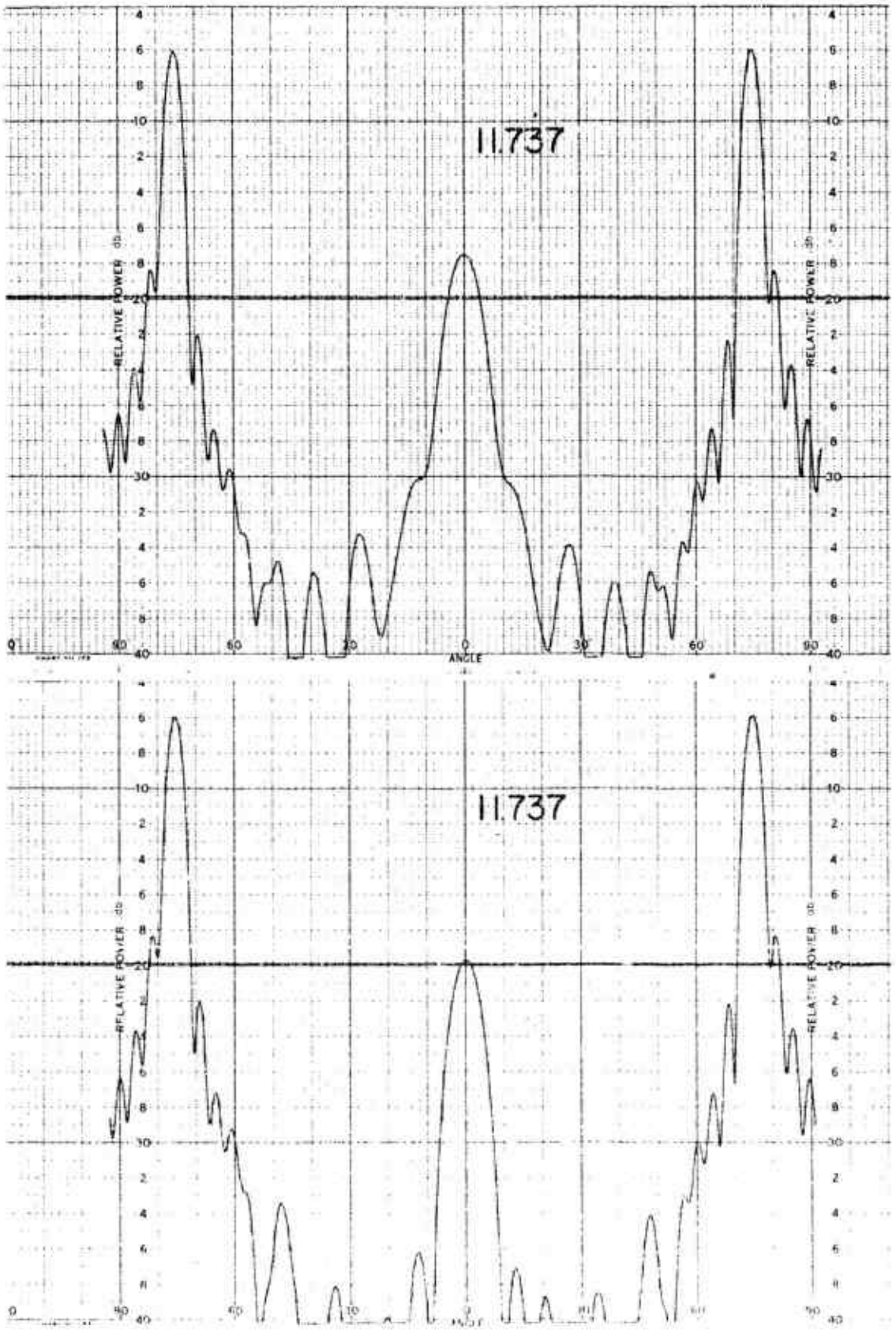
11.737
RELATIVE POWER db
ANGLE
11.737
RELATIVE POWER db

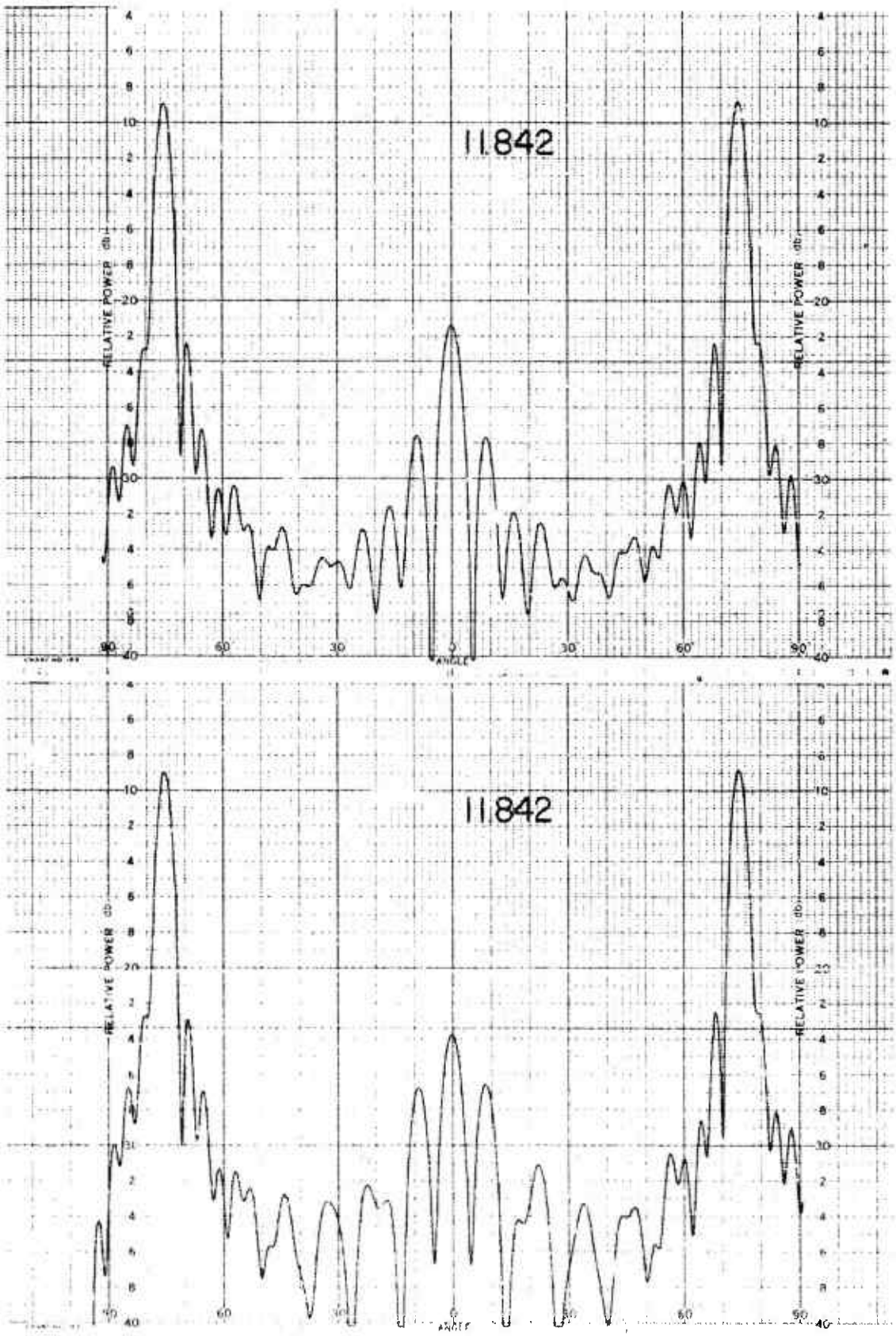
11.842
RELATIVE POWER db
ANGLE
11.842
RELATIVE POWER db
ANGLE

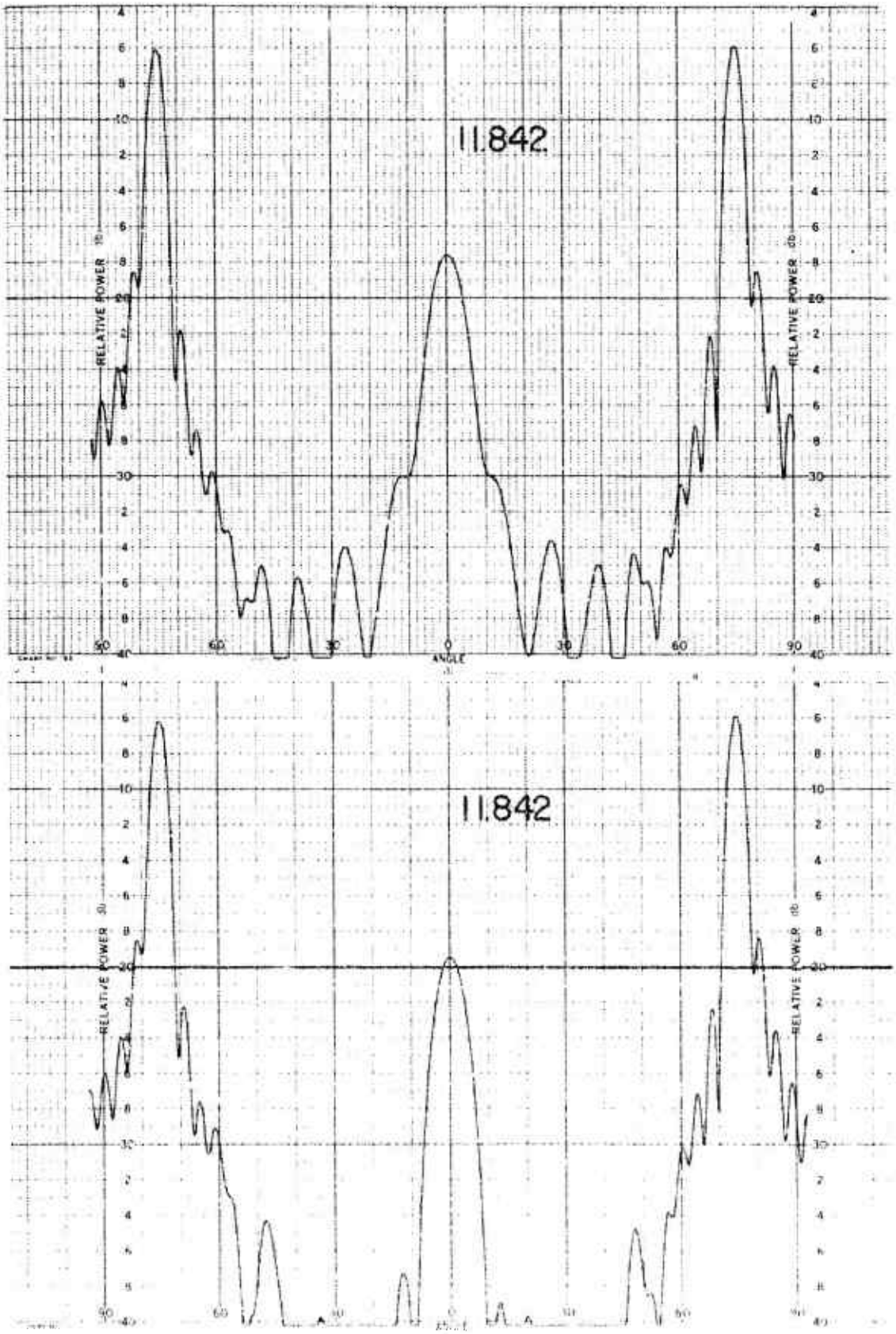
11.842
RELATIVE POWER db
ANGLE
11.842
RELATIVE POWER db

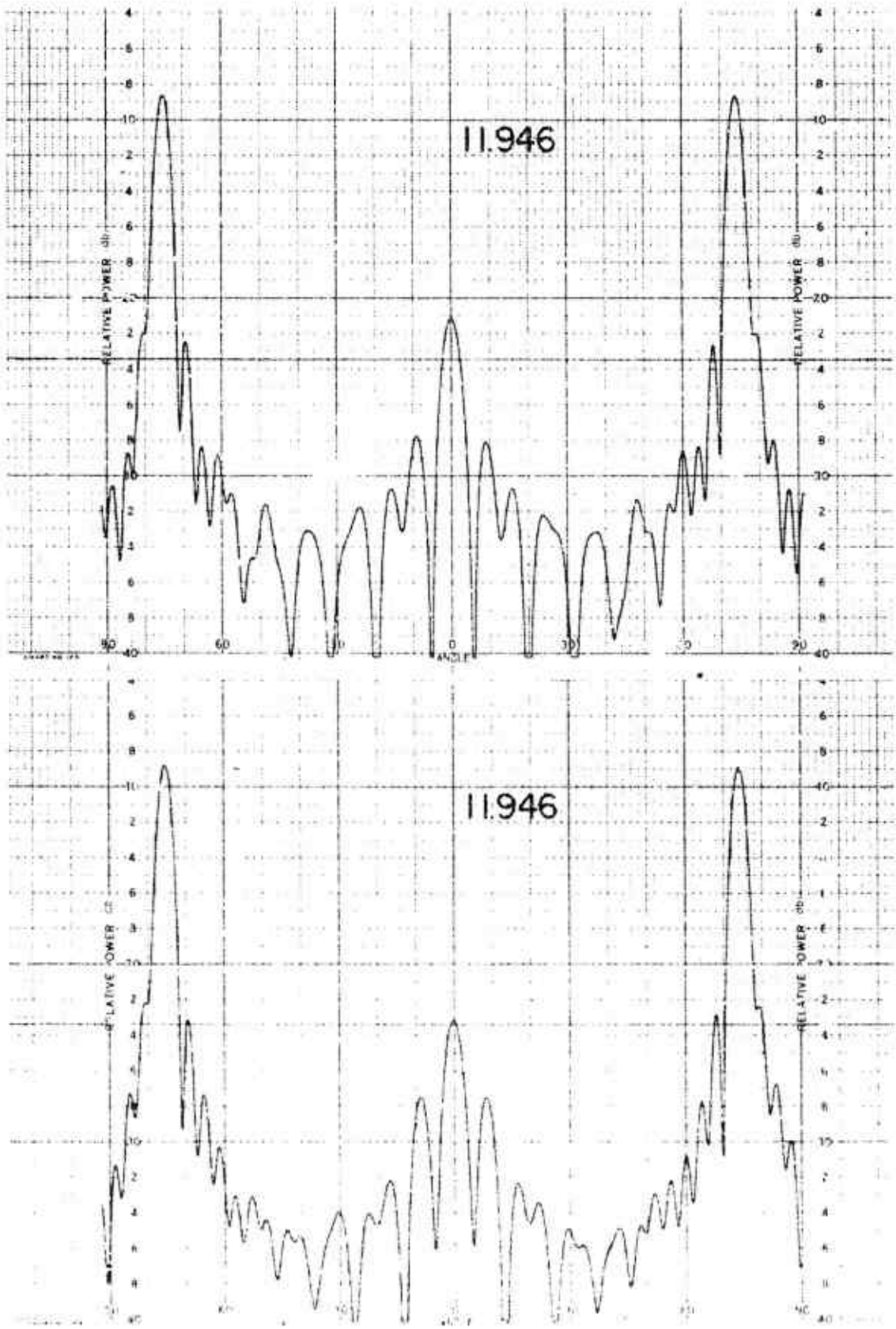
11.946
RELATIVE POWER db
ANGLE
11.946
RELATIVE POWER db

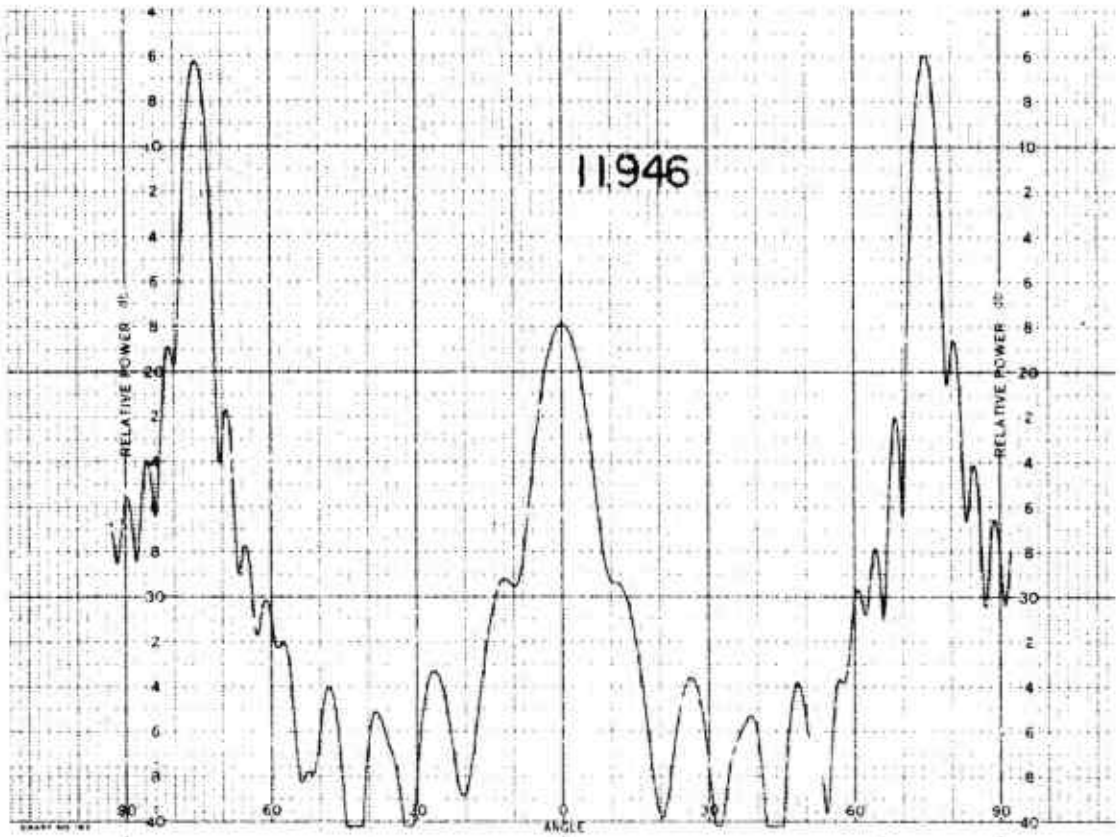
11.946
RELATIVE POWER dB
ANGLE

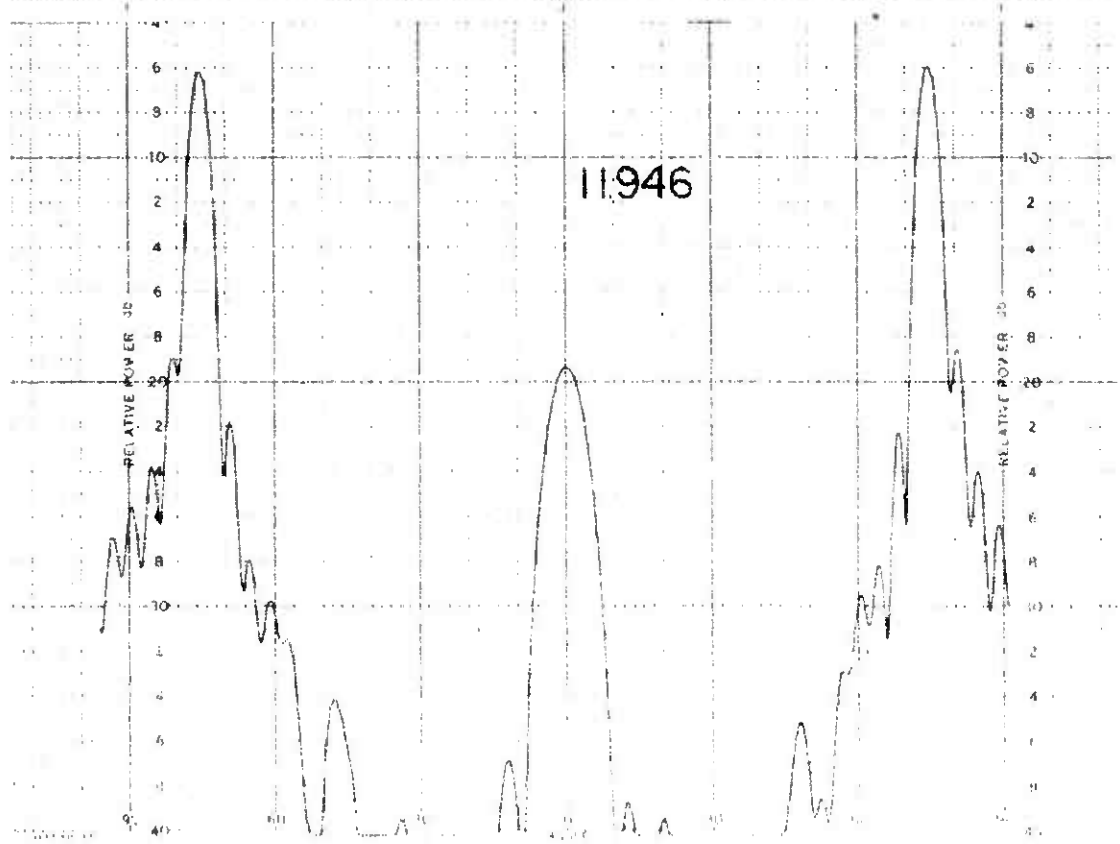
11.946
RELATIVE POWER dB

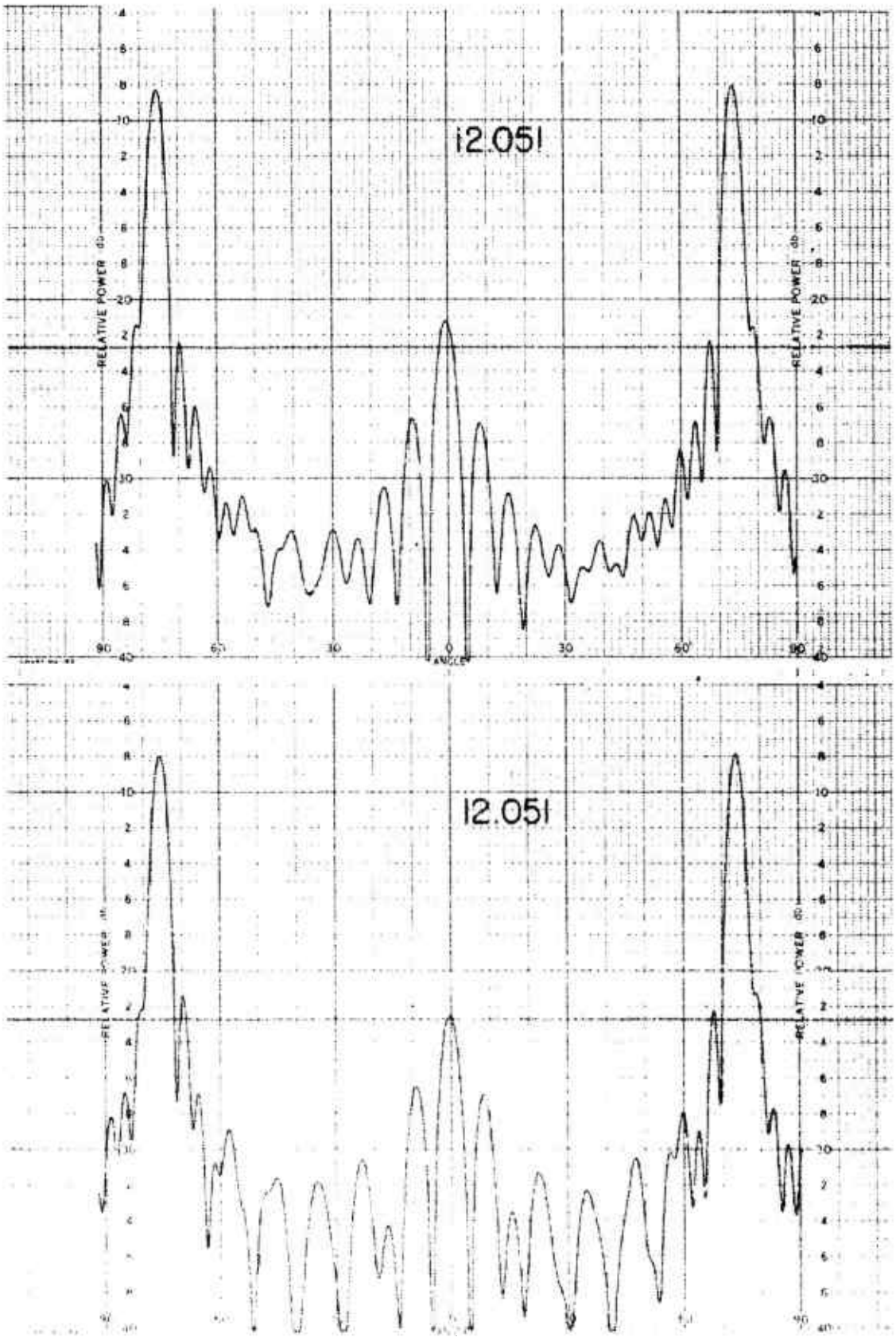
12.051
RELATIVE POWER dB
12.051
RELATIVE POWER dB

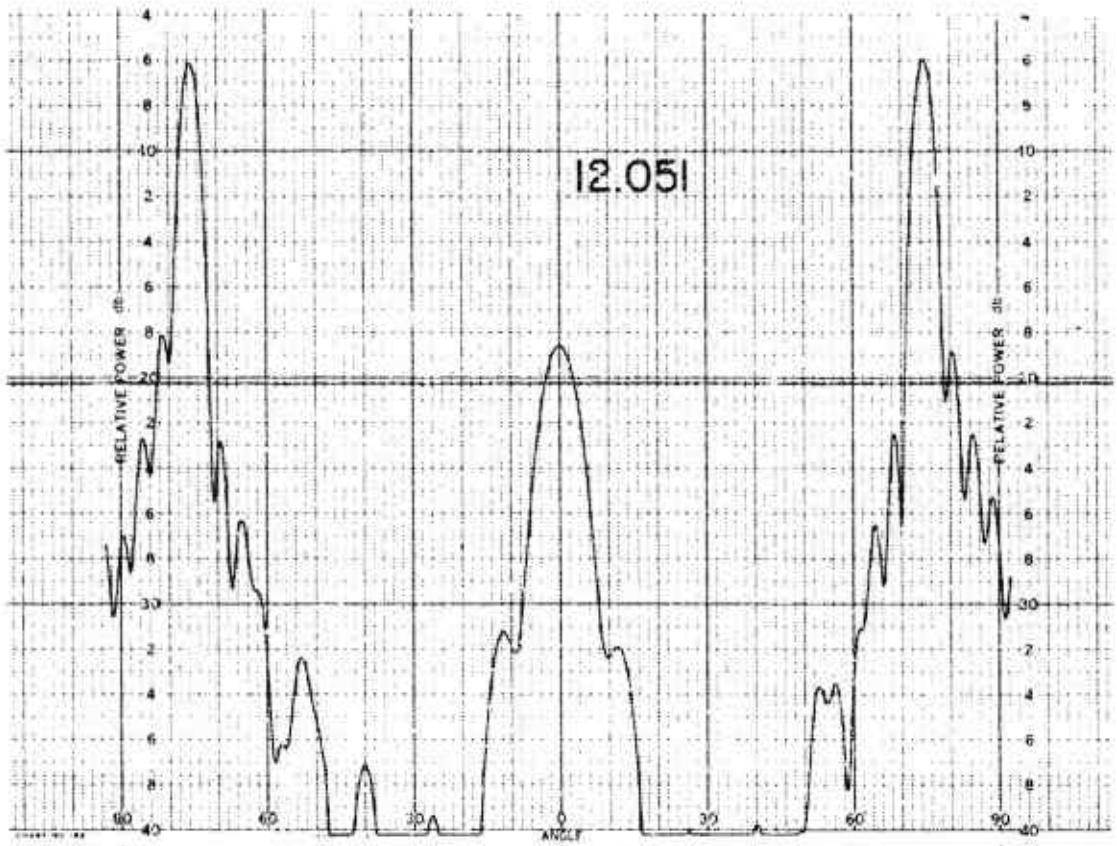
12.051
RELATIVE POWER dB
ANGLE

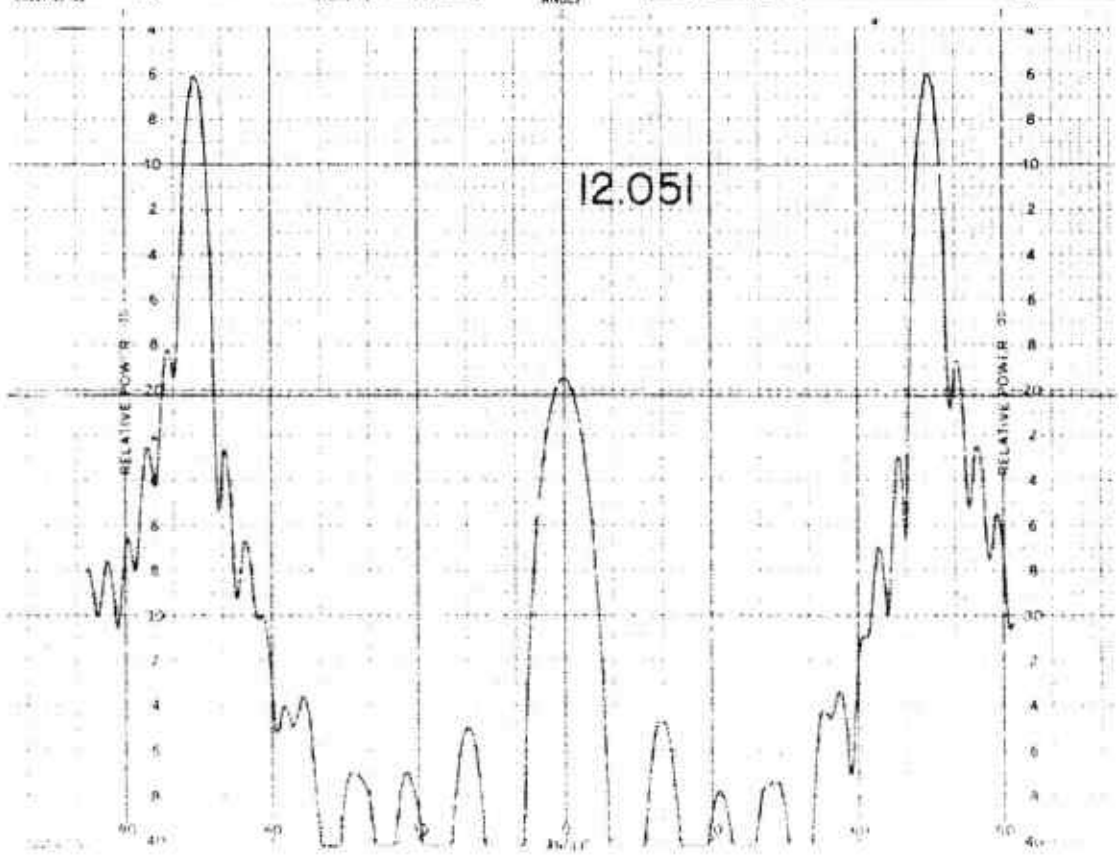
12.051
RELATIVE POWER dB
ANGLE

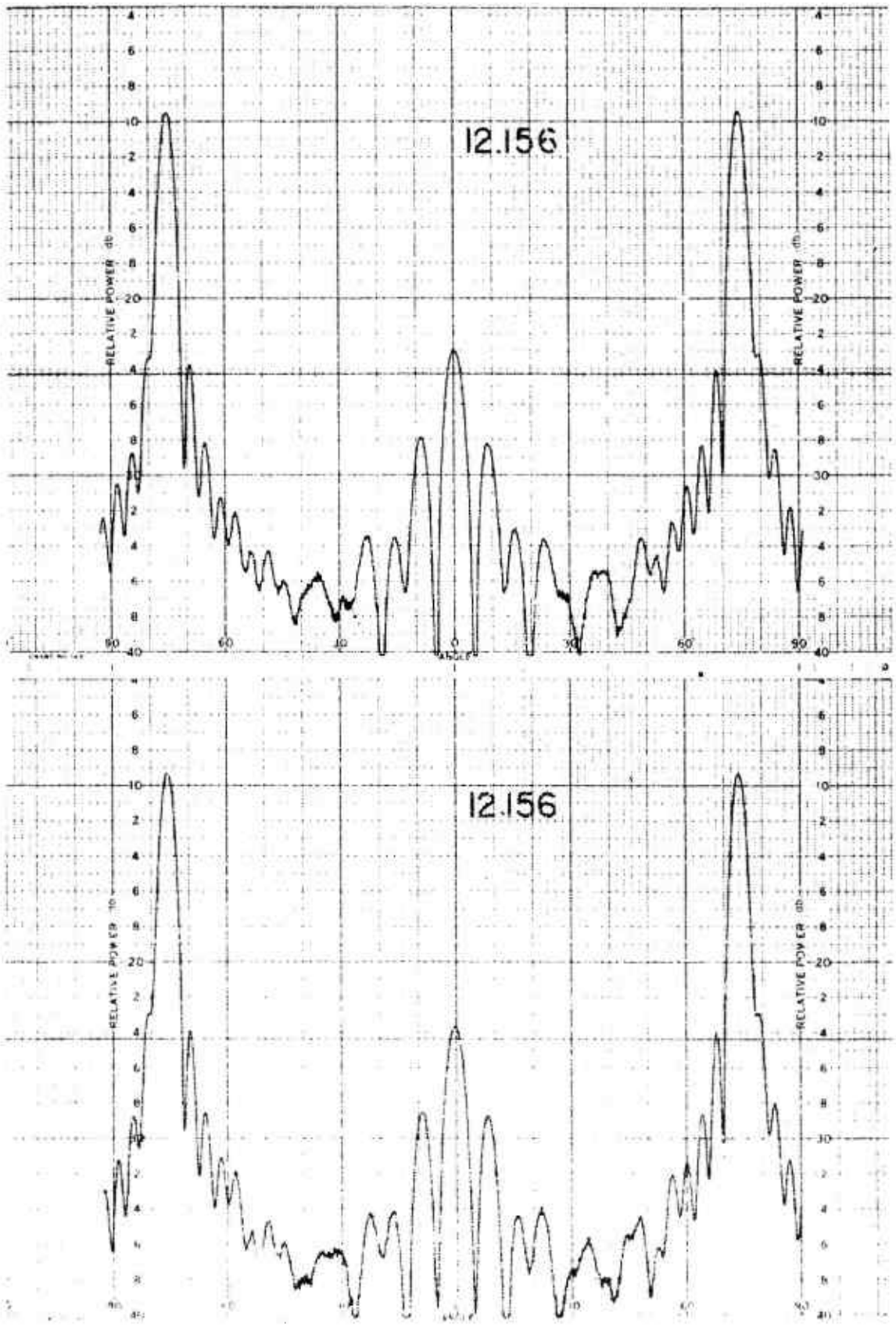
12.156
RELATIVE POWER db
12.156
RELATIVE POWER db

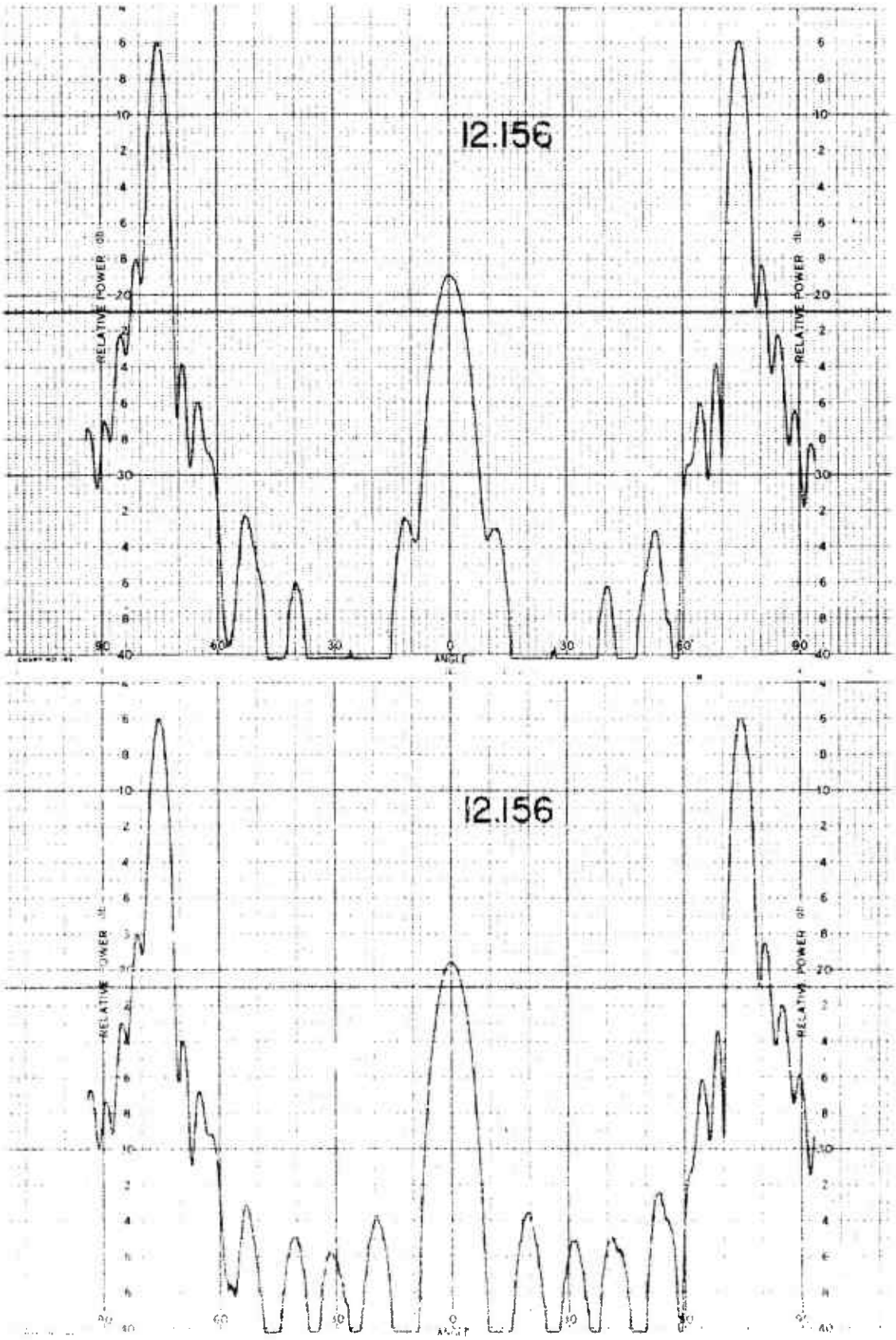
12.156
RELATIVE POWER dB
ANGLE
12.156
RELATIVE POWER dB
ANGLE

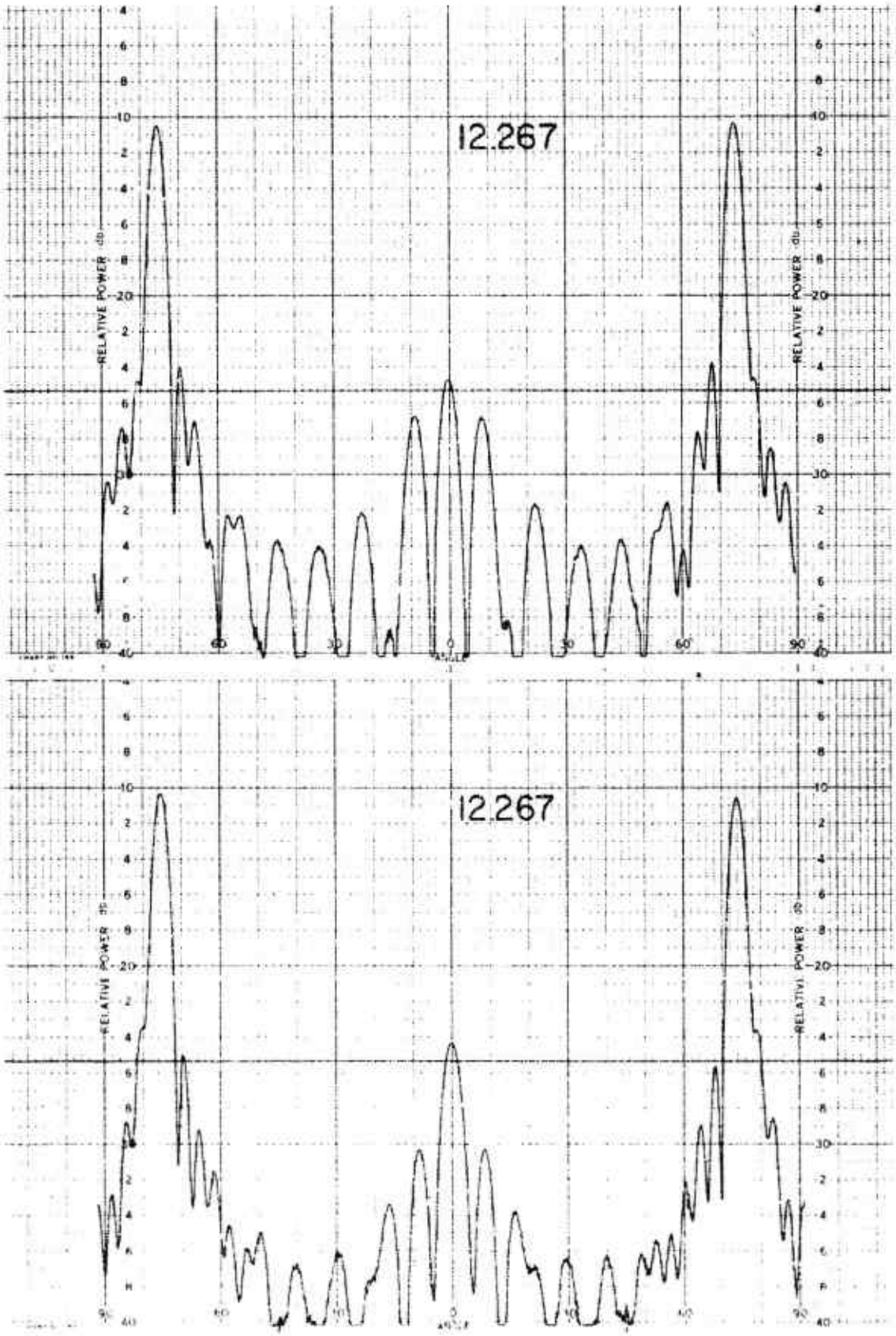
12.267
RELATIVE POWER dB
12.267
RELATIVE POWER dB

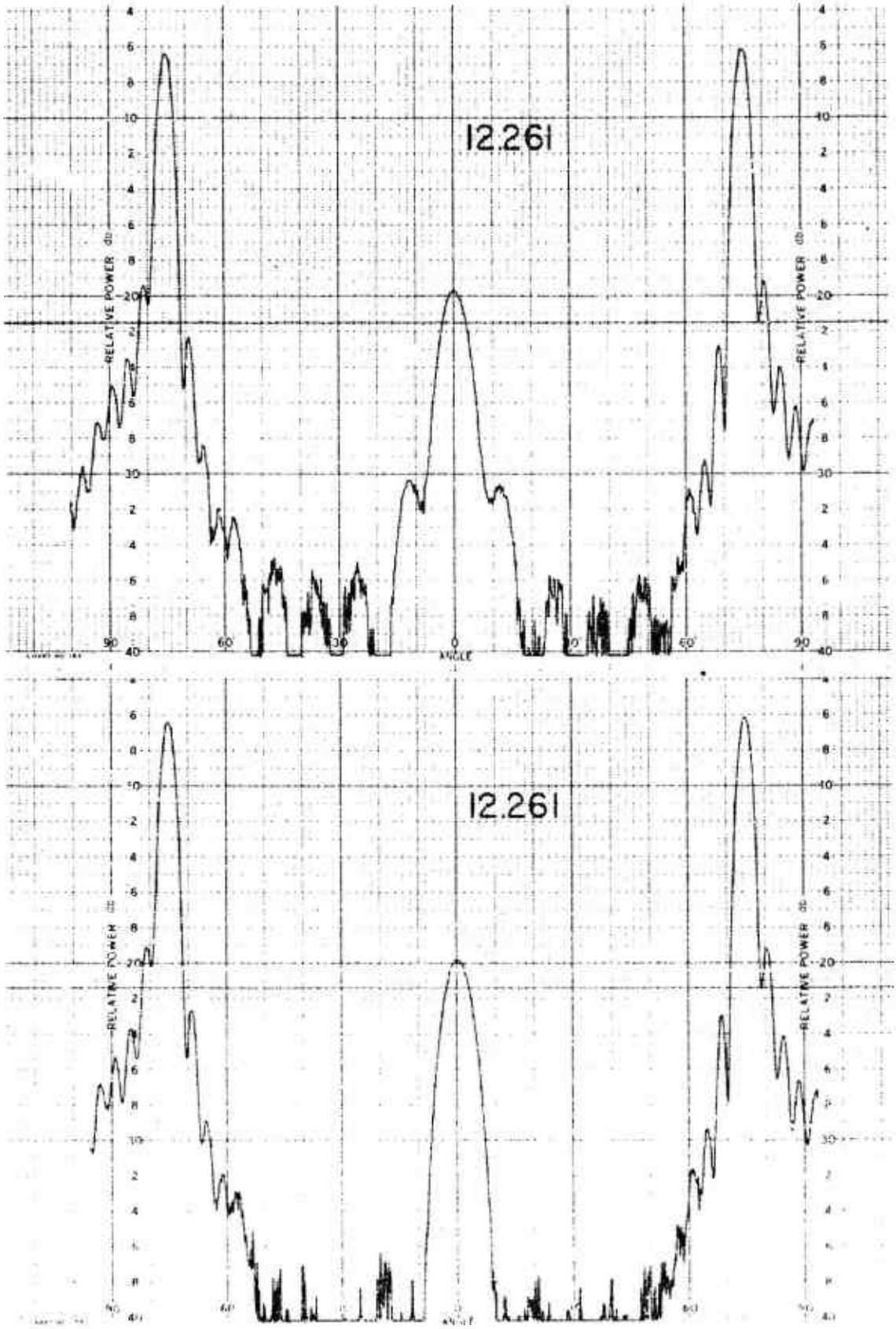
12.261
RELATIVE POWER dB
ANGLE
12.261
RELATIVE POWER dB

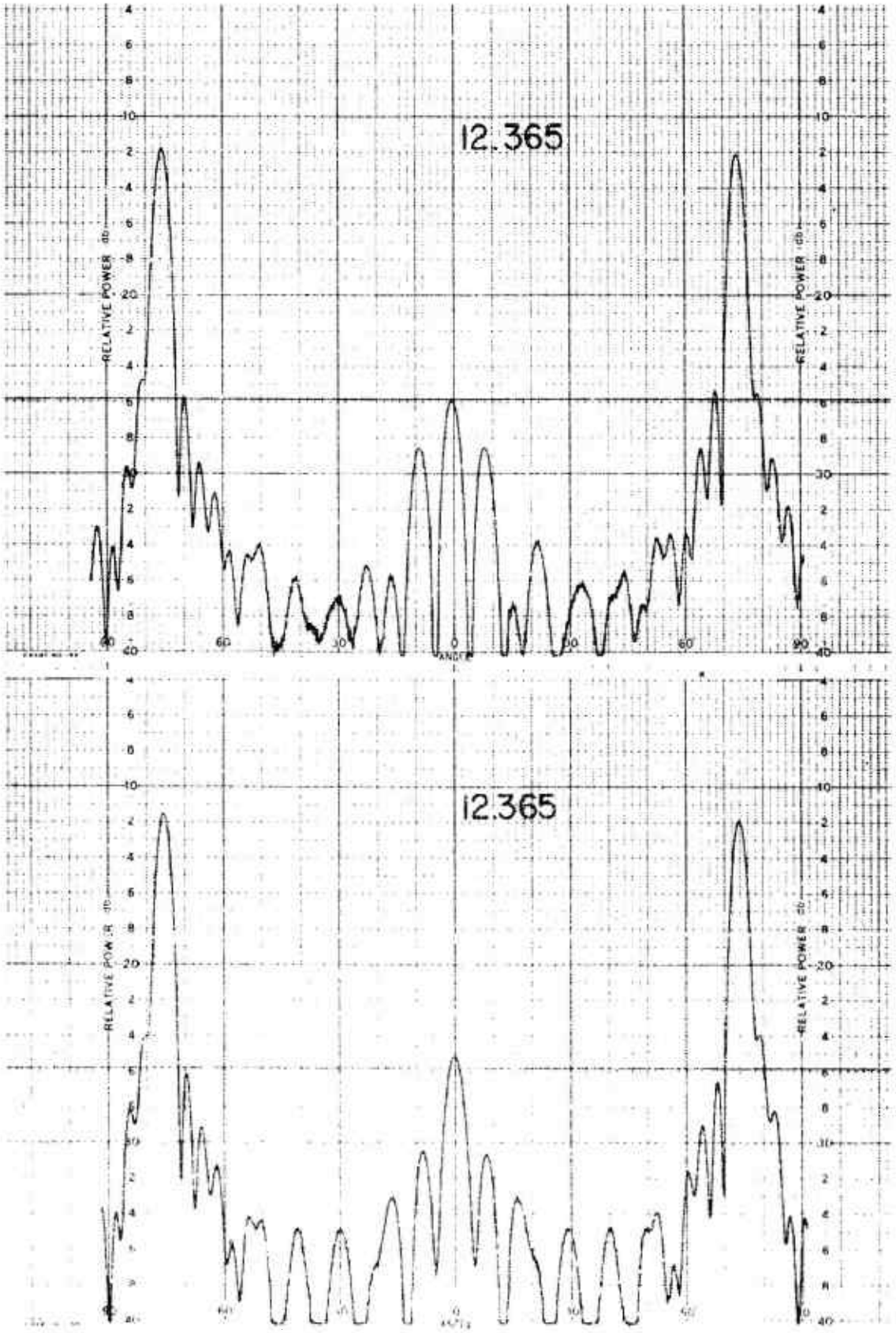
12.365
RELATIVE POWER db
12.365
RELATIVE POWER db

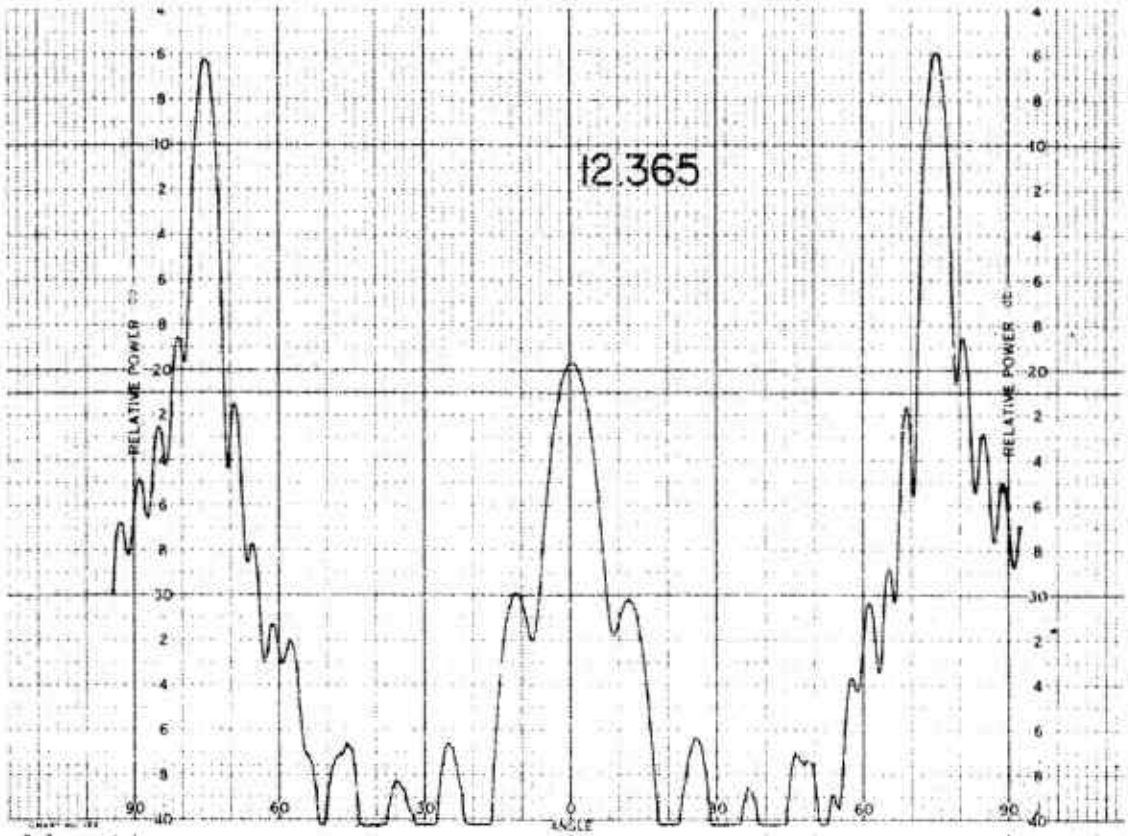
12.365
RELATIVE POWER dB
ANGLE

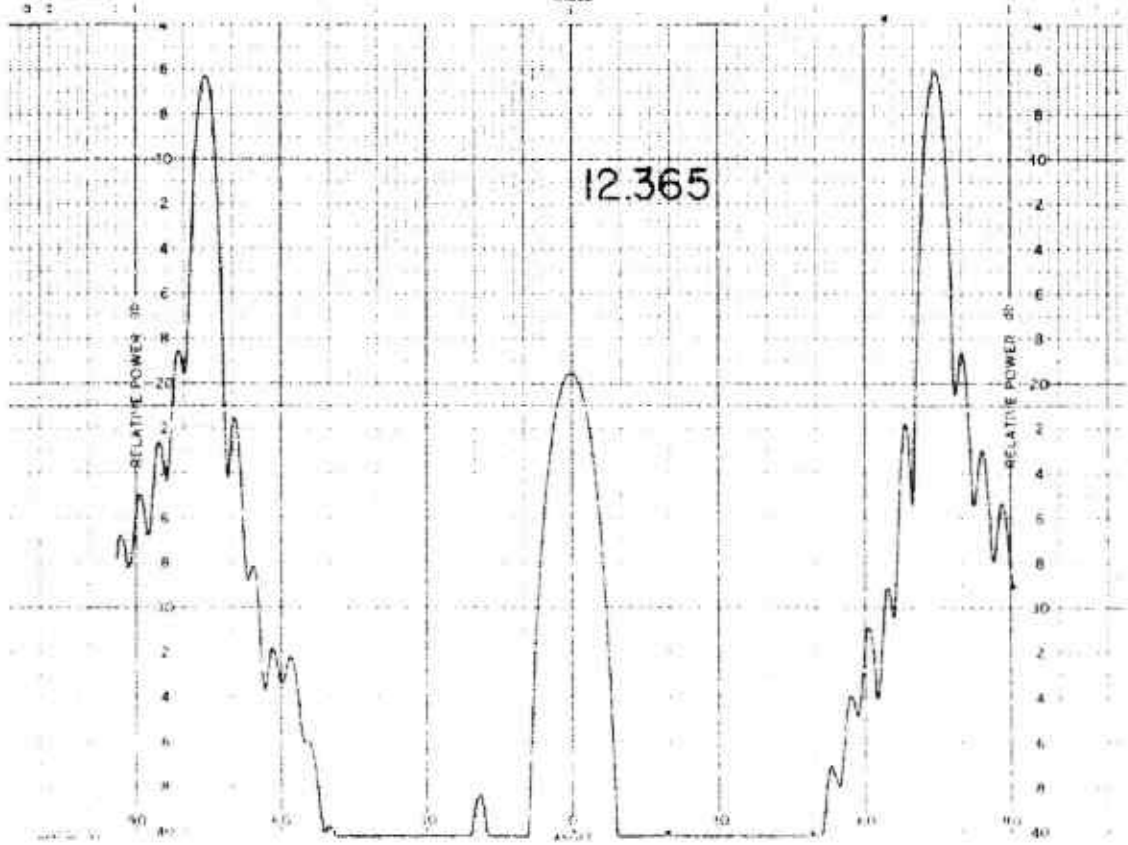
12.365
RELATIVE POWER dB

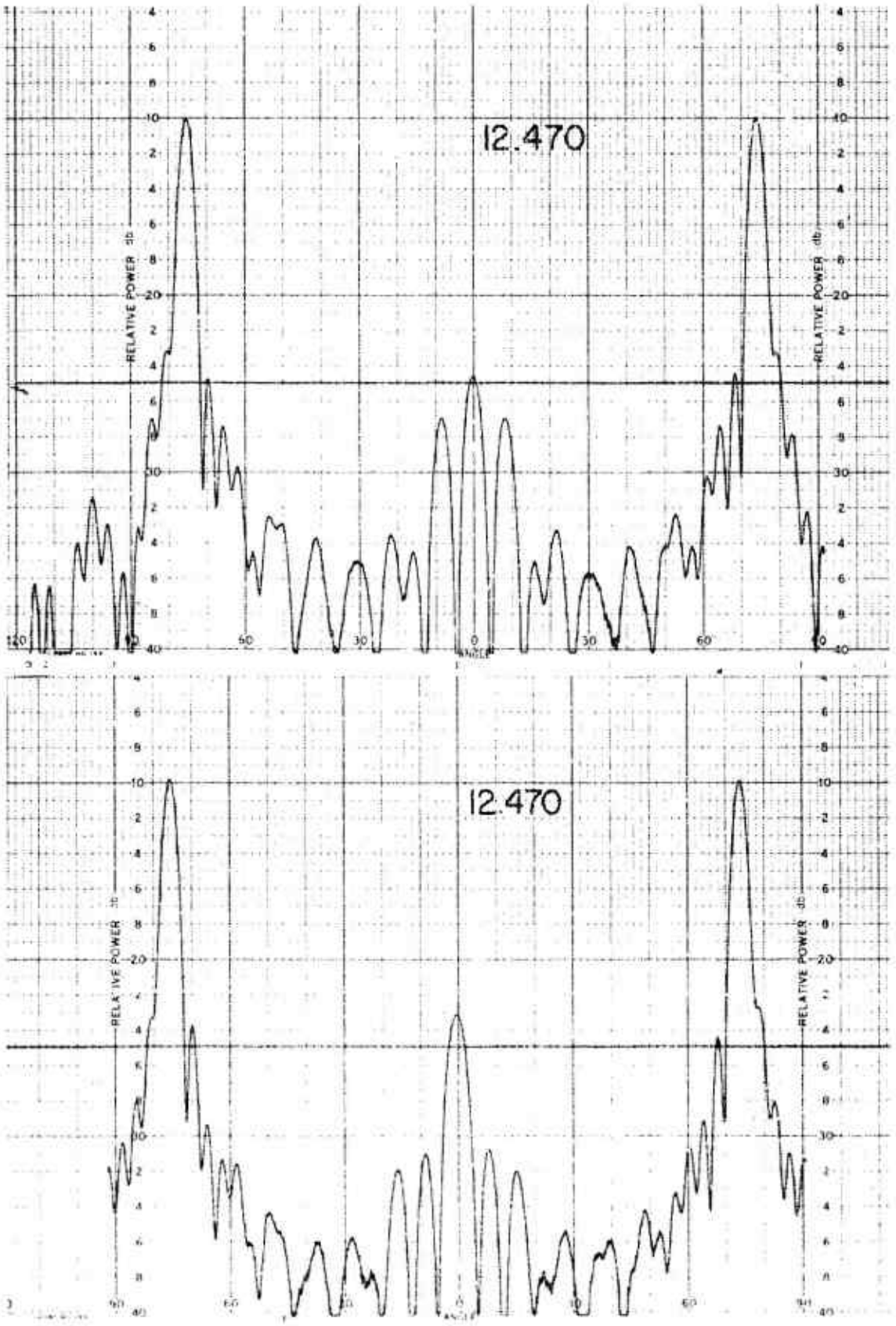
12.470
RELATIVE POWER db
12.470
RELATIVE POWER db

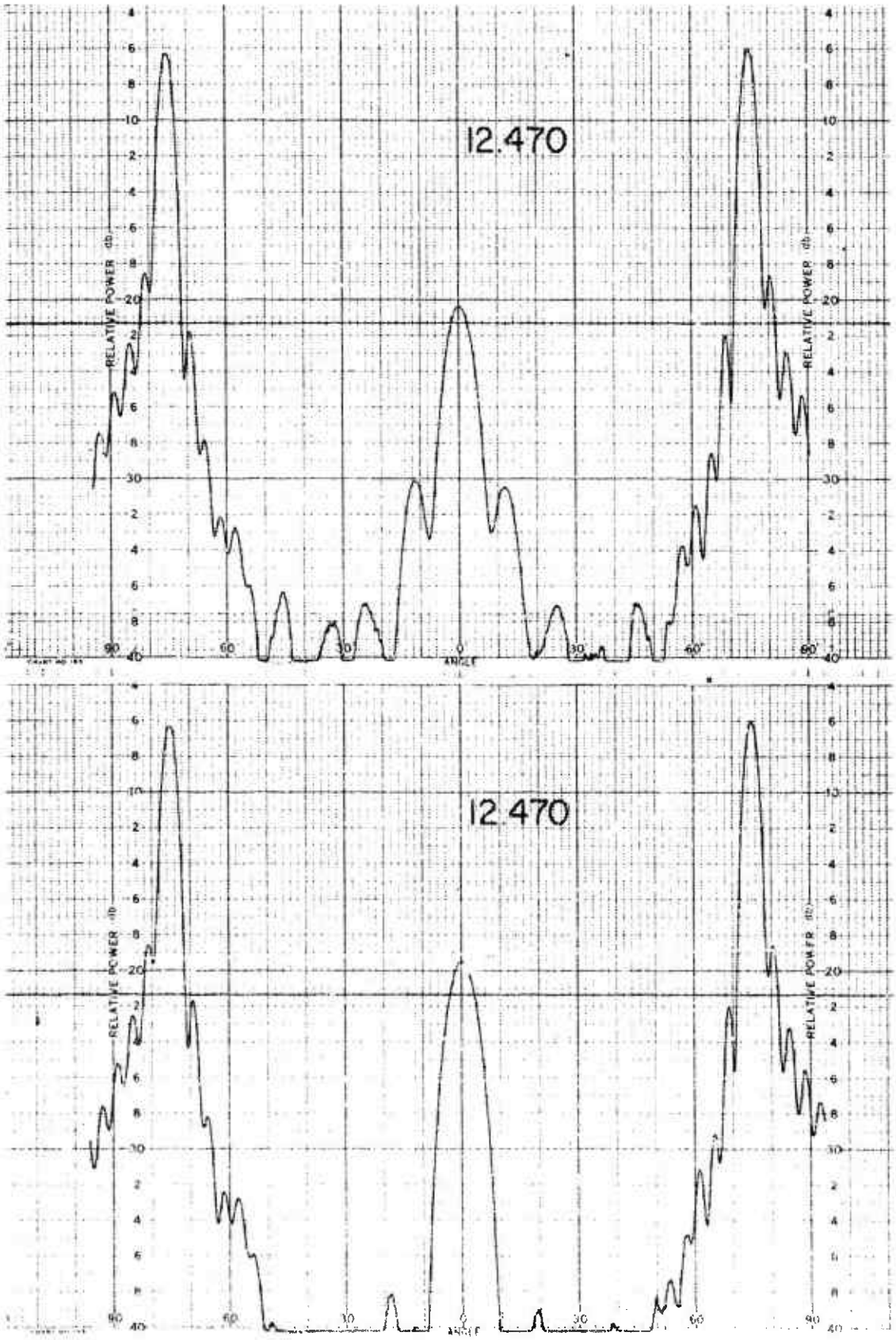
12.470
RELATIVE POWER db
ANGLE
12.470
RELATIVE POWER db
ANGLE

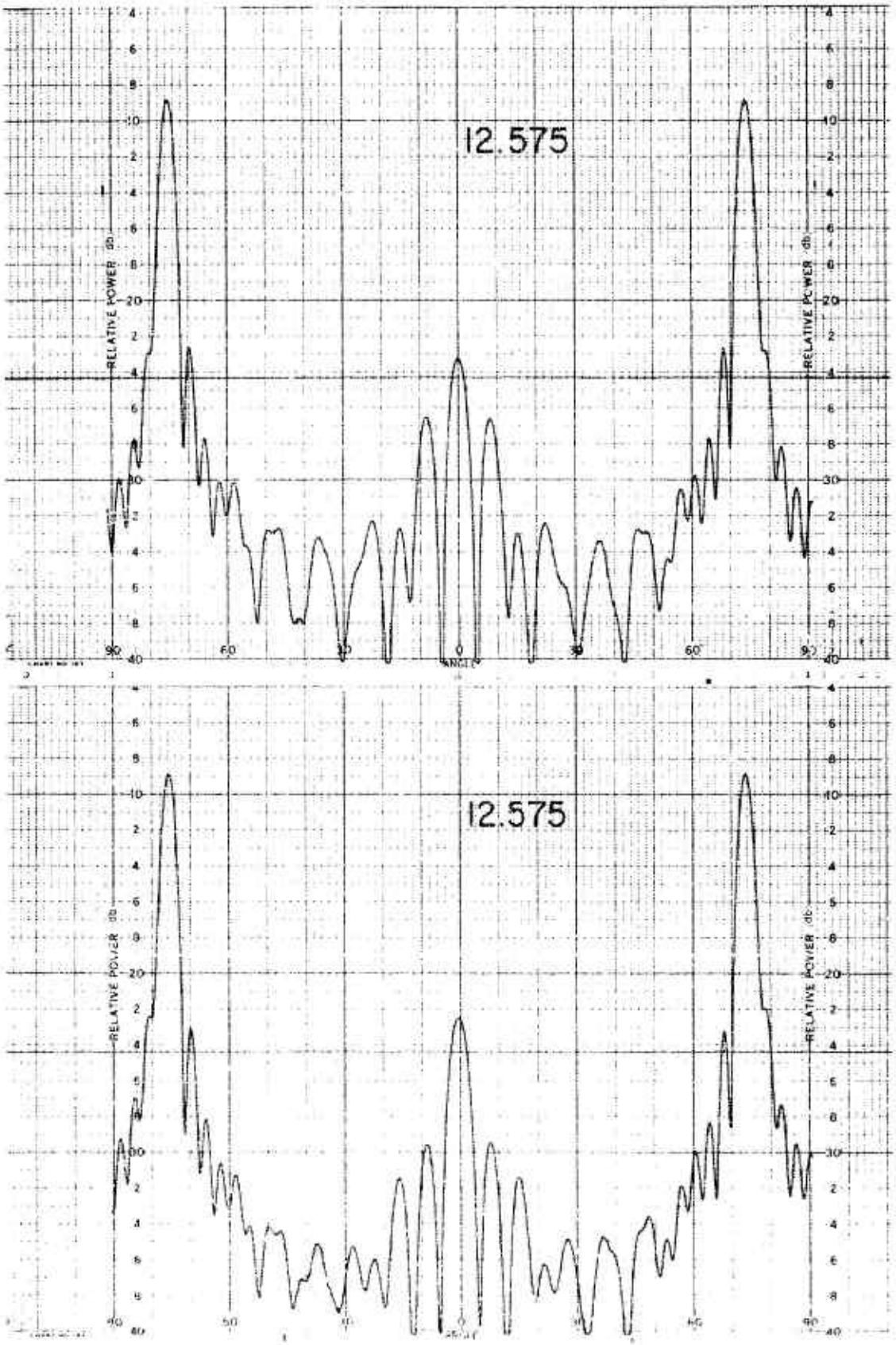
12.575
RELATIVE POWER db
12.575
RELATIVE POWER db

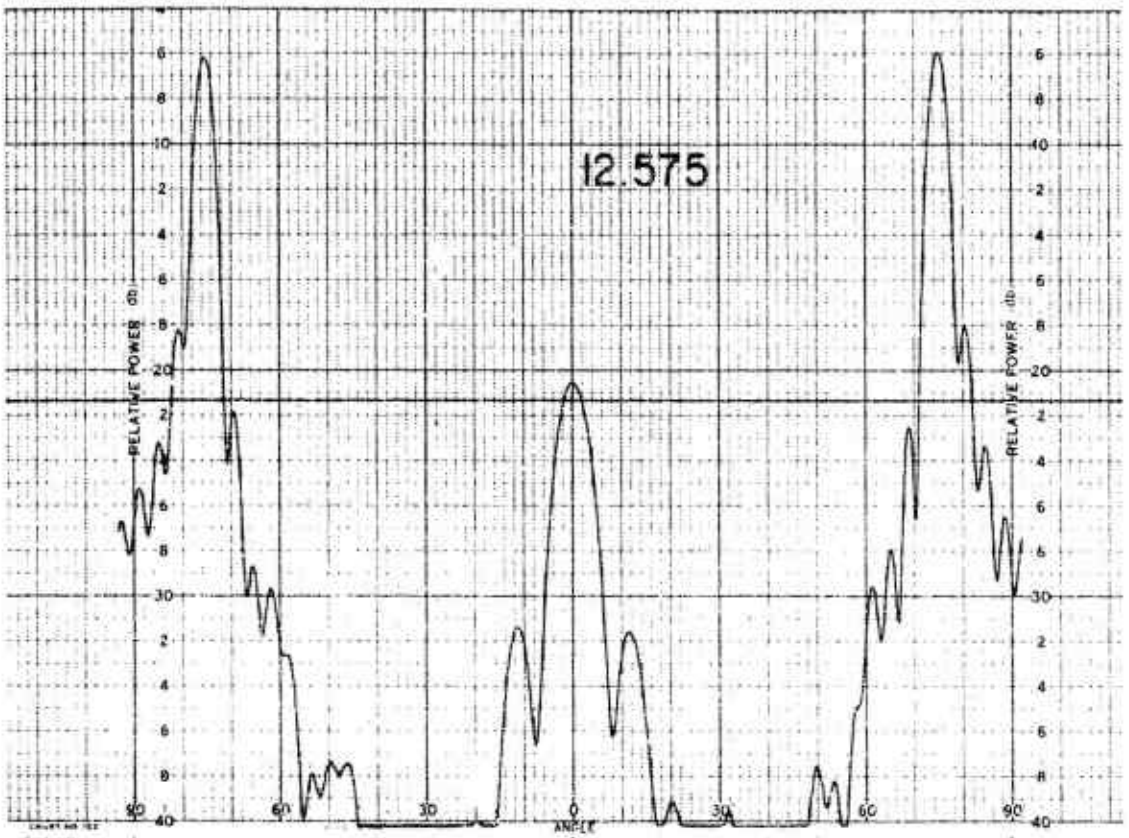
12.575
RELATIVE POWER db
ANGLE

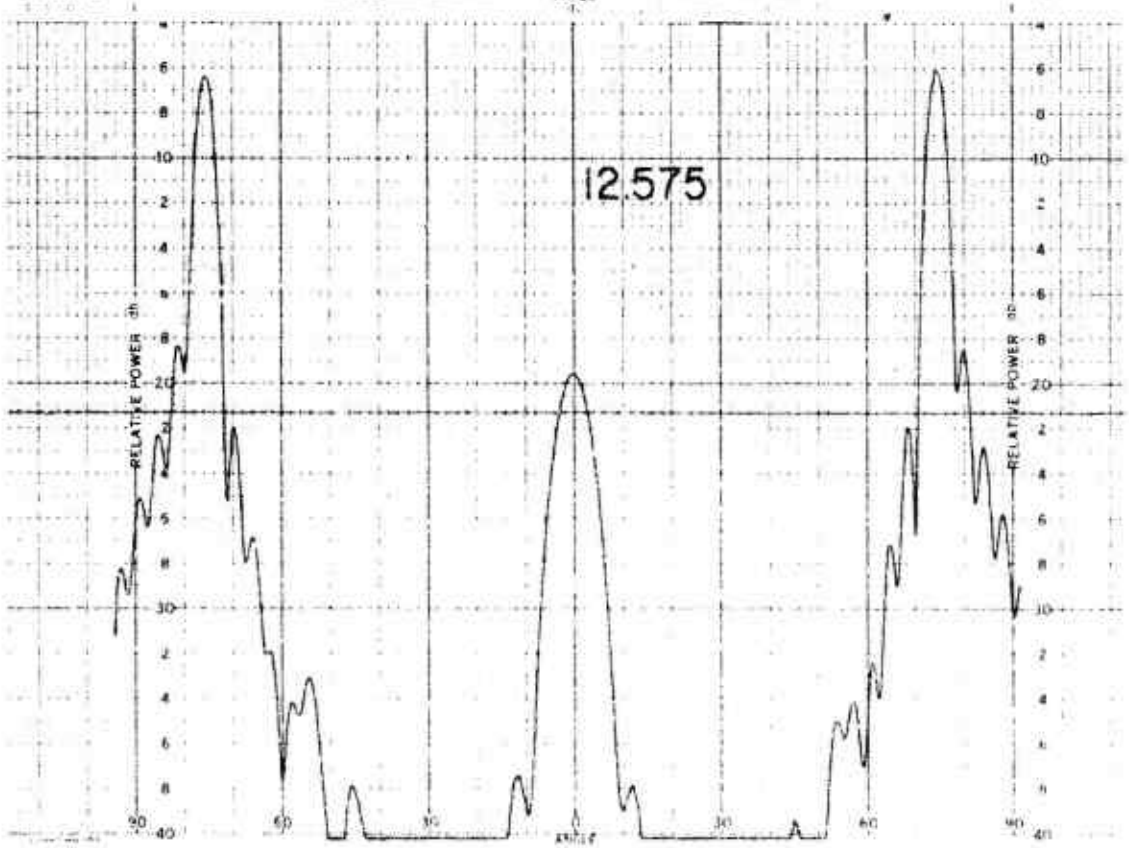
12.575
RELATIVE POWER db
ANGLE

40^{O} CONE


12.798
RELATIVE POWER (db)
ANGLE

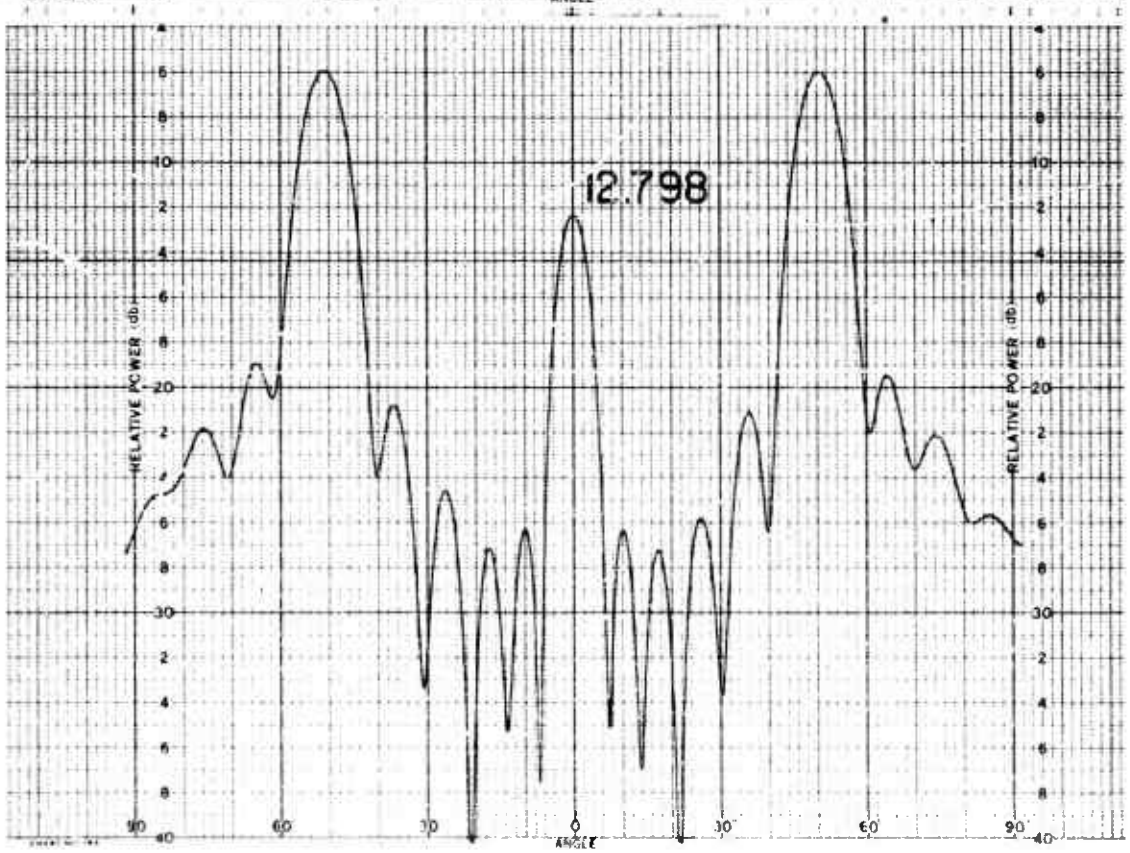
12.798
RELATIVE POWER (db)
ANGLE

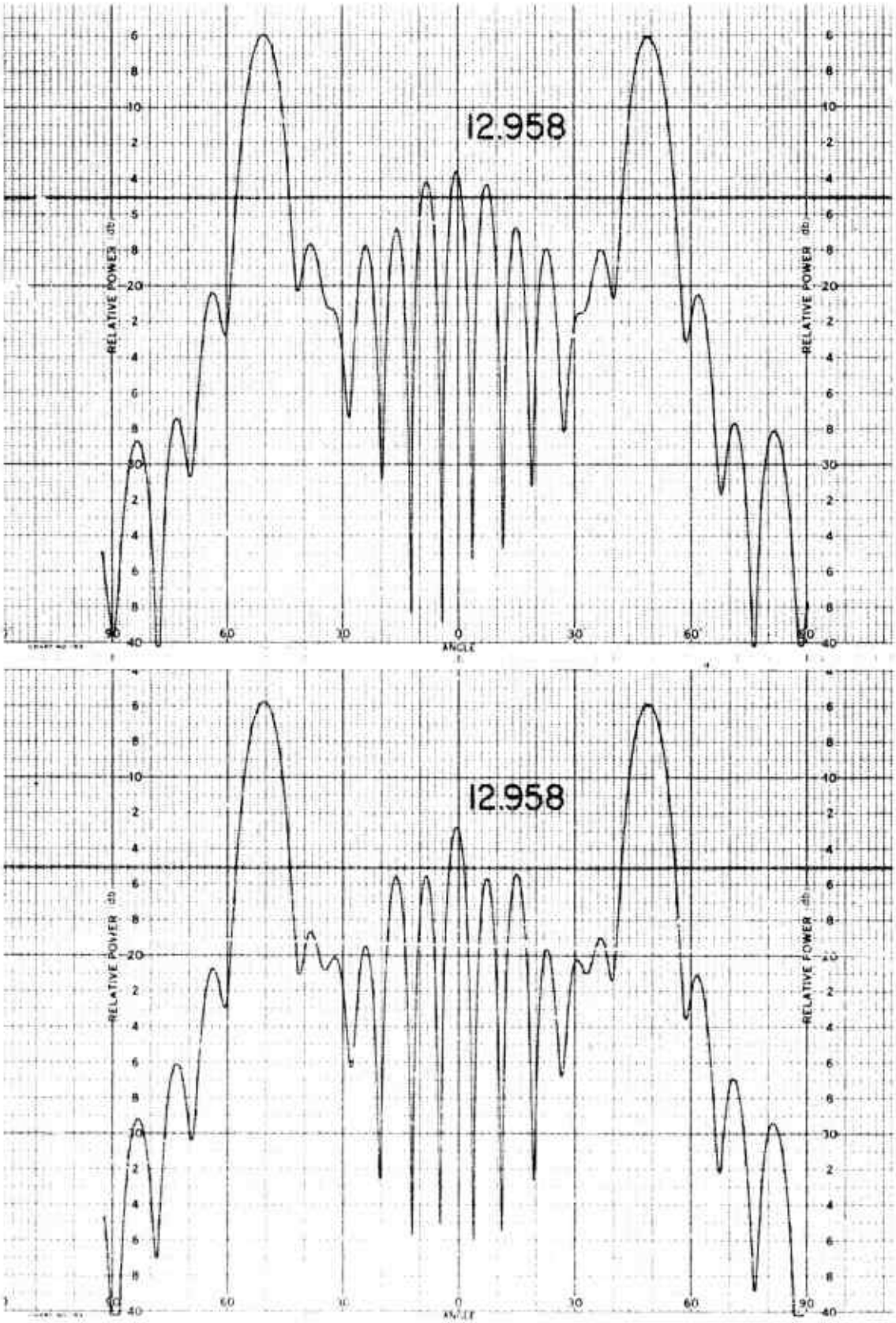
12.958
RELATIVE POWER (db)
ANGLE
12.958
RELATIVE POWER (db)
ANGLE

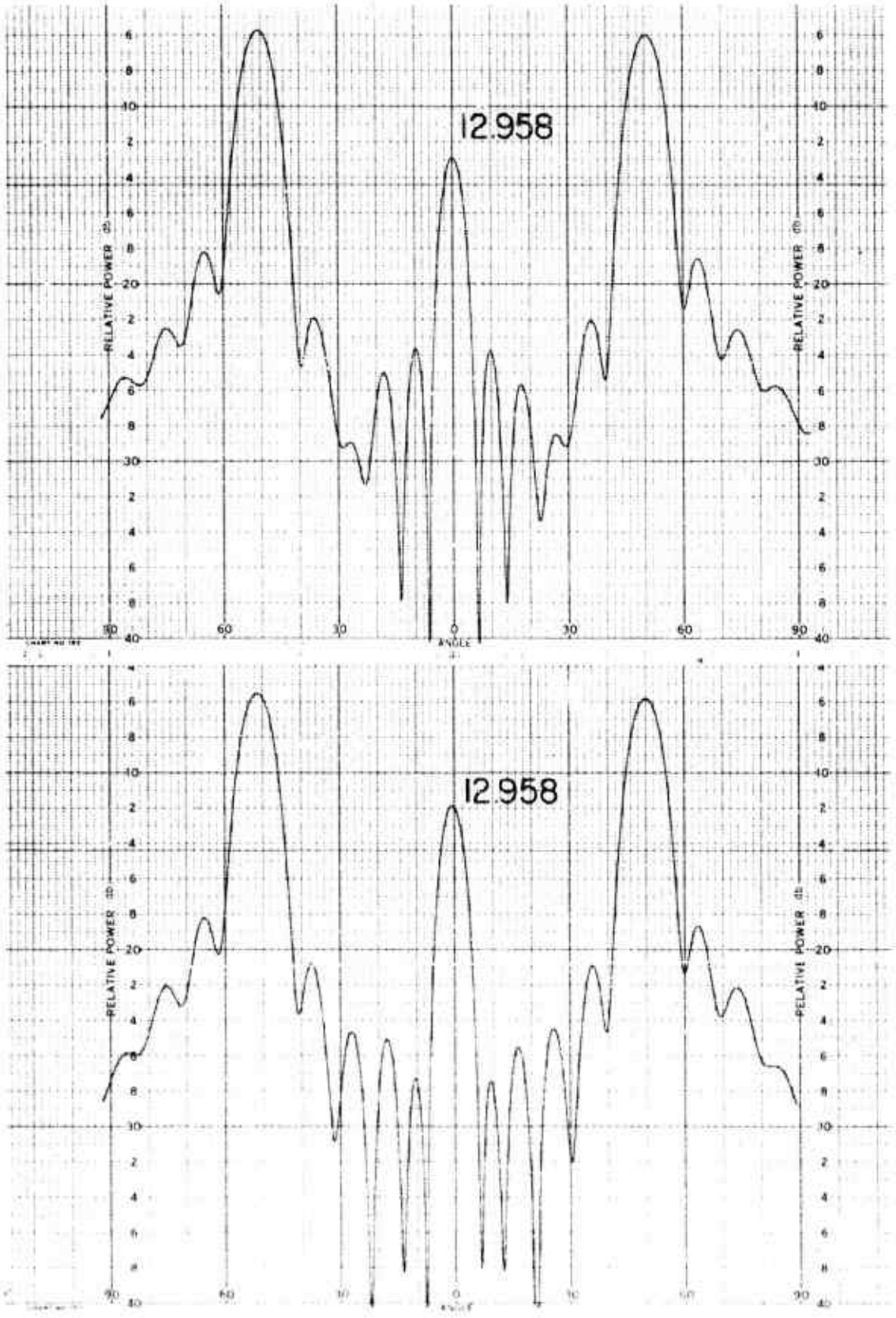
12.958
RELATIVE POWER (db)
ANGLE
12.958
RELATIVE POWER (db)

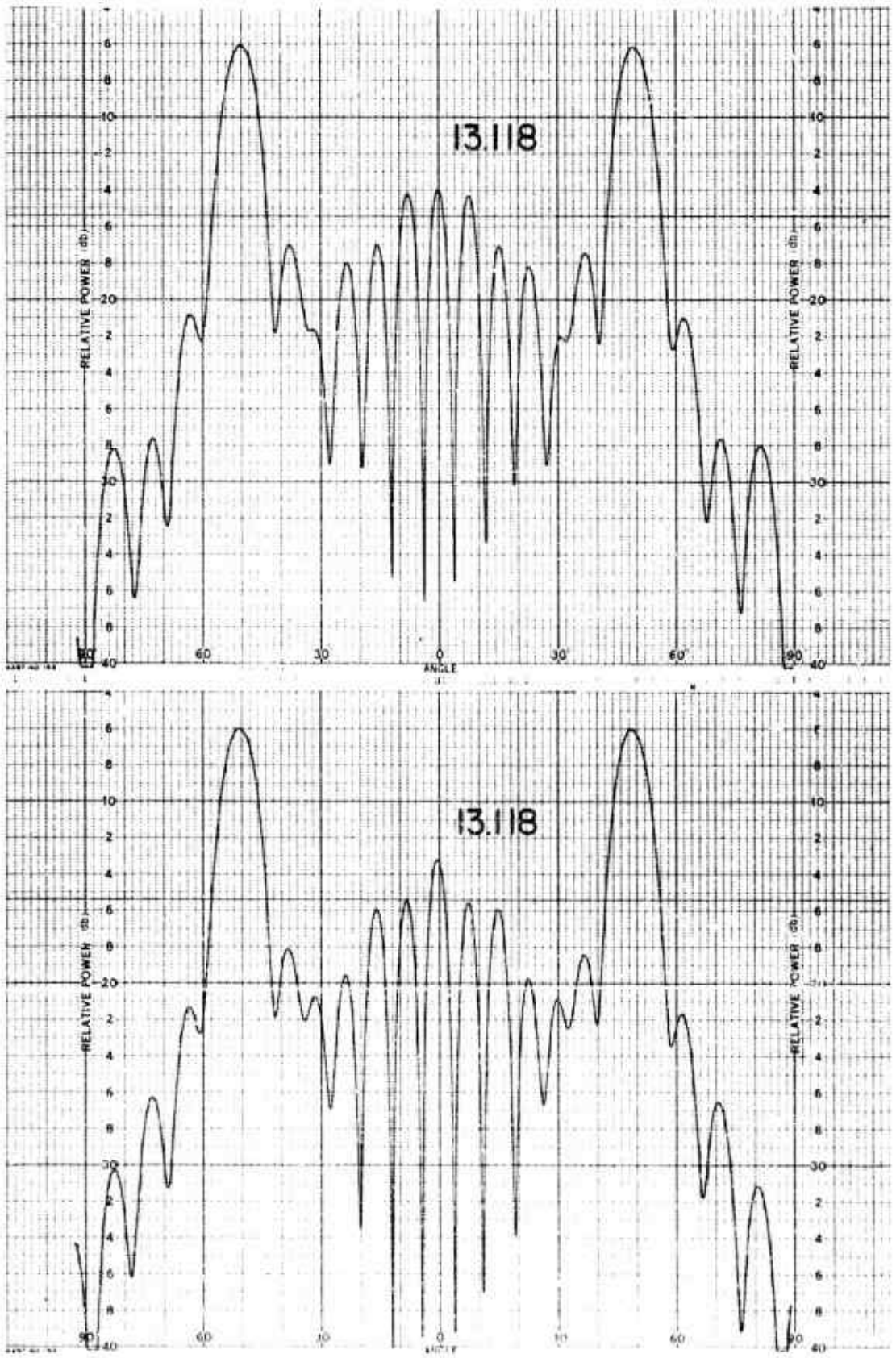
13.118
RELATIVE POWER (db)
ANGLE
13.118
RELATIVE POWER (db)

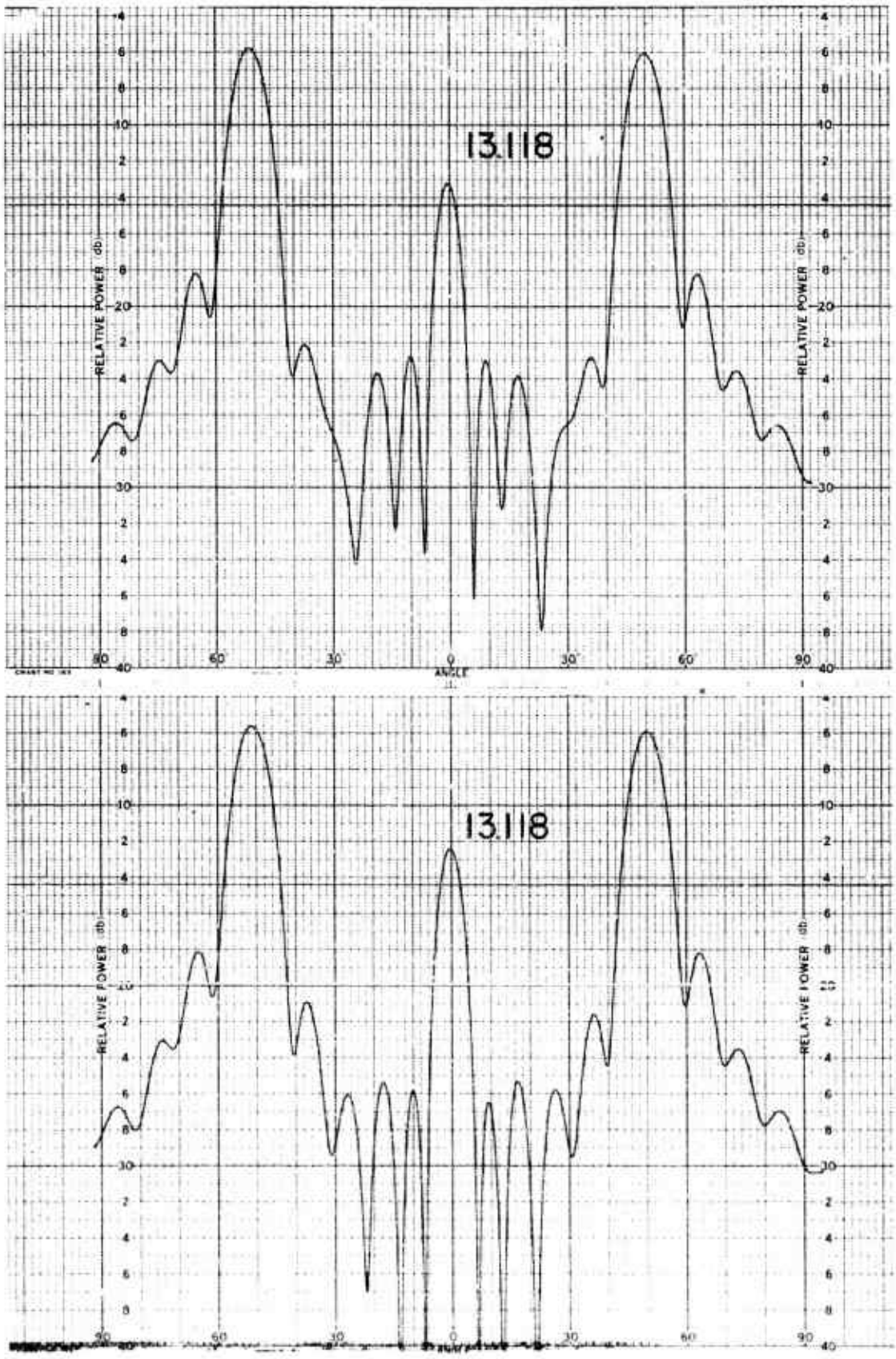
13.118
RELATIVE POWER (db)
ANGLE
13.118
RELATIVE POWER (db)

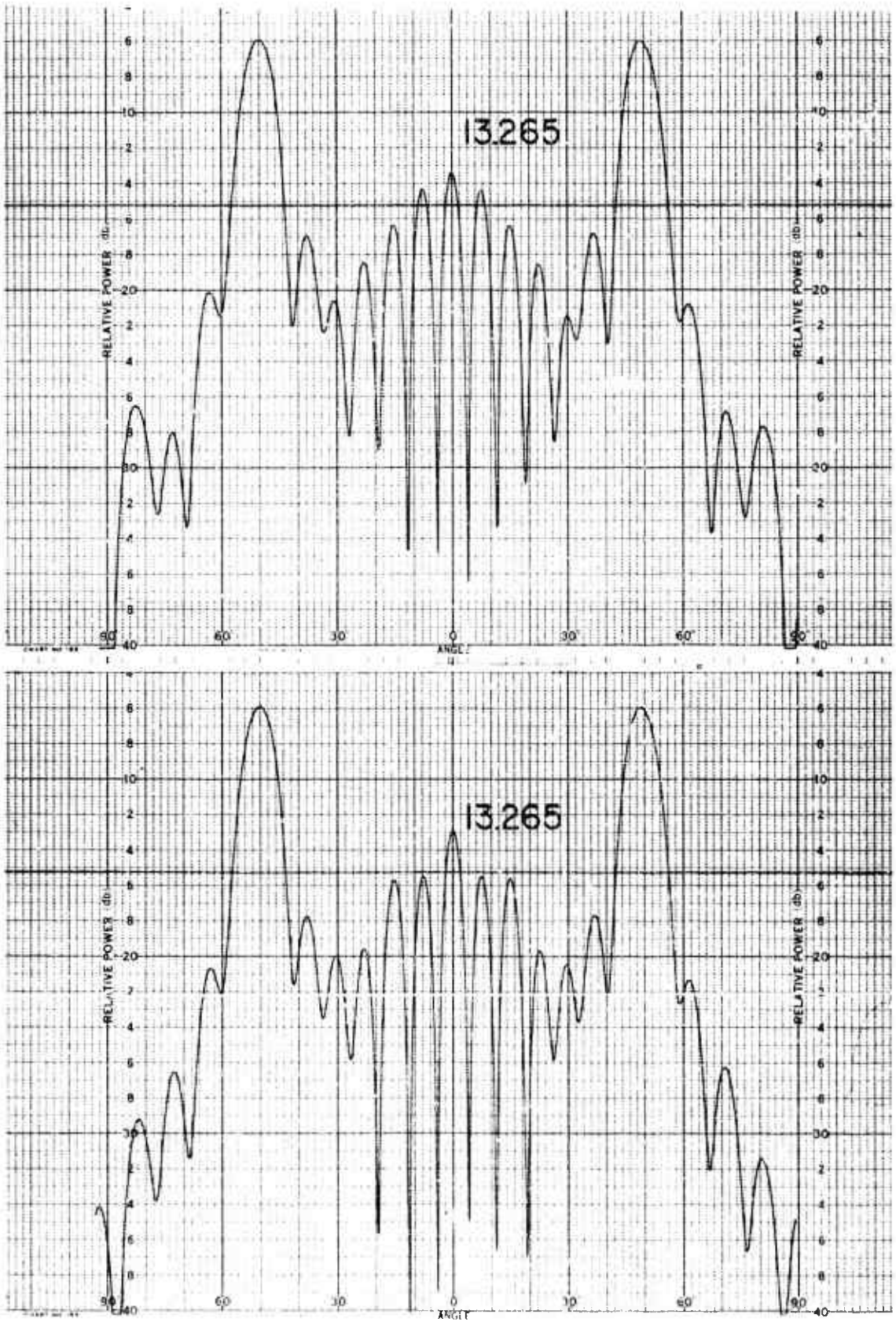
13.265
RELATIVE POWER (db)
ANGLE
13.265
RELATIVE POWER (db)
ANGLE

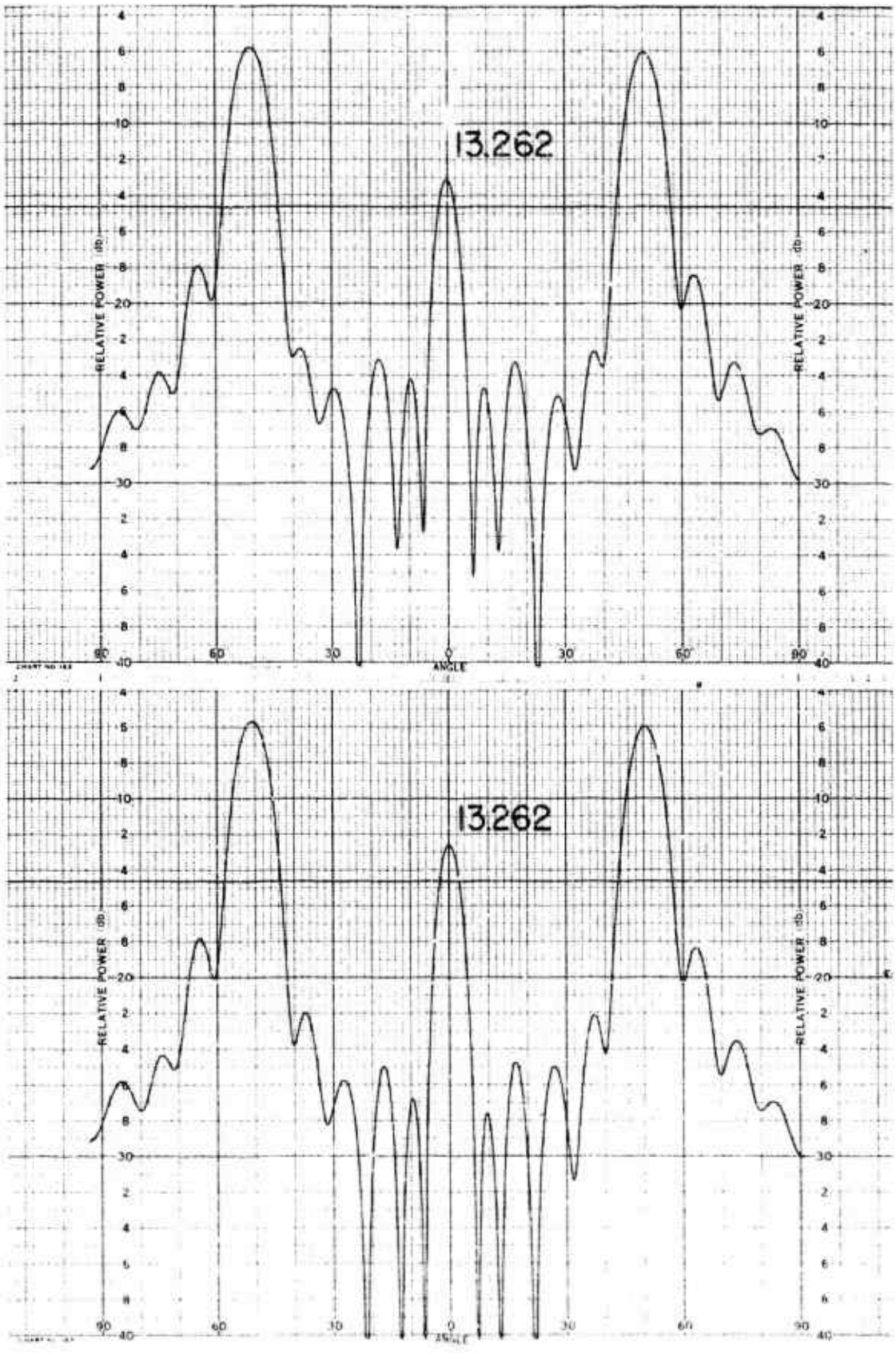
13.262
RELATIVE POWER (dB)
ANGLE
90
60
30
0
30
60
90
13.262
RELATIVE POWER (dB)
ANGLE

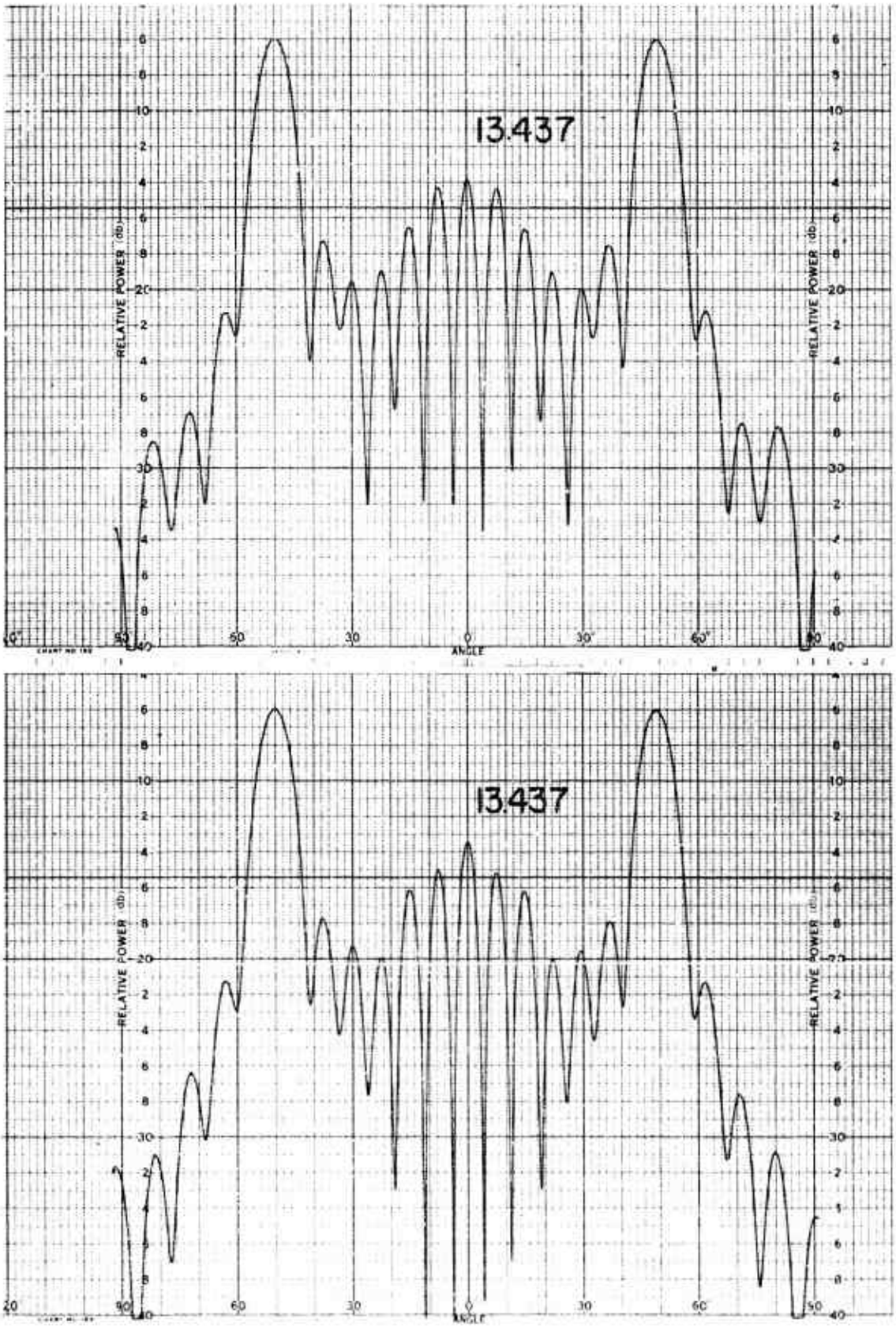
13.437
RELATIVE POWER (db)
ANGLE
13.437
RELATIVE POWER (db)
ANGLE

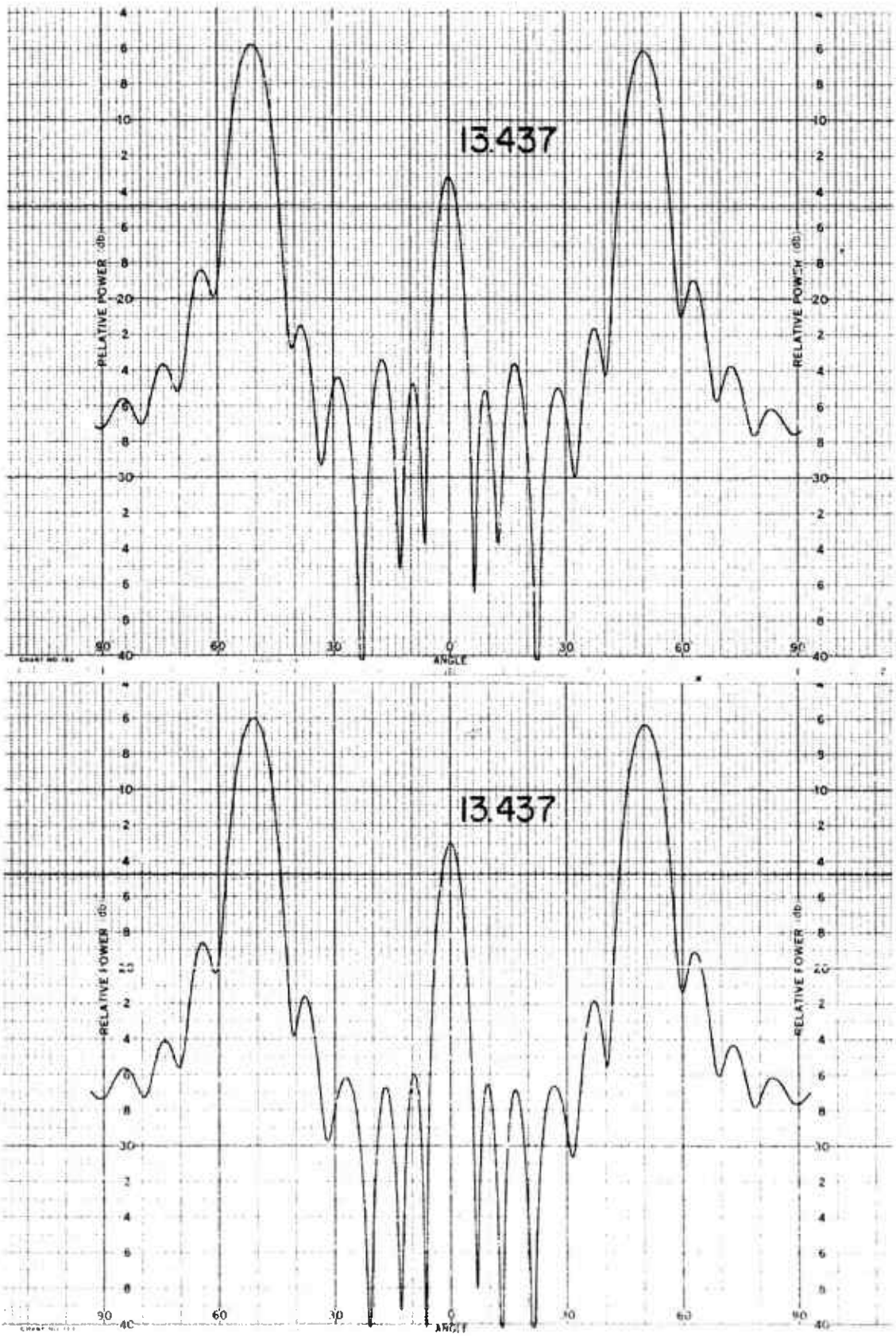
13.437
RELATIVE POWER (db)
ANGLE
90
60
30
0
30
60
90
13.437
RELATIVE POWER (db)
ANGLE

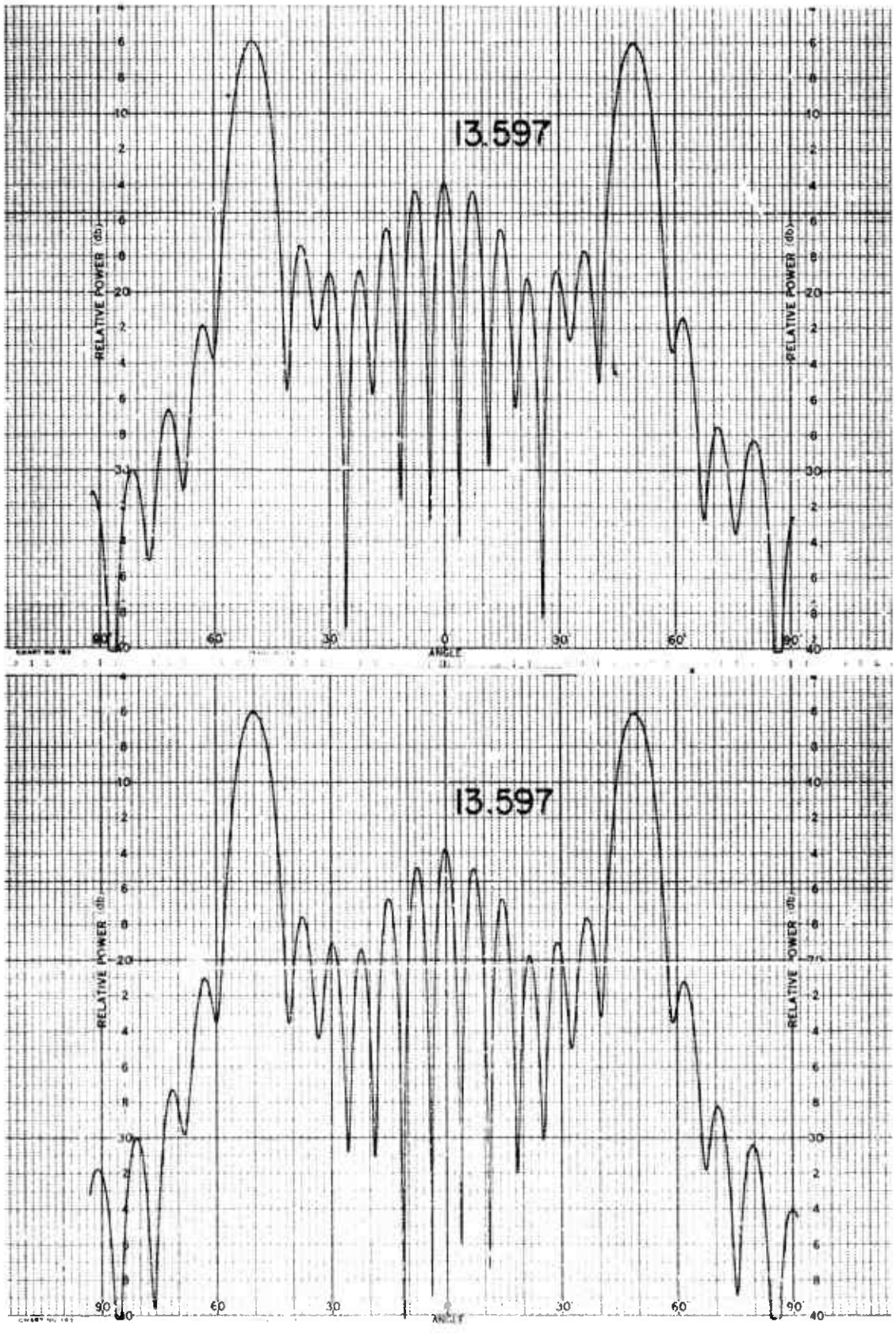
13.597
RELATIVE POWER (db)
ANGLE
90°
60°
30°
0
30°
60°
90°
13.597
RELATIVE POWER (db)
ANGLE

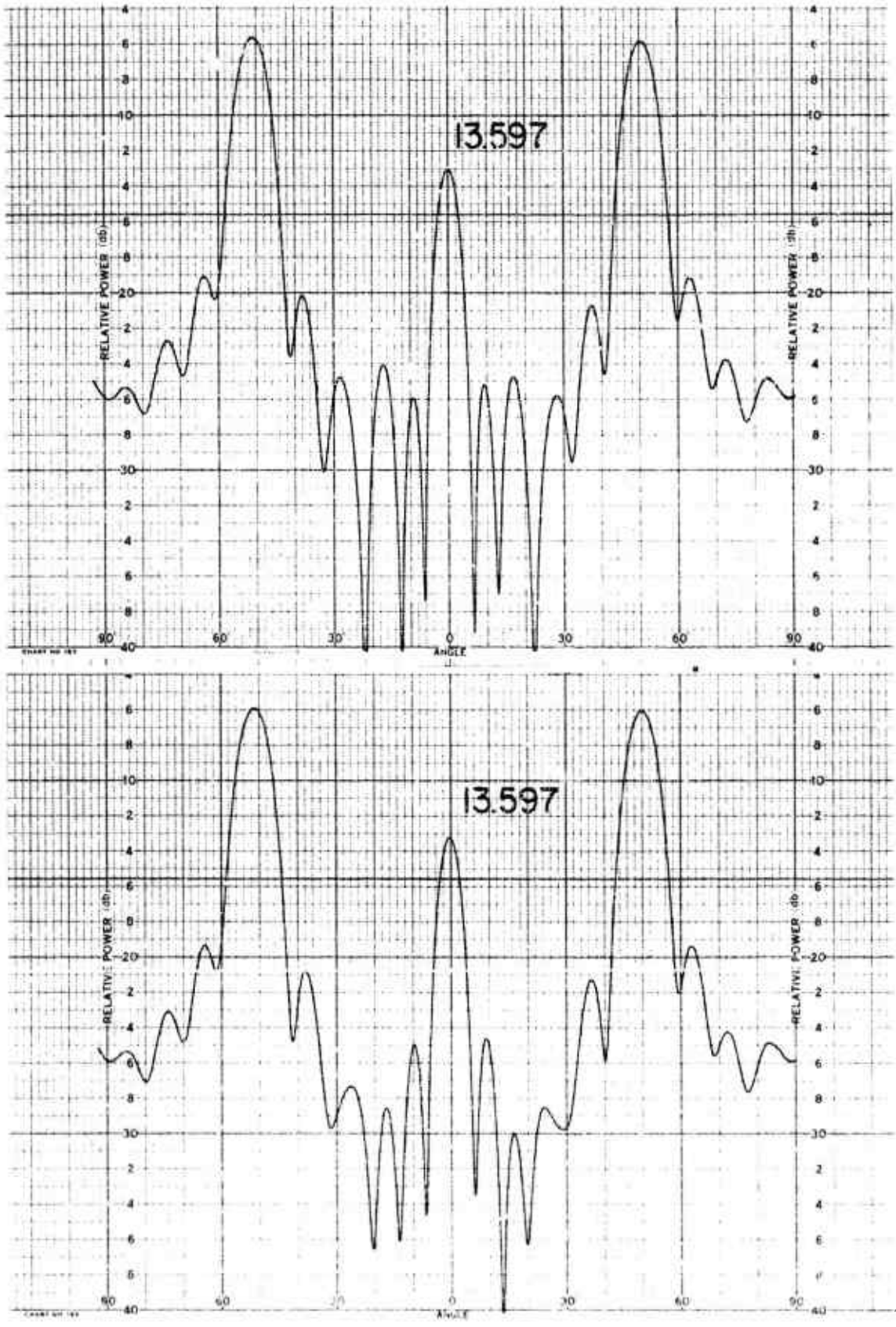
13.597
RELATIVE POWER (db)
ANGLE
13.597
RELATIVE POWER (db)
ANGLE

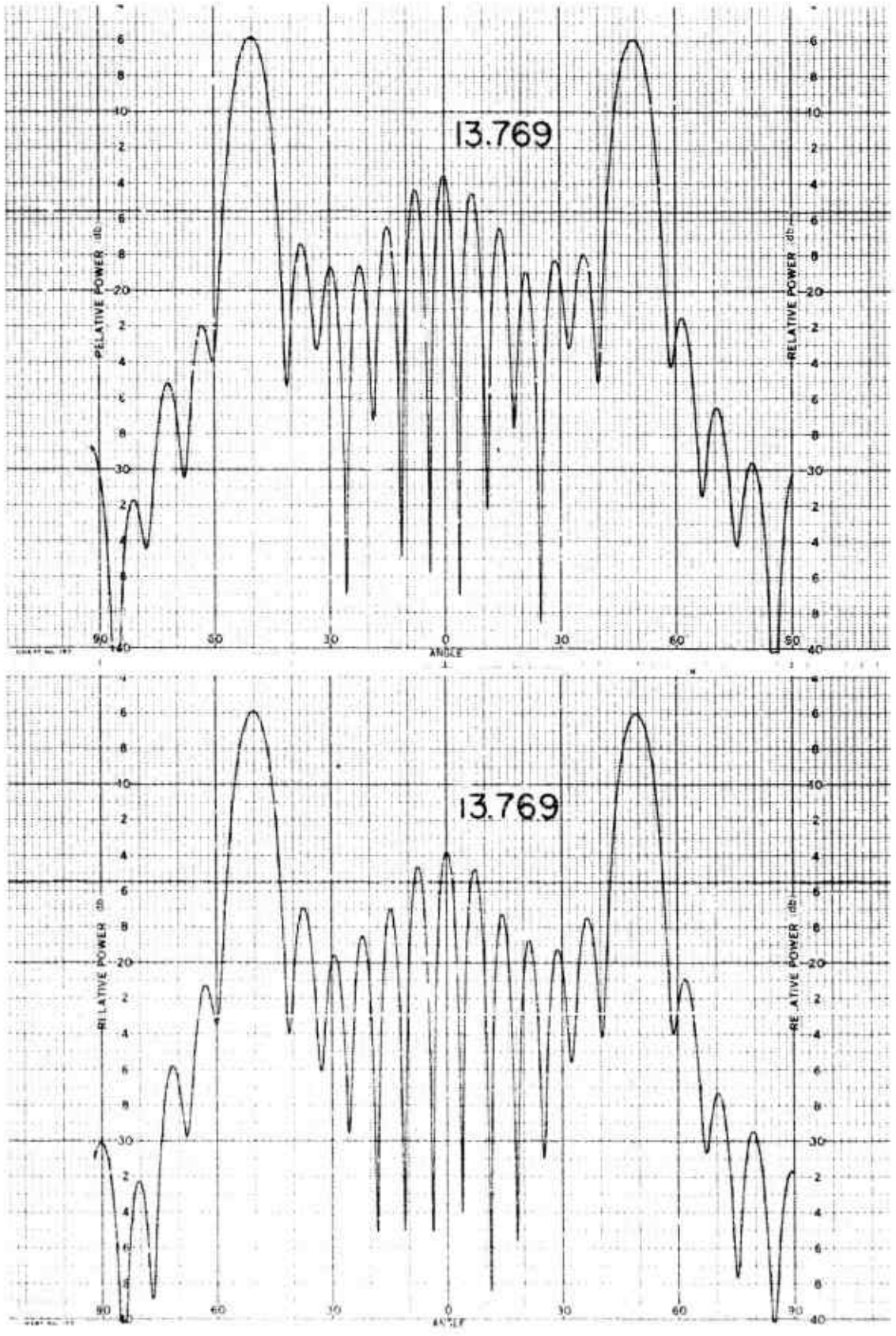
13.769
RELATIVE POWER db
ANGLE
13.769
RELATIVE POWER db
ANGLE

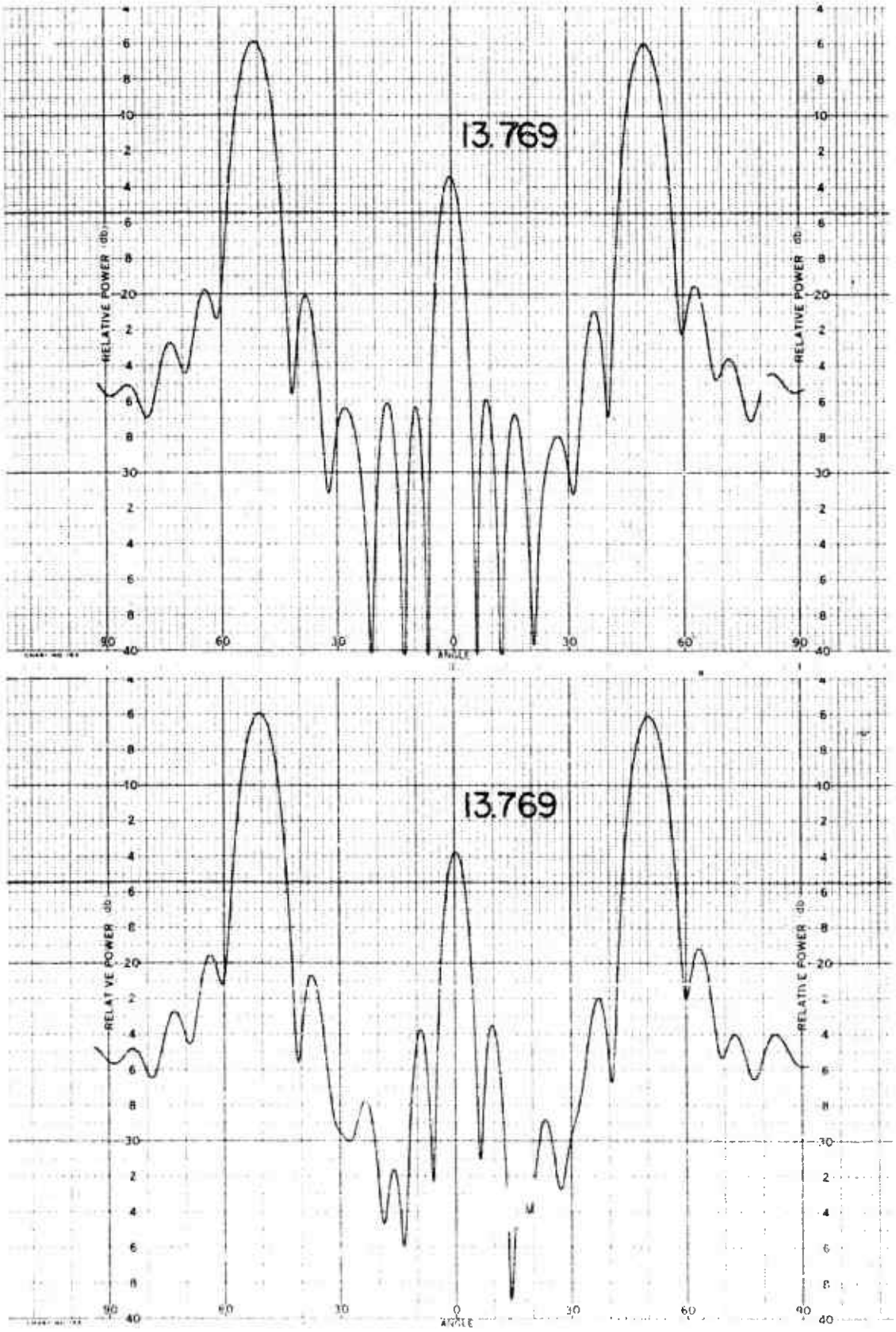
13.769
RELATIVE POWER (db)
ANGLE
13.769
RELATIVE POWER (db)
ANGLE

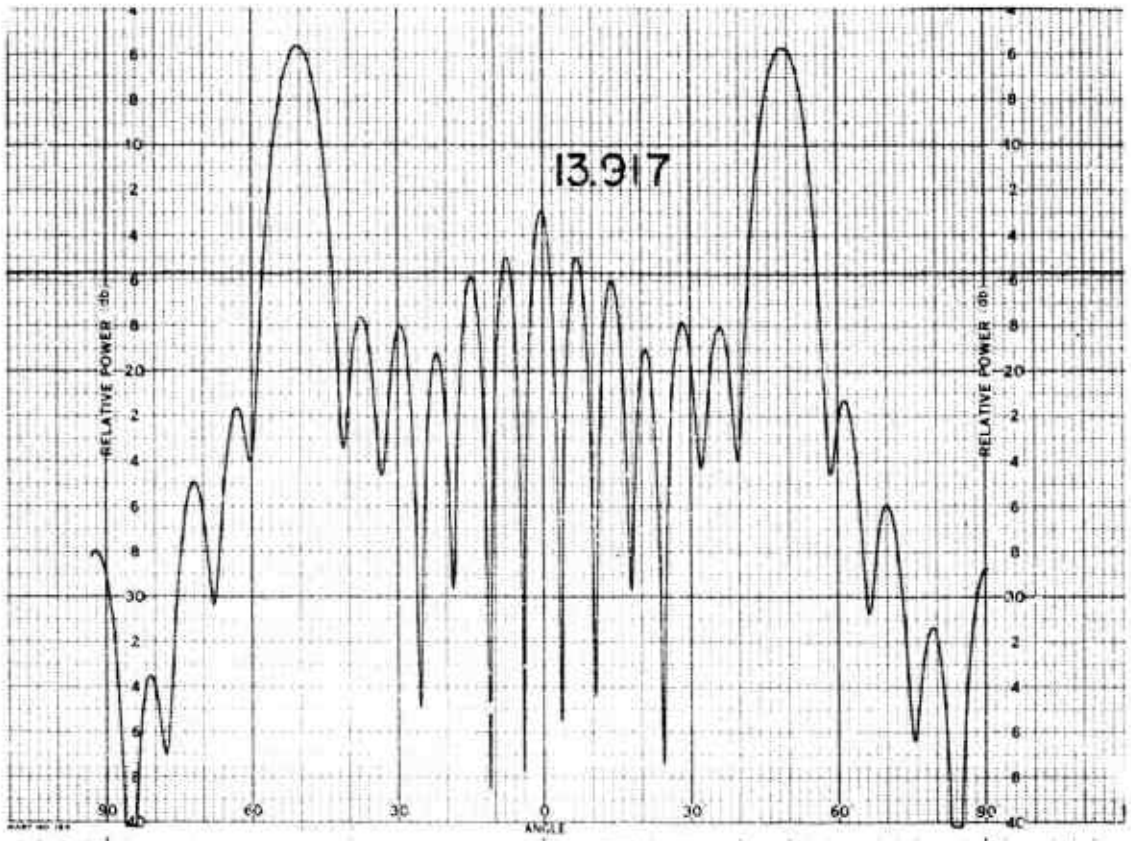
13.917
RELATIVE POWER db
ANGLE

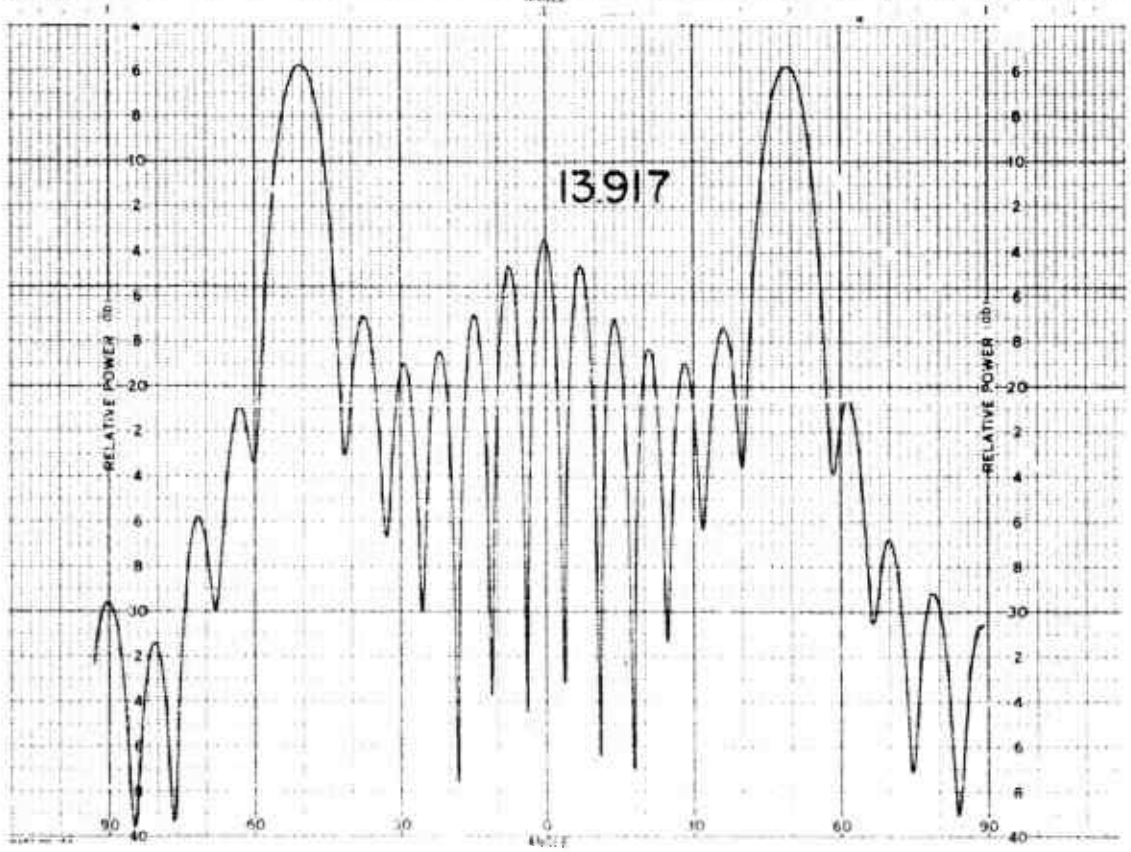
13.917
RELATIVE POWER db
ANGLE

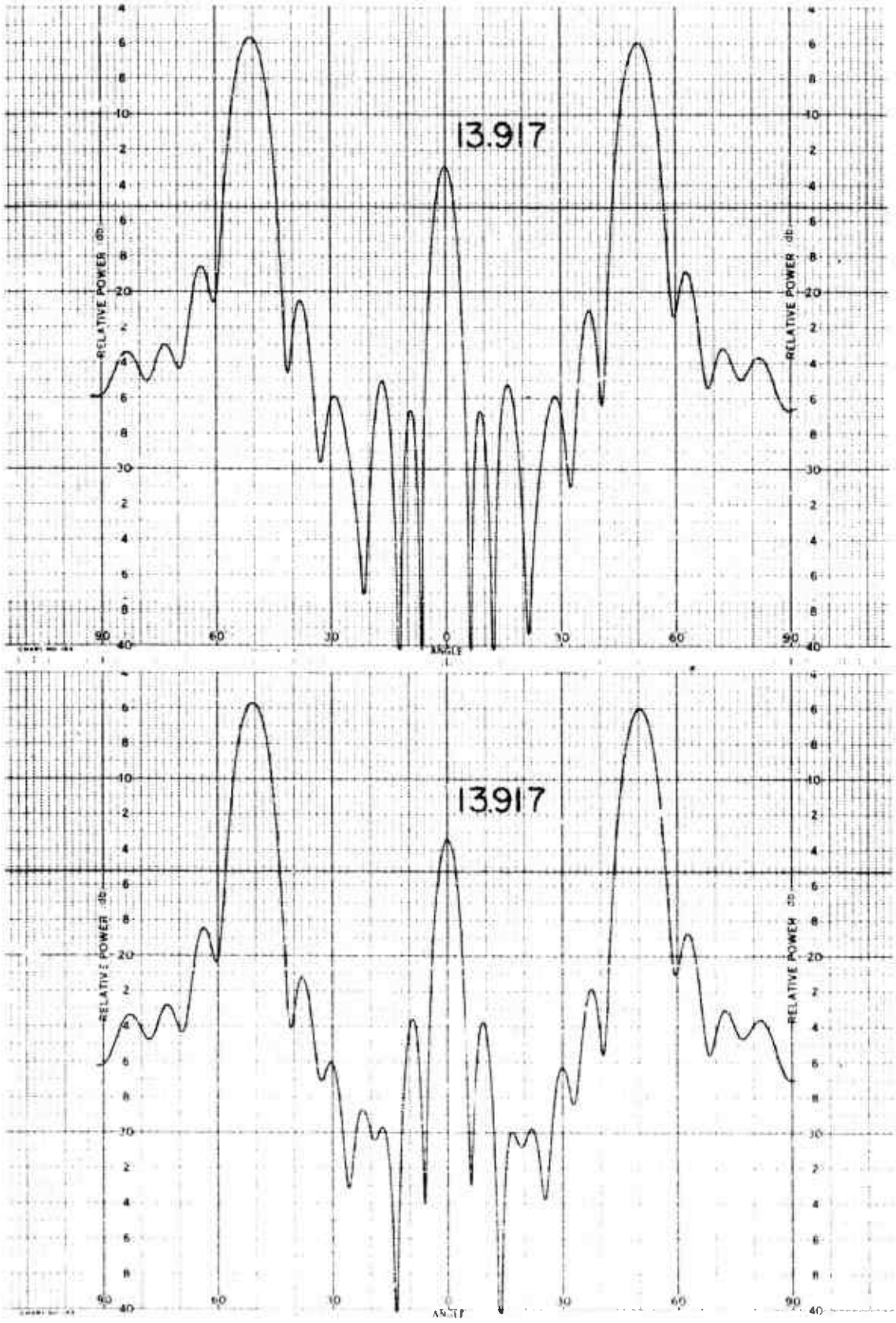
13.917
RELATIVE POWER db
ANGLE
13.917
RELATIVE POWER db
ANGLE

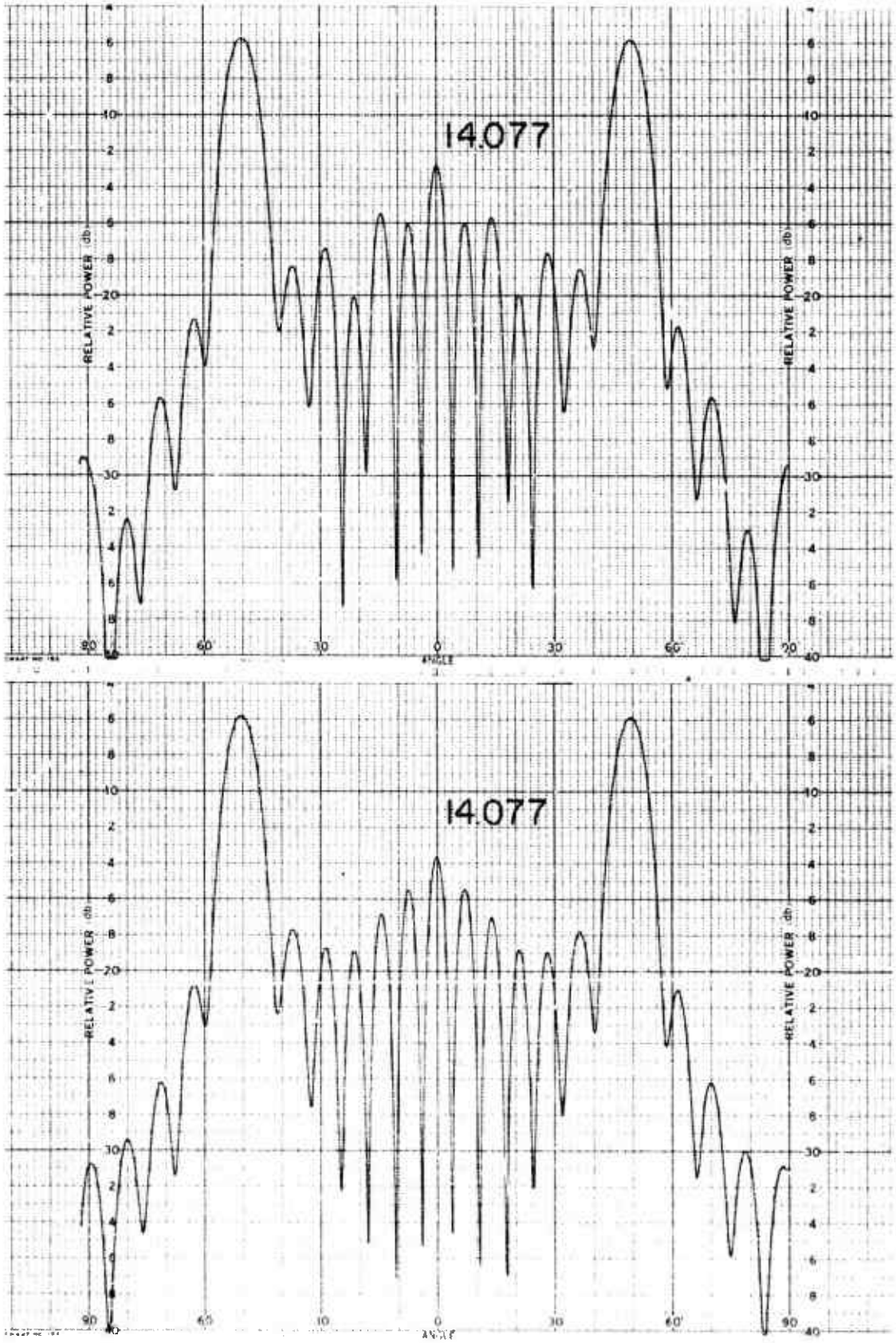
14.077
RELATIVE POWER (db)
ANGLE
14.077
RELATIVE POWER (db)
ANGLE

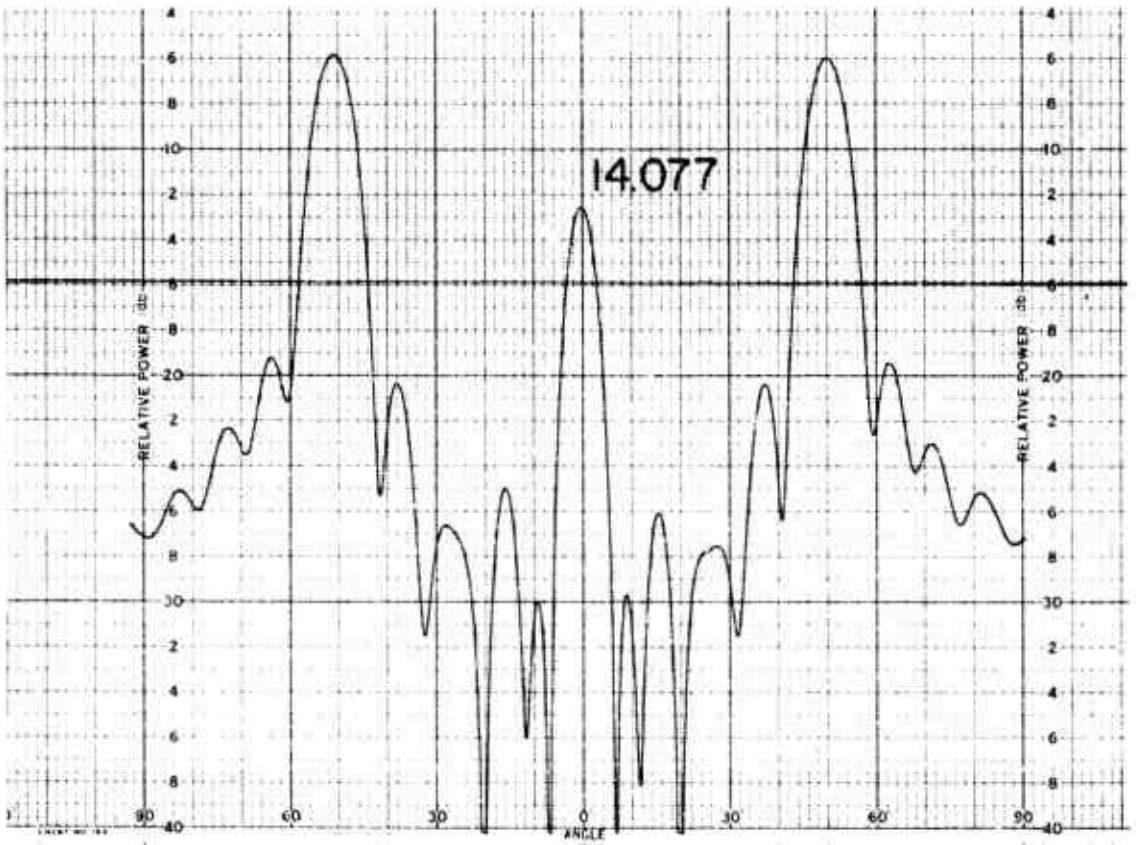
14.077
RELATIVE POWER db
ANGLE

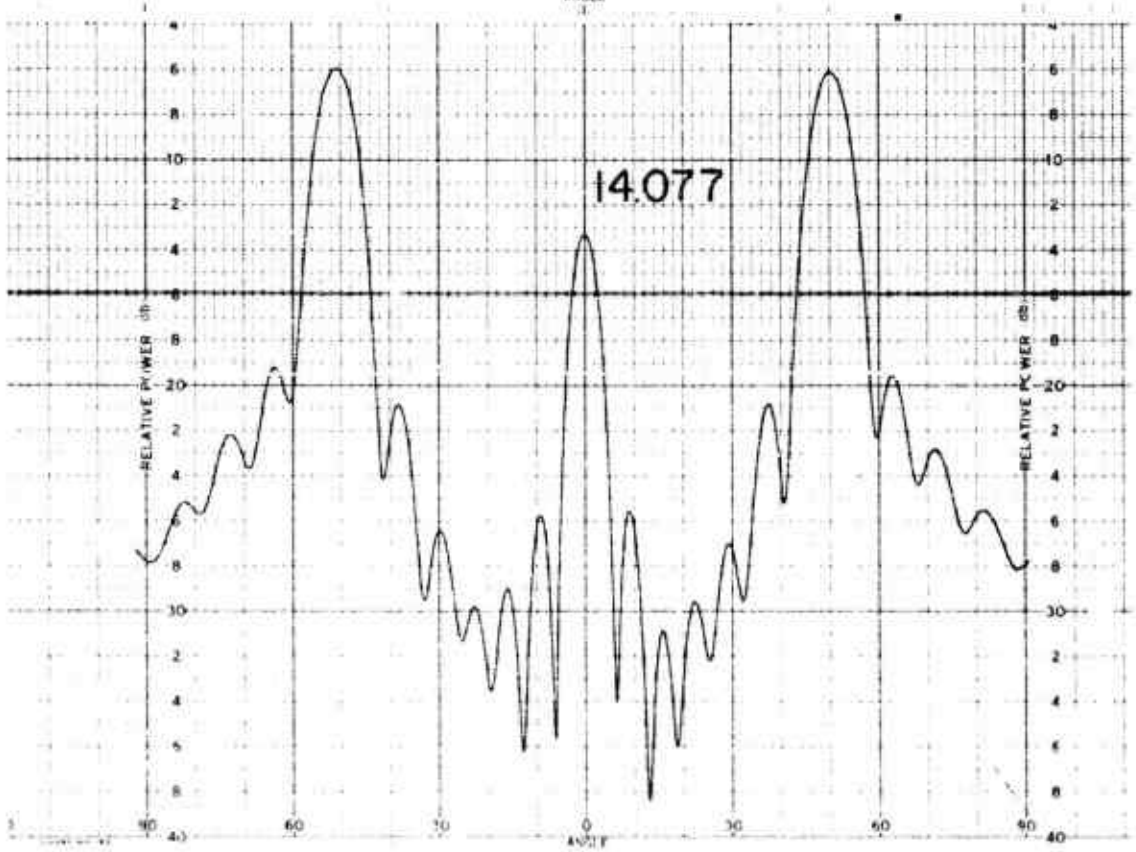
14.077
RELATIVE POWER db

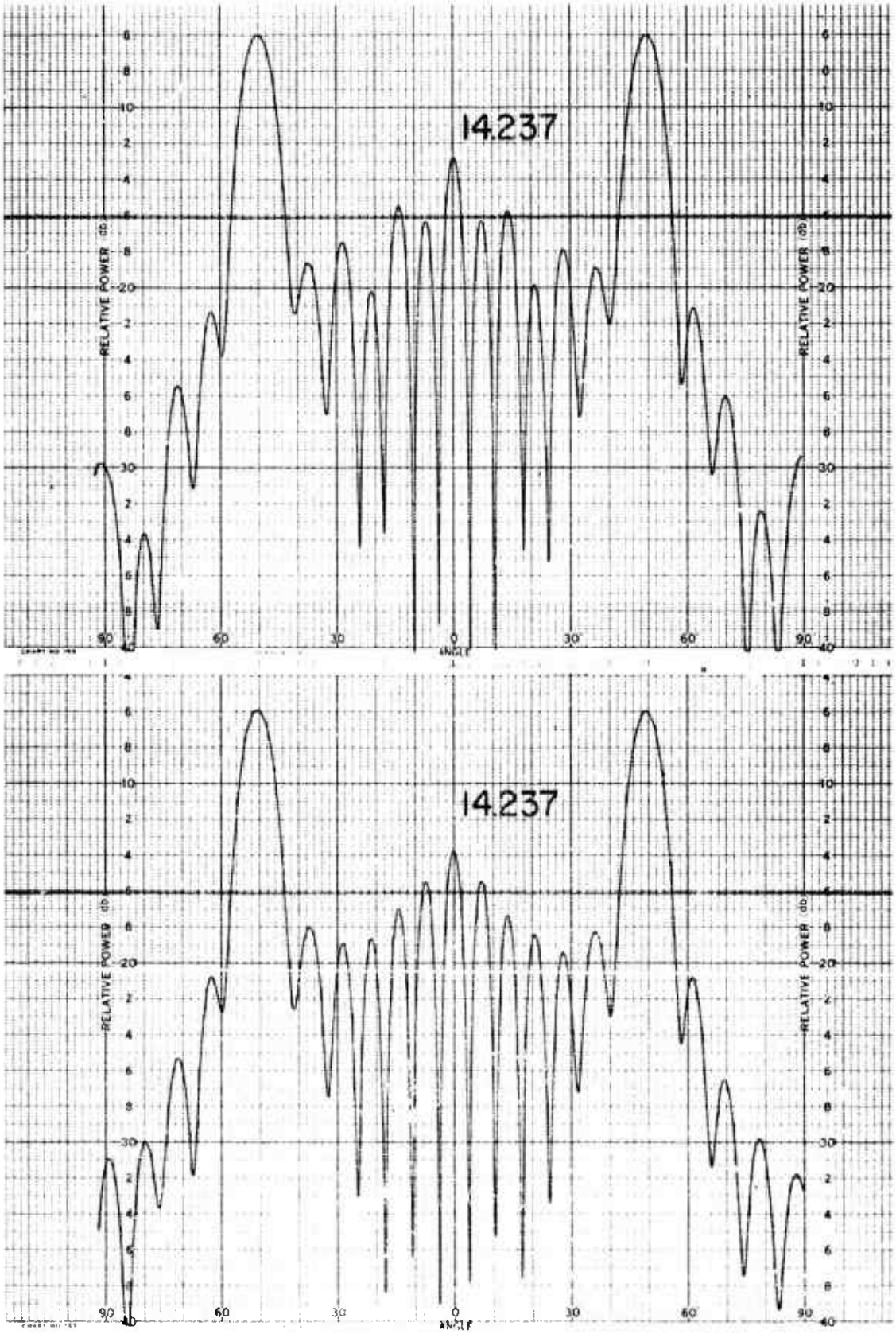
14.237
RELATIVE POWER db
ANGLE
14.237
RELATIVE POWER db
ANGLE

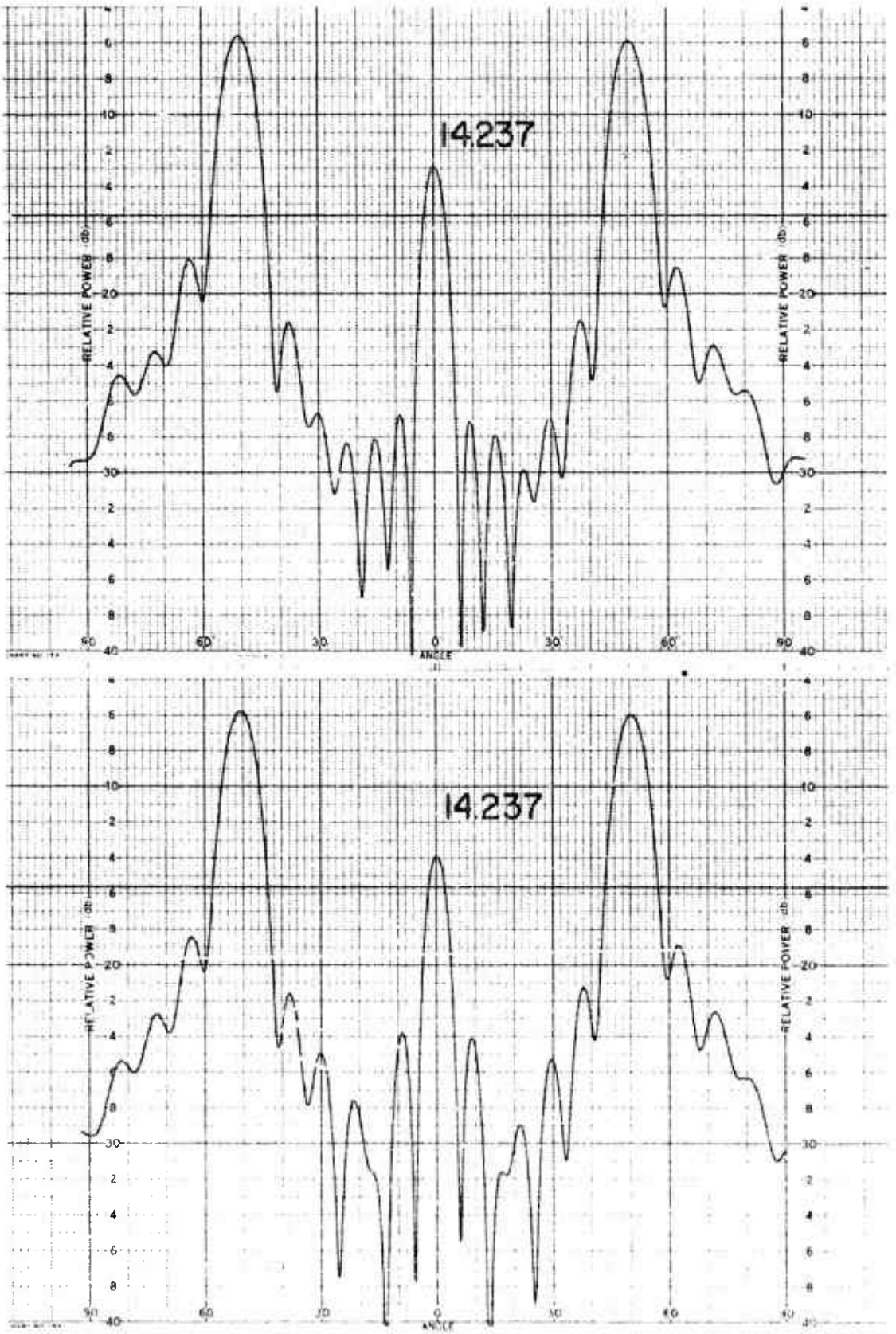
14,237
RELATIVE POWER (db)
ANGLE
14,237
RELATIVE POWER (db)
ANGLE

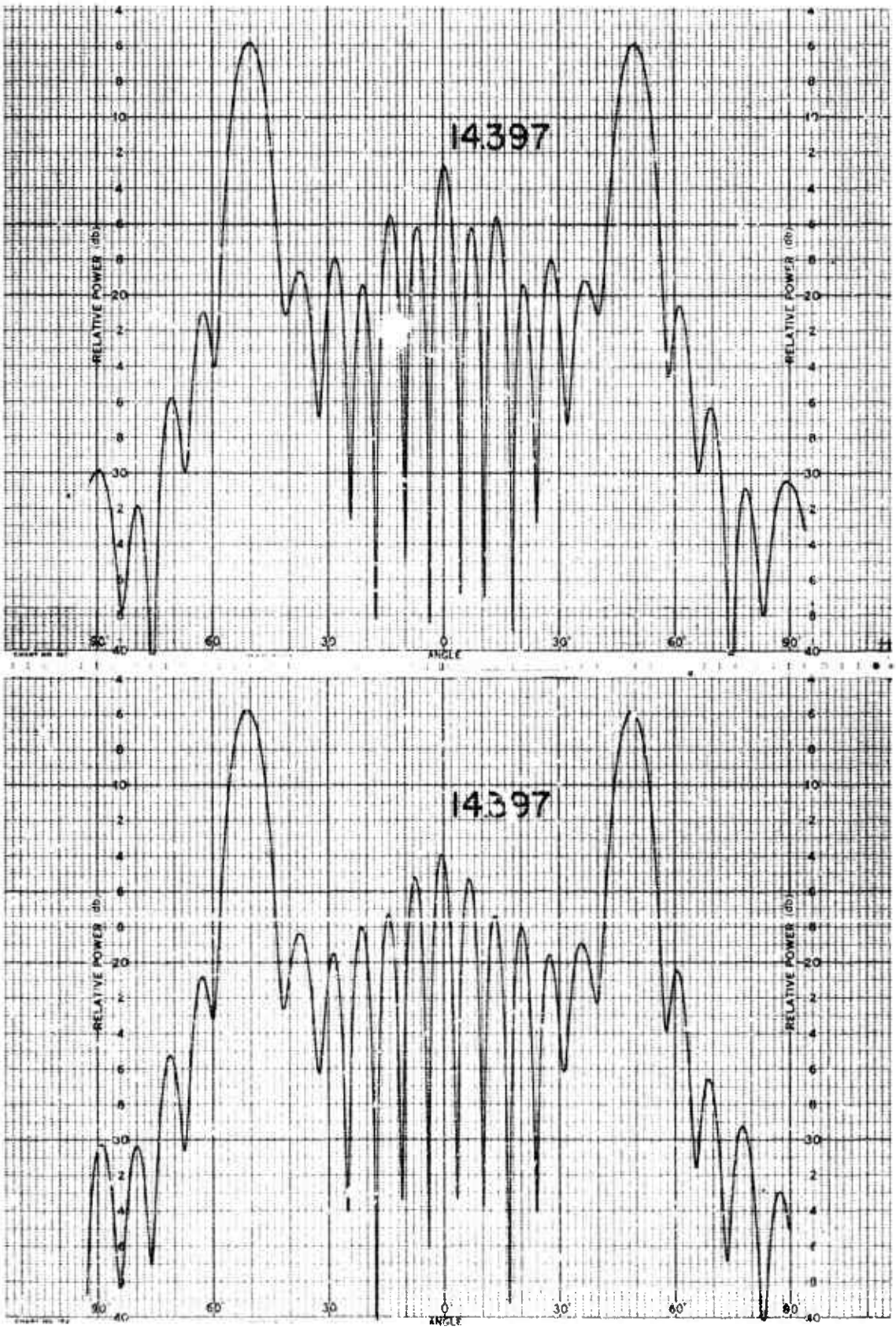
14397
RELATIVE POWER (db)
ANGLE
14397
RELATIVE POWER (db)
ANGLE

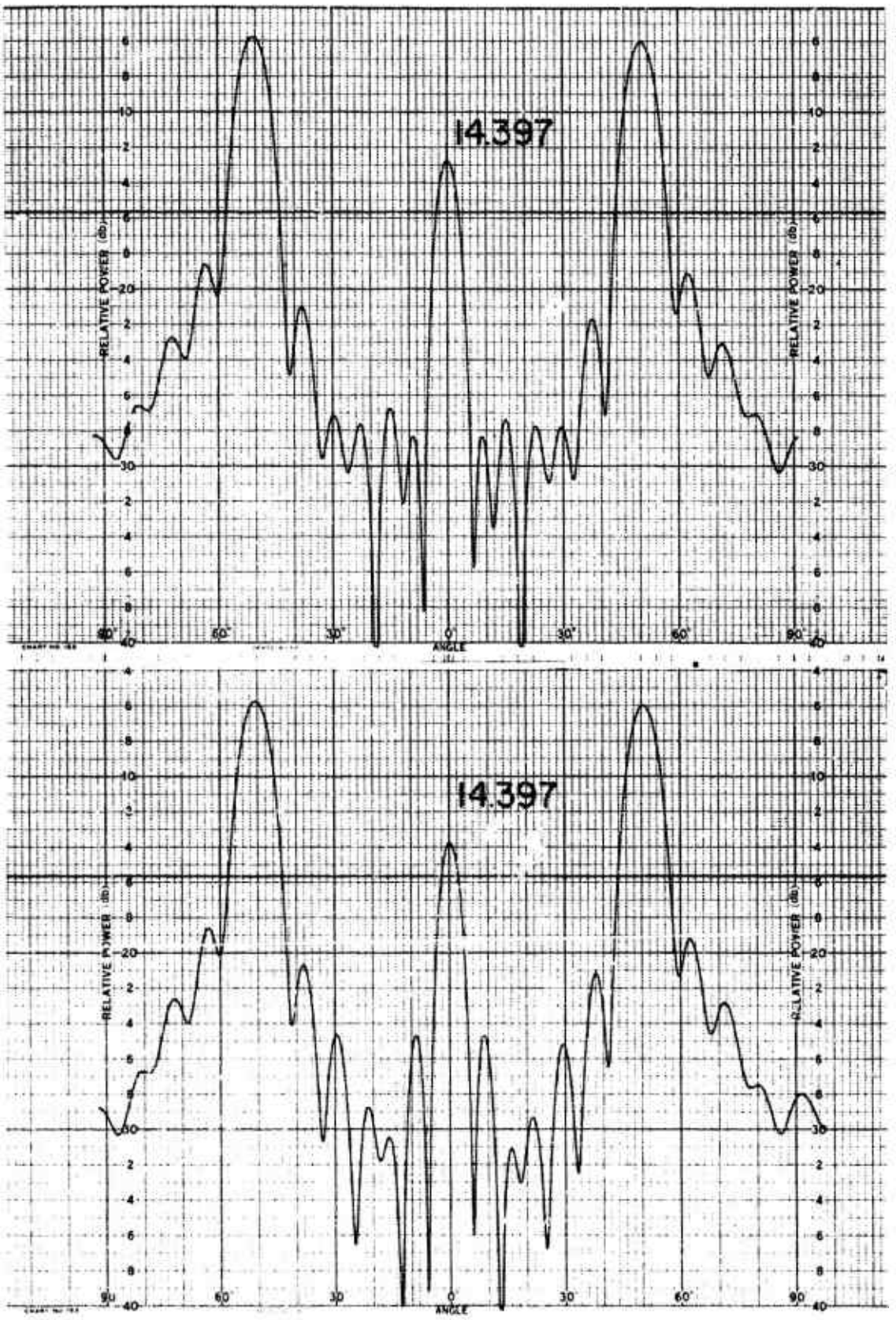
14.397
RELATIVE POWER (db)
ANGLE
14.397
RELATIVE POWER (db)
ANGLE

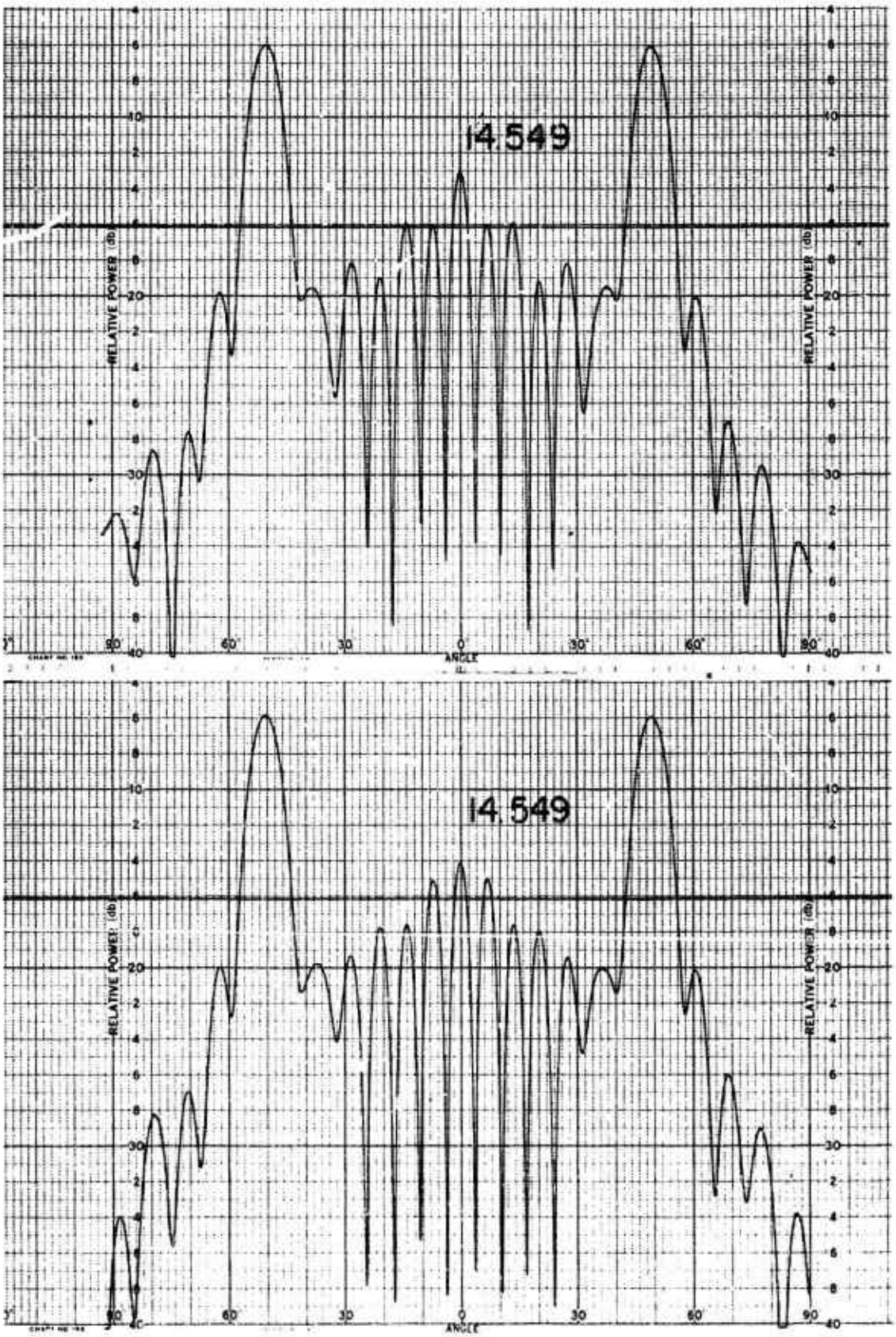
14.549
RELATIVE POWER (db)
ANGLE
90°
60°
30°
0
30°
60°
90°
14.549
RELATIVE POWER (db)
ANGLE

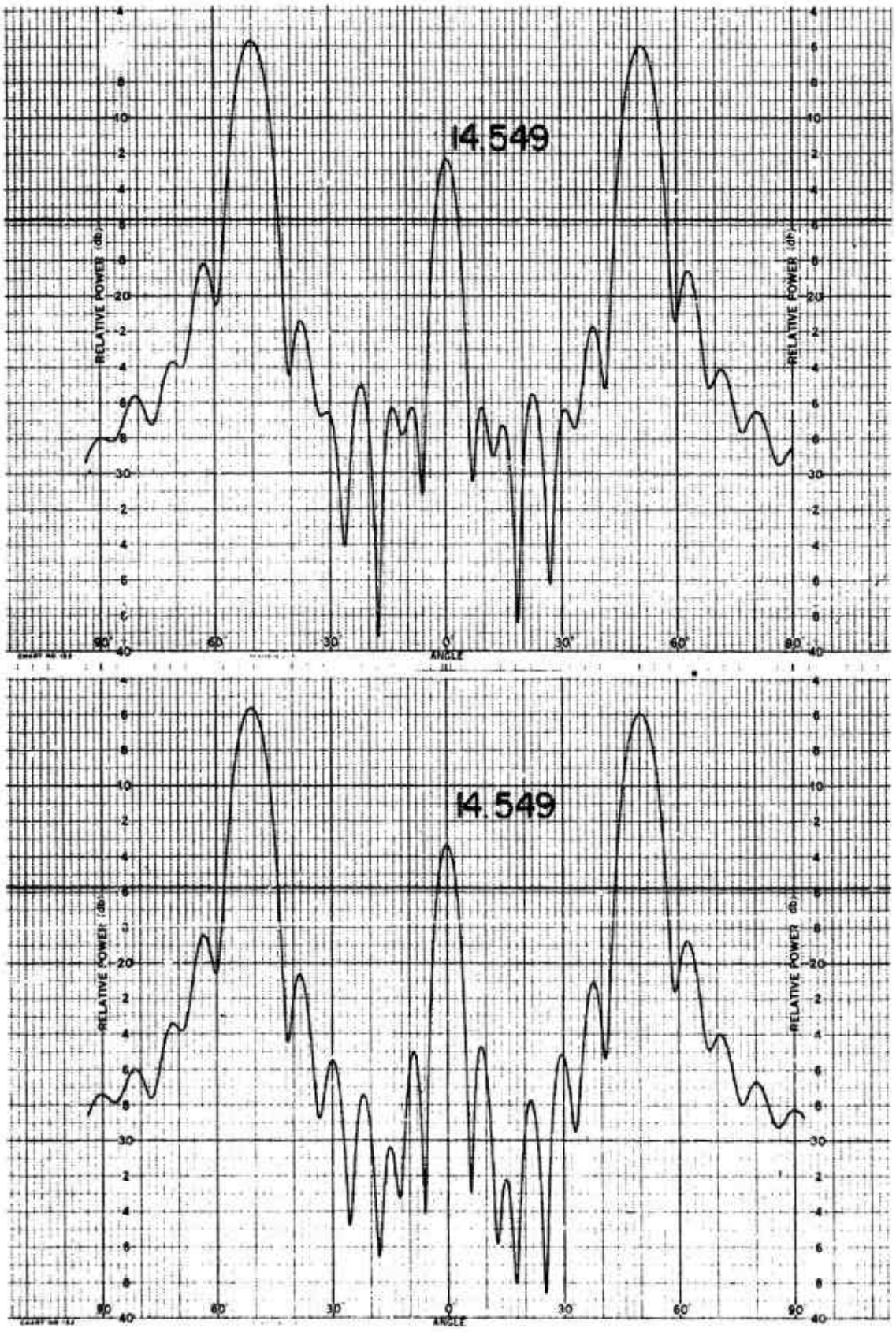
14.549
RELATIVE POWER (db)
ANGLE
14.549
RELATIVE POWER (db)
ANGLE

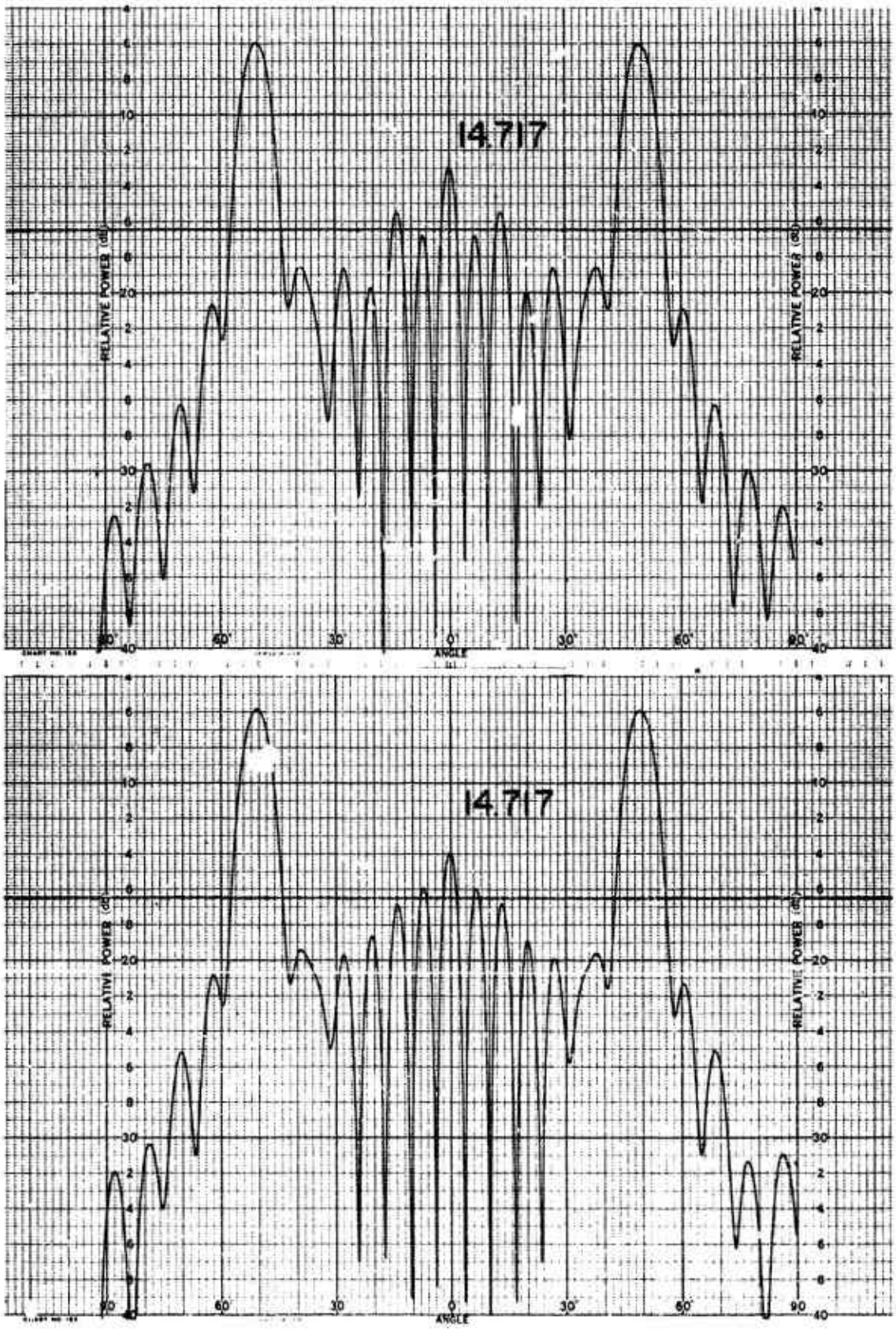
14.717
RELATIVE POWER (dB)
ANGLE
14.717
RELATIVE POWER (dB)
ANGLE

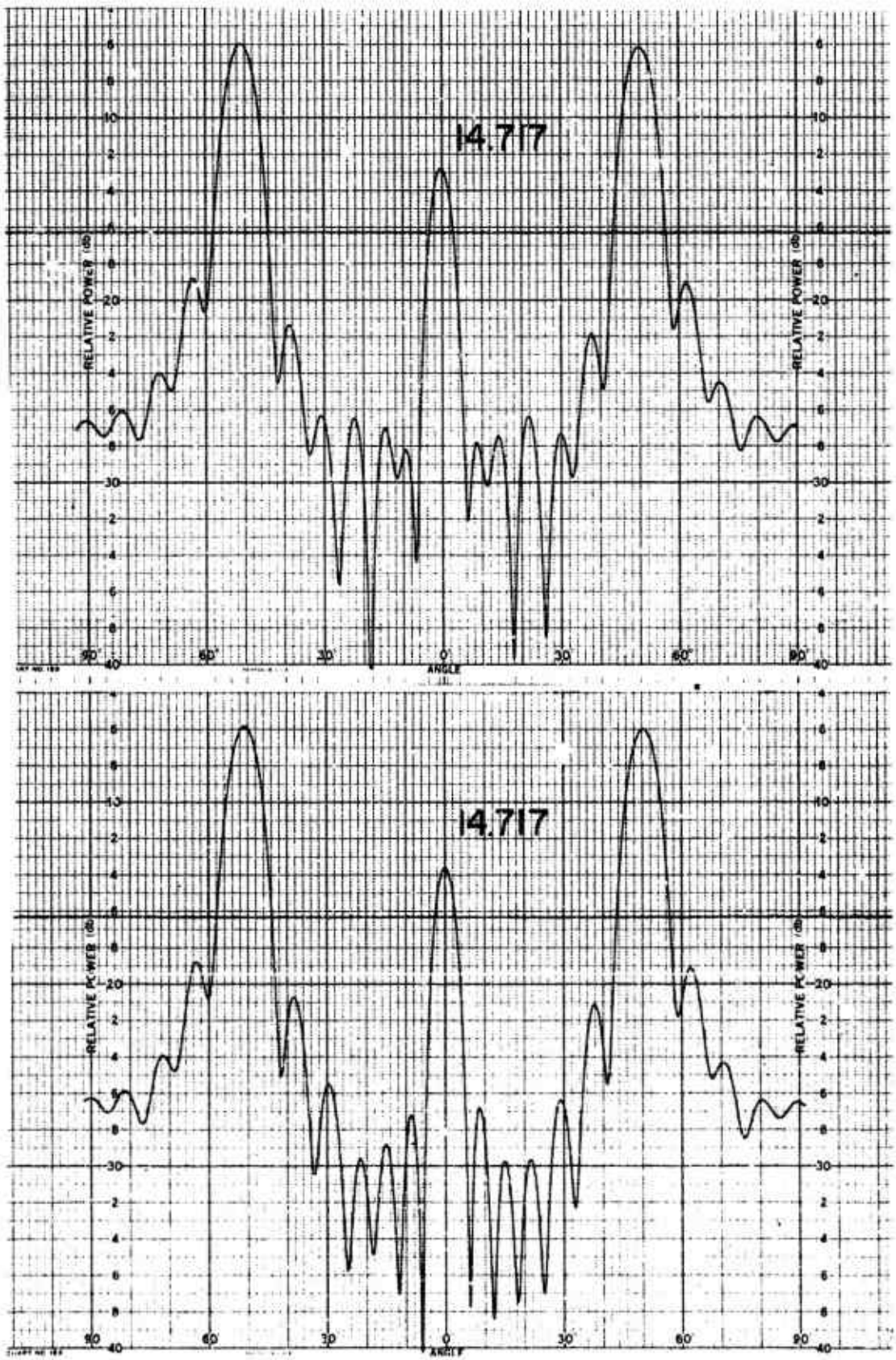
14.717
RELATIVE POWER (dB)
ANGLE
14.717
RELATIVE POWER (dB)
ANGLE

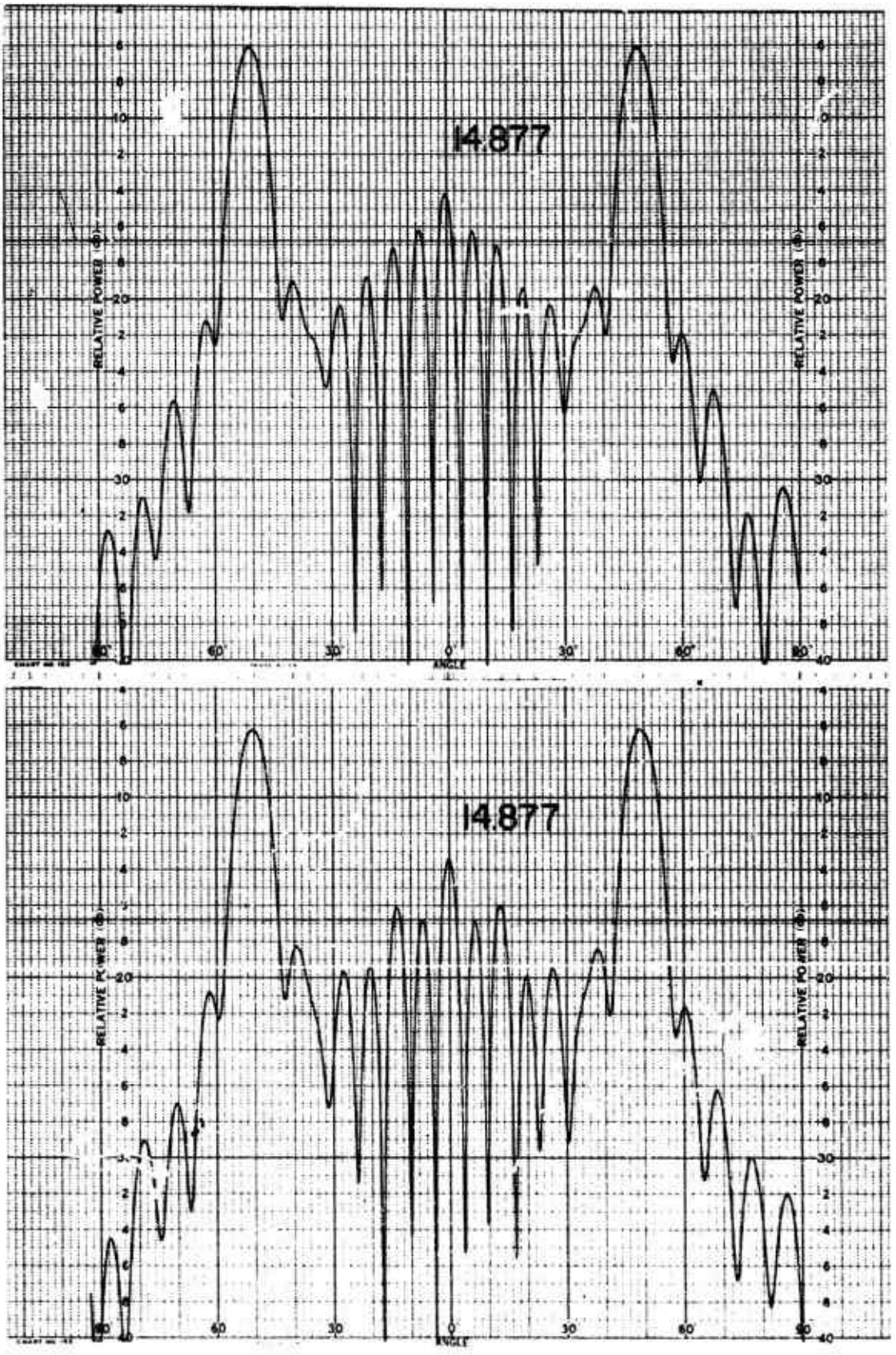
14.877
RELATIVE POWER (dB)
ANGLE
14.877
RELATIVE POWER (dB)
ANGLE

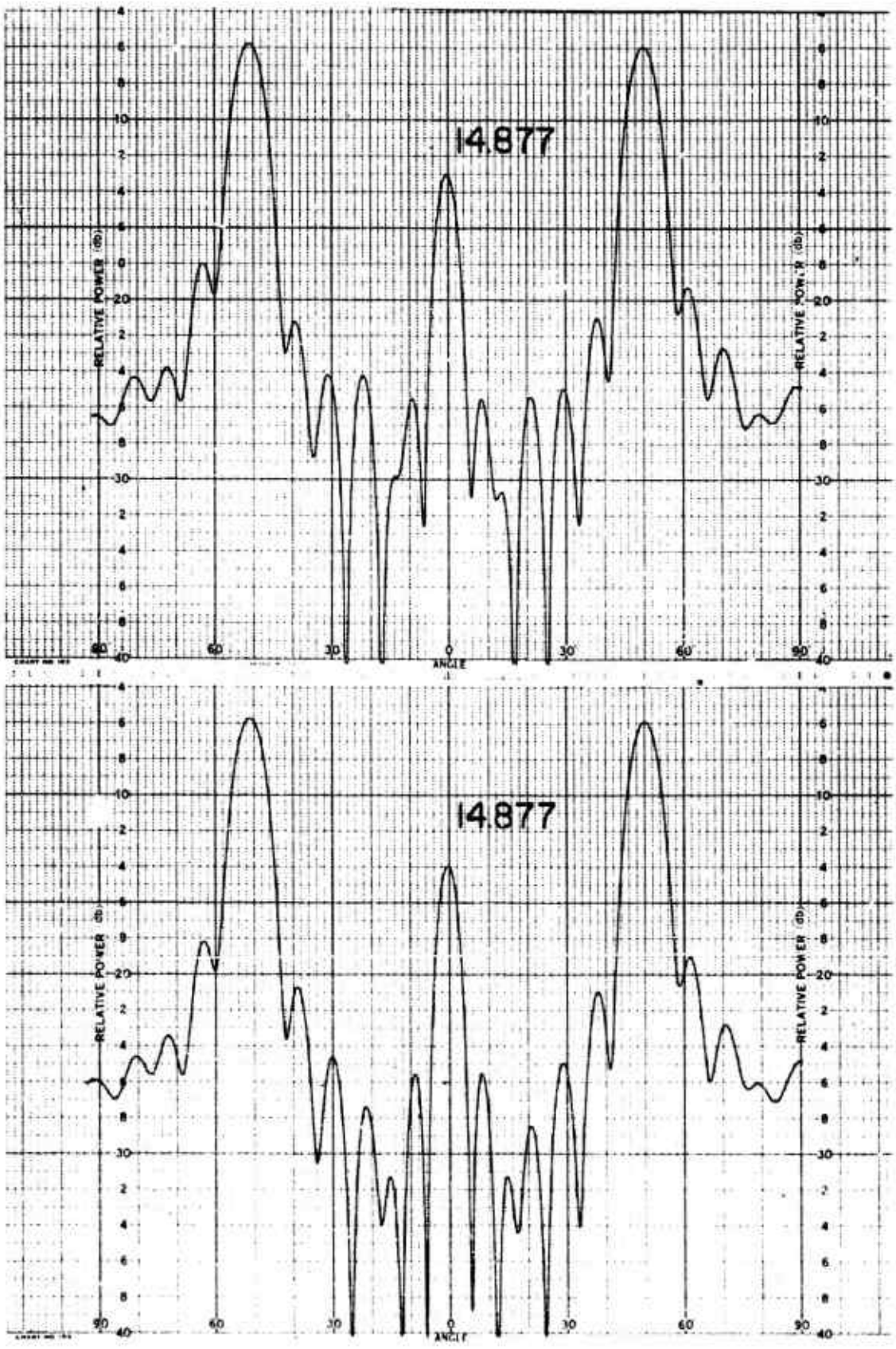
14.877
RELATIVE POWER (db)
ANGLE
14.877
RELATIVE POWER (db)
ANGLE

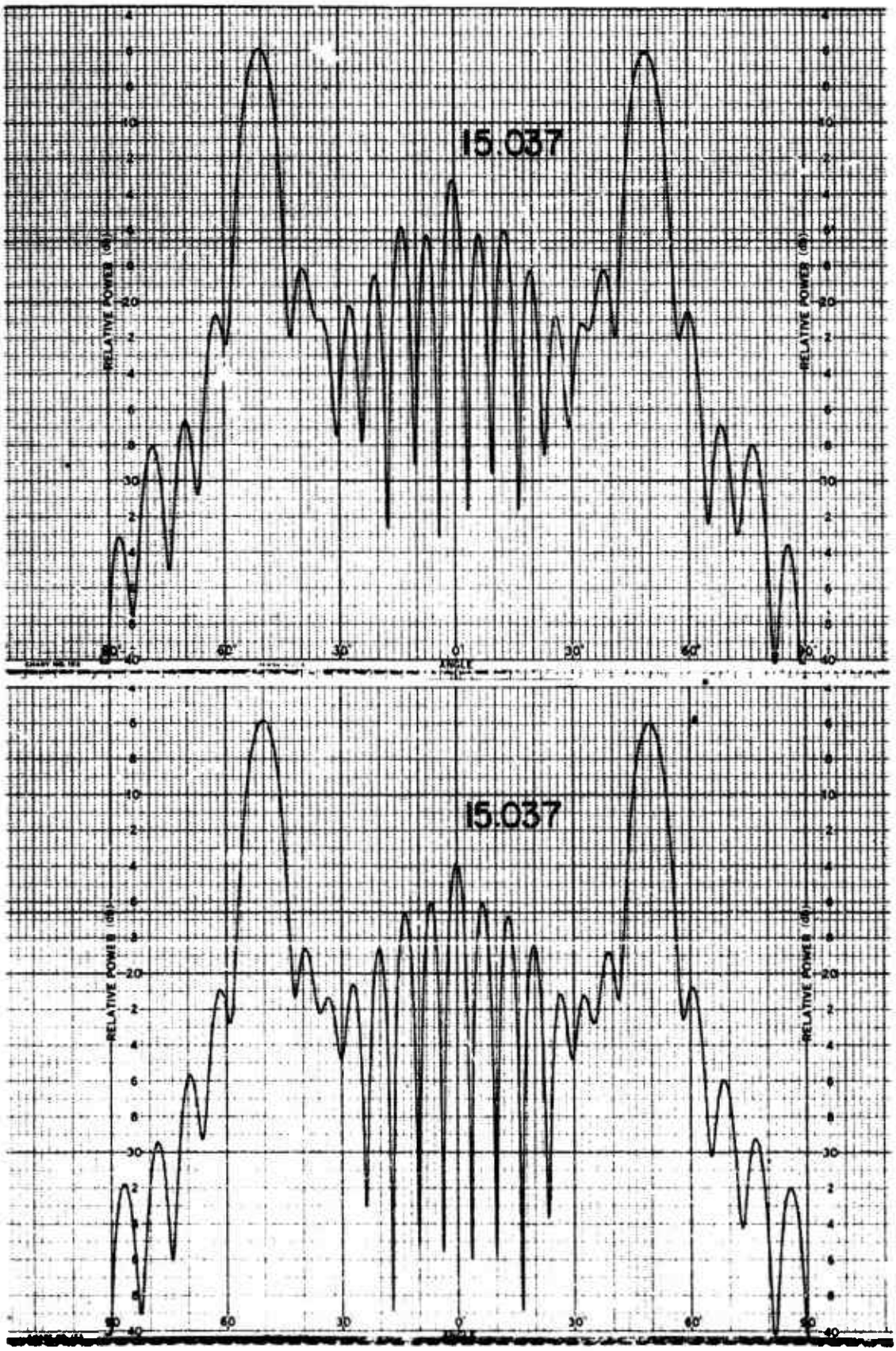
15.037
RELATIVE POWER (dB)
ANGLE
15.037
RELATIVE POWER (dB)

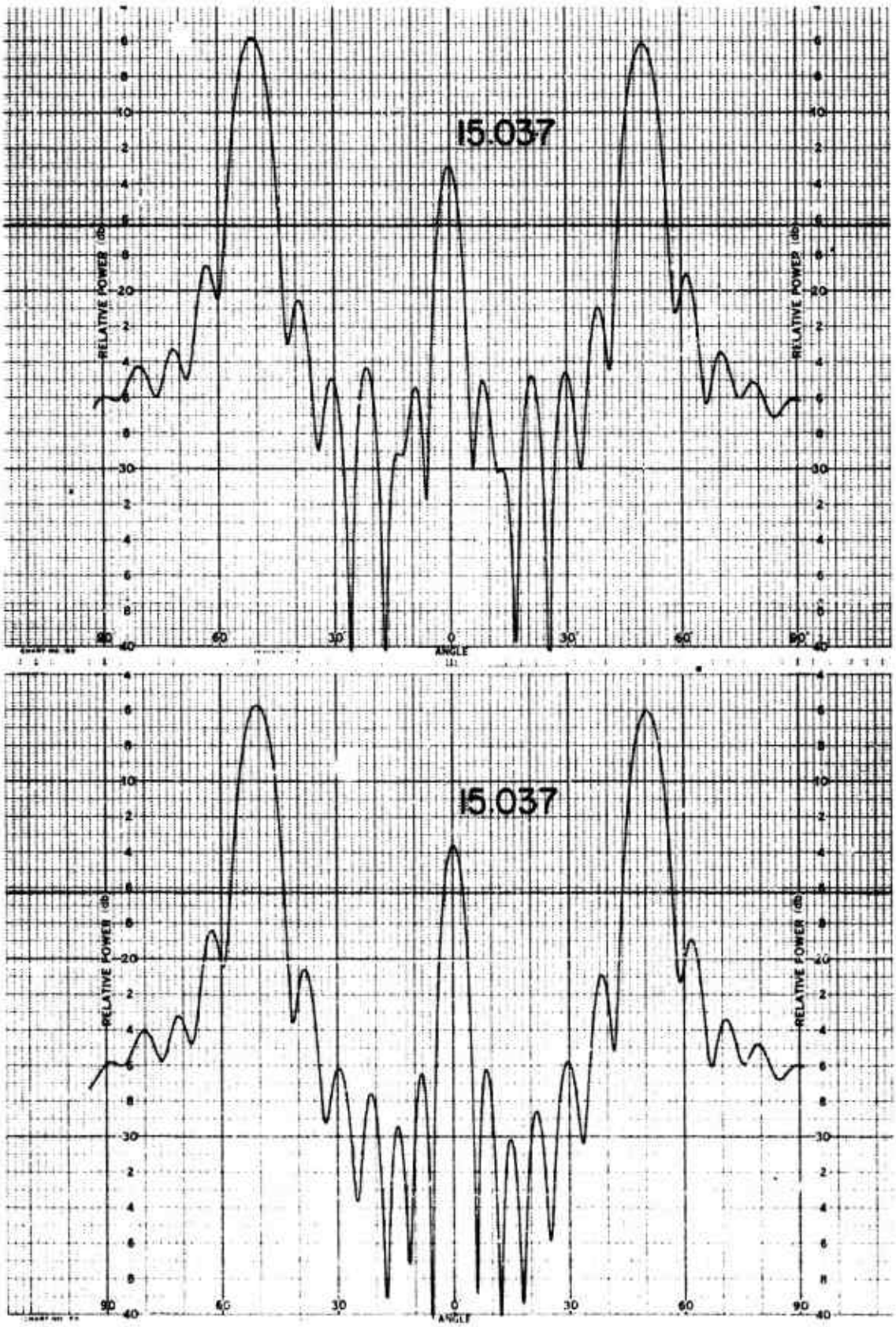
15.037
RELATIVE POWER (db)
ANGLE
15.037
RELATIVE POWER (db)
ANGLE

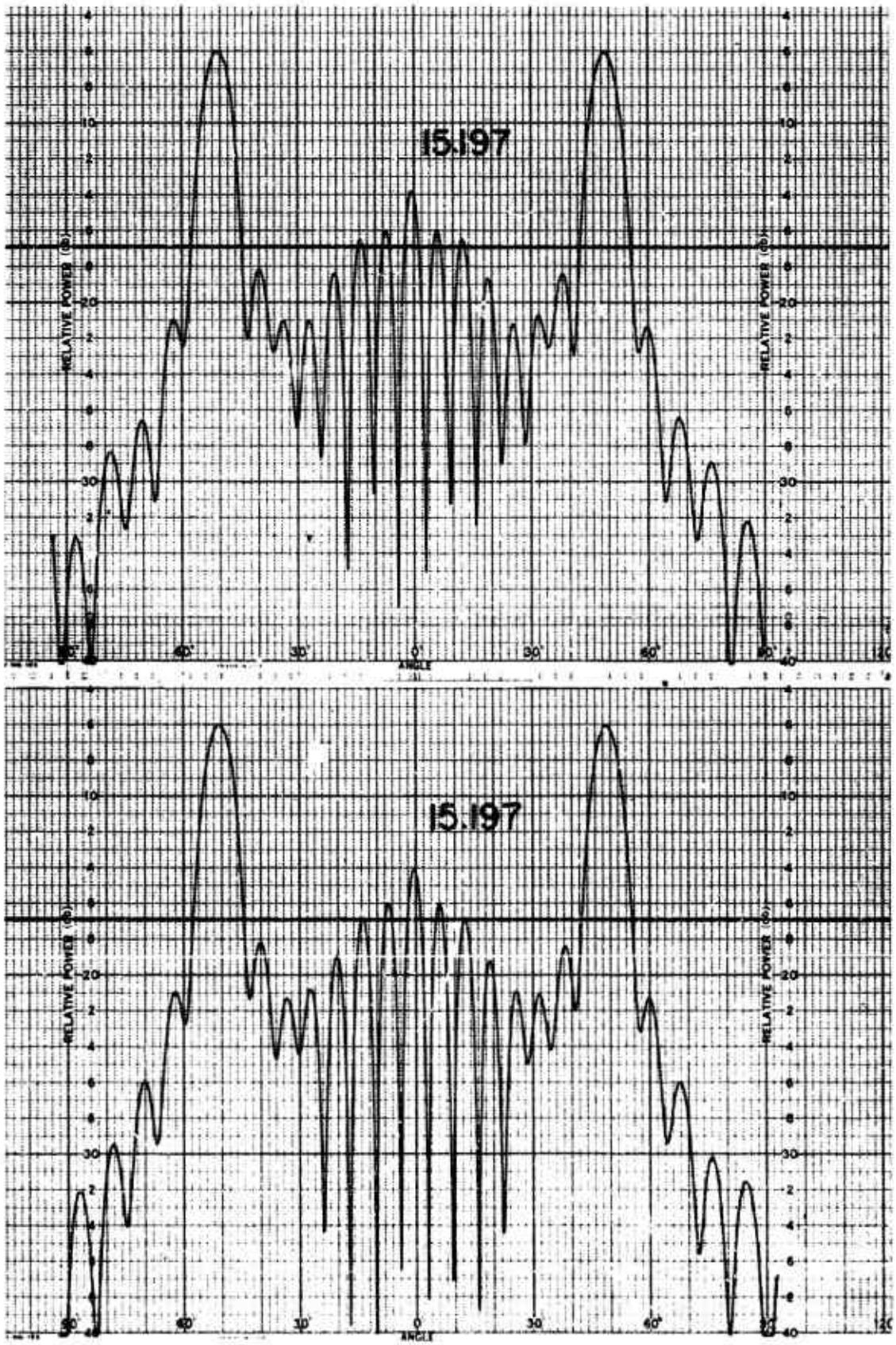
15.197
RELATIVE POWER (db)
ANGLE
15.197
RELATIVE POWER (db)
ANGLE

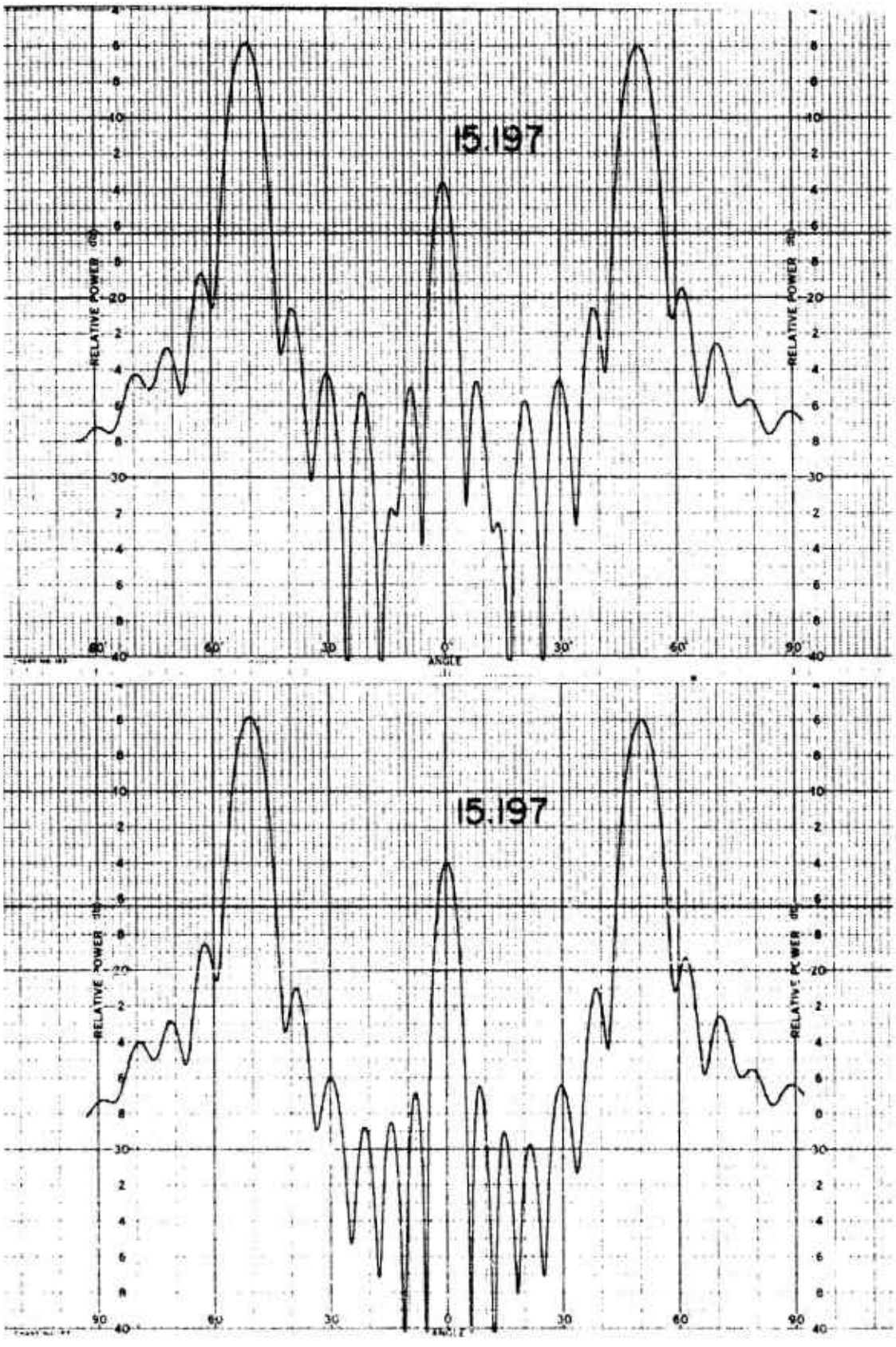
15.197
RELATIVE POWER db
ANGLE
60°
30°
0°
30°
60°
90°
15.197
RELATIVE POWER db
ANGLE
90°
60°
30°
0°
30°
60°
90°

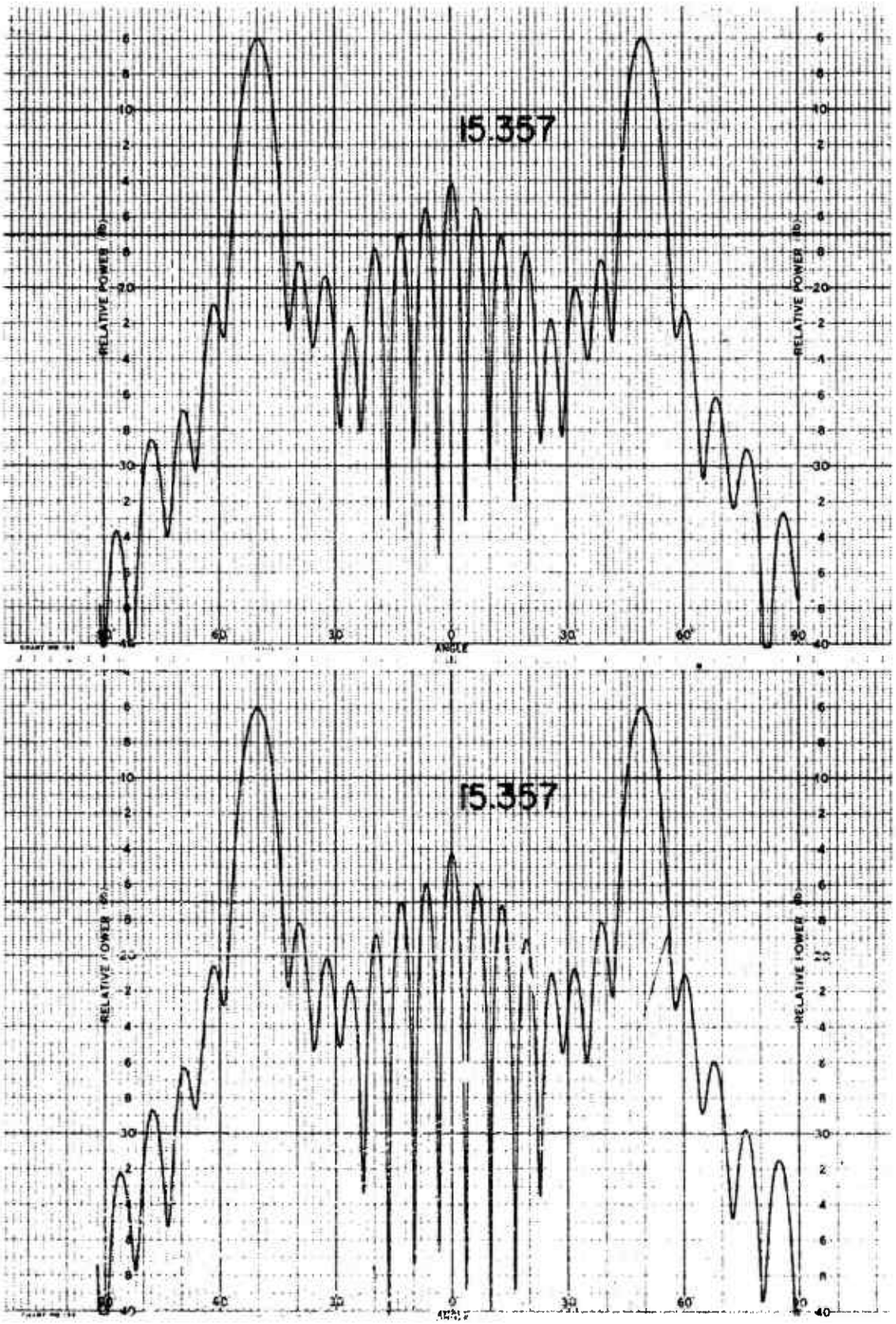
15.357
RELATIVE POWER (dB)
ANGLE
15.357
RELATIVE POWER (dB)
ANGLE

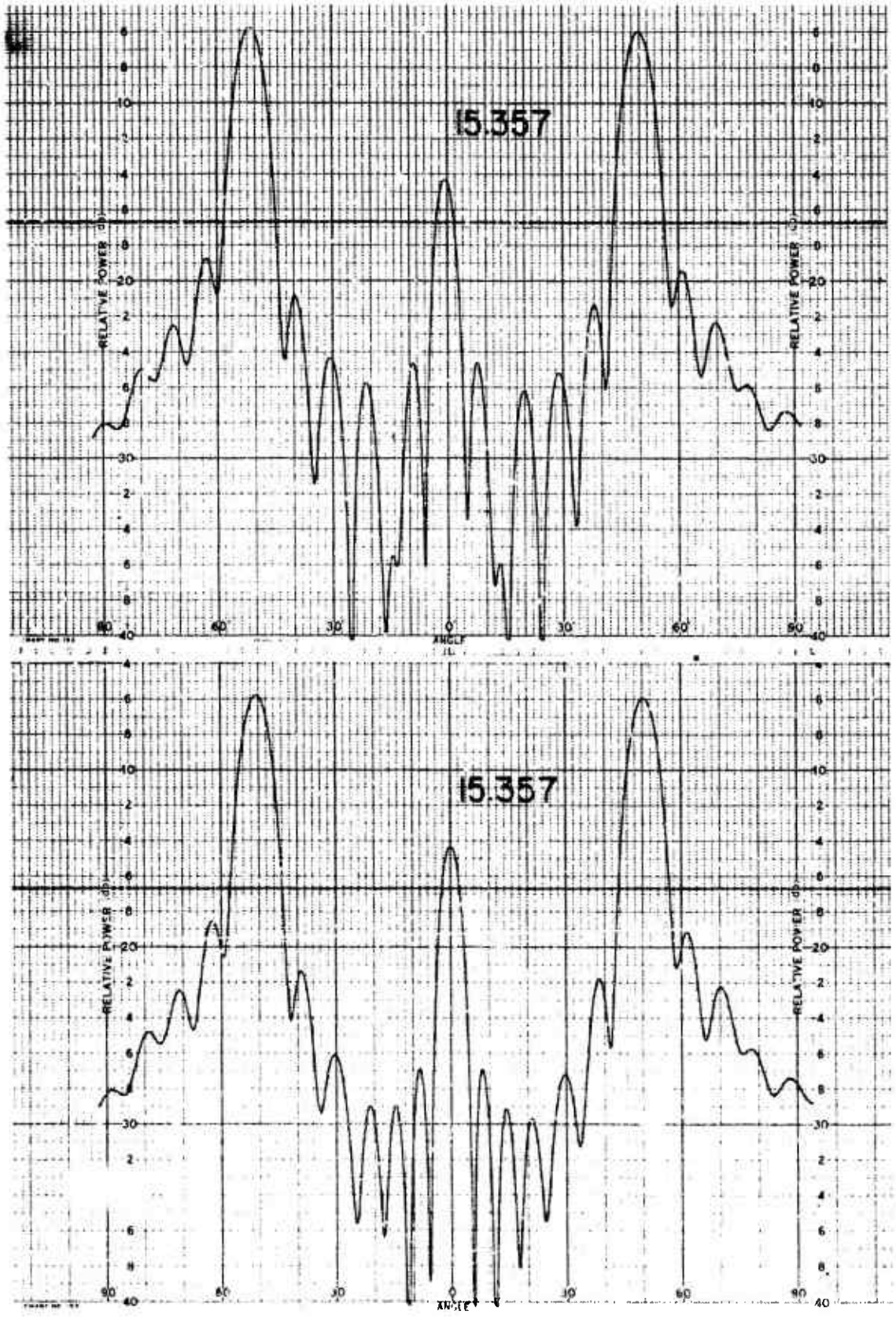
15.357
RELATIVE POWER (db)
ANGLE
15.357
RELATIVE POWER (db)
ANGLE

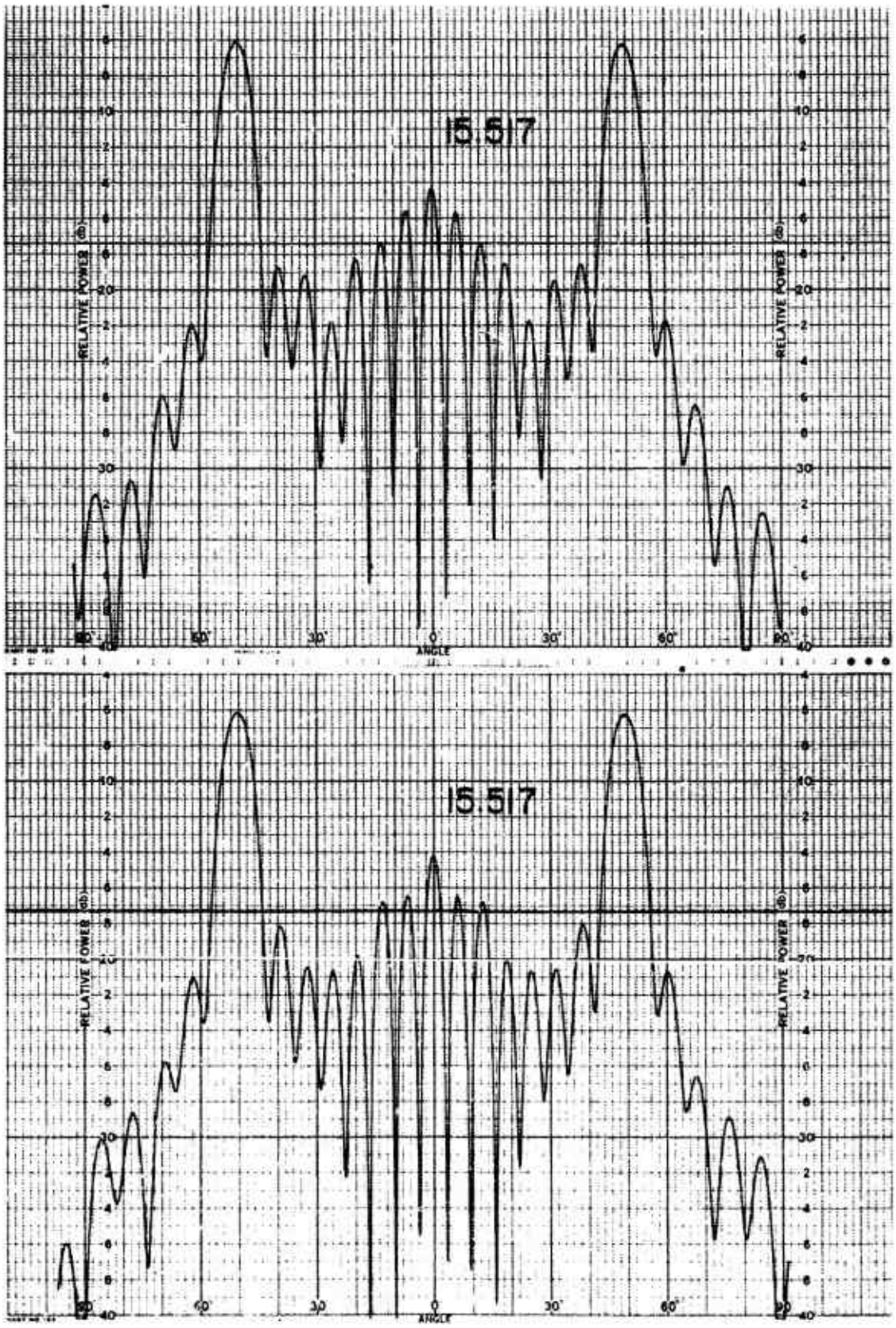
15.517
RELATIVE POWER (db)
ANGLE
15.517
RELATIVE POWER (db)
ANGLE

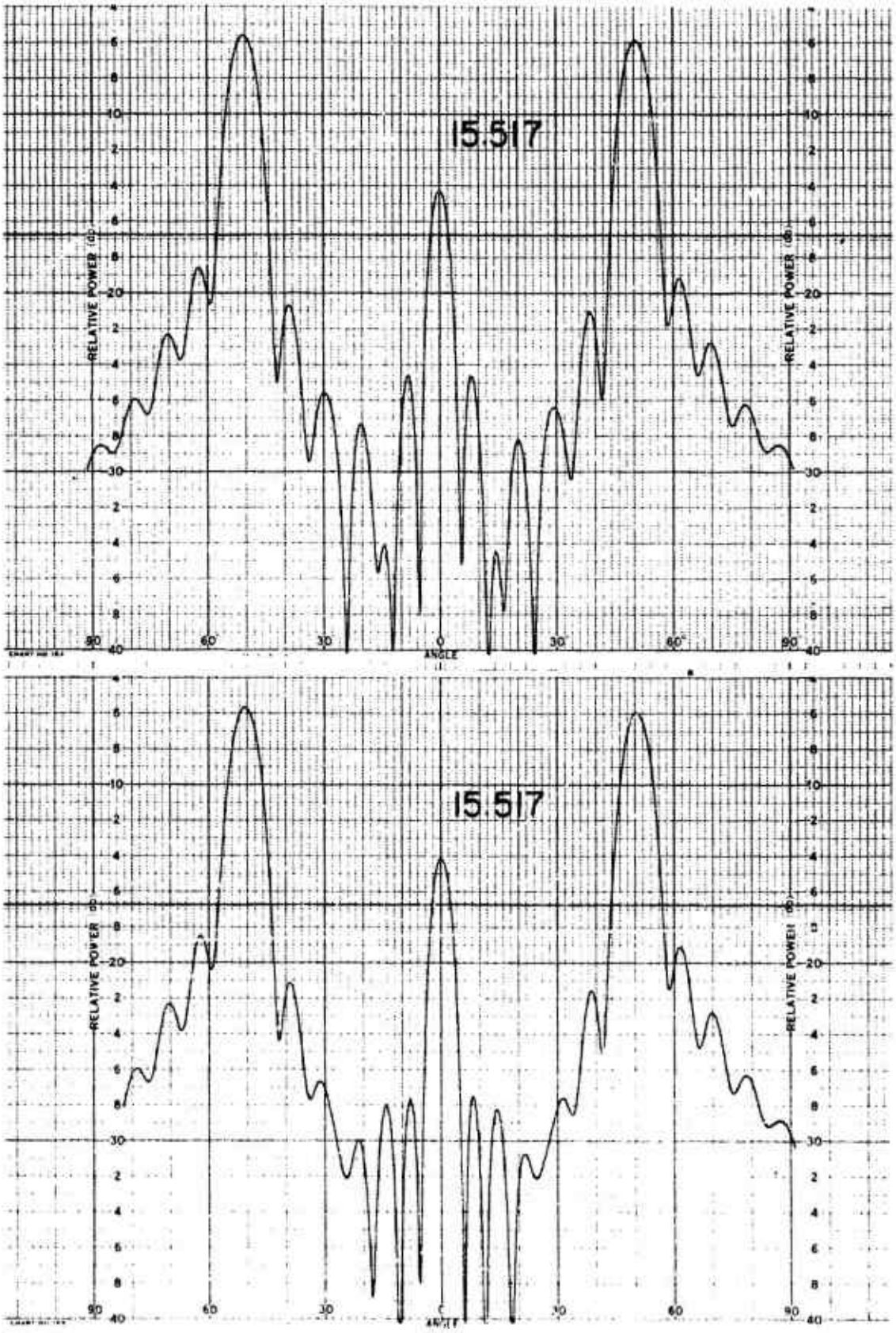
15.517
RELATIVE POWER (dB)
ANGLE
90
60
30
0
30
60
90
15.517
RELATIVE POWER (dB)
ANGLE

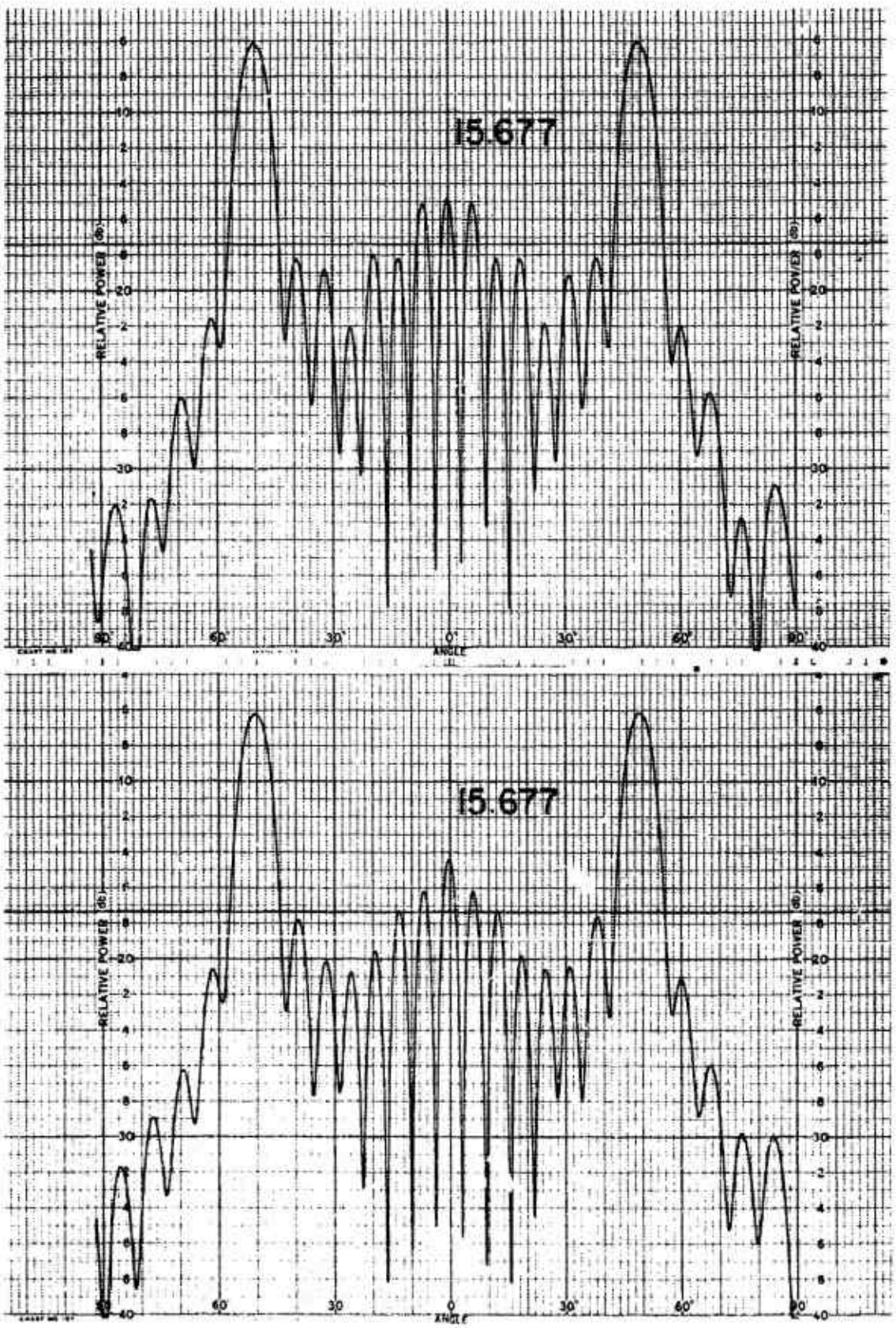
15.677
RELATIVE POWER (dB)
ANGLE
15.677
RELATIVE POWER (dB)
ANGLE

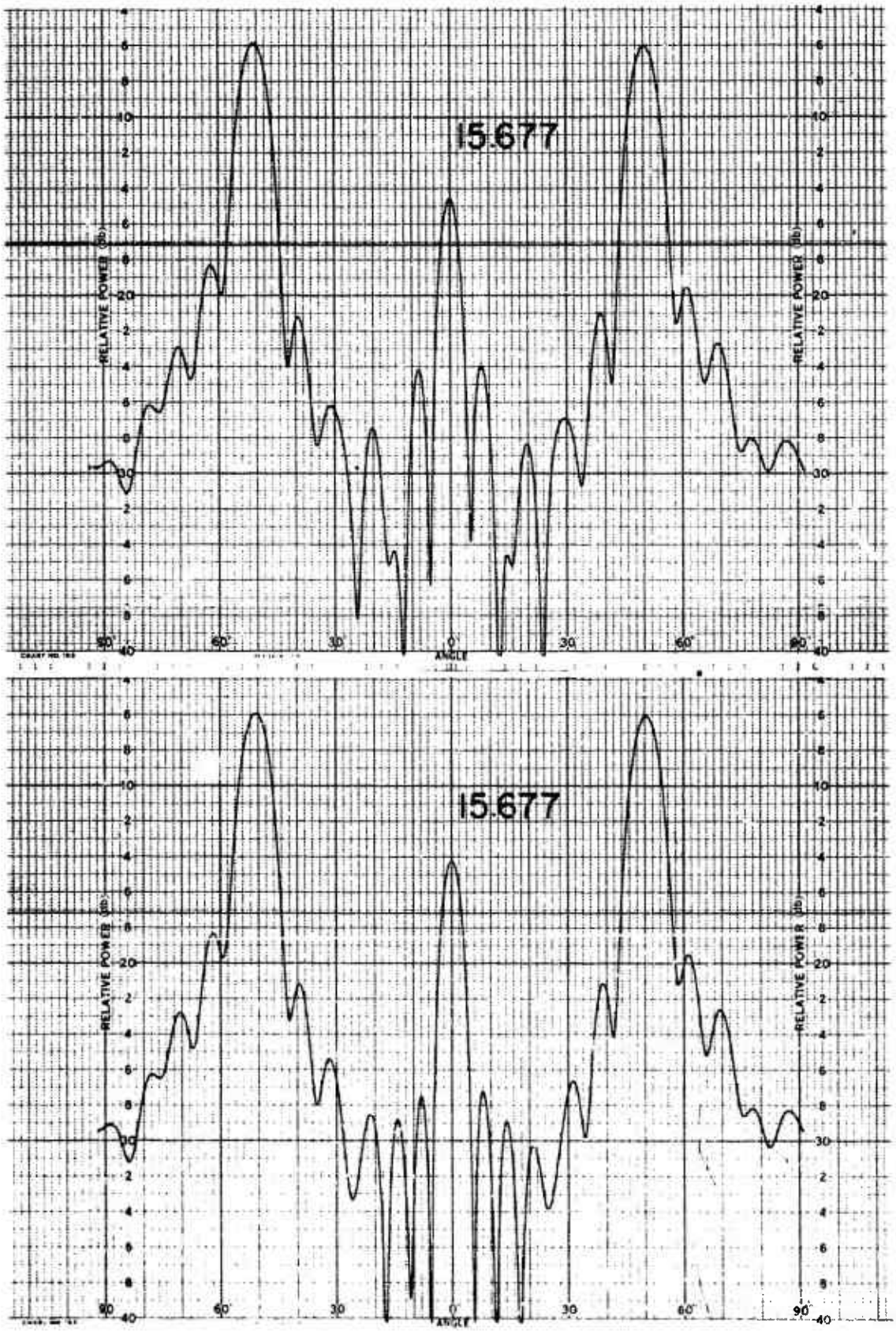
15.677
RELATIVE POWER (DB)
ANGLE
90°
60°
30
0°
30
60°
90°
15.677
RELATIVE POWER (DB)
ANGLE

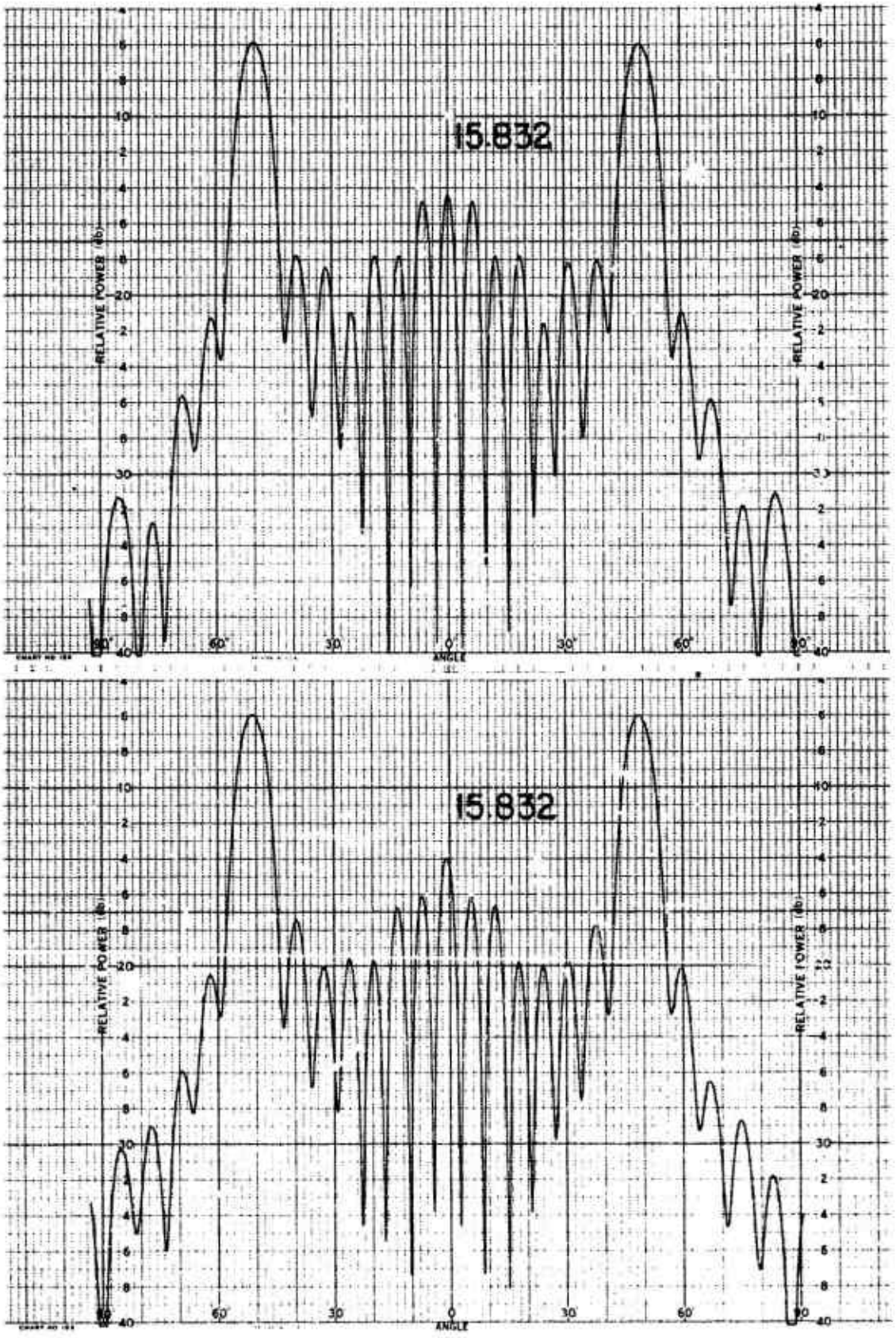
15.832
RELATIVE POWER (db)
ANGLE
15.832
RELATIVE POWER (db)
ANGLE

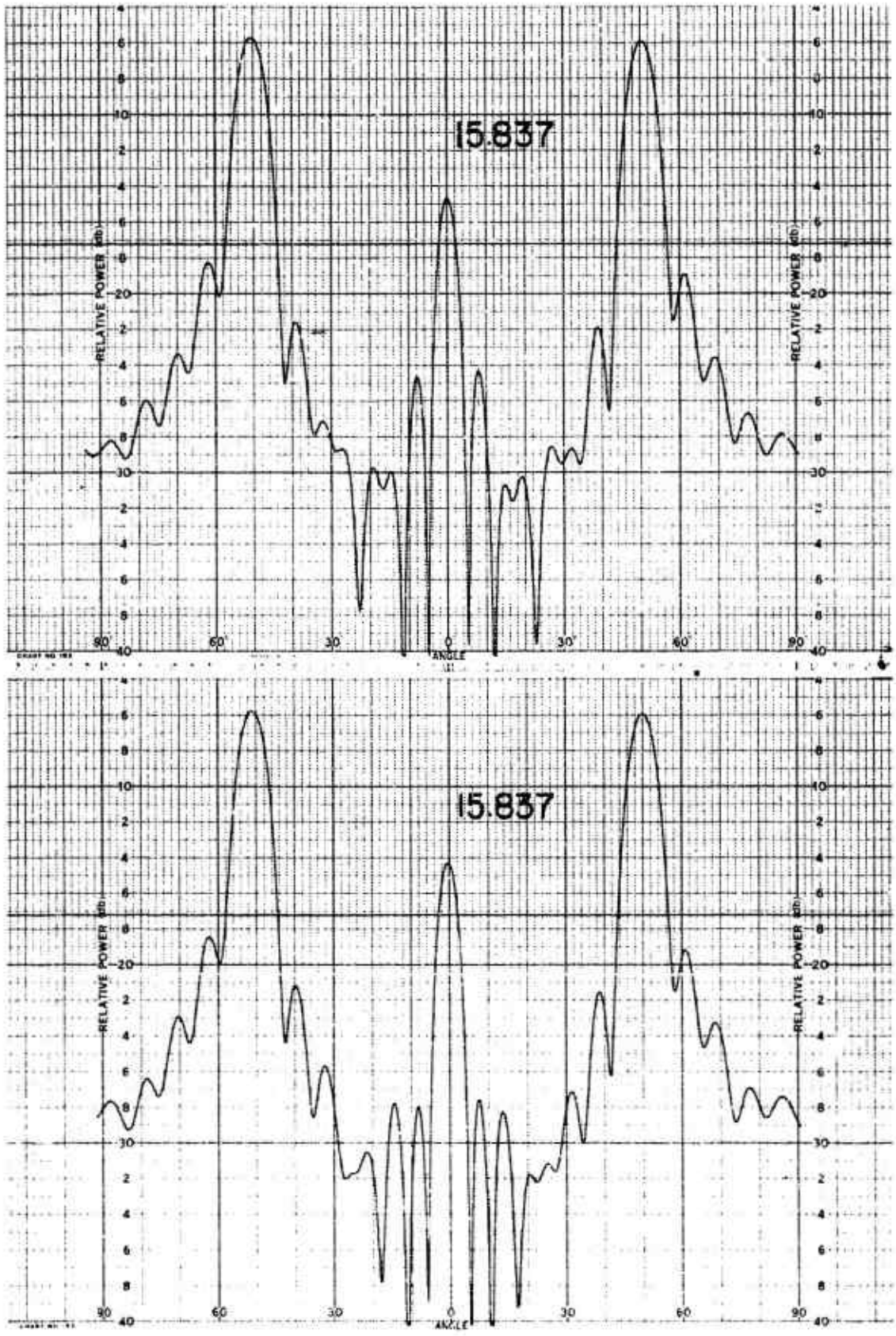
15.837
RELATIVE POWER (dB)
ANGLE
80°
60°
30°
0
30°
60°
90°
15.837
RELATIVE POWER (dB)
ANGLE

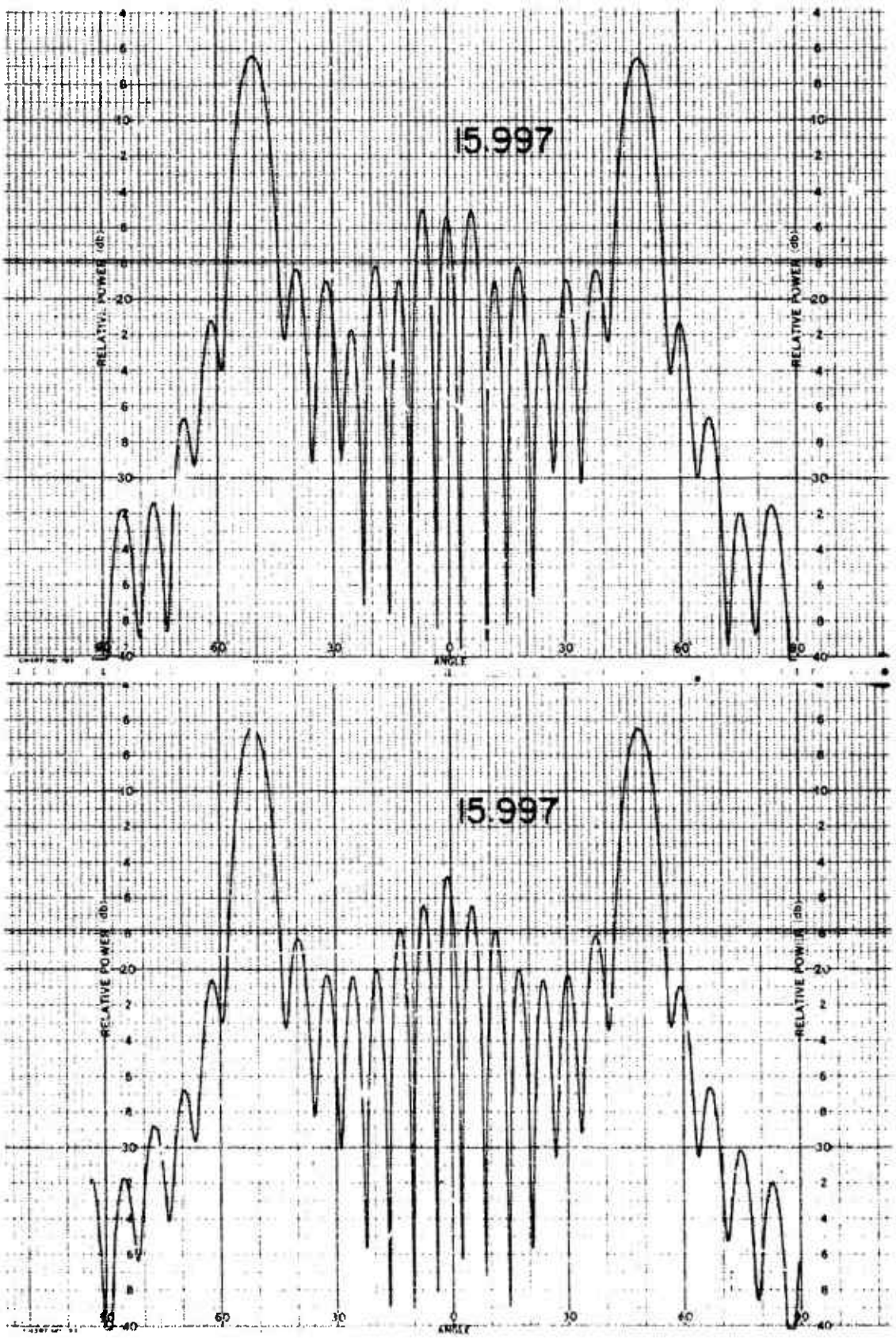
15.997
RELATIVE POWER (db)
ANGLE
15.997
RELATIVE POWER (db)
ANGLE

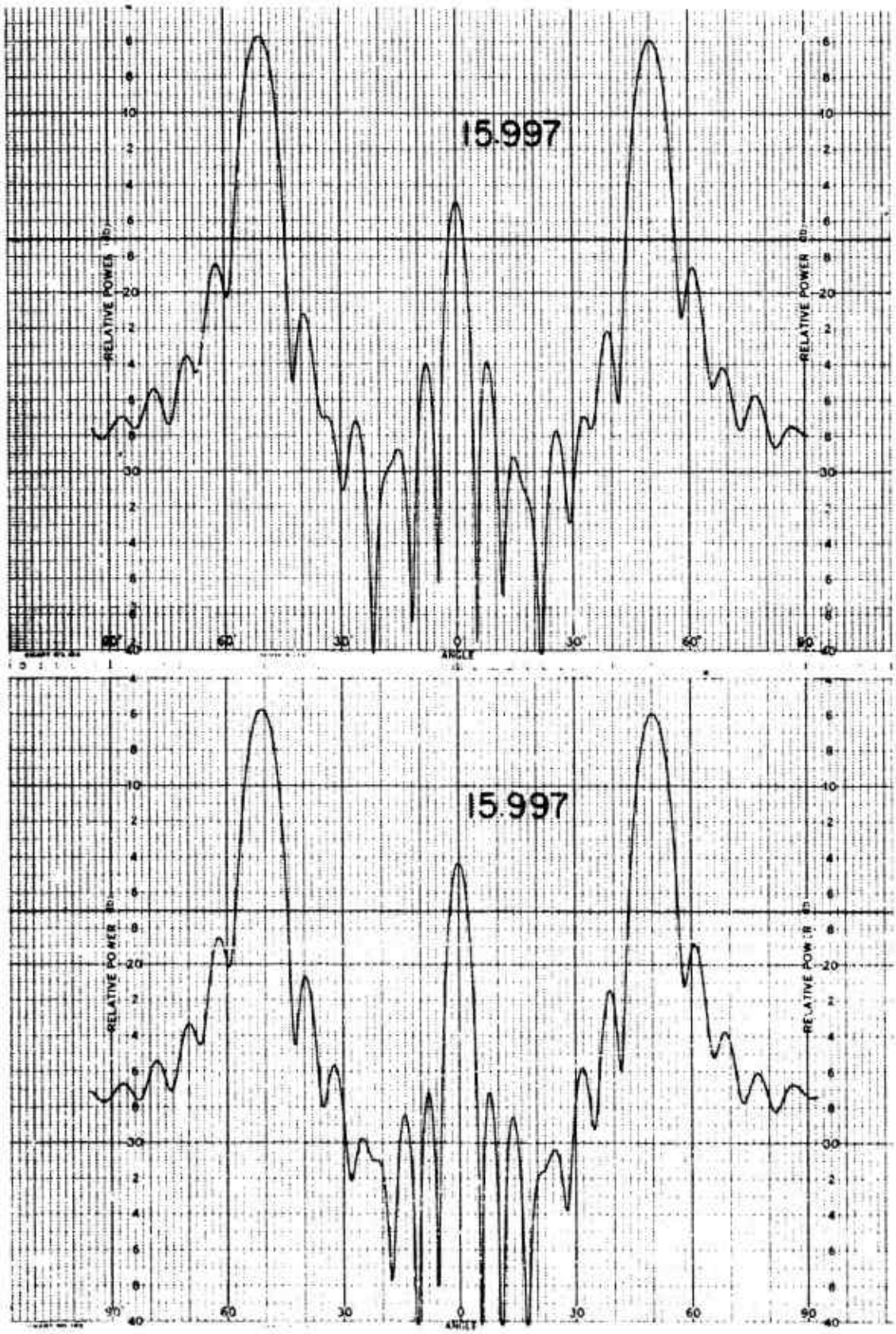
15.997
RELATIVE POWER (dB)
ANGLE
15.997
RELATIVE POWER (dB)
ANGLE

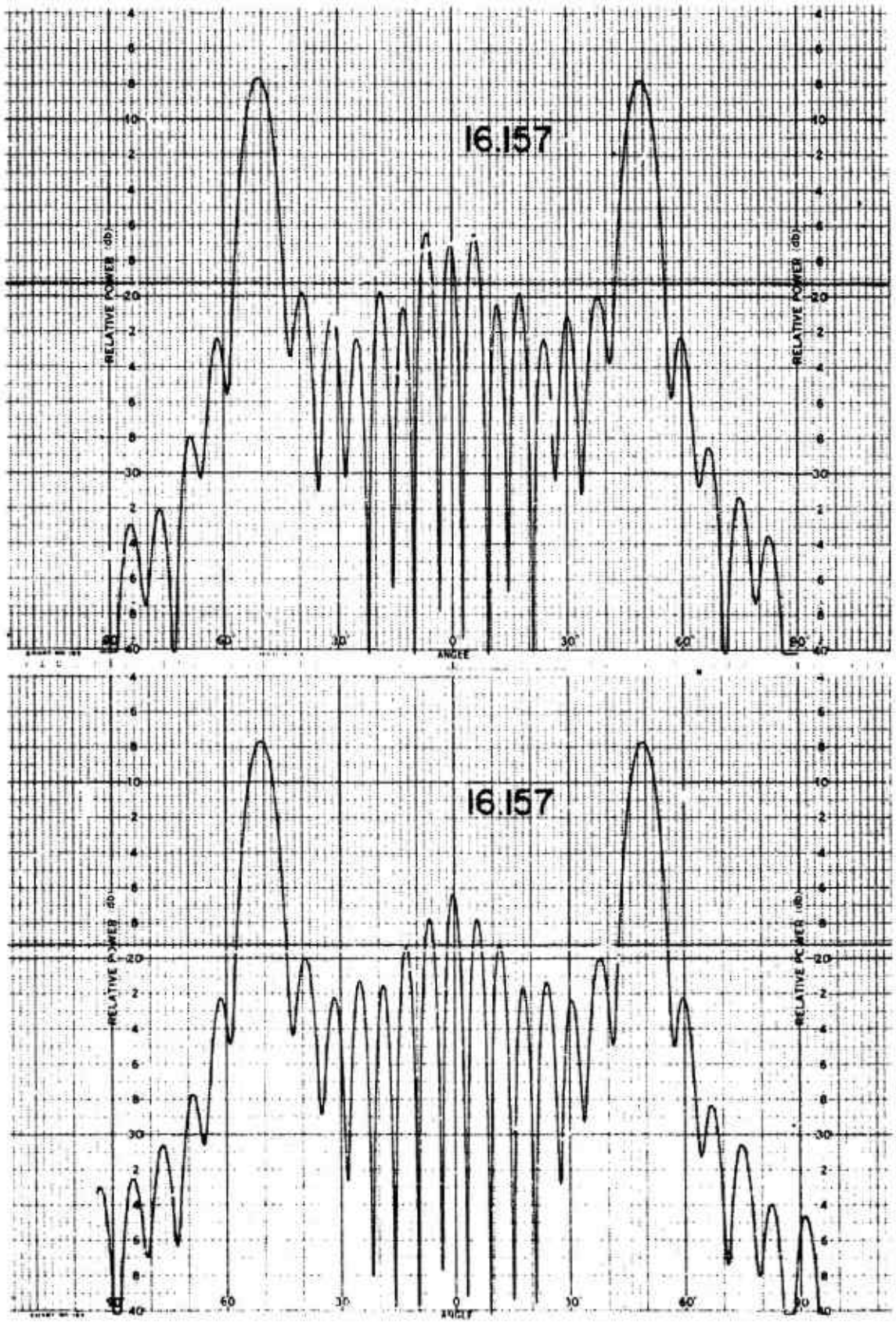
16.157
RELATIVE POWER (db)
ANGEE
16.157
RELATIVE POWER (db)
ANGLE

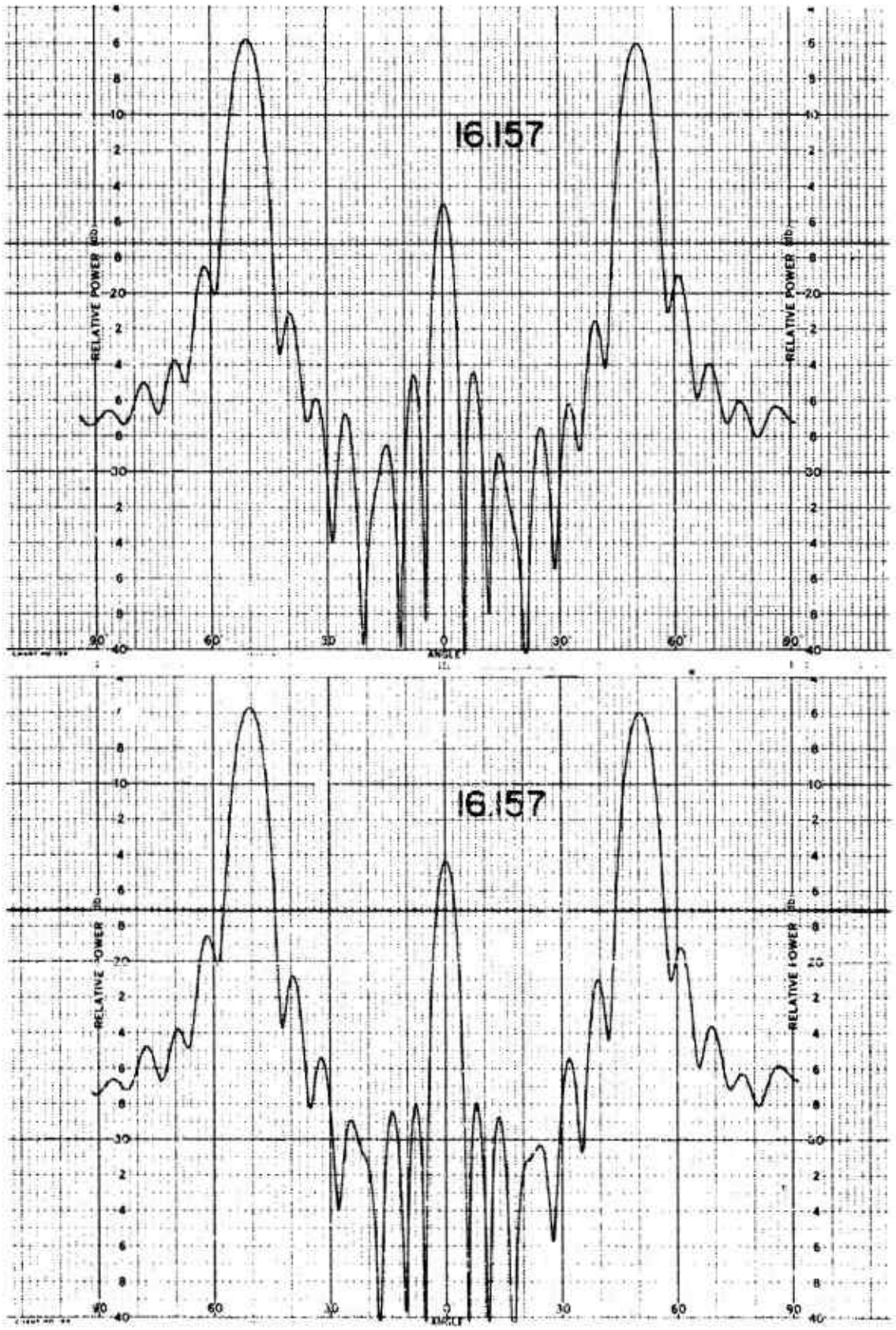
16.157
RELATIVE POWER (db)
ANGLE
16.157
RELATIVE POWER (db)
ANGLE

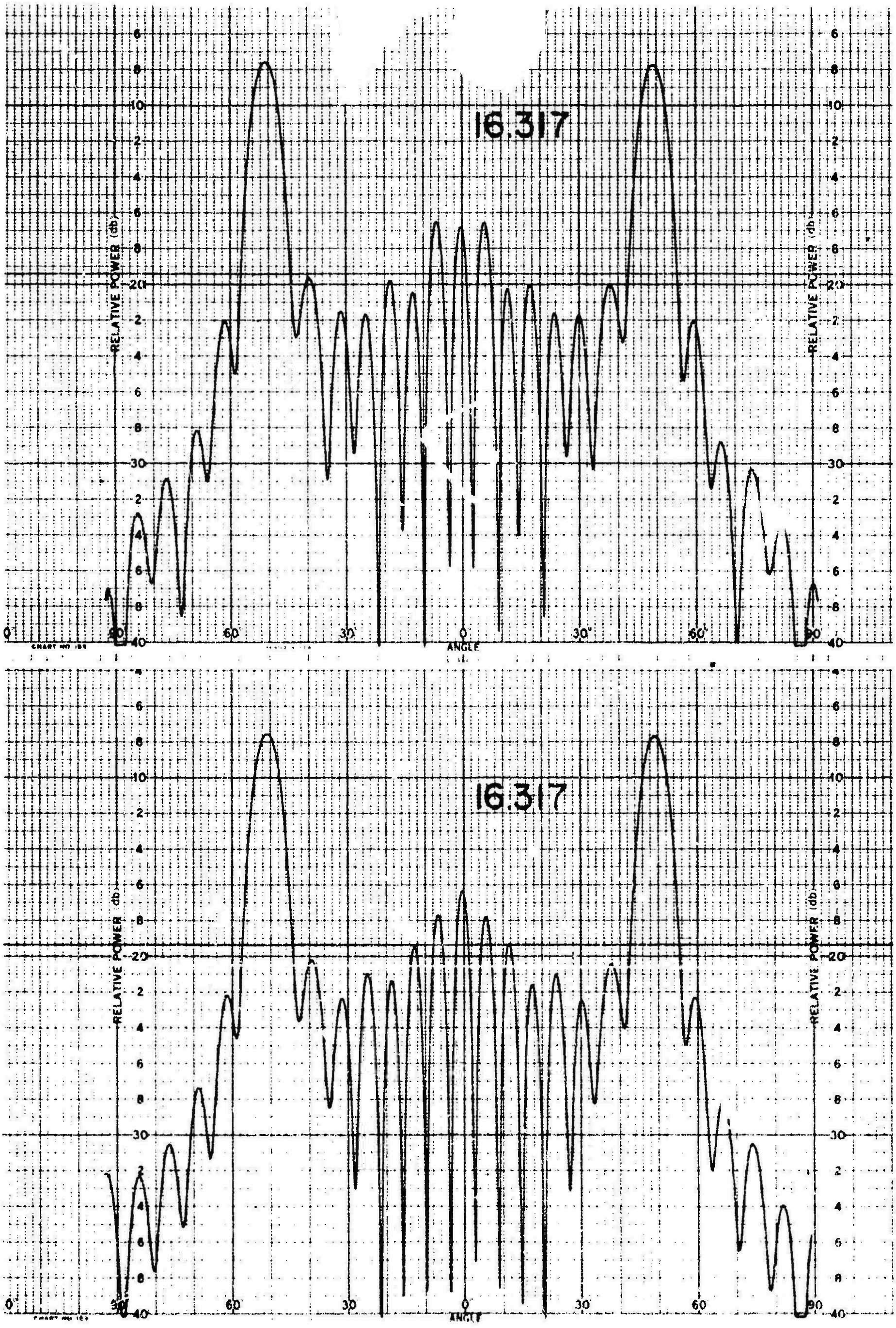
16,317
RELATIVE POWER (db)
ANGLE
0°
30°
60°
90°

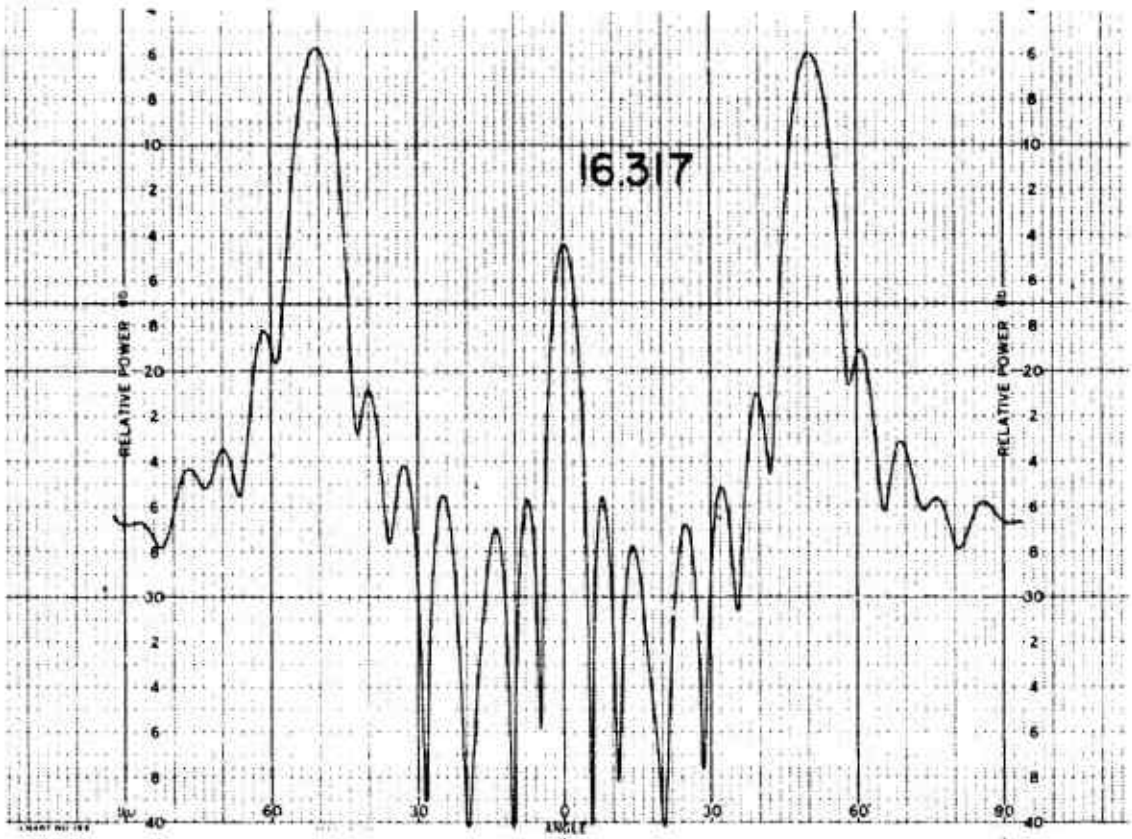
16.317
RELATIVE POWER
RELATIVE POWER
ANGLE

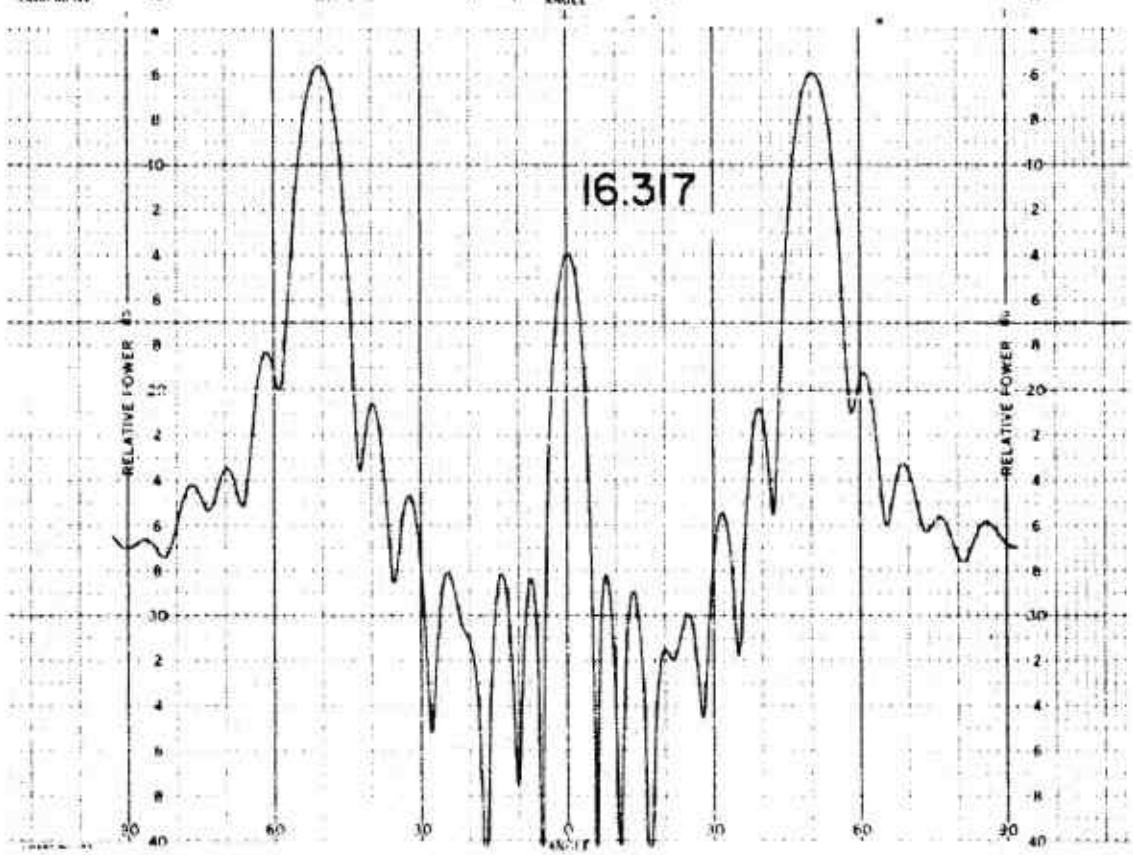
16.317
RELATIVE POWER
RELATIVE POWER

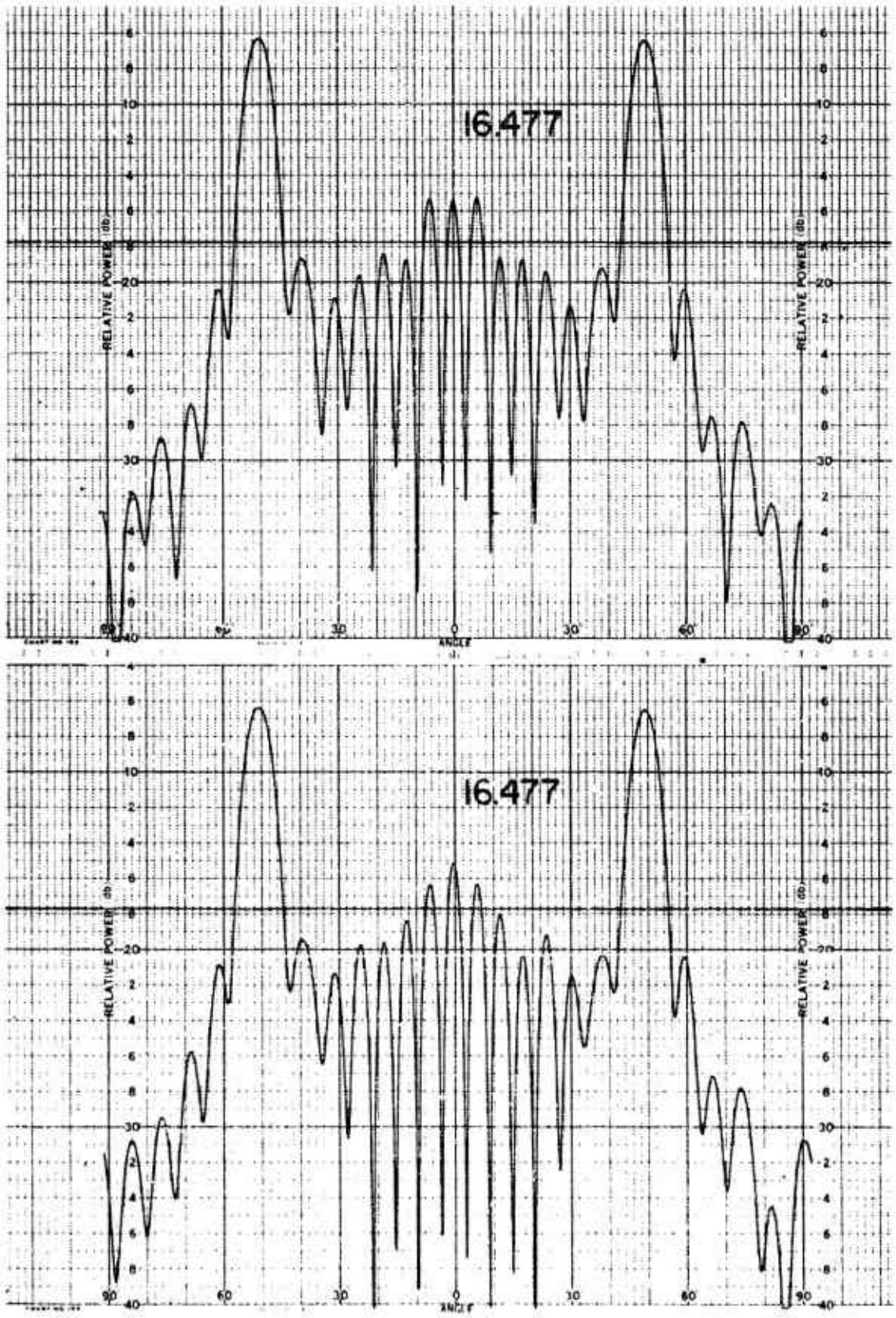
16.477
RELATIVE POWER (db)
ANGLE
16.477
RELATIVE POWER (db)
ANGLE

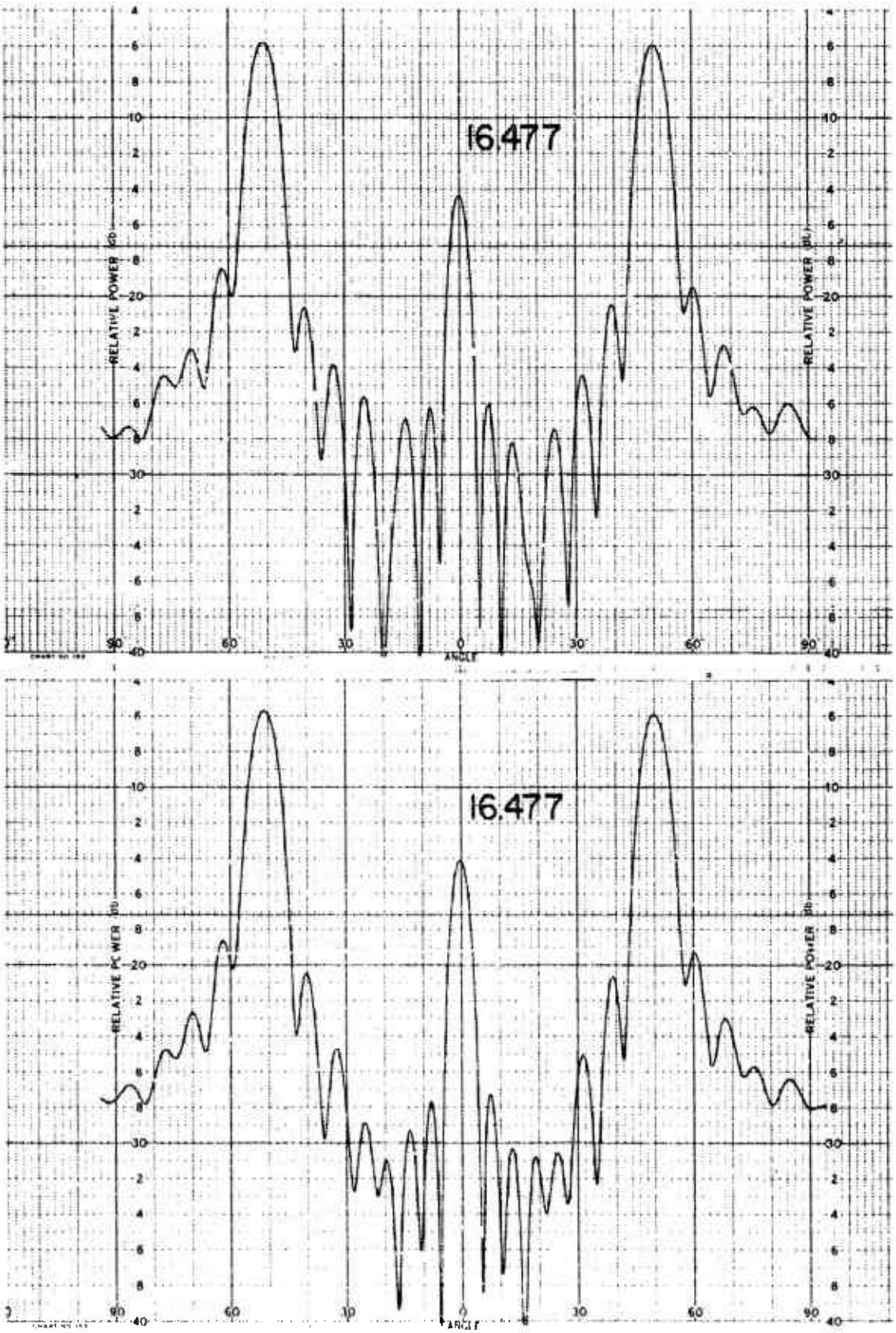
16.477
RELATIVE POWER (db)
ANGLE
16.477
RELATIVE POWER (db)
ANGLE

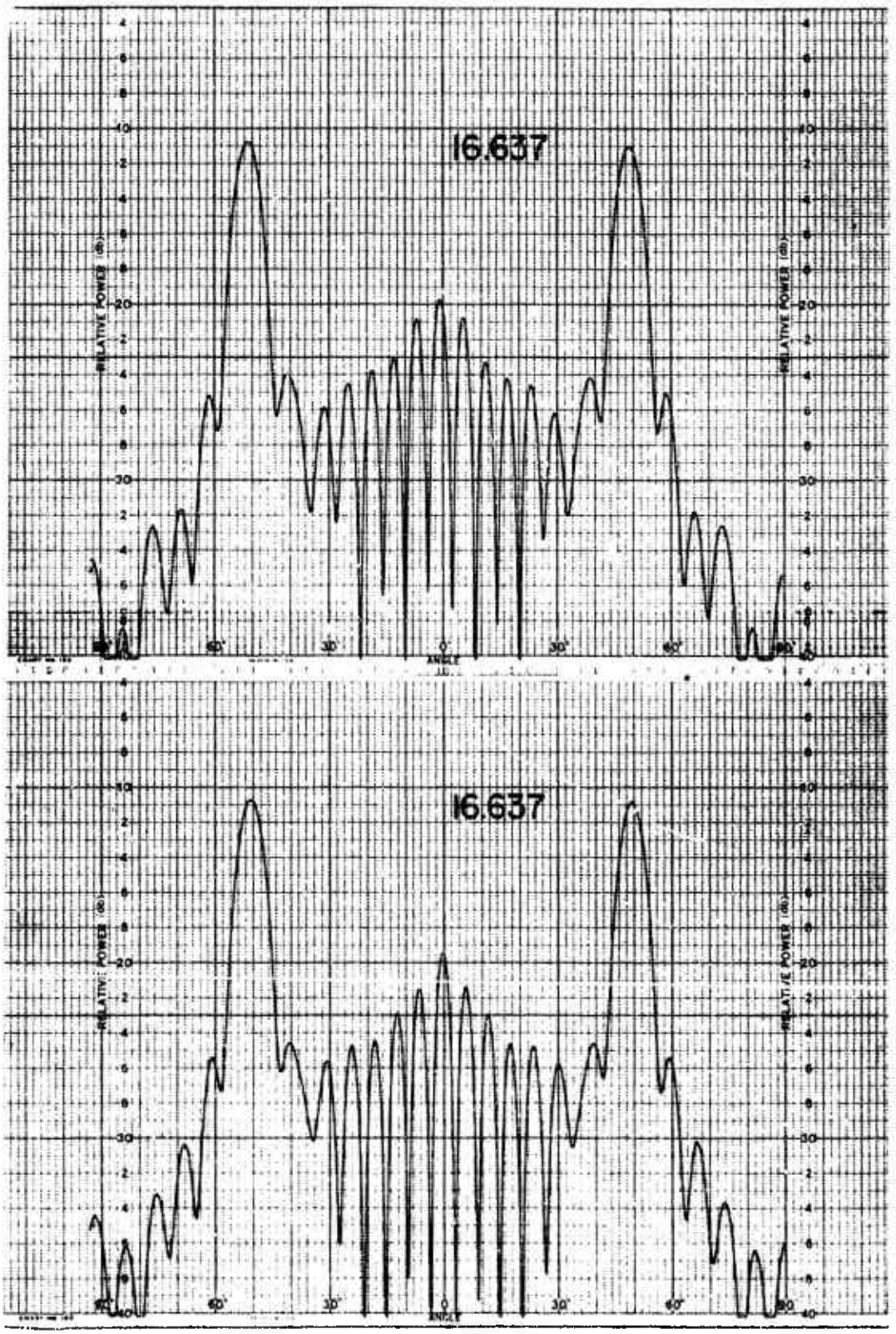
16.637
RELATIVE POWER (db)
ANGLE
16.637
RELATIVE POWER (db)
ANGLE

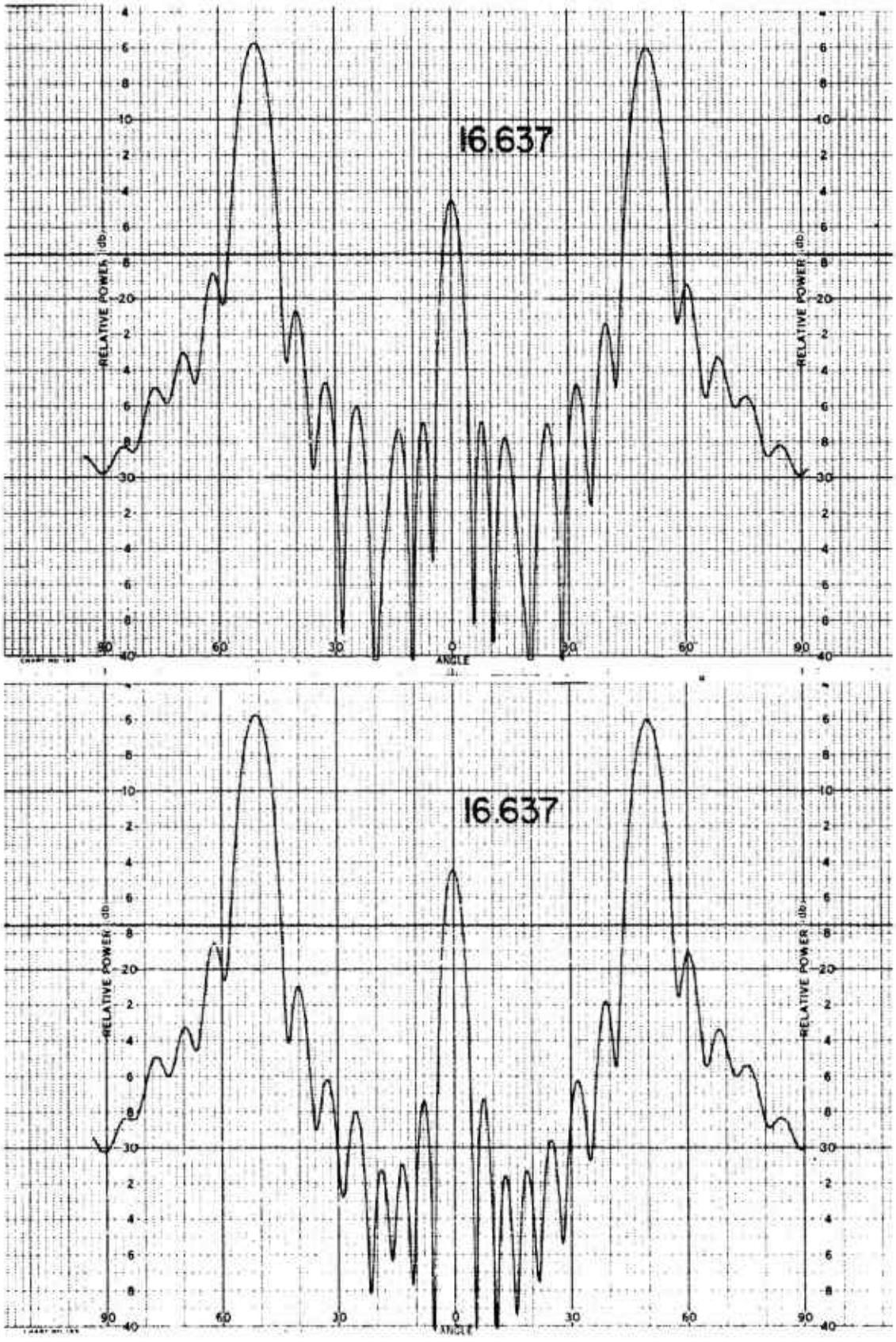
16.637
RELATIVE POWER (db)
ANGLE
16.637
RELATIVE POWER (db)
ANGLE

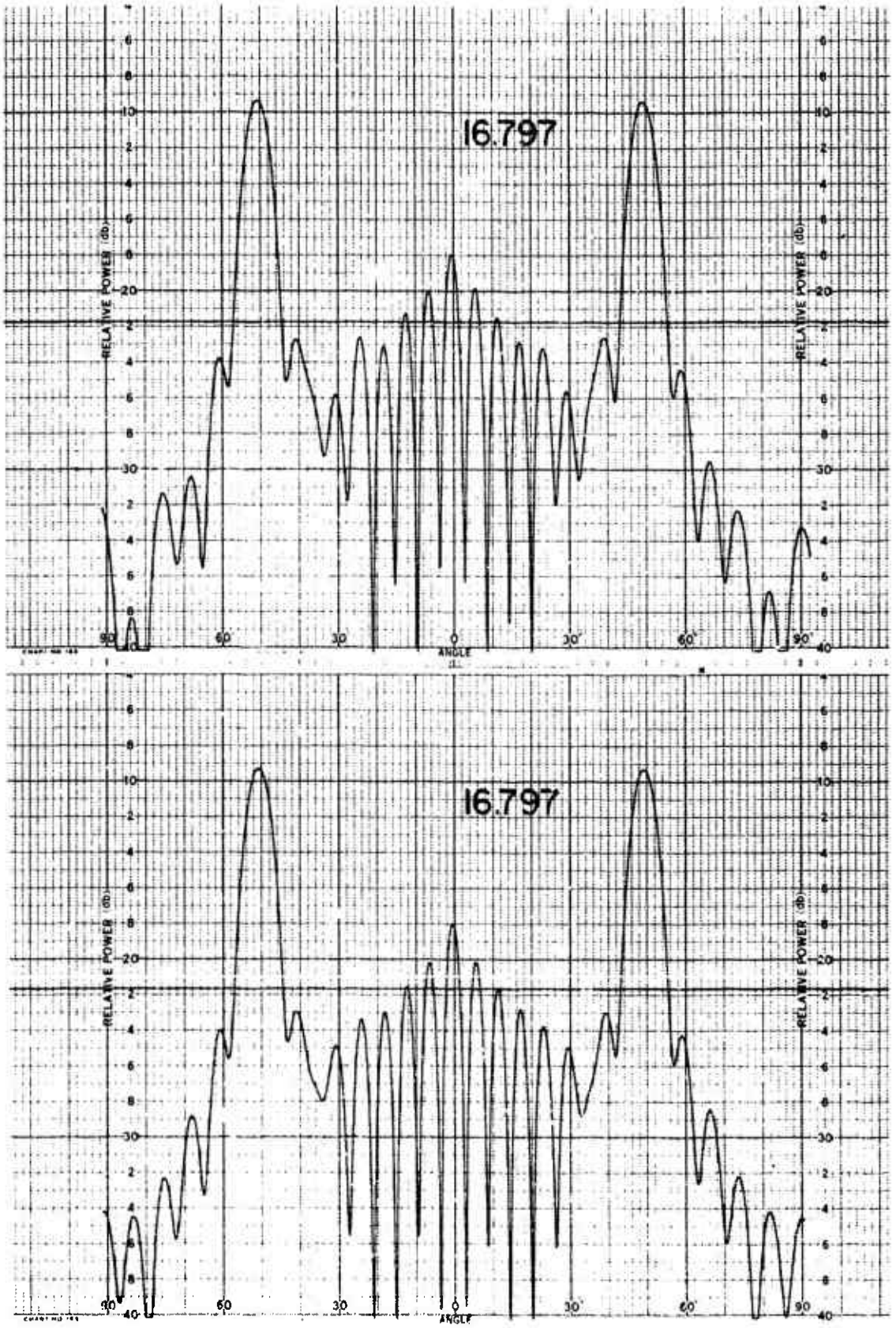
16.797
RELATIVE POWER (db)
ANGLE
16.797
RELATIVE POWER (db)
ANGLE

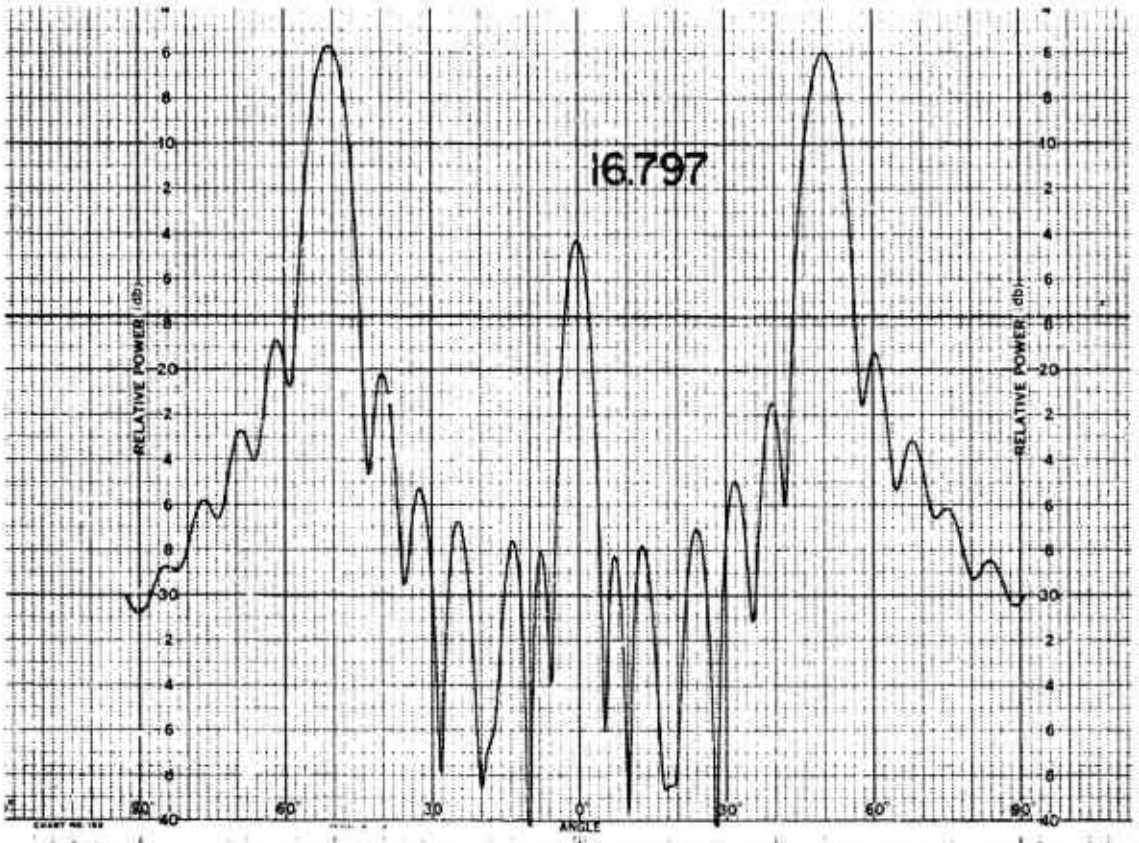
16.797
RELATIVE POWER (db)
ANGLE
60°
30
0°
30°
60°
90°

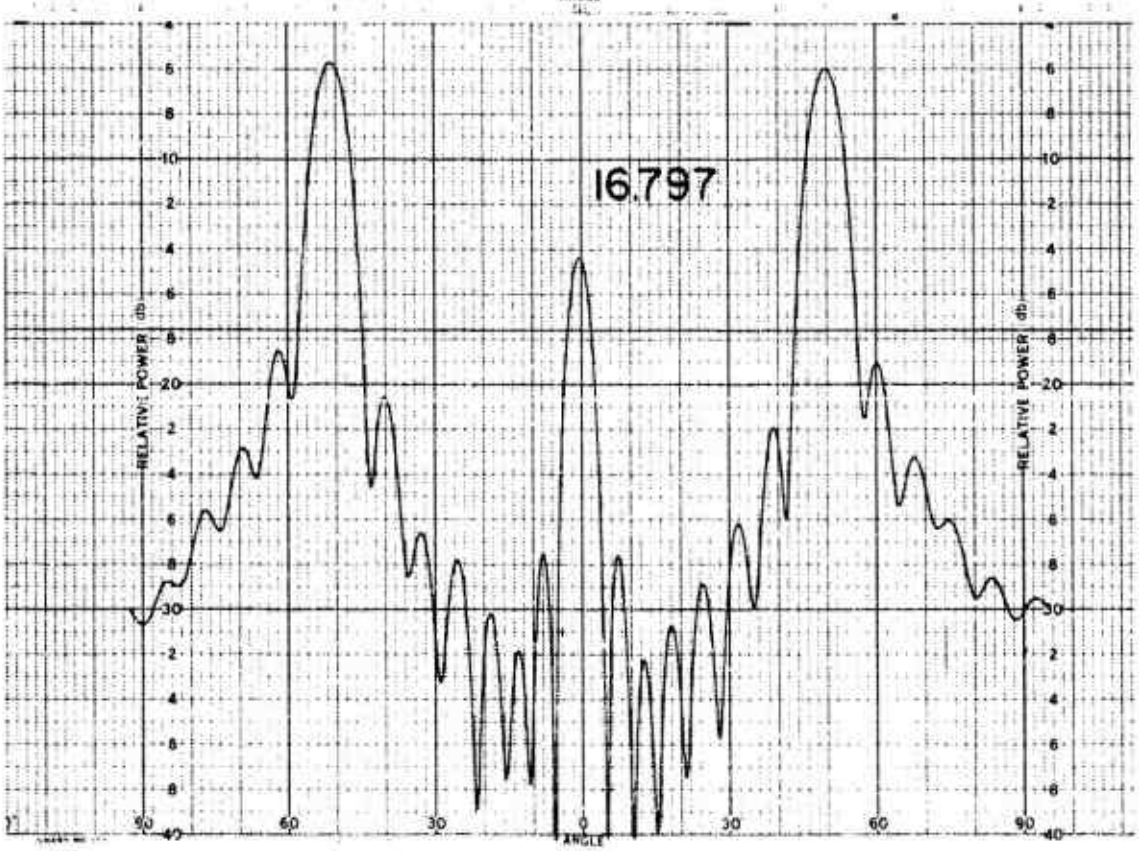
16.797
RELATIVE POWER (db)
ANGLE
60°
30
0°
30°
60°
90°

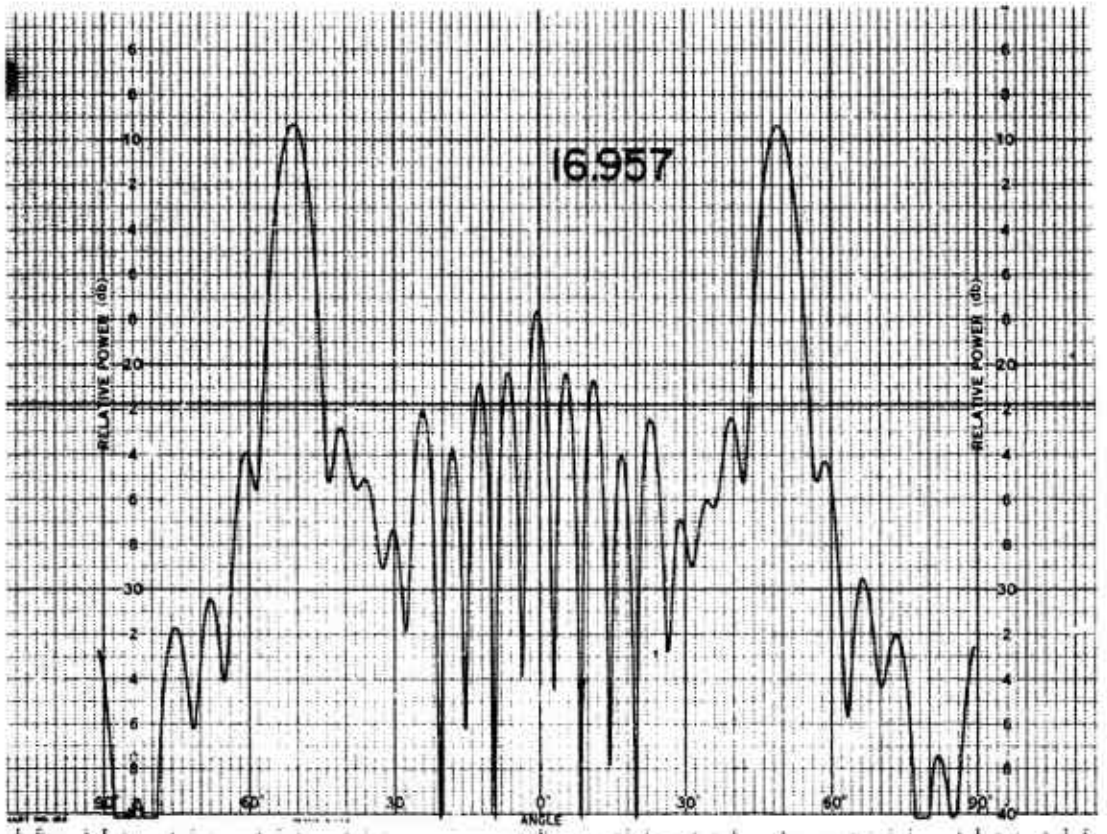
16.957
RELATIVE POWER (db)
ANGLE
90°
60°
30°
0°
30°
60°
90°

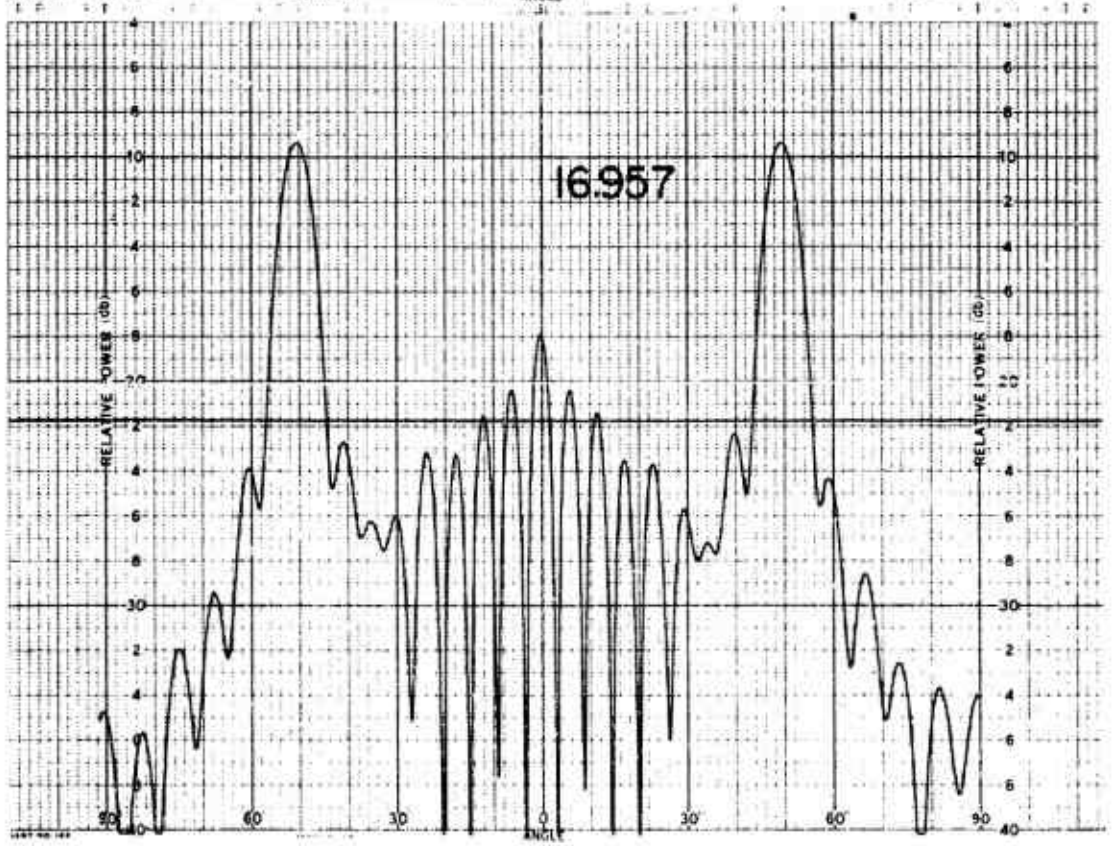
16.957
RELATIVE POWER (db)
ANGLE
90°
60°
30°
0°
30°
60°
90°

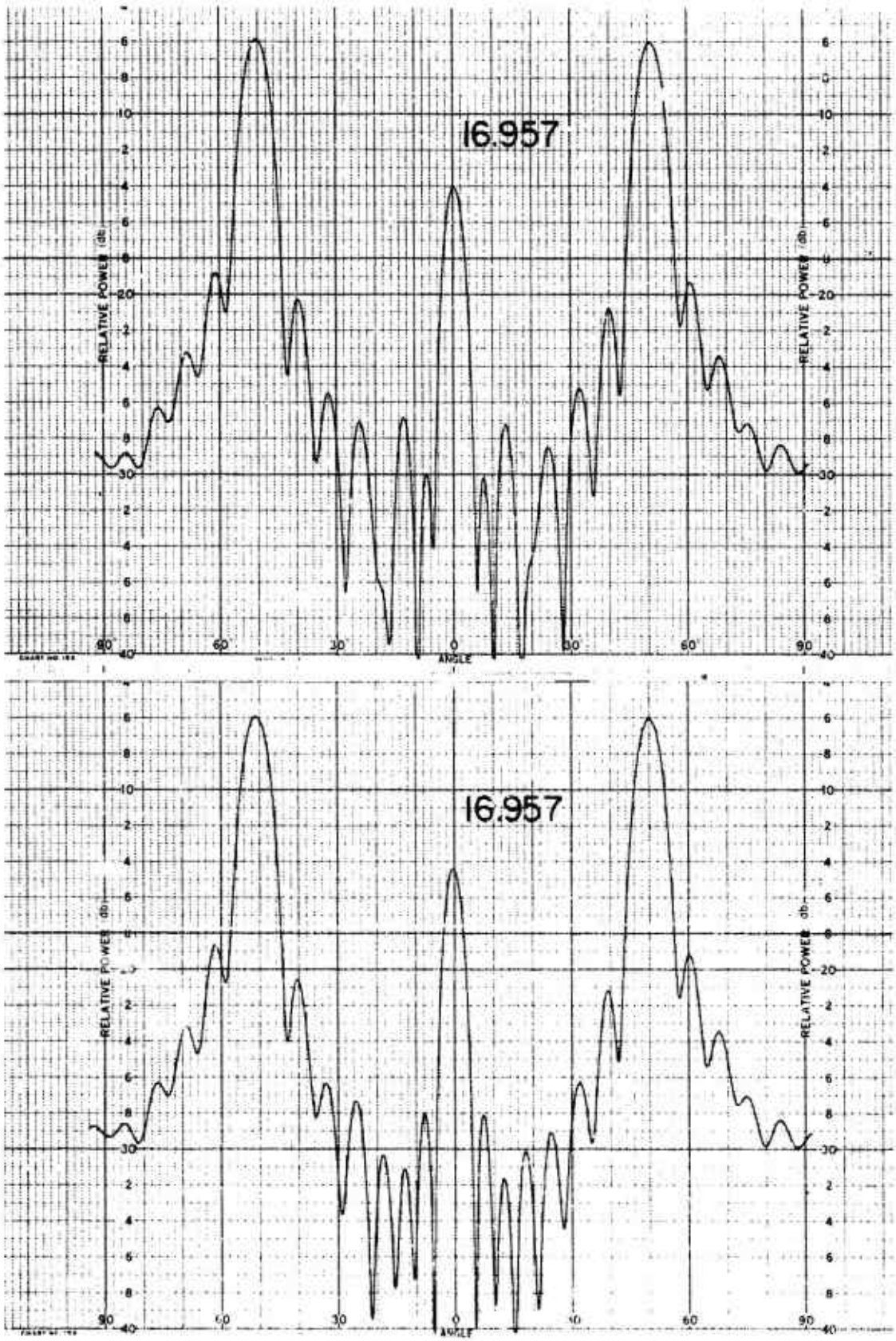
16.957
RELATIVE POWER (db)
ANGLE
16.957
RELATIVE POWER (db)
ANGLE

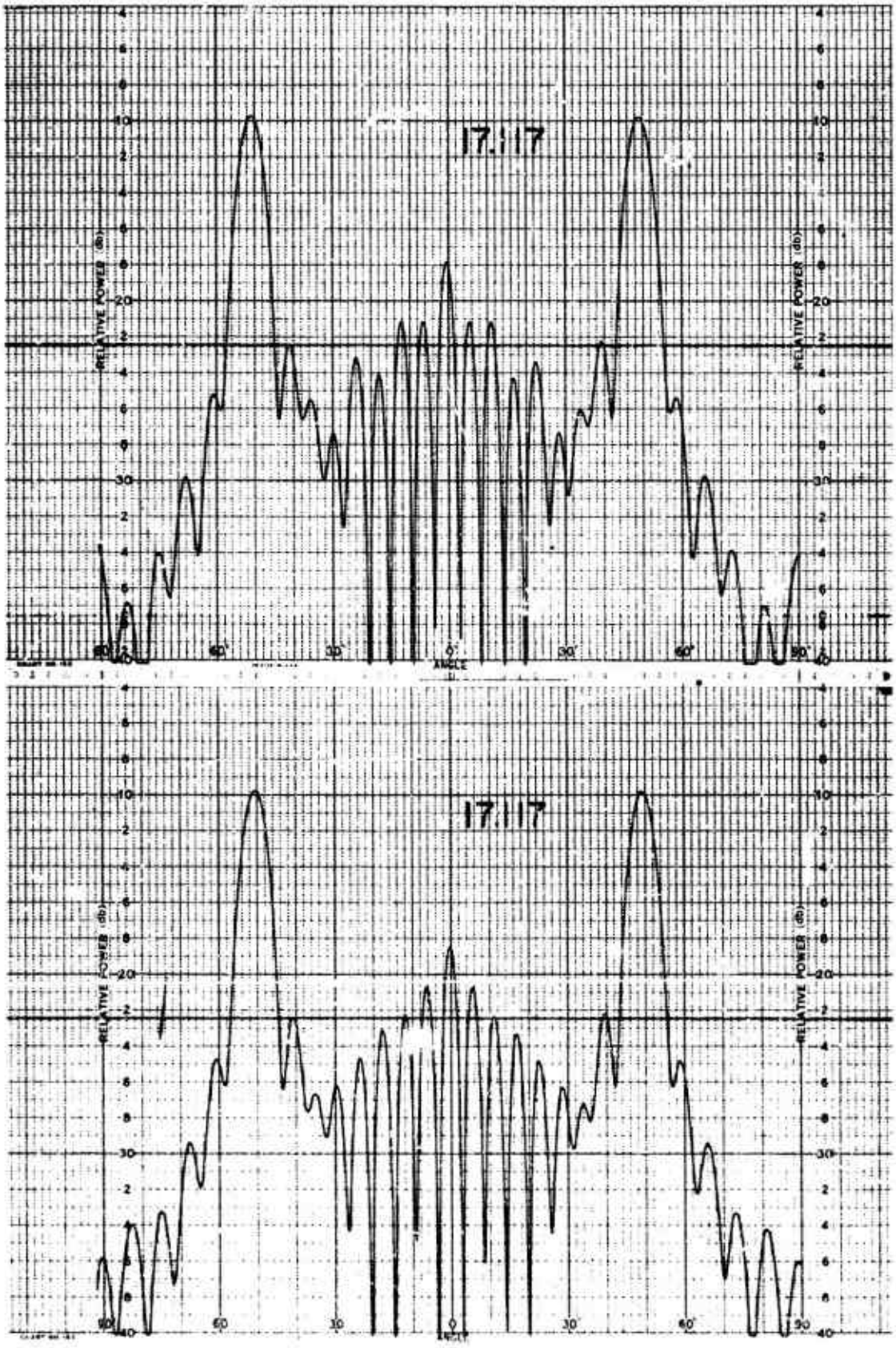
17.117
RELATIVE POWER (db)
ANGLE
17.117
RELATIVE POWER (db)

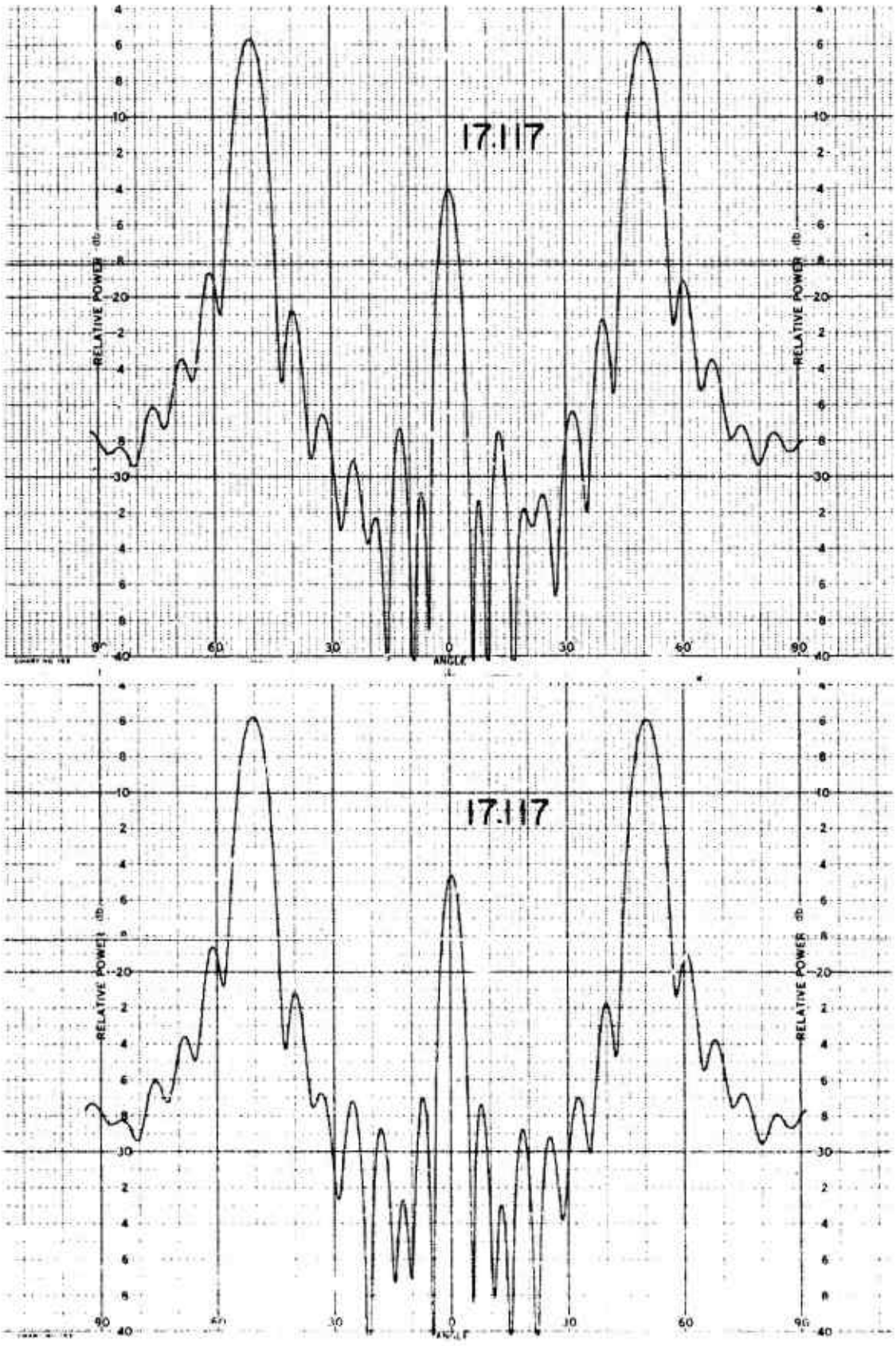
17.117
RELATIVE POWER db
ANGLE
90
60
30
0
30
60
90
17.117
RELATIVE POWER db
ANGLE

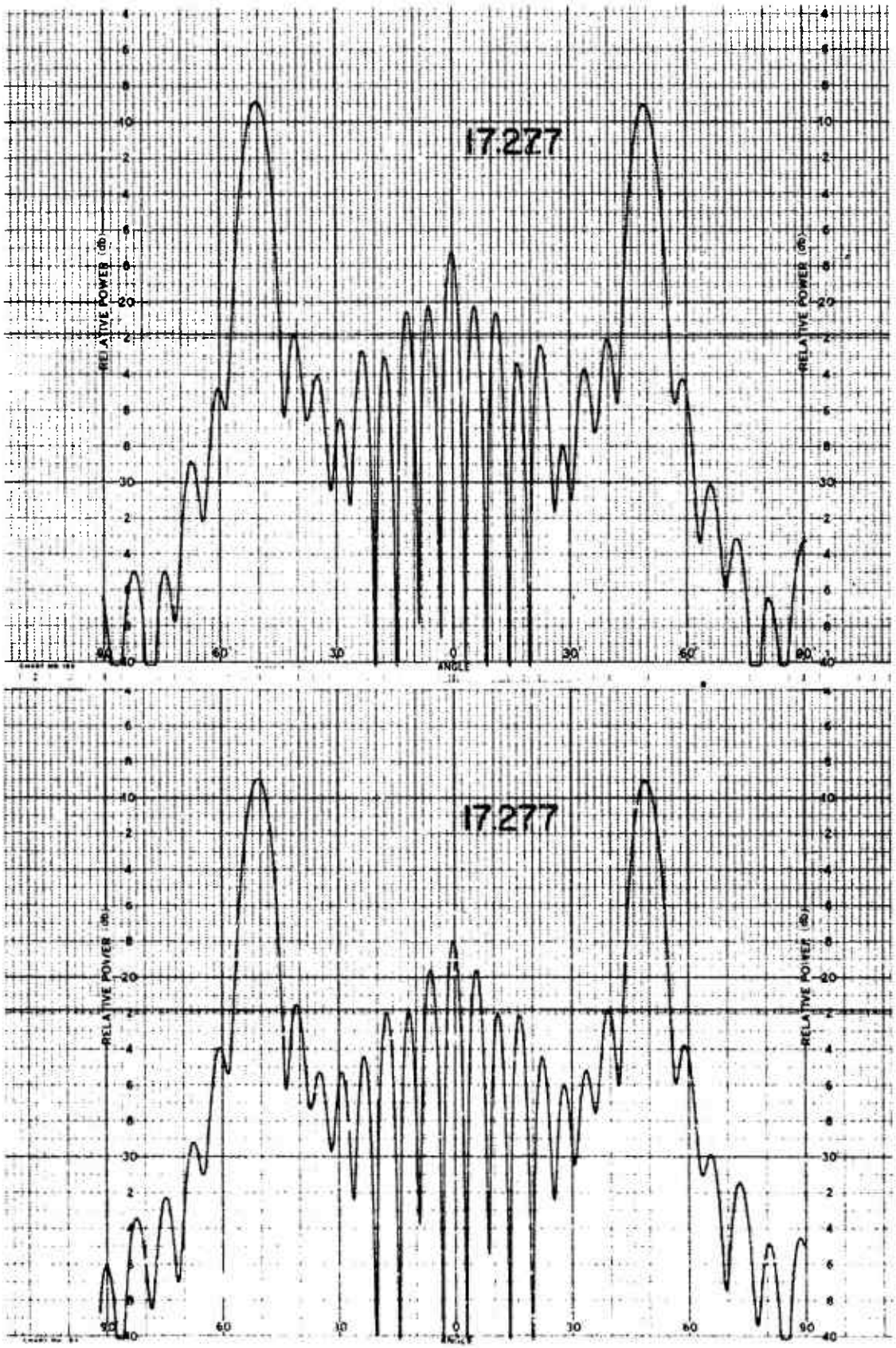
17.277
RELATIVE POWER (dB)
ANGLE
17.277
RELATIVE POWER (dB)

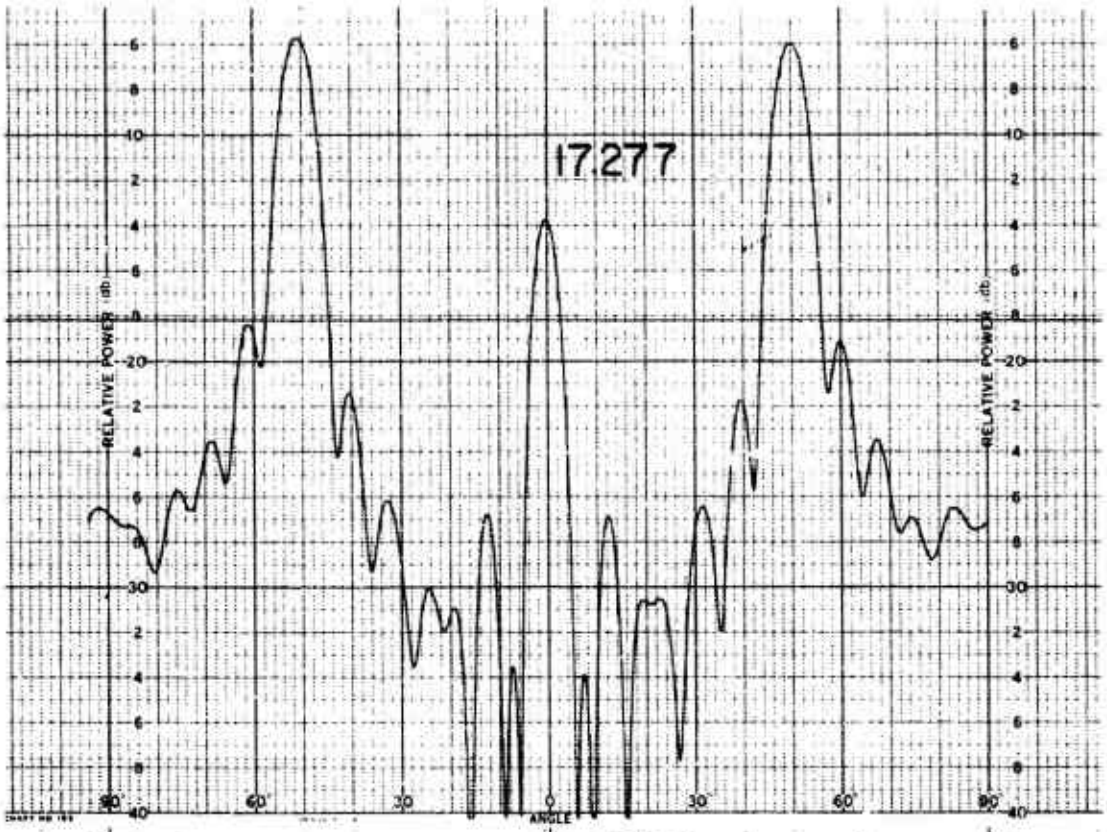
17.277
RELATIVE POWER (dB)
ANGLE

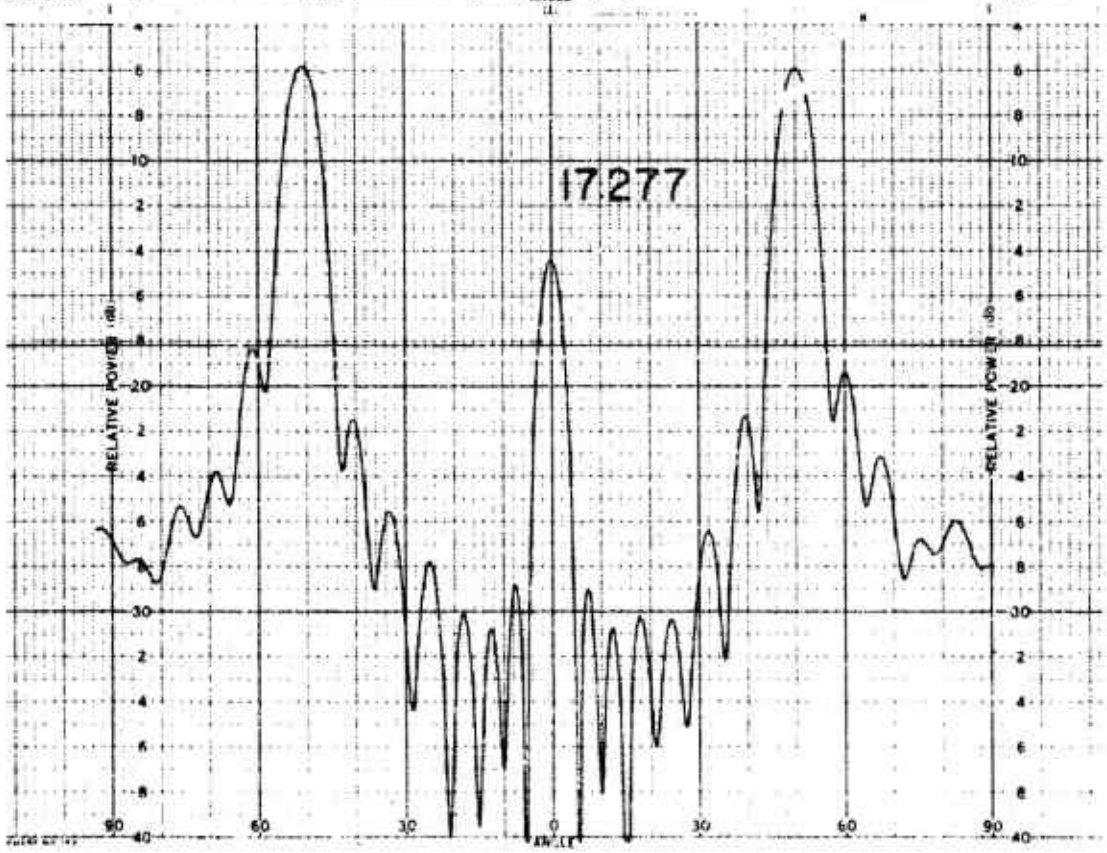
17.277
RELATIVE POWER (dB)
ANGLE

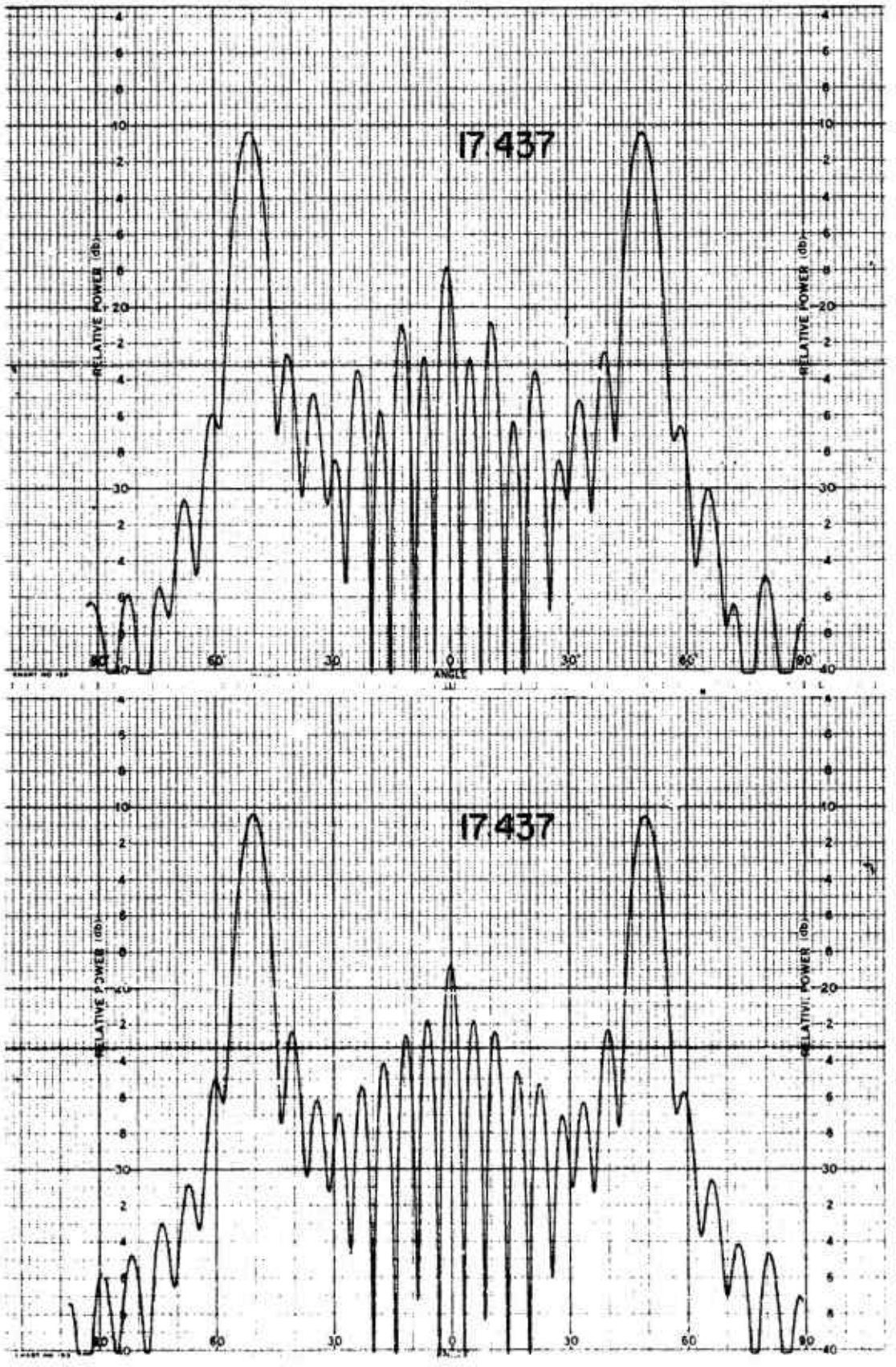
17.437
RELATIVE POWER (db)
ANGLE
17.437
RELATIVE POWER (db)

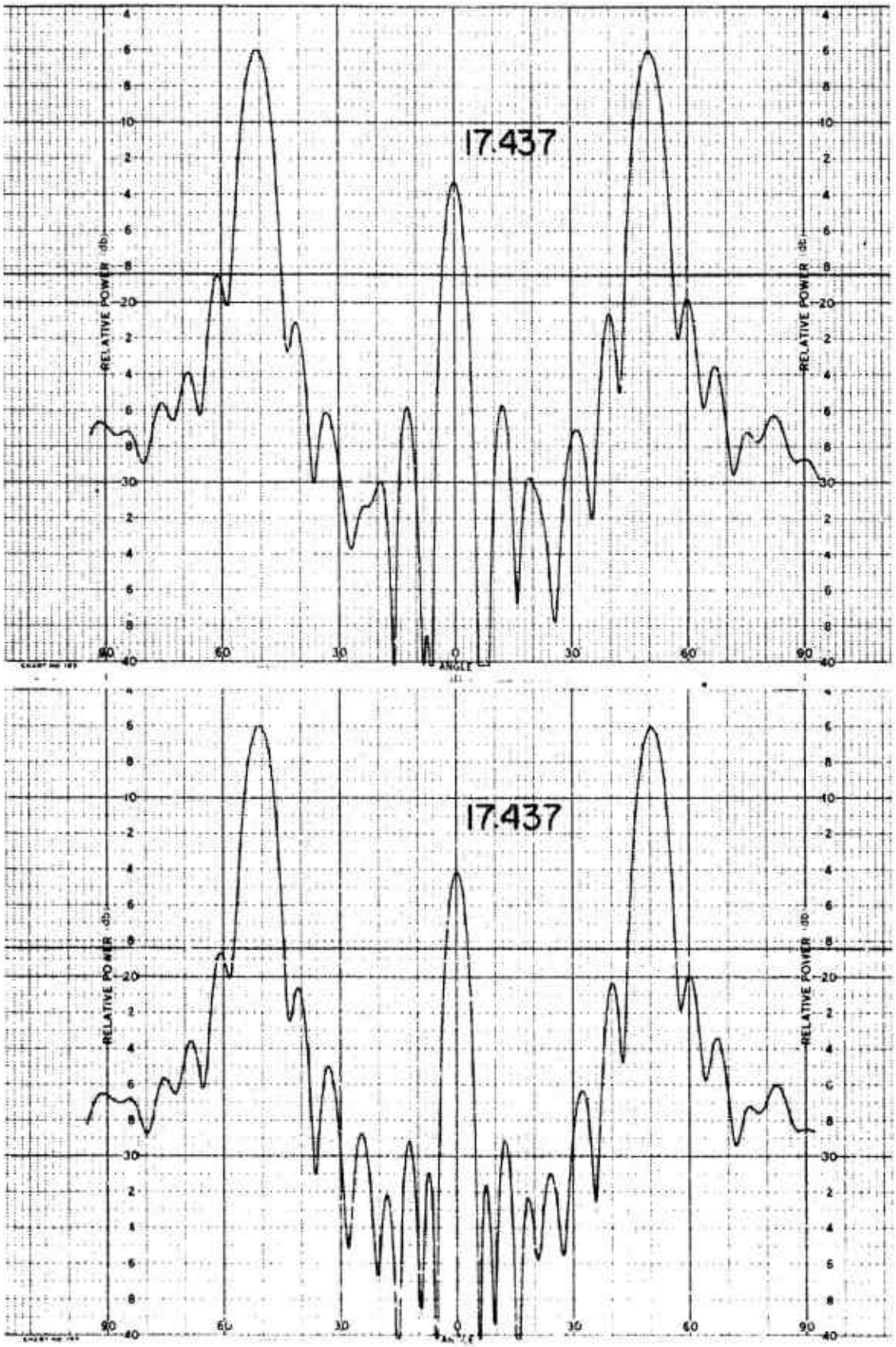
17.437
RELATIVE POWER (db)
ANGLE
90
60
30
0
30
60
90
17.437
RELATIVE POWER (db)
ANGLE

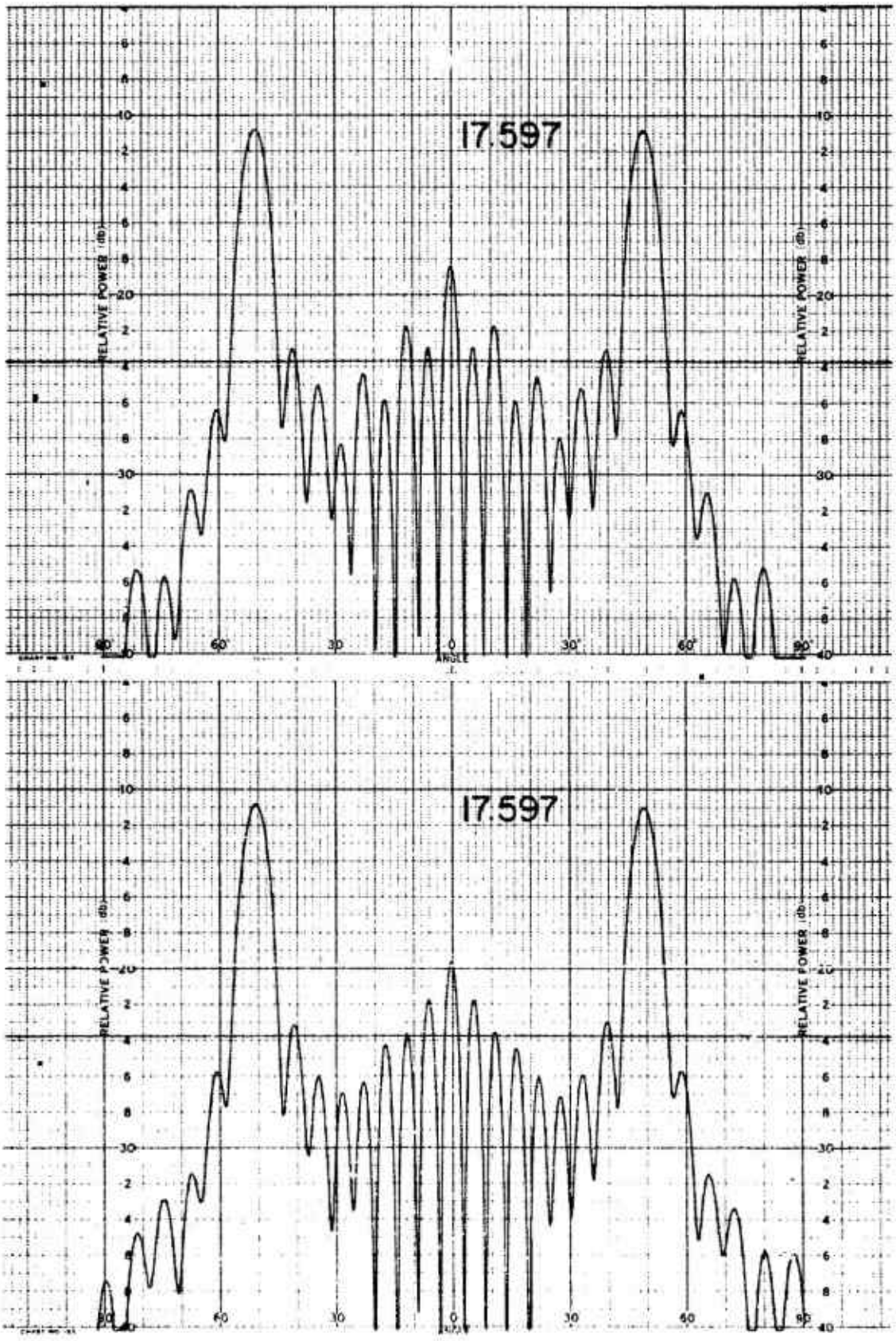
17.597
RELATIVE POWER (db)
ANGLE
60°
30°
0
30°
60°
90°
17.597
RELATIVE POWER (db)

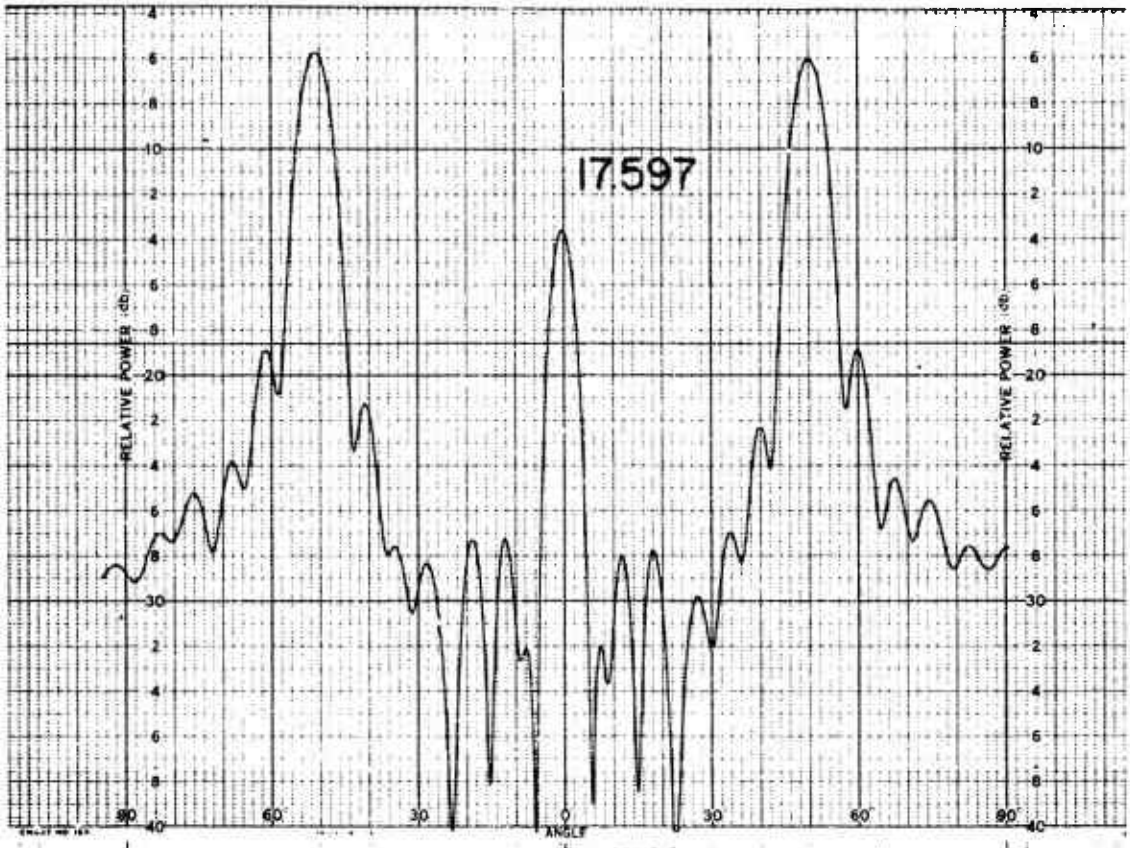
17.597
RELATIVE POWER (db)
ANGLE
90
60
30
0
30
60
90

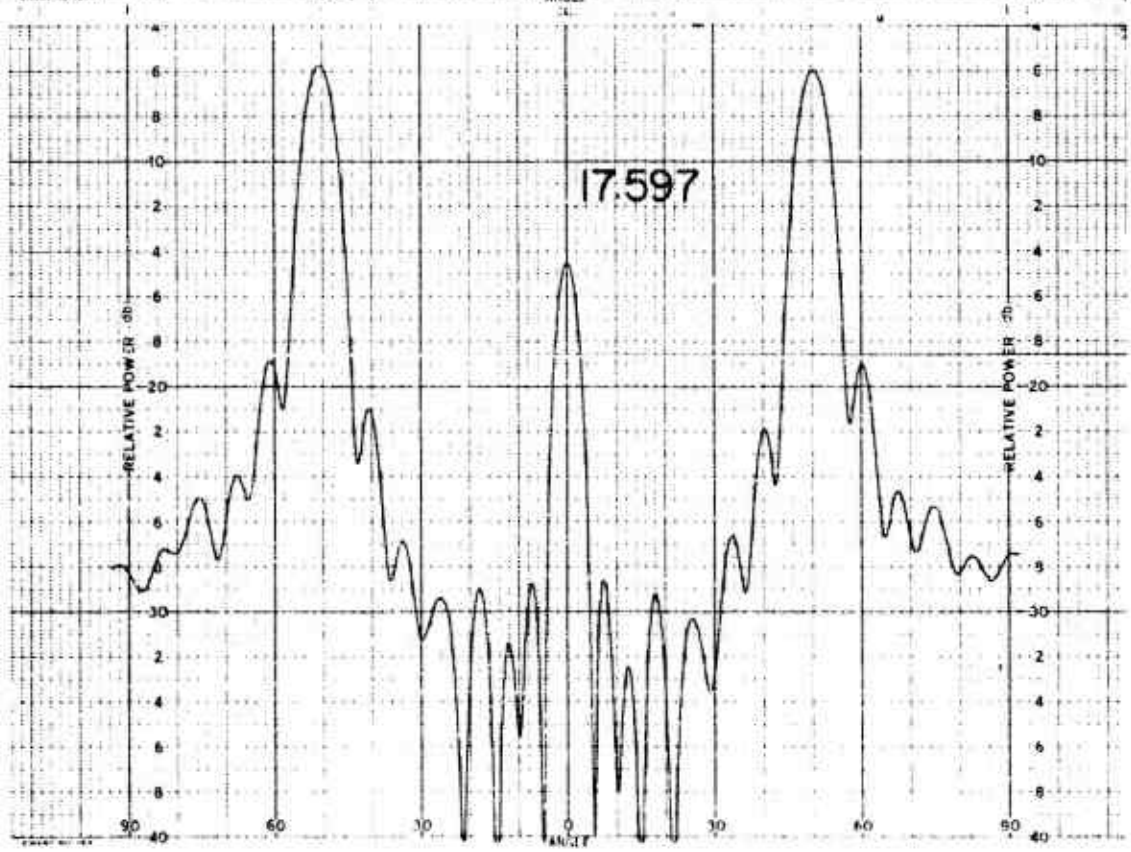
17.597
RELATIVE POWER (db)
ANGLE
90
60
30
0
30
60
90

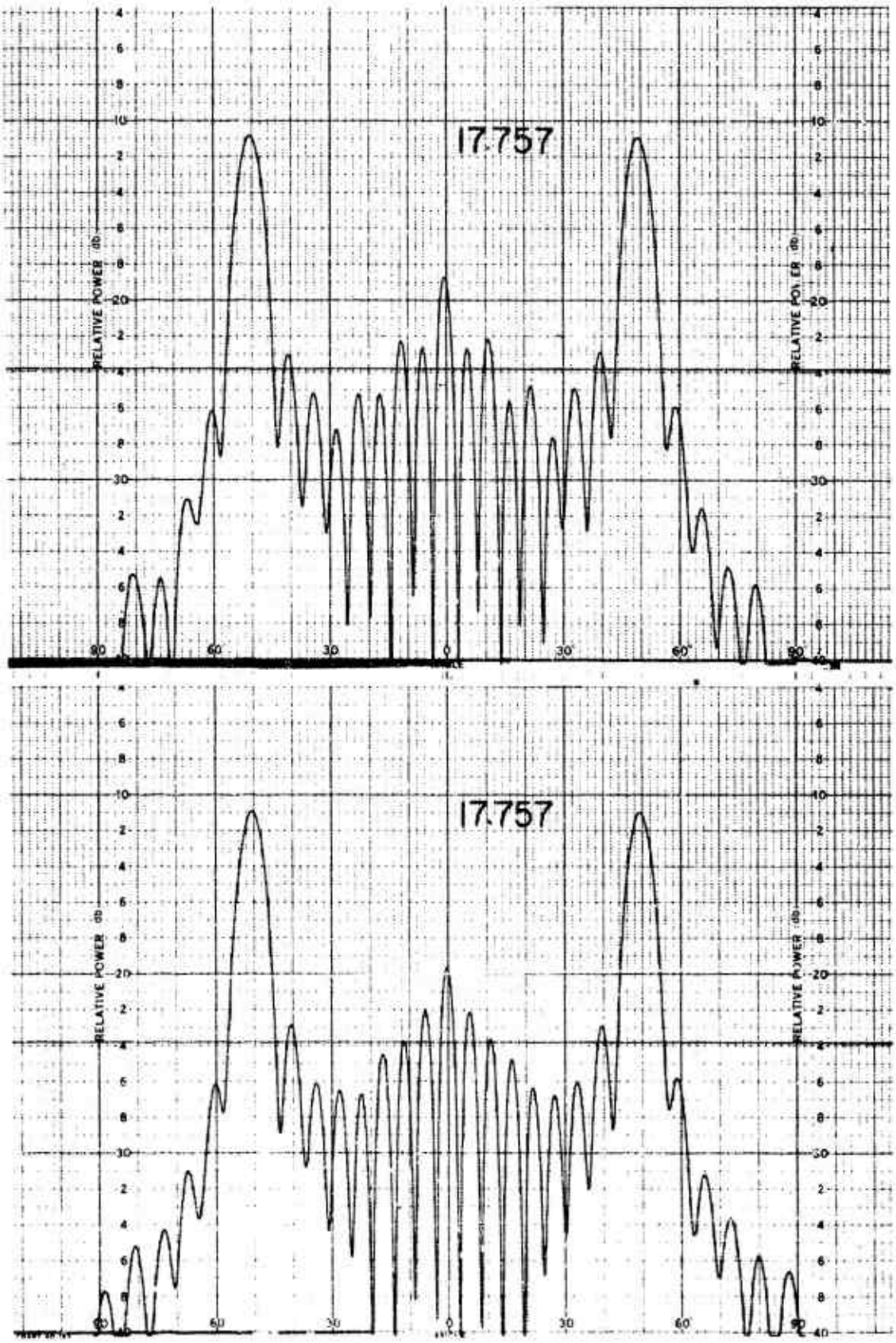
17.757
RELATIVE POWER db
90
60
30
0
30
60
90
17.757
RELATIVE POWER db
90
60
30
0
30
60
90

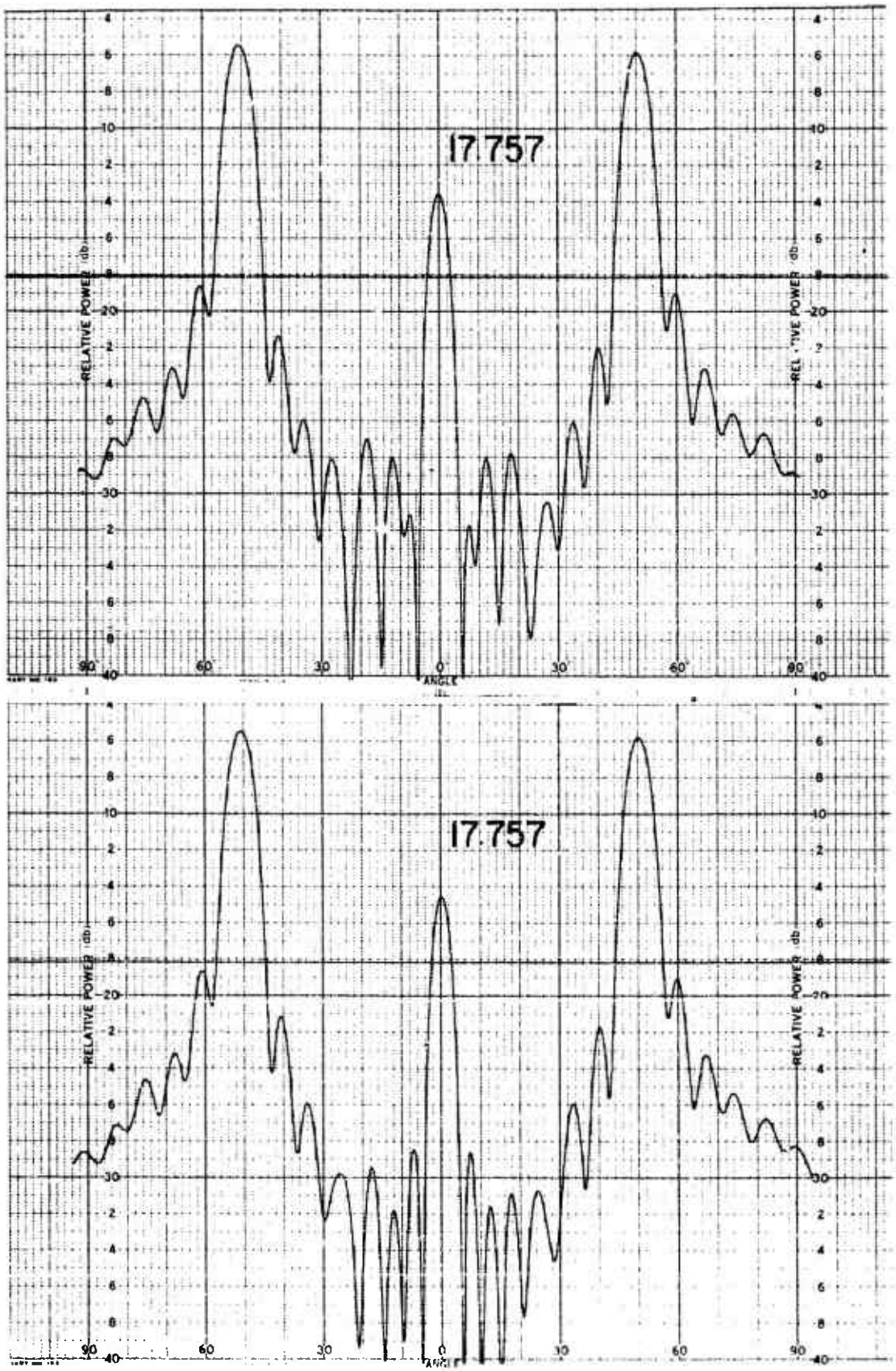
17.757
RELATIVE POWER db
ANGLE
90
60
30
0
30
60
90
17.757
RELATIVE POWER db
ANGLE

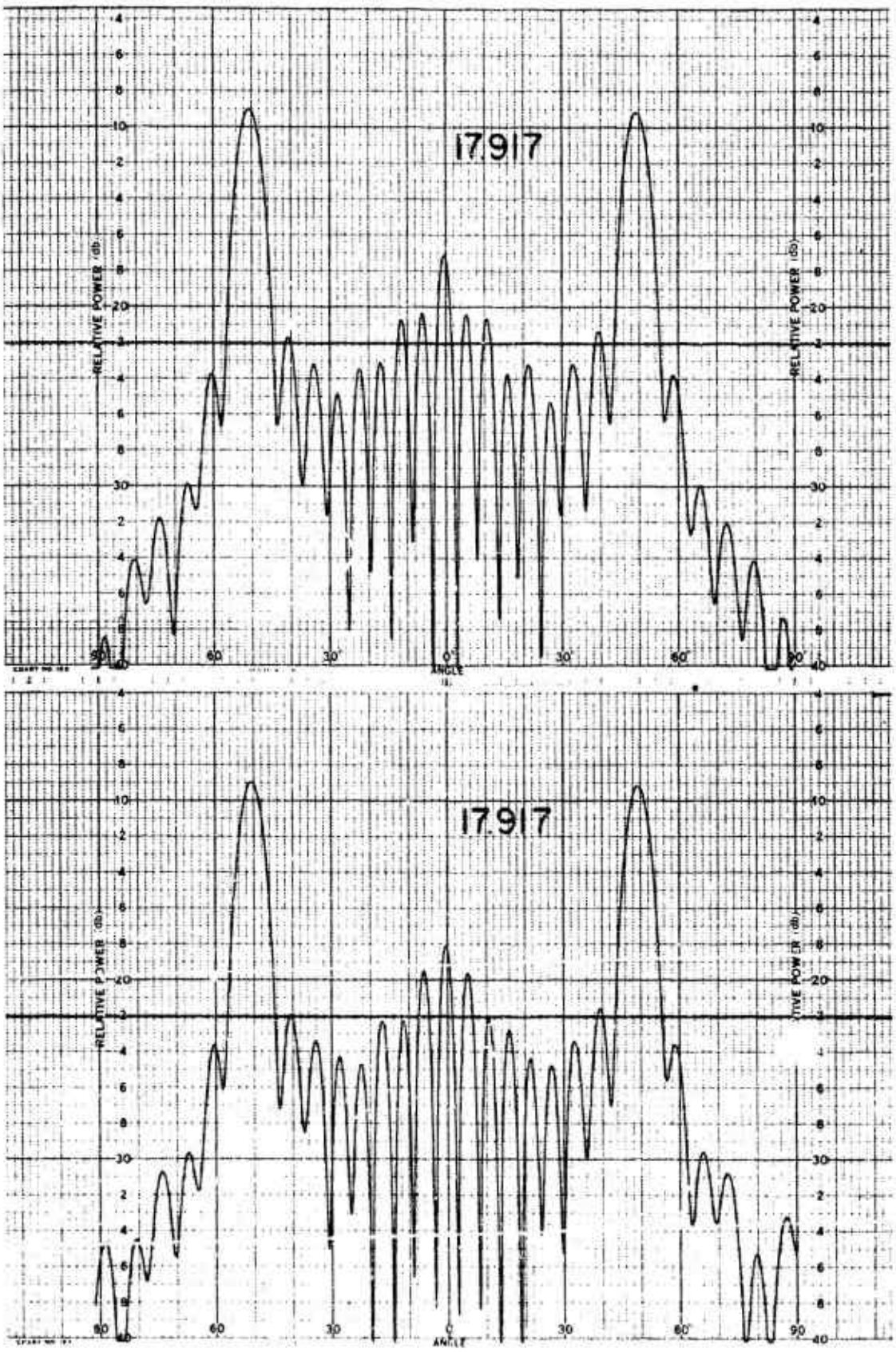
17.917
RELATIVE POWER (db)
ANGLE
17.917
RELATIVE POWER (db)
ANGLE

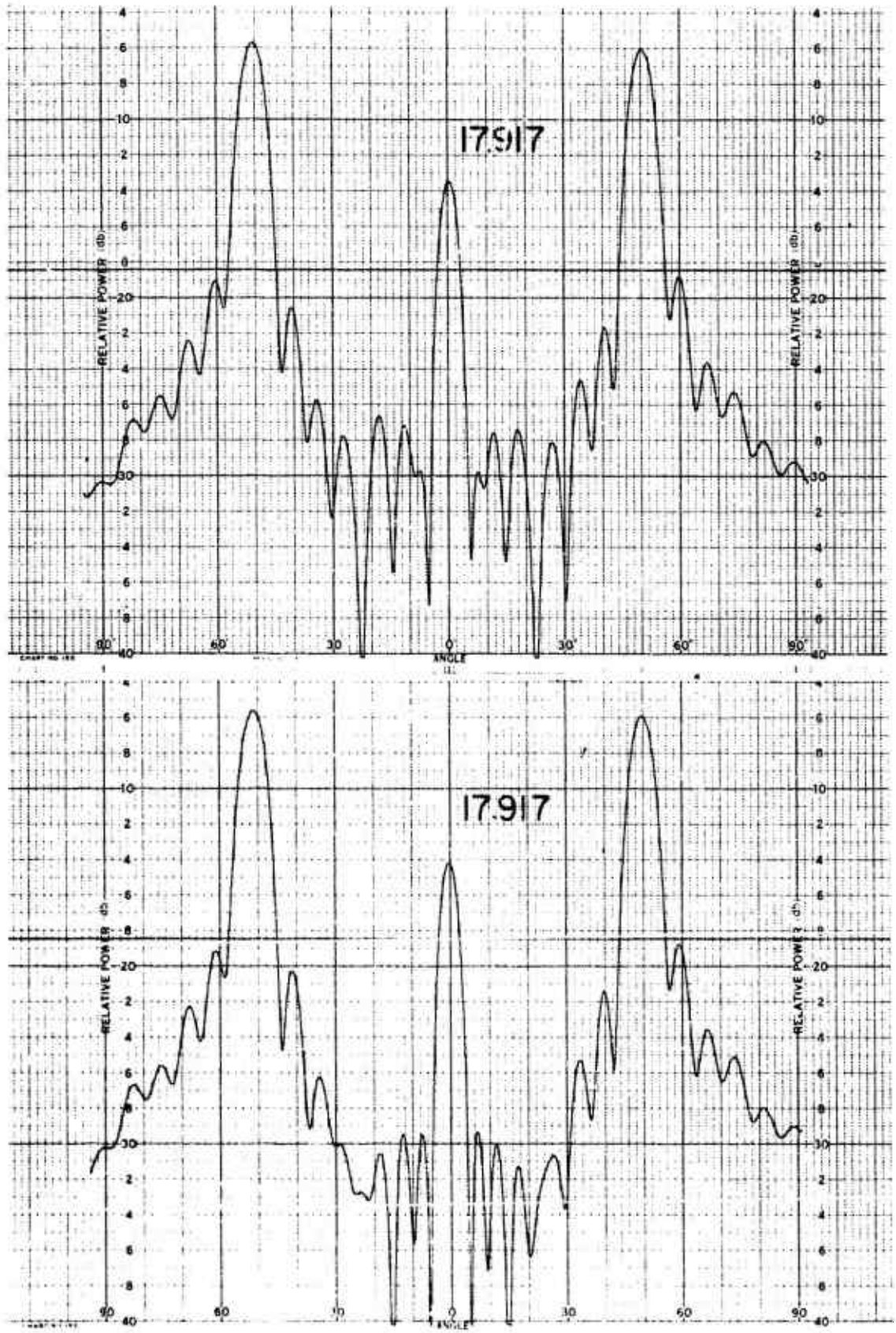
17.917
RELATIVE POWER (db)
ANGLE
17.917
RELATIVE POWER (db)
ANGLE

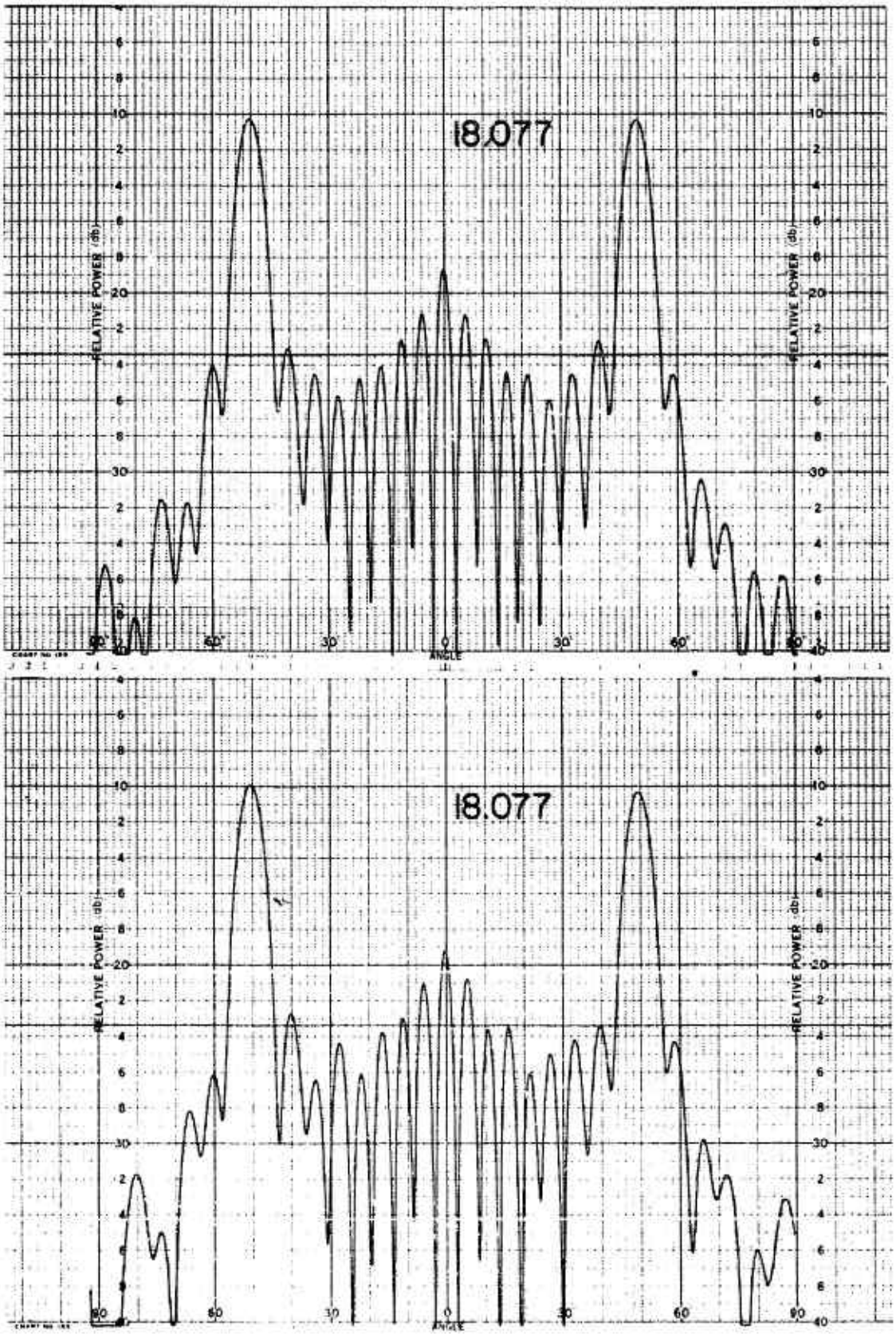
18.077
RELATIVE POWER (db)
ANGLE
18.077
RELATIVE POWER (db)
ANGLE

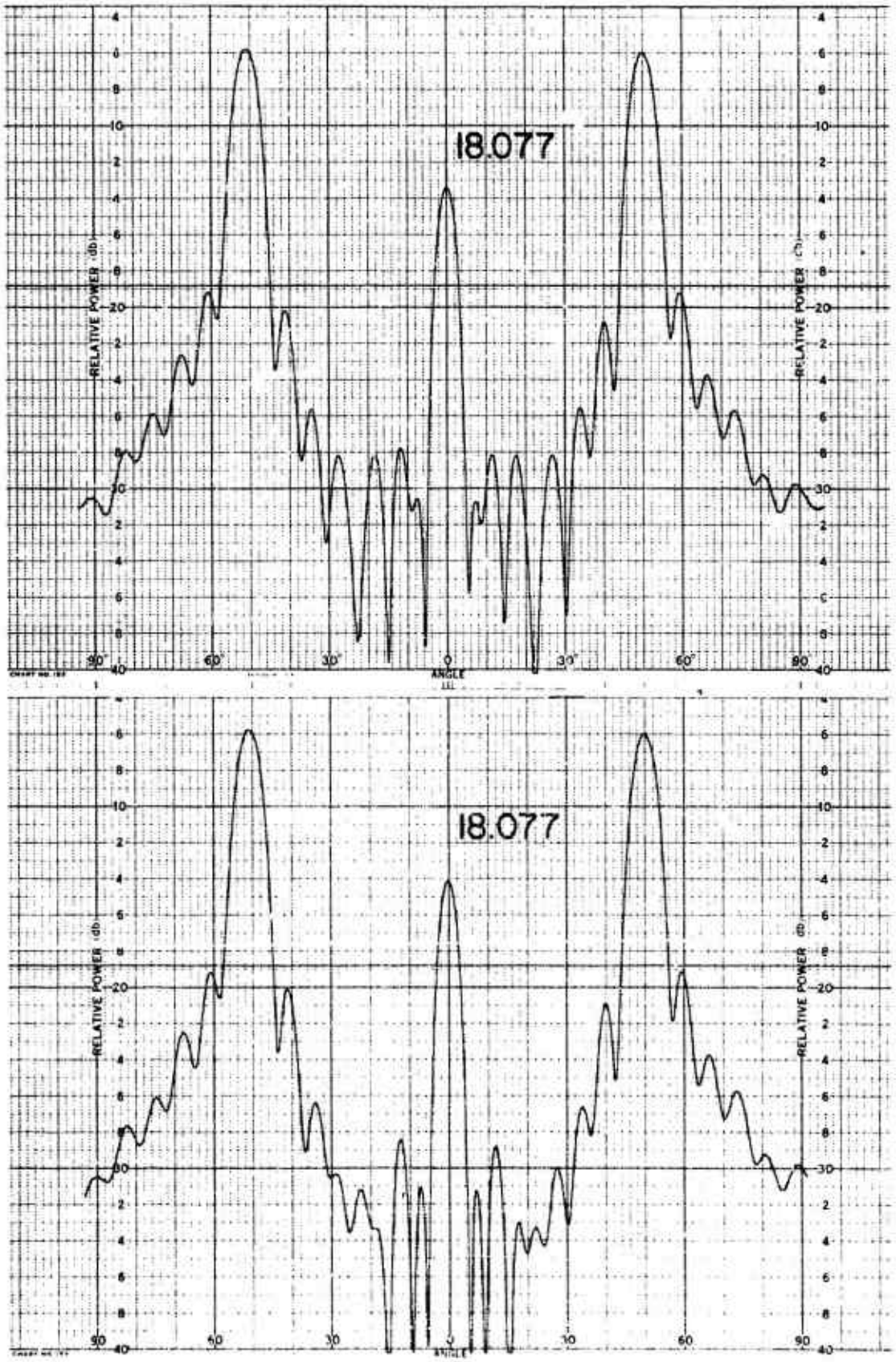
18.077
RELATIVE POWER (db)
RELATIVE POWER (db)
90°
60°
30°
0
ANGLE
30°
60°
90°
18.077
RELATIVE POWER (db)
RELATIVE POWER (db)

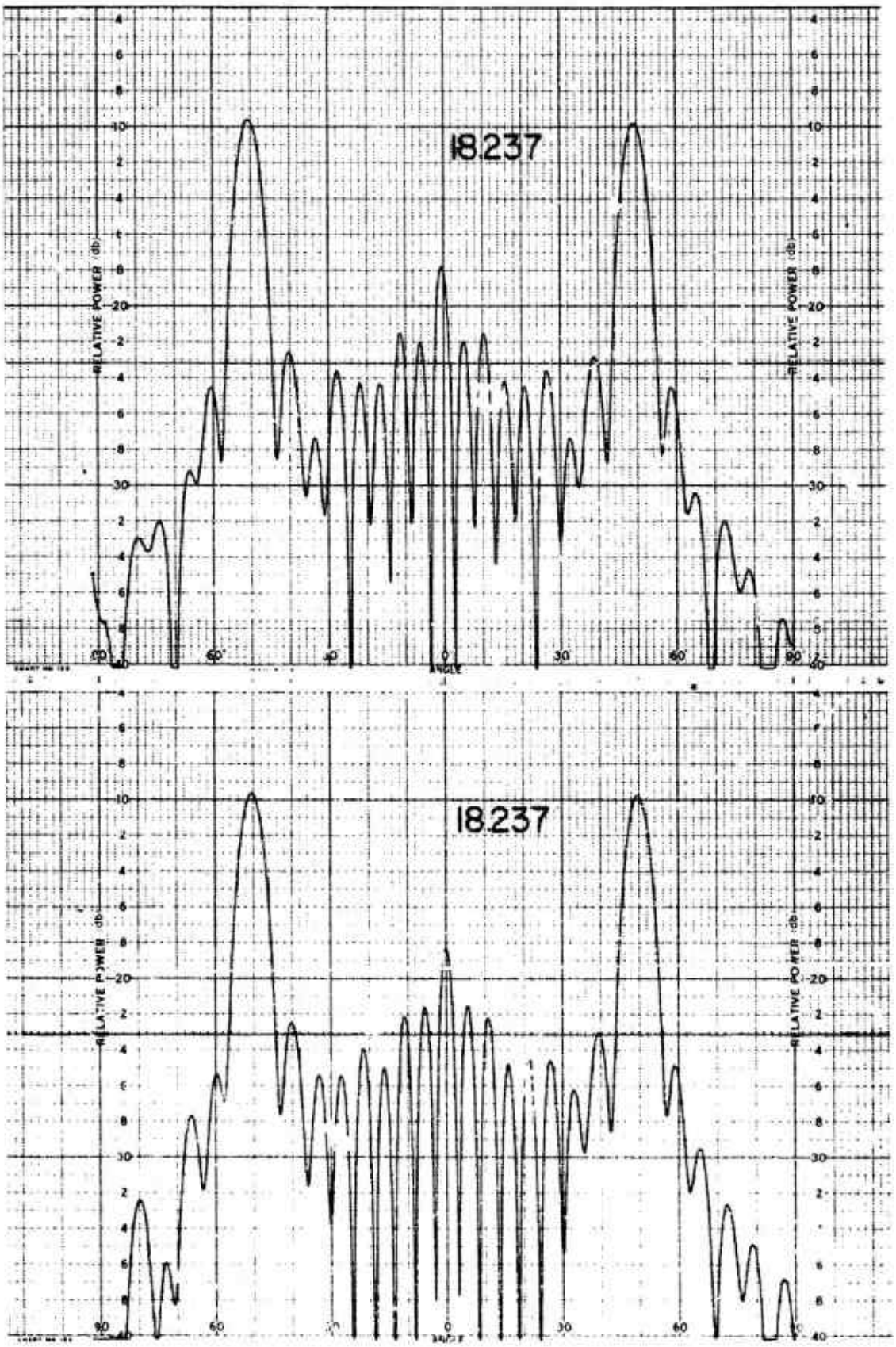
18.237
RELATIVE POWER (db)
ANGLE
18.237
RELATIVE POWER (db)
ANGLE

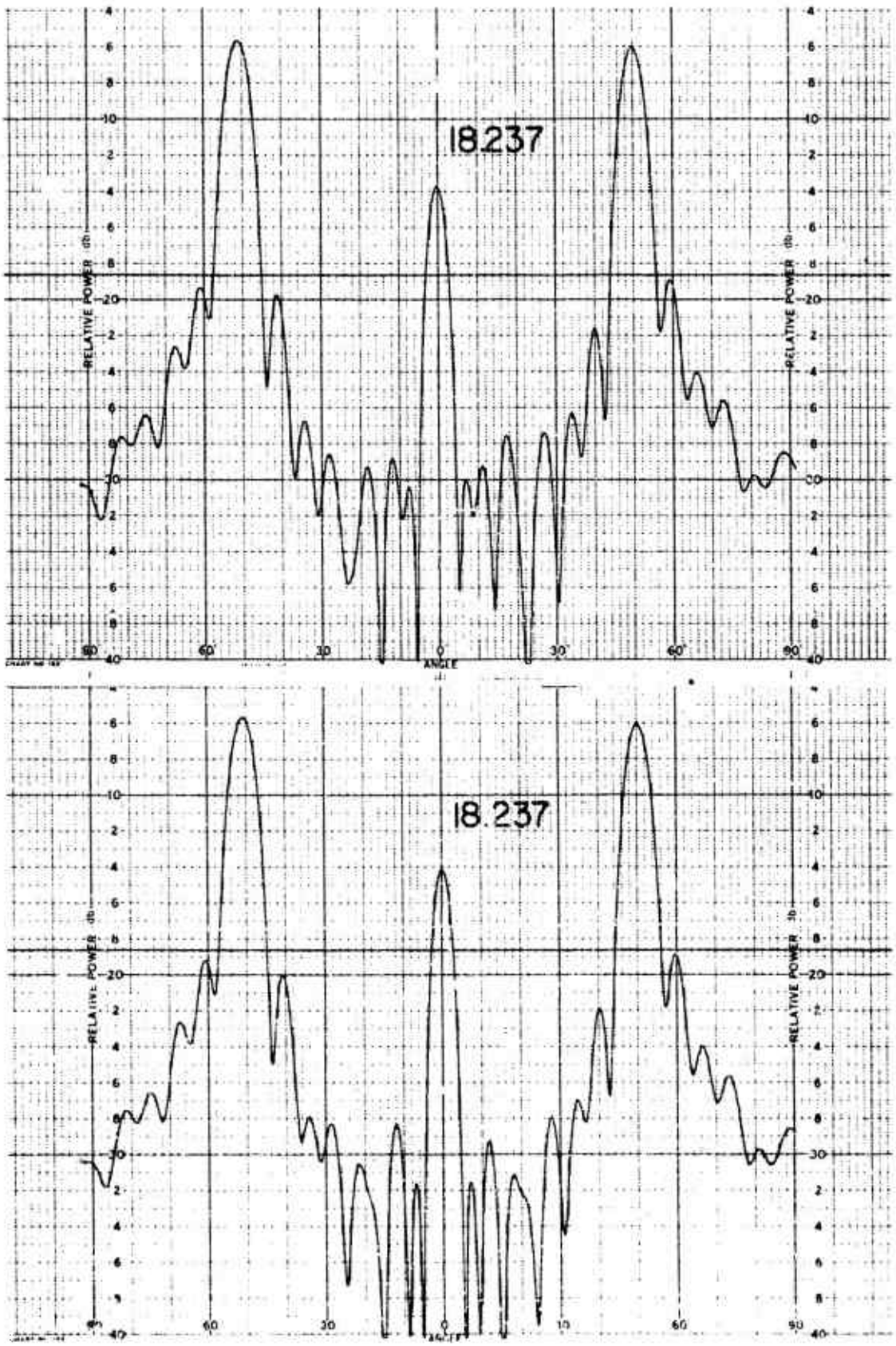
18.237
RELATIVE POWER (db)
ANGLE
18.237
RELATIVE POWER (db)

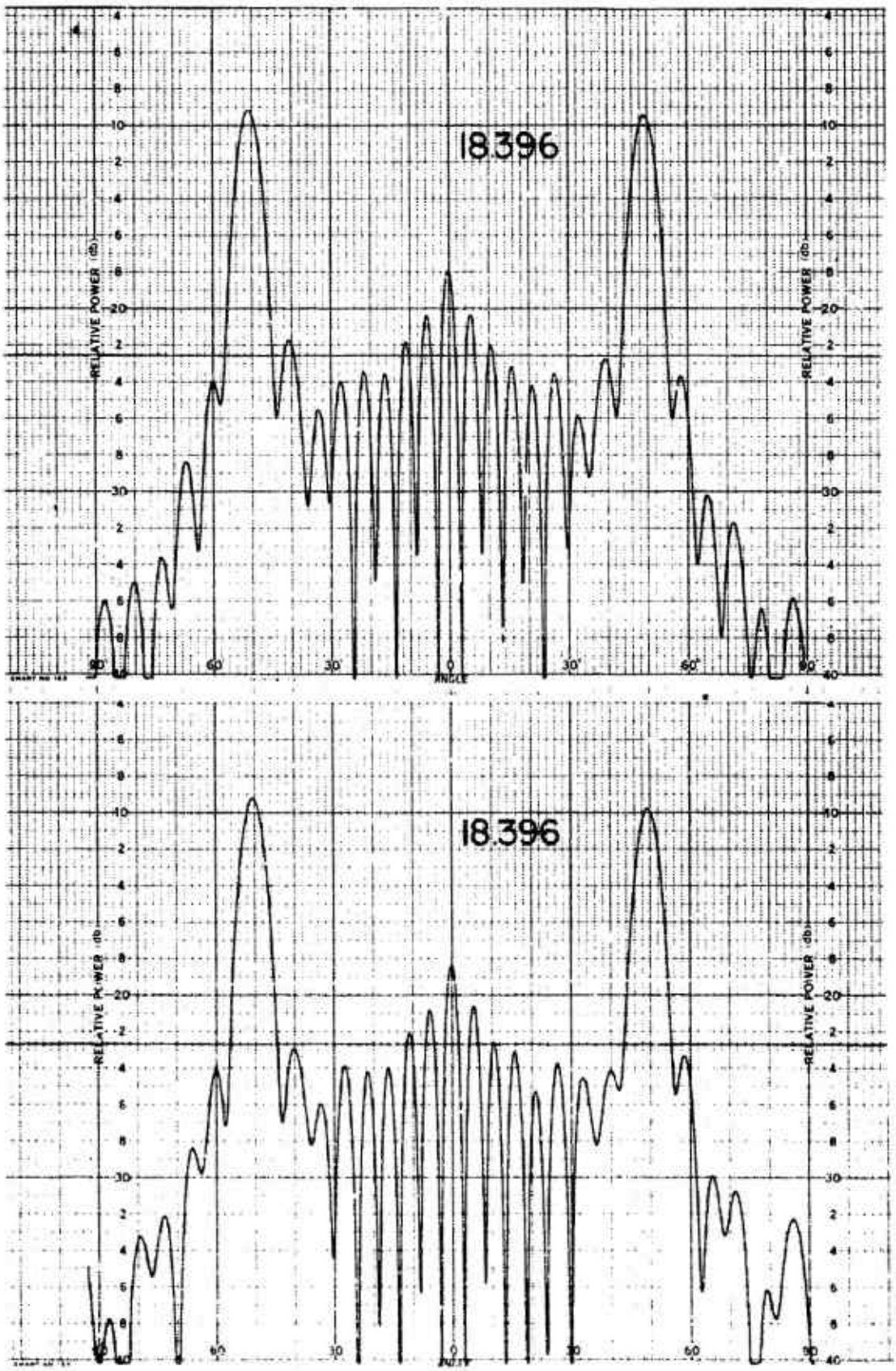
18396
RELATIVE POWER (db)
ANGLE
18396
RELATIVE POWER (db)
ANGLE

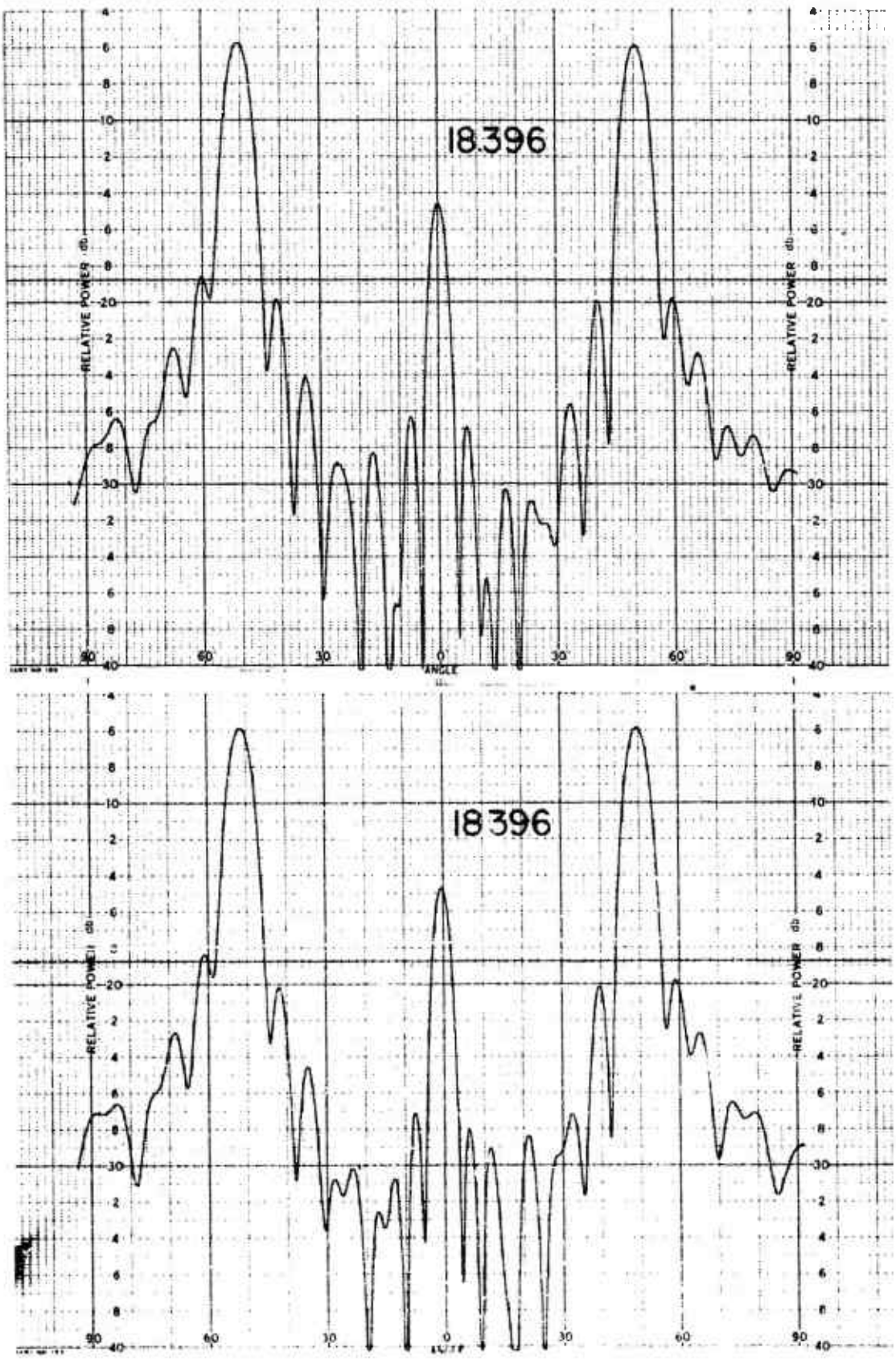
18396
RELATIVE POWER db
ANGLE
90
60
30
0
30
60
90
18396
RELATIVE POWER db
RELATIVE POWER db

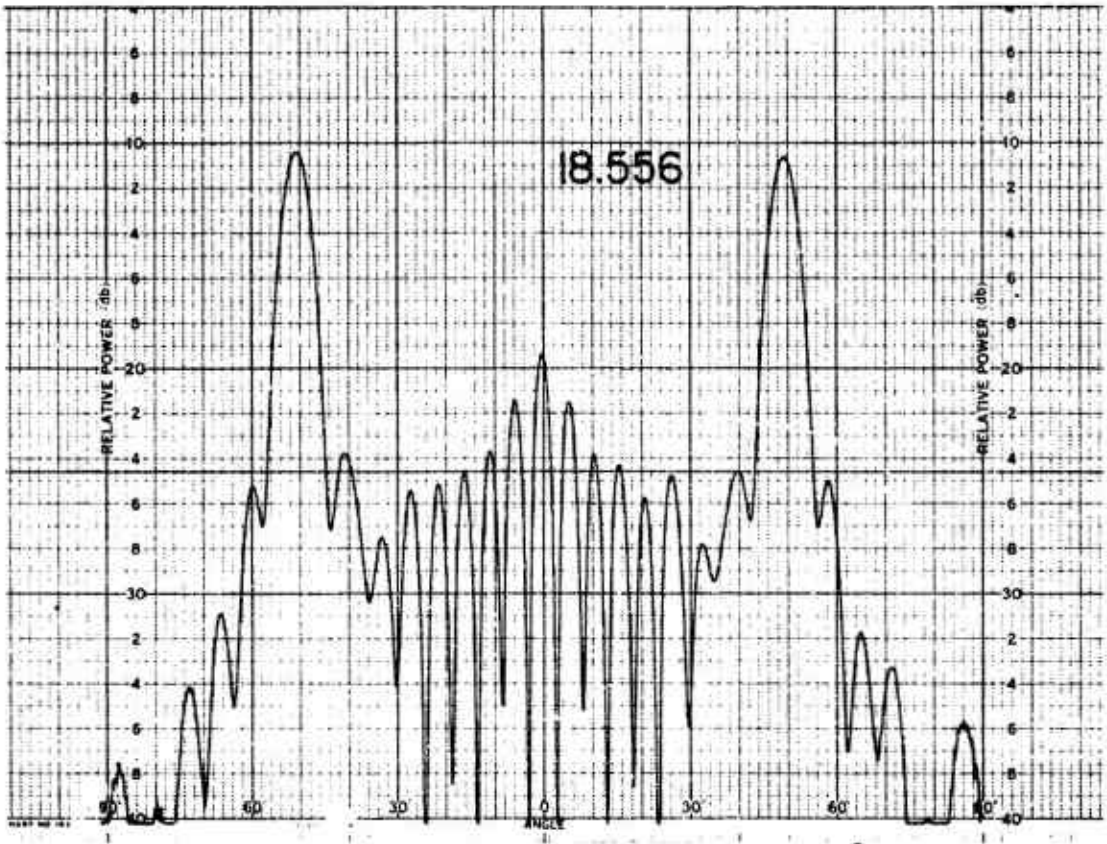
18.556
RELATIVE POWER (db)
ANGLE

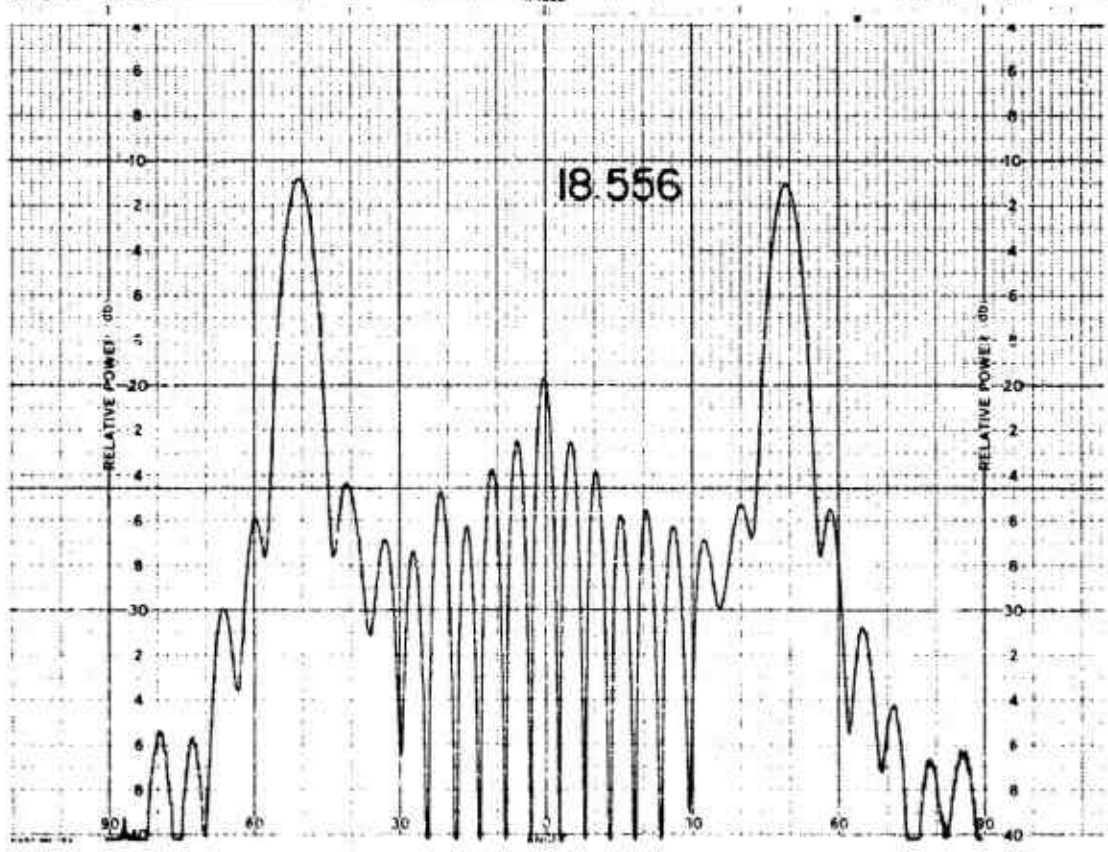
18.556
RELATIVE POWER (db)

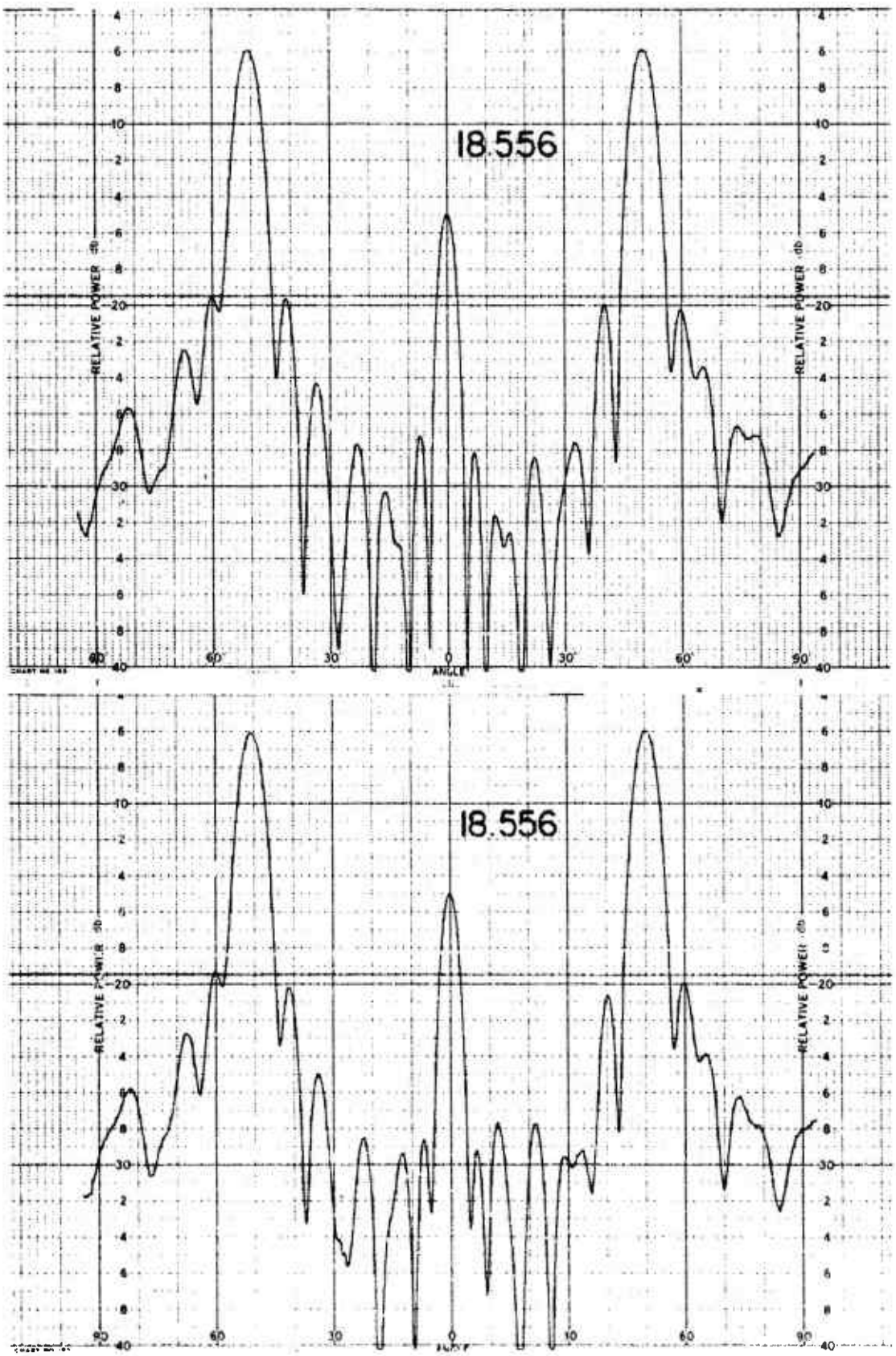
18.556
RELATIVE POWER db
ANGLE
60°
30°
0
30°
60°
90°
18.556
RELATIVE POWER db
ANGLE

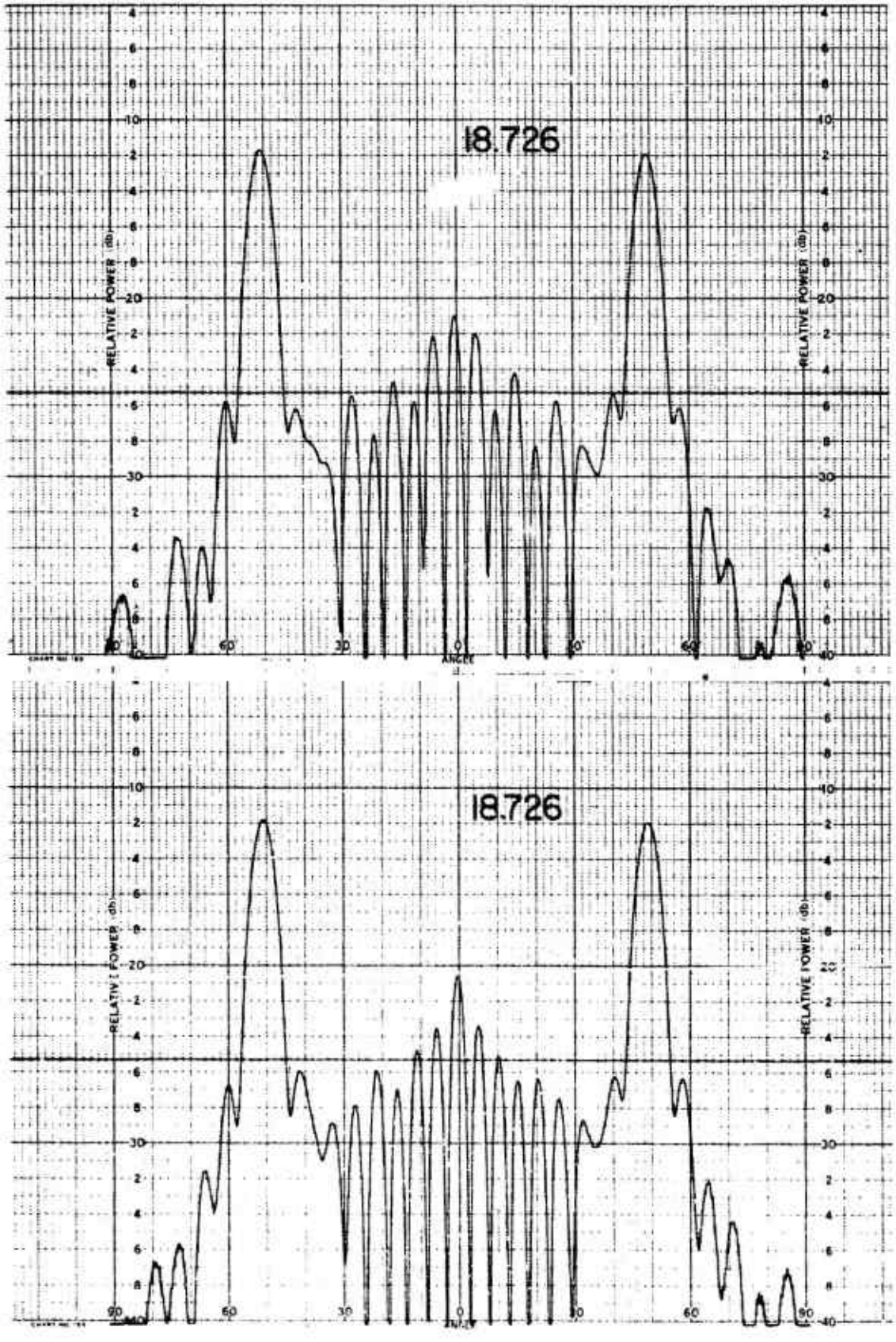
18.726
RELATIVE POWER (db)
ANGLE
18.726
RELATIVE POWER (db)
ANGLE

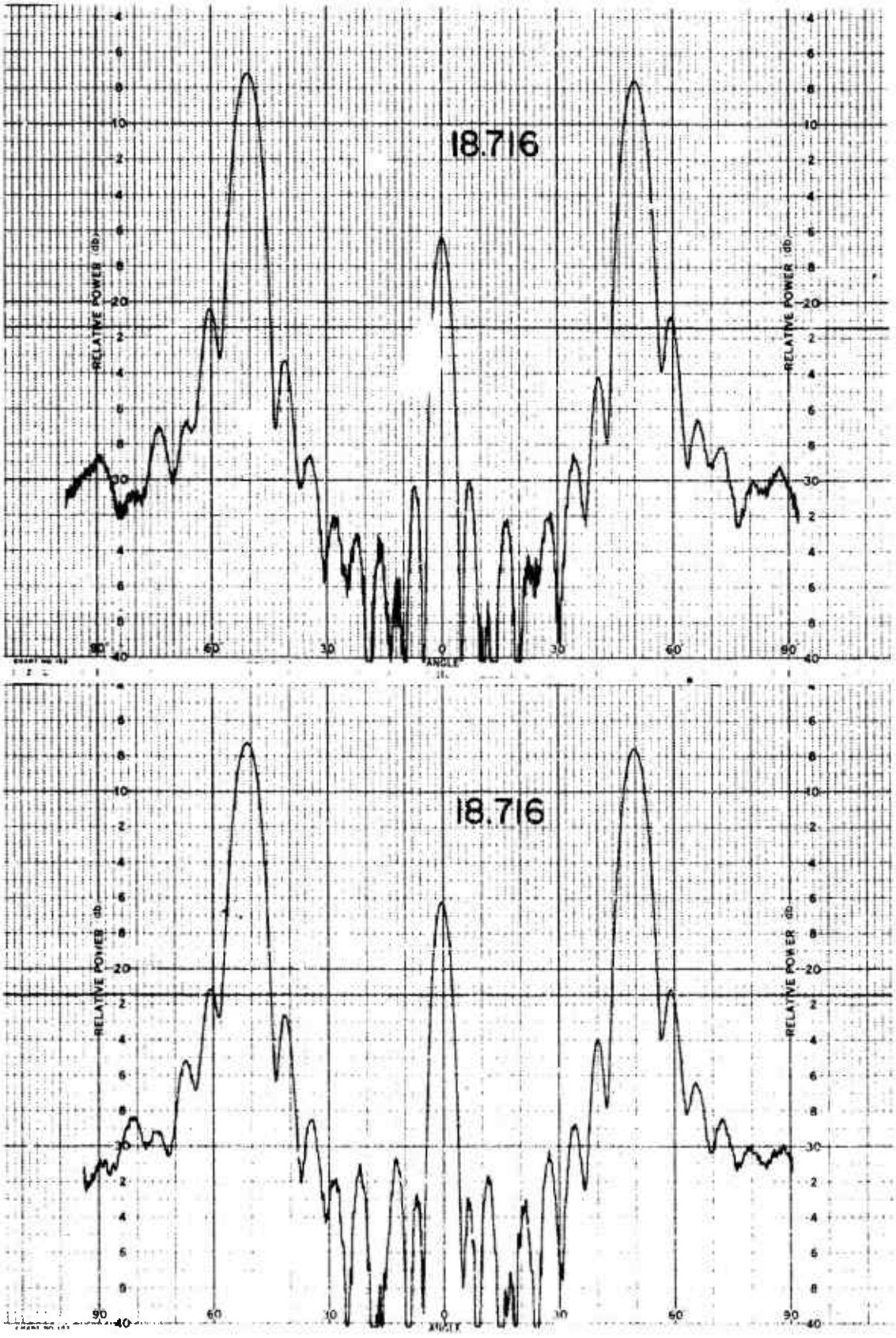
18.716
RELATIVE POWER db
ANGLE
18.716
RELATIVE POWER db
ANGLE

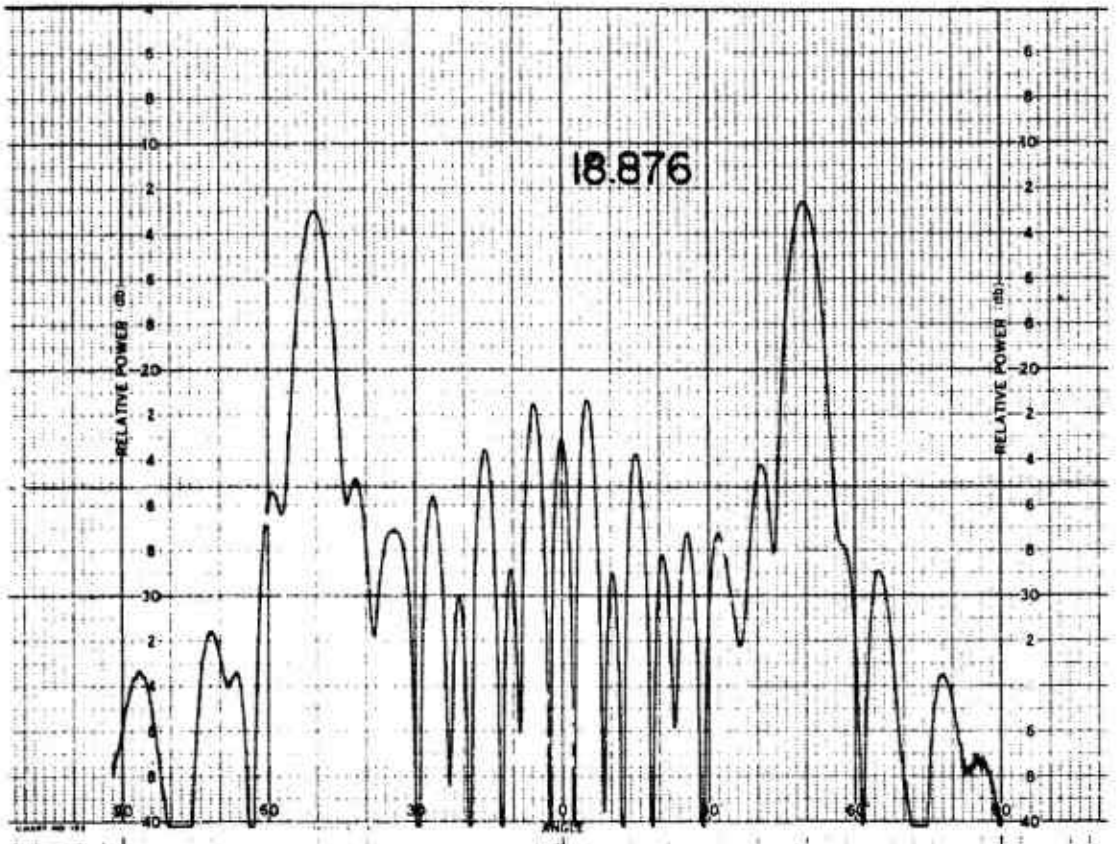
18.876
RELATIVE POWER (dB)
ANGLE

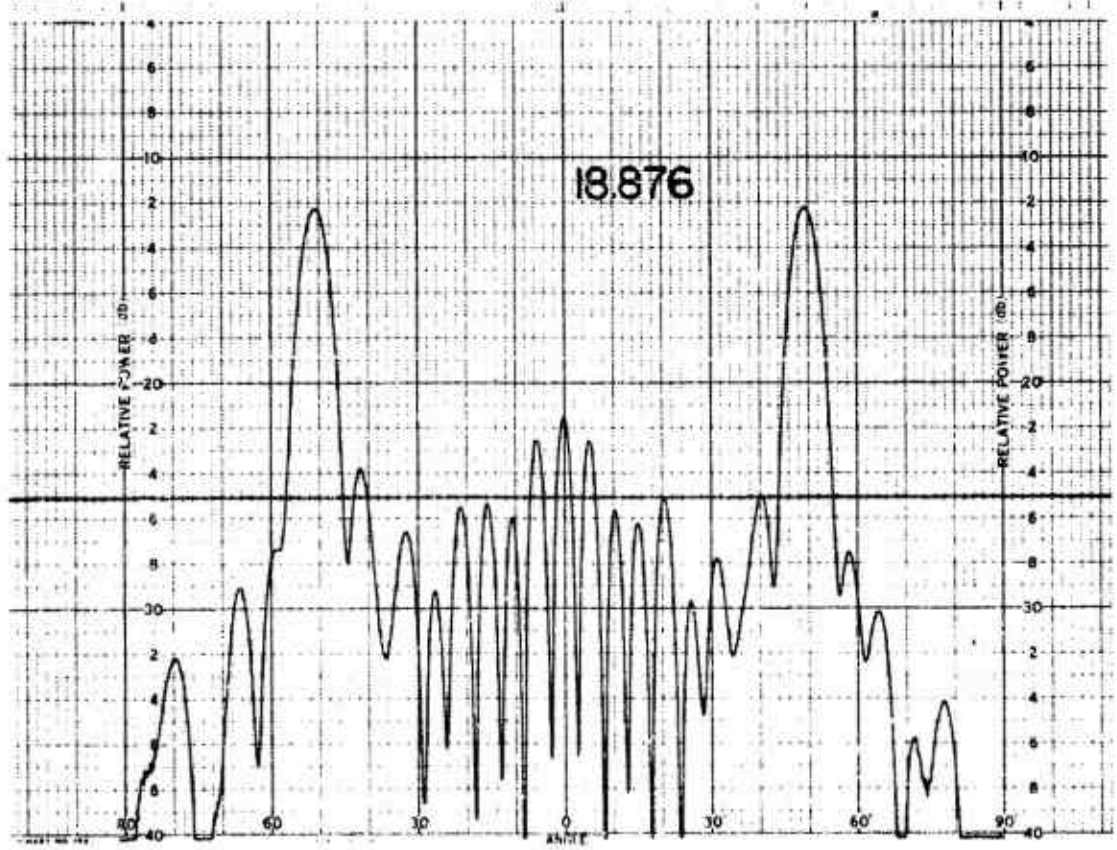
18.876
RELATIVE POWER (dB)
ANGLE

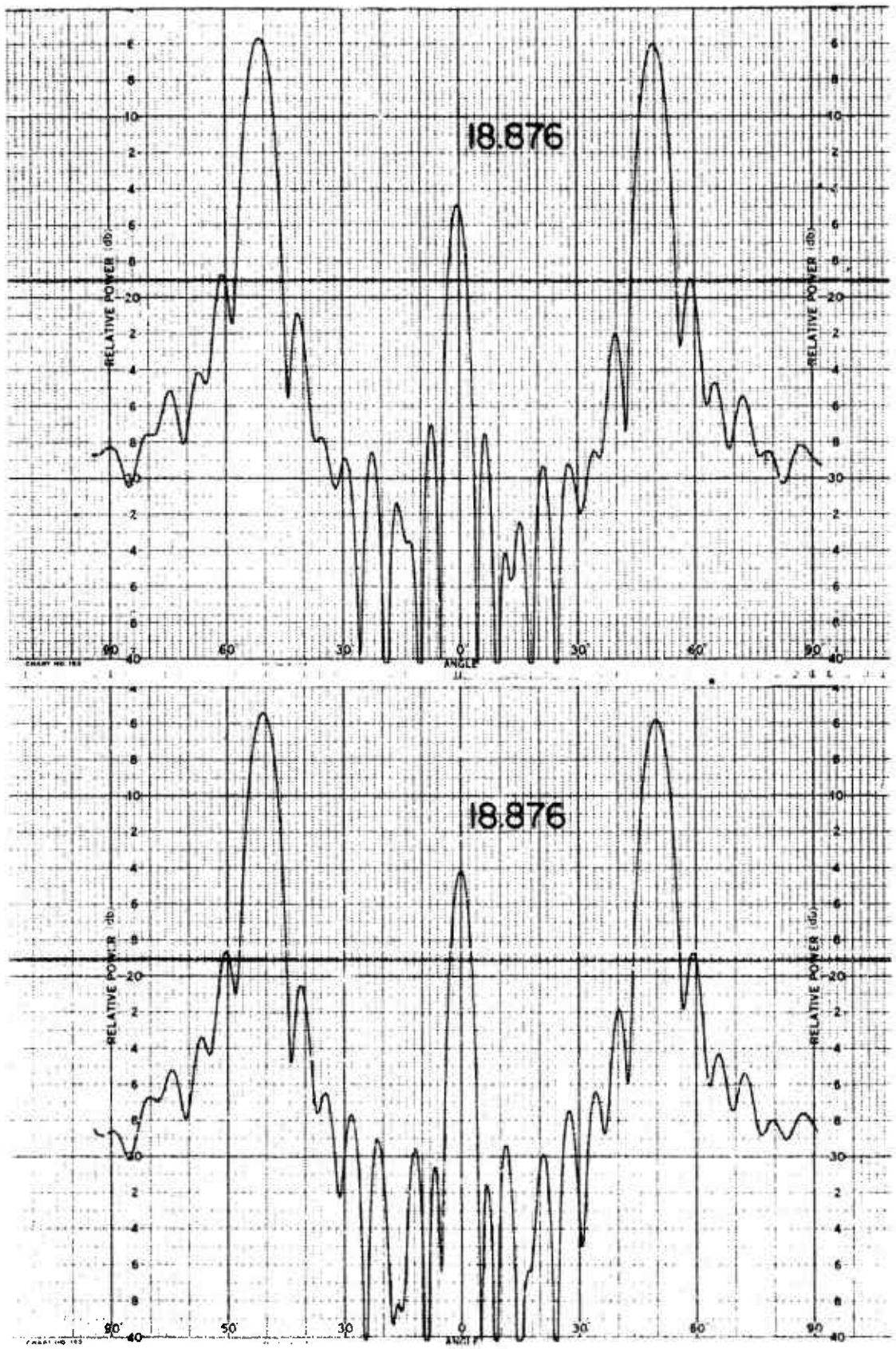
18.876
RELATIVE POWER (db)
ANGLE
18.876
RELATIVE POWER (db)

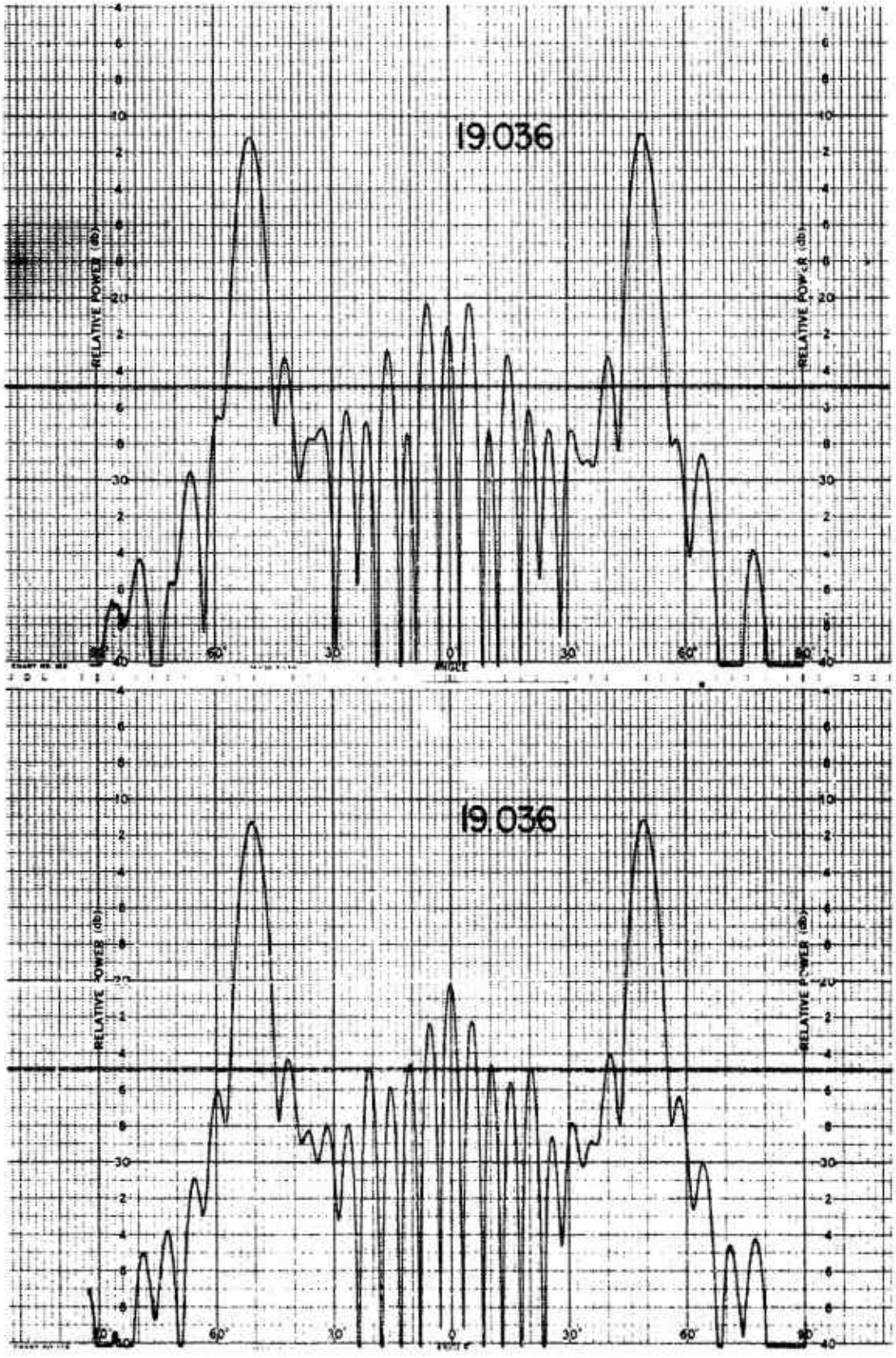
19.036
RELATIVE POWER (db)
ANGLE
19.036
RELATIVE POWER (db)

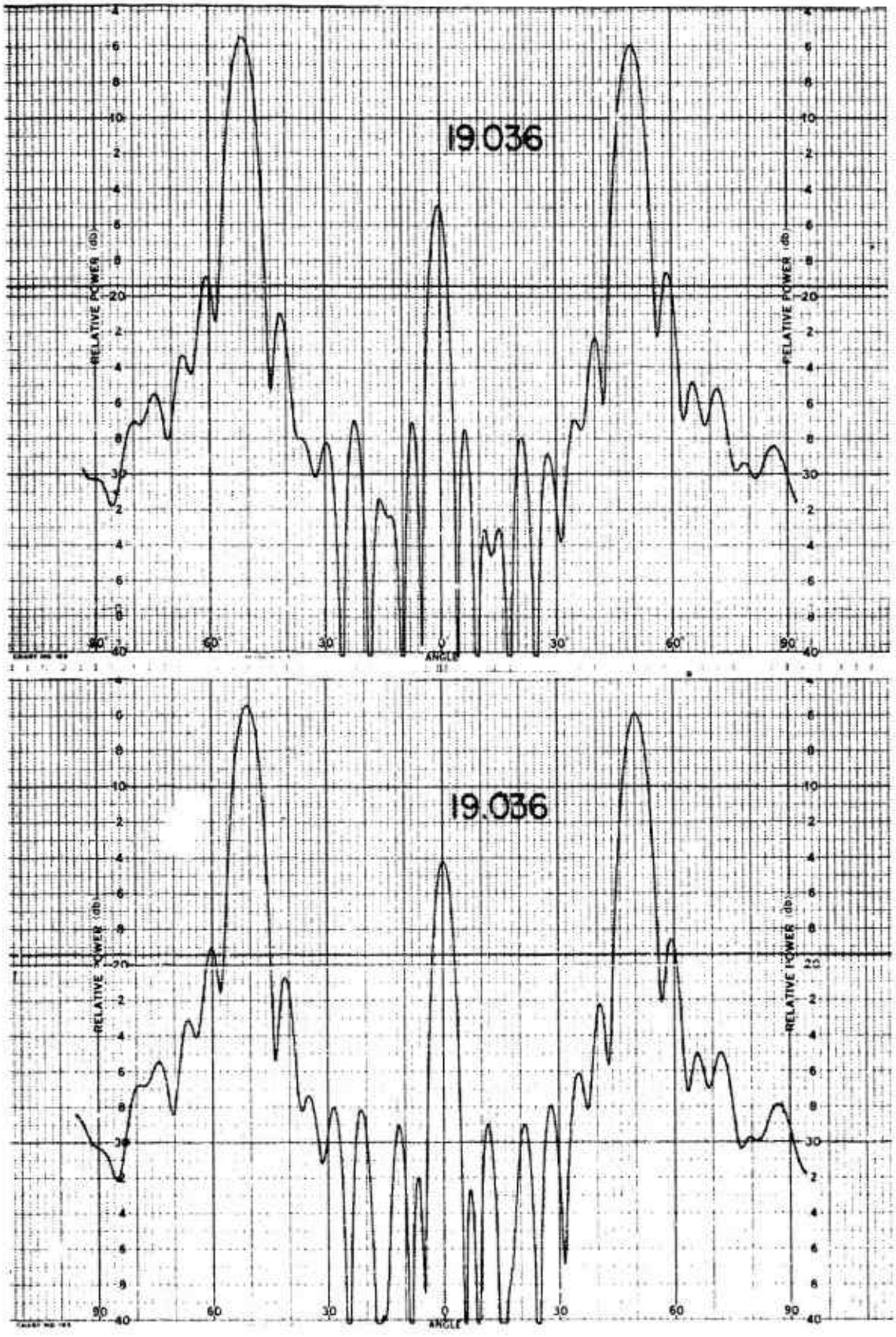
19.036
RELATIVE POWER (dB)
ANGLE
19.036
RELATIVE POWER (db)
ANGLE

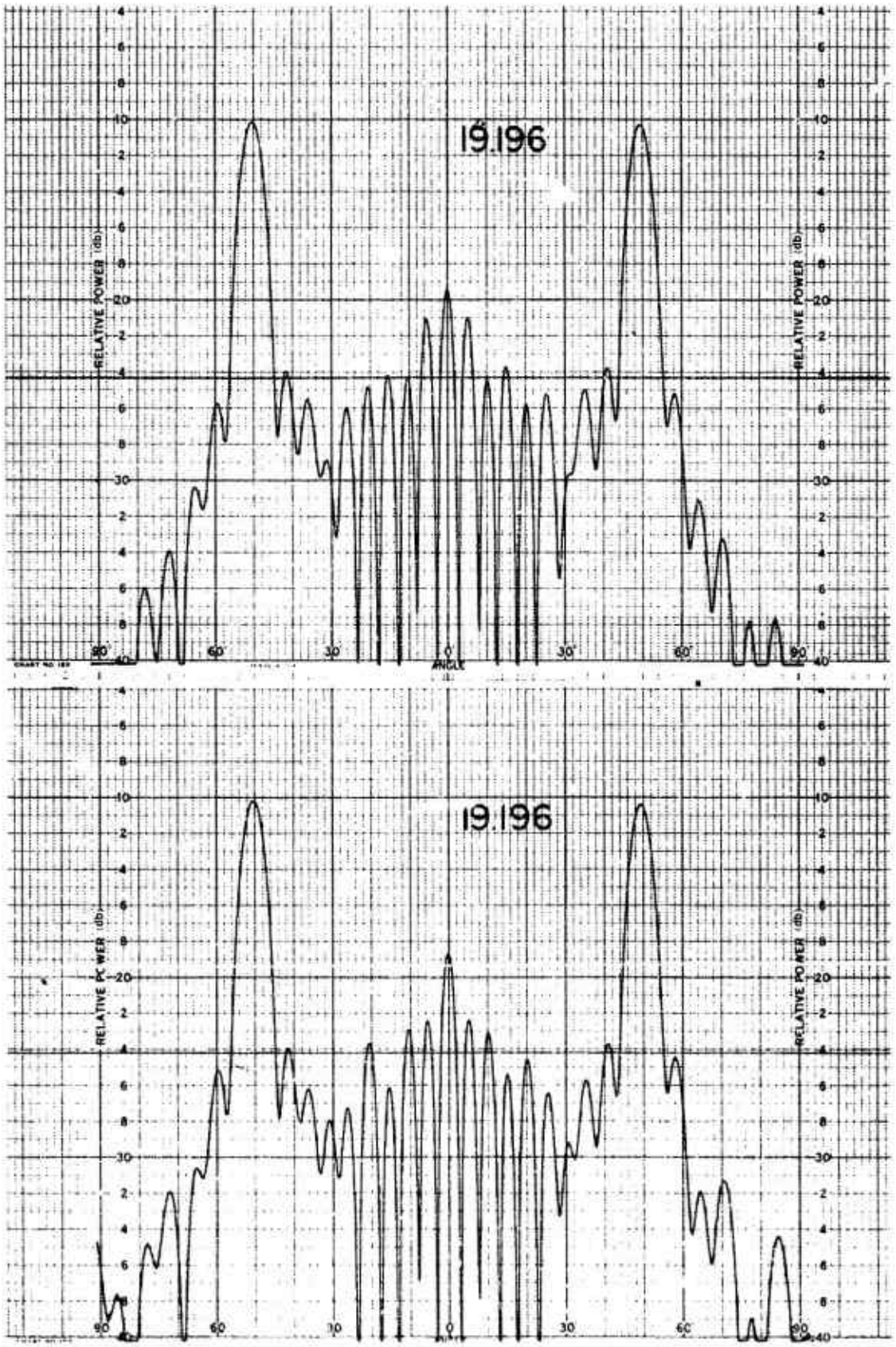
19.196
RELATIVE POWER (db)
ANGLE
19.196
RELATIVE POWER (db)

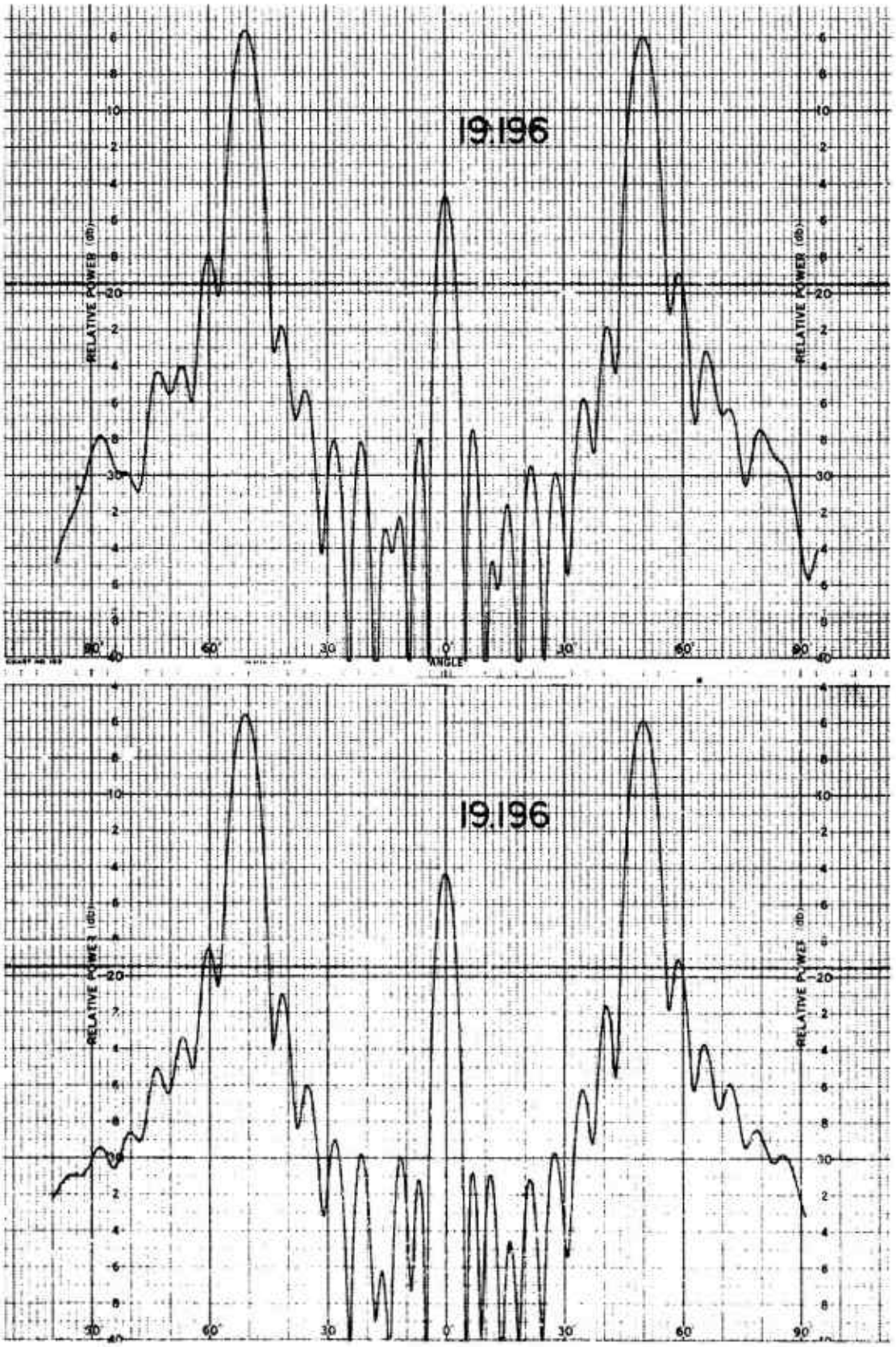
19.196
RELATIVE POWER (dB)
90°
60°
30
0°
ANGLE
30
60°
90°
19.196
RELATIVE POWER (dB)